Universidade do Minho
Escola de Engenharia

Sofia Afonso Alves

A new concept of bio-multifunctional nanotubular surfaces for dental implants: tribocorrosion resistant, antibacterial and osteogenic

March 2017

FCT
Fundação para a Ciência e a Tecnologia
MINISTÉRIO DA EDUCAÇÃO E CIÊNCIA

POPH
QUALIFICAR É CRESCER.

QREN
QUADRO DE REFERÊNCIA ESTRATÉGICO NACIONAL
PORTUGAL 2007.2013

Governo da República Portuguesa

UNIÃO EUROPEIA
Fundo Social Europeu

A new concept of bio-multifunctional nanotubular surfaces for dental implants: tribocorrosion resistant, antibacterial and osteogenic
Sofia Afonso Alves
UMinho | 2017

Universidade do Minho
Escola de Engenharia

Sofia Afonso Alves

A new concept of bio-multifunctional nanotubular surfaces for dental implants: tribocorrosion resistant, antibacterial and osteogenic

PhD thesis in Biomedical Engineering

Work developed under supervision of:
Luís Augusto Sousa Marques da Rocha
Ana Maria Pires Pinto
Jean-Pierre Celis

March 2017

STATEMENT OF INTEGRITY

I hereby declare having conducted my thesis with integrity. I confirm that I have not used plagiarism or any form of falsification of results in the process of the thesis elaboration.

I further declare that I have fully acknowledged the Code of Ethical Conduct of the University of Minho.

Universidade do Minho, 31/03/2017

Full name: Sofia Afonso Alves

Signature: Sofia Afonso Alves

Acknowledgements

Along the last four years I have spent one of the most intense and enriching periods of my life. I feel so blessed and thankful for the opportunity I had to conduct my work in several institutions all over the world, and meet people who greatly contributed to the success of this thesis. So, I would like to thank them from the bottom of my heart.

To my supervisor, Luís Rocha, for his motivation, guidance and support throughout the project. For his friendship and encouragement in every moment, and for the given opportunity to perform my experimental activities in a multicultural environment, which have allowed me to improve my research skills, and contributed highly to my personal progress.

To Prof. Ana Maria Pinto, for all the support and friendship along the past years.

To my co-supervisor Prof. Jean-Pierre Celis for his availability for scientific discussions, sharing with me his experience and broad knowledge in the area, providing key ideas for the successful development of the work.

To Prof. Mariana Henriques and Elisa Rodrigues for all their availability on helping me in the execution of an important part of this work. Their kindness and generosity made a difference in the upshot of this thesis.

To Prof. Tolou Shokuhfar, who has given me the opportunity to discover the "nano-scale world". I will be eternal grateful for your guidance and support throughout the time I spent at UIC. She welcomed me in her research group, always believing and encouraging throughout the time I spent in the wonderful Chicago city.

I'm grateful to Prof. Cortino Sokotjo, Prof. Mathew Mathew and Prof. Christos Takoudis from IBTN-US group for their mentoring by providing important comments and suggestions, which were fundamental to increase my knowledge in the field, and contributed to the development of this work.

To Prof. José Mauro Granjeiro for giving me the opportunity to work in INMETRO, which really contributed to the success of this work.

To Prof. Radovan Borojevic for the opportunity to work in Rio the January cell bank, for his extraordinary expertise and providing of important ideas and suggestions throughout the work, contributing to the good quality of my research.

To André Rossi, for all his persistence, expertise and experience, which provided me the opportunity to overcome several obstacles and allowed the development of a crucial part of this work.

To Prof. Paulo Noronha who has welcomed me in UNESP and contributed with his experience and knowledge to this work.

To several friends and colleagues from all the institutions that I have the opportunity to work and that contributed to the success of this project, to name a few, Sara Piperni, Renata Carvalho, Jacques Werckmann, Rafaela Santos, Rosana Bizon, Marcus Teixeira, Esther Takamori, Wanderson Studzel, Priscila Laviola, António Saraiva, Bruno Cosme, Márcia Maru, Vanessa Kapps, Ana Beatriz e Bruna Costa.

To several colleagues and friends, for their help on this work and constant support. From University of Minho, Portugal, to Alexandra Alves, Fatih Toptan, Sandra Lopes, Luisa Oliveira. From the IBTN-US group, to Maria Alfaro, Isabella Marques, Luciana Trino, Bahvani Patel, Arman Butt and Azhang Hamlekhan. A special thanks to my dear friend Sweetu Patel who have welcomed me with a smile, always encouraging and helping me, unconditionally.

To Ana Ribeiro, for her friendship, motivation, wisdom, and always useful comments and suggestions on my work.

To my unforgettable PhD colleagues and friends, Helena Cruz, Fernando Oliveira, Sonia Costa and Maria João Runa who were always by my side.

Diana Morais, my eternal and loyal partner, who really inspired and encouraged me throughout the duration of this project.

Most importantly, my acknowledgement to all my family, all of their members whose names are uncountable. Their unconditional love, patience and understanding encouraged me every single day. I may consider myself really blessed for having you by me side.

A great thank, to my parents, Jacinto Alves e Teresa Alves, who are the ones to whom I dedicate this thesis. Without them, nothing would be possible.

Finally, I would like to acknowledge the Portuguese Foundation for Science and Technology (FCT) Portugal, for the financial support provided through the grant SFRH/BD/88517/2012.

FCT Fundação para a Ciência e a Tecnologia
MINISTÉRIO DA EDUCAÇÃO E CIÊNCIA

POPH QUALIFICAR É CRESCER.

QREN QUADRO DE REFERÊNCIA ESTRATÉGICO NACIONAL PORTUGAL 2007.2013

GOVERNO DA REPÚBLICA PORTUGUESA

UNIÃO EUROPEIA
Fundo Social Europeu

A new concept of bio-multifunctional nanotubular surfaces for dental implants: tribocorrosion resistant, antibacterial and osteogenic

Abstract

Dental implant market is continuously growing due to the constant increase in life expectancy and higher concerns on oral hygiene and aesthetics. Titanium-based materials are the most widely used in dental implants due to their superior biocompatibility, mechanical properties, and excellent corrosion resistance. However, despite the high overall success rate of dental implants, a significant number of failures still occur.

Implant failures in dentistry may be ascribed essentially to three main causes, namely the lack of an adequate implant-bone integration, microbial infection, and corrosion/tribocorrosion processes. The modification of Ti surface features has been a strategy currently adopted in the attempt to overcome these complications. Ideally, the implant should be able to display concomitantly two contradictory properties: the enhancement of human cell adhesion and the inhibition of the adhesion of undesirable microorganisms. Additionally, the implant surface should be also tailored with the ability to withstand the combined actions of corrosion and wear (tribocorrosion), at which they are exposed to in the human body. Nanotechnology is an emerging area in the field of dentistry, and in particular, nanotubular TiO_2 surfaces have been widely recognized as promising candidates to improve the performance of dental implants. However, the construction of effective nanotubular systems based on an integrated approach addressing, simultaneously, the three main causes of failure, is still missing.

This thesis aims the synthesis of multifunctional TiO_2 nanotubes (NTs) in Ti surfaces, tailored to exhibit simultaneously tribo-electrochemical resistance, antibacterial activity, and an adequate osseointegration ability. To achieve the main aim, TiO_2 NTs were synthesized by anodization, and functionalized with bone-constituting elements such as calcium, phosphorous, and zinc, through a novel methodology based on reverse polarization anodization processes. After bio-functionalization, Ti surfaces decorated with TiO_2 NTs displayed an outstanding tribo-electrochemical behavior, the capacity to impair bacterial viability, and the ability to improve human cell responses. These multiple functions were ascribed to the morphological, topographical, and physicochemical features of bio-functionalized TiO_2 NTs, as well as to their mechanical properties and adhesion strength to Ti.

The outcomes of this work remarkably show that significant improvements have been achieved. By means of a simple approach, key functionalities of conventional TiO_2 NTs were improved, which are expected to have a major clinical impact in dental implant therapies.

Um novo conceito de superfícies nanotubulares bio-multifuncionais para implantes dentários: resistentes à tribocorrosão, antibacterianas e osteogénicas

Resumo

O mercado de implantes dentários tem vindo a crescer, devido ao aumento constante da esperança de vida e maiores preocupações no que respeita higiene oral e estética. Materiais à base de titânio (Ti) são os mais usados em implantes dentários devido à sua elevada biocompatibilidade, propriedades mecânicas e excelente resistência à corrosão. No entanto, apesar da alta taxa de sucesso, um número significativo de falhas ainda ocorrem.

As falhas de implantes em odontologia podem ser atribuídas essencialmente a três causas, nomeadamente, a falta de uma adequada integração implante-osso, infeção microbiana e processos de corrosão/tribocorrosão. A modificação das características de superfície do Ti tem sido uma estratégia atualmente adotada, na tentativa de superar essas complicações. Idealmente, o implante deveria ser capaz de exibir concomitantemente duas propriedades contraditórias: o aumento da adesão de células humanas e a inibição da adesão de microrganismos indesejáveis. Além disso, a superfície do implante deveria também ser adaptada com a capacidade de resistir às ações combinadas de corrosão e desgaste (tribocorrosão), às quais estão expostas no corpo humano. A nanotecnologia é uma área emergente na área da odontologia e, em particular, as superfícies de TiO_2 nanotubulares têm sido amplamente reconhecidas como potencial candidatas para melhorar o desempenho dos implantes dentários. No entanto, ainda está em falta a construção de sistemas nanotubulares eficazes, assentes numa abordagem integrada que considere, simultaneamente, as três principais causas de falha.

Esta tese objetiva a síntese de nanotubos (NTs) de TiO_2 multifuncionais em superfícies de Ti, adaptados para exibir simultaneamente resistência tribo-eletroquímica, atividade antibacteriana e adequada capacidade de osteointegração. Neste sentido, NTs de TiO_2 foram sintetizados via anodização e funcionalizados com elementos constituintes do osso, como cálcio, fósforo e zinco, através de uma nova metodologia baseada em processos de anodização via polarização inversa. Após bio-funcionalização, as superfícies de Ti decoradas com NTs de TiO_2 apresentaram um excelente comportamento tribo-eletroquímico, a capacidade de prejudicar a viabilidade bacteriana e a aptidão de melhorar a resposta de células humanas. Estas múltiplas funções foram atribuídas às características morfológicas, topográficas e físico-químicas dos NTs de TiO_2 bio-funcionalizados e às suas propriedades mecânicas e força de adesão ao Ti.

Os resultados deste trabalho mostram notavelmente que melhorias significativas foram alcançadas. Por intermédio de uma abordagem simples, as funcionalidades chave dos NTs de TiO_2 convencionais foram melhoradas, as quais são esperadas ter um impacto clínico relevante nas terapias de implantes dentários.

Table of Contents

List of Abbreviations

NH_4F	Ammonium Fluoride
Ag	Silver
AS	Artificial Saliva
Al_2O_3	Alumina
C	Carbon
Ca	Calcium
CaO	Calcium Oxide
$Ca_2(PO_4)_2$	Calcium Phosphate
$CaCO_3$	Calcium Carbonate
CLSM	Confocal Laser Scanning Microscopy
CO_2	Carbon Dioxide
COF	Coefficient of Friction
cp-Ti	commercially pure Titanium
DMSO	Dimethyl sulfoxide
ECM	Extracellular Matrix
EDS	Energy Dispersive X-Ray Spectroscopy
EG	Ethylene Glicol
F^-	Fluoride
FBS	Fetal Bovine Serum
Fe	Iron
FESEM	Field Emission Scanning Electron Microscopy
HA	Hydroxyapatite
hMSC	Human Mesenchymal Stem Cell
HDMS	Hexamethyldisilazane
HF	Hydrofluoric Acid
HNO_3	Nitric Acid
K	Potassium
Mg	Magnesium
MTT	3-(4,5-dimethyl-2-thiazolyl)-2,5-diphenyl-2H-tetrazolium bromide
NTs	Nanotubes
Na	Sodium
NaF	Sodium Fluoride

O	Oxygen
OCP	Open Circuit Potential
OH^-	Hydroxide
P	Phosphorous
PBS	Phosphate Buffered Saline
PO_4^{3-}	Phosphate
Pt	Platinum
R_a	Average Roughness
SCE	Saturated Calomel Electrode
SD	Standard Deviation
SEM	Scanning Electron Microscopy
SHE	Standard Hydrogen Electrode
Si	Silicon
TEM	Transmission Electron Microscopy
Ti	Titanium
TiO_2	Titanium Dioxide
Zn	Zinc
WCA	Water Contact Angle
XPS	X-Ray Photoelectron Spectroscopy

List of Figures

CHAPTER 4

CHAPTER 5

CHAPTER 6

CHAPTER 7

List of Tables

CHAPTER 1

General introduction

1.1. Motivation

Tooth loss due to decay, trauma or periodontal diseases is a common problem generally followed by several complications such as the reduction of masticatory function, fracture of the mandible due to loss of underlying bone, and also compromise the aesthetics of the person [1]. Dental implants have become an effective and long-term treatment option for replacing missing teeth by restoring the patient to normal function, speech, health and physical appearance [2].

More than 35 million people in the United States (U.S.) are missing all their teeth in one or both jaws. Statistics show that 69 % of adults aged between 35 – 44 have lost at least one permanent tooth, while 26 % of adults by age 74 have lost all of their permanent teeth [3, 4]. It is estimated that about 3 million Americans have dental implants, and another 500,000 implants are placed annually, according to American Academy of Implant Dentistry [3]. The growing concern over oral hygiene, an increasing life expectancy and the availability of advanced solutions with increased procedure efficiency are some of the key factors leading to the global boom in dental implant therapies [5]. It is expected that the total population in the U.S. will grow by almost 50 % between 2000 and 2050, and furthermore, by 2050 it is estimated that the elderly will make up 20.6 % of the total population [1]. Nowadays, there are numerous dental implant companies worldwide producing several hundreds of different implant systems [6]. The worldwide dental implant market has been rising with expectancy to be continuously growing over the next years with an annual growth rate of 10 %, from US$3.4 billion in 2011 to US$6.6 billion by 2018 [5].

Titanium (Ti) materials are known as the most biocompatible and have been successfully used for dental implants [2]. Notwithstanding the high success rates that Ti-based dental implant therapies have reached, a significant number of failures are still being reported. In accordance with different clinical studies covering follow up periods of 2 – 16 years, the overall survival rates of dental implants ranged between 76 % and 98.7 %, with clinically relevant implant failure rates found comprised 1 – 25 % [7-11]. As above mentioned, the number of dental implant procedures have been on the rise. Life expectancy is increasing and age alone should not be considered a limiting factor for dental implant therapy [9]. Therefore, if the current complications are not surpassed, a massive increase in dental implant failures is expected within the upcoming years. Hence, it is urgent the demand for strategies to overcome them.

Despite the good biocompatibility of Ti, its poor osteogenic ability and the lack of antimicrobial properties are the main factors leading to delayed osseointegration and complicated bacterial infections, which are known as two main causes of failures in implant dentistry [11, 12]. Functionalization of implant surfaces through the modification of features such as morphology, topography, chemistry, structure, and energy has been widely recognized

as a promising strategy to mitigate these issues [13, 14]. In accordance with the literature review reported by Ballo *et al.* [15], the currently available implant systems in the market mainly offer three different kinds of surfaces: 1) machined surfaces, 2) sandblasted and/or acid-etched surfaces, and 3) advanced functionalized surfaces with specific features such as morphology, topography and chemistry. In general, the main aim on surface modification has been to provide a faster, stronger and safer osseointegration. Dental implant companies have been focused on the development of bone-integrating surfaces, however, less attention has been devoted to microbial colonization issues.

Besides poor osseointegration and infection, there is a third main issue that has been gathering the attention of the scientific community, which is related to the degradation of dental implant materials through the simultaneous action of wear and corrosion (tribocorrosion). Dental implants may be exposed to tribocorrosive actions, either at the time of implantation or in a later stage after osseointegration. Generally, degradation of Ti implant material through wear-corrosion processes, is accompanied by the release of wear debris/corrosion products to the implant surroundings, which may induce to several biological complications that may end up in implant failure [16, 17]. Despite a wide range of surface modification strategies have been applied to improve Ti surface features, in general, the effect of those treatments on the tribocorrosion behavior of the material, is unknown.

More recently, nanostructured surfaces have demonstrated to play a crucial role in osseointegration by modulating cell functions. Wennernerg *et al.* [18] showed that different dental implant companies have already launched novel implant surfaces with modifications implemented at a nano-scale level to improve biofunctionality, emphasizing the promising prospects of nanotechnology in dentistry field. In particular, research studies have effectively shown that the decoration of Ti-based materials with TiO_2 NTs (NTs), is a simple way to promote cellular functions due to their unique morphological and physicochemical properties [19, 20]. Beyond the promising potential to induce osseointegration and reduce infection, nanotubular surfaces can behave as efficient drug delivery systems, and be tailored to incorporate multiple functionalities [21-23]. However, the construction of effective nanotubular systems based on an integrated and multidisciplinary approach that addresses, simultaneously, the three main problems related to dental implant failure, is still missing. To further emphasize this need, it has been reported that TiO_2 NTs display poor adhesion strength to the Ti substrate what might compromise their widespread applications [24], and lead researchers to query about the clinical application of several scientific works published in this field up to date. For all these reasons, the understanding of the degradation behavior of TiO_2 NTs by wear and corrosion processes is required. In fact, as a step forward, it is urgent the demand for new and innovative strategies to

develop new tribocorrosion resistant implant surfaces with potential to avoid infection, and simultaneously, promote osseointegration, towards a new generation of dental implants.

1.2. Objectives

The central **hypothesis** of this thesis was stated as **"Titanium surfaces decorated with TiO_2 nanotubes display multiple bio-functionalities: tribo-electrochemical resistance, antibacterial activity and osseointegration ability"**.

To validate this hypothesis, the main aim of this project was to synthesize bio-multifunctional TiO_2 NTs in Ti surfaces, tailored to simultaneously exhibit enhanced tribo-electrochemical resistance, antibacterial activity, and an adequate osseointegration ability. The main steps followed to achieve the main aim of this thesis, were set as objectives, which intended to address the validation process of the main hypothesis, through a systematic and multidisciplinary approach. Hereafter follows the specific objectives of the thesis:

1) Synthesize and characterize bone-inspired TiO_2 NTs in Ti surfaces, and further bio-functionalize them with calcium, phosphorous and zinc.

2) Study the bio-functionalization mechanisms of TiO_2 NTs and their influence on the characteristics of TiO_2 NTs/Ti interface.

3) Examine the potential of bio-functionalized nanotubular surfaces to induce osseointegration and avoid bacterial infection.

4) Investigate the electrochemical and tribo-electrochemical behaviors of conventional and bio-functionalized TiO_2 NTs, under single and multiple reciprocating sliding conditions in artificial saliva.

1.3. Structure of the thesis

This thesis is composed by a total of 9 chapters. For a better comprehension of its structure, henceforward is a brief overview explaining the main topics addressed in each section.

The main goal of the present chapter, **chapter 1**, is to introduce the key motivating factors that stimulated the execution of this project. The main hypothesis of this thesis is stated, as well as the description of the main aim and specific objectives.

The **chapter 2** is intended to review the state of the art of the main topics addressed along the main body of the thesis. Relevant information on Ti dental implants is provided, and important topics related to the three main causes of osseointegrated implant failures are reported, for a better understanding of the failure mechanisms. Basic definitions of some key concepts related to osseointegration, microbial infection, corrosion, and tribocorrosion are

described. Furthermore, a literature review on the surface modification strategies currently adopted for enhancing Ti implants performance is provided, with special focus on nanotechnological approaches. Finally, the state of the art regarding the synthesis of TiO_2 NTs by anodization is reviewed, focusing on their use for osseointegrated implant applications.

The main findings of this work are compiled in the form of five scientific papers, already published or submitted for publication in international journals, and these are reported from chapter 3 to chapter 7.

The **chapter 3** initiates the core of the thesis, and reports the first publication of this work. It concerns to the synthesis and characterization of bio-functionalized TiO_2 NTs with calcium (Ca) and phosphorous (P), by reverse polarization anodization. The first biocompatibility studies were described, and the novel methodology adopted for NTs functionalization shows up as a very promising way to improve cell functions, and minimize bio-degradation of Ca/P-based TiO_2 NTs by corrosion.

The study described in **chapter 4** was determinant for the understanding of the upcoming work. This paper focused on the bio-functionalization of TiO_2 NTs with zinc (Zn), together with Ca and P, through the previously reported methodology in chapter 3. For the first time, the thorough characterization of the interface between Ti substrate and TiO_2 NTs was carried out, aiming a better understanding of the mechanisms governing bio-functionalization.

In **chapter 5,** the potential of bio-functionalized TiO_2 NTs to induce osseointegration and avoid infection was investigated. To achieve this objective, the influence of nanotubular surface features on osteoblast-like and human mesenchymal stem cells (hMSCs) was investigated, as concerns metabolic activity and adhesion ability. Furthermore, the osteoblastic differentiation of hMSCs was examined as well as their angiogenesis capability. Finally, the adhesion and viability of *Staphylococcus aureus* on bio-functionalized NTs was also studied.

Based on the scientific knowledge acquired from chapter 4, the **chapter 6** aimed to investigate the tribo-electrochemical degradation behavior of TiO_2 NTs, before and after bio-functionalization, when submitted to reciprocating sliding tests in artificial saliva (AS). A first insight on the degradation mechanisms of NTs exposed to tribocorrosive actions was proposed for the first time.

The **chapter 7** is related to the last scientific work performed in this thesis and was undertaken based on the outcomes obtained in the preceding chapter. This paper aimed to investigate, for the first time, the tribo-electrochemical performance of bio-functionalized NTs submitted to multiple reciprocating sliding actions in AS, to better simulate the *in vivo* conditions. In this study, the adhesion strength and mechanical properties of the nanotubular films are studied, before and after bio-functionalization, and correlated with their tribo-

electrochemical responses.

In **chapter 8,** the main outcomes reported in the five previous chapters are summarized, and the interrelation existing between them is established along with a general discussion.

To finalize, in **chapter 9** some important questions that have arisen during the different stages of development of the thesis, and could not be answered based on the existing literature, are described. Furthermore, a few future studies are proposed for further improvement of this work, or either to provide new insights for exploring other topics.

References

[1] Babbush CA, Hahn JA, Krauser JT and Rosenlicht JL. Dental implants: the art and science, Elsevier Health Sciences, 2010.
[2] Oshida Y, Tuna EB, Aktören O and Gençay K. Dental implant systems, International journal of molecular sciences 11 (2010), 1580-1678.
[3] American Academy of Implant Dentistry. Facts and Figures on Dental Implants. Accessed on December 12, 2016. Available from: http://www.aaid.com/about/Press_Room/Dental_Implants_FAQ.html.
[4] Gaviria L, Salcido JP, Guda T and Ong JL. Current trends in dental implants, Journal of the Korean Association of Oral and Maxillofacial Surgeons 40 (2014), 50-60.
[5] Global boom in dental implants, British Dental Journal 214 (2013), 219.
[6] Jokstad A, Esposito M, Grusovin MG, Coulthard P, Worthington H and Pætursson BE. Implant Dentistry: a Technology Assessment, in: Jokstad A (Eds.), Osseointegration and Dental Implants, Wiley-Blackwell, 2009, pp. 3-26.
[7] Paquette DW, Brodala N and Williams RC. Risk factors for endosseous dental implant failure, Dental Clinics of North America 50 (2006), 361-374.
[8] Schwartz-Arad D, Laviv A and Levin L. Failure causes, timing, and cluster behavior: an 8-year study of dental implants, Implant dentistry 17 (2008), 200-207.
[9] Srinivasan M, Meyer S, Mombelli A and Müller F. Dental implants in the elderly population: a systematic review and meta-analysis, Clinical oral implants research 00 (2016), 1-11.
[10] Wittneben JG, Buser D, Salvi GE, Bürgin W, Hicklin S and Brägger U. Complication and Failure Rates with Implant-Supported Fixed Dental Prostheses and Single Crowns: A 10-Year Retrospective Study, Clinical implant dentistry and related research 16 (2014), 356-364.
[11] Porter JA and Von Fraunhofer JA. Success or failure of dental implants? A literature review with treatment considerations, General dentistry 53 (2004), 423-432.
[12] Kronström M, Svenson B, Hellman M and Persson GR. Early Implant Failures in Patients Treated with Brånemark System Titanium Dental Implants: A Retrospective Study, International Journal of Oral & Maxillofacial Implants 16 (2001), 201-207.
[13] Liu X, Chu PK and Ding C. Surface modification of titanium, titanium alloys, and related materials for biomedical applications, Materials Science and Engineering: R: Reports 47 (2004), 49-121.
[14] Neoh KG, Hu X, Zheng D and Kang ET. Balancing osteoblast functions and bacterial adhesion on functionalized titanium surfaces, Biomaterials 33 (2012), 2813-2822.
[15] Ballo AM, Omar O, Xia W and Palmquist A. Dental Implant Surfaces-Physicochemical Properties, Biological Performance, and Trends, in Implant Dentistry – A Rapidly Evolving Practice, Intech, 2011, pp. 19-56.
[16] Goodman SB. Wear particles, periprosthetic osteolysis and the immune system, Biomaterials 28 (2007), 5044-5048.
[17] Huber M, Reinisch G, Trettenhahn G, Zweymüller K and Lintner F. Presence of corrosion products and hypersensitivity-associated reactions in periprosthetic tissue after aseptic loosening of total hip replacements with metal bearing surfaces, Acta Biomaterialia 5 (2009), 172-180.
[18] Wennerberg A and Albrektsson T. On implant surfaces: a review of current knowledge and opinions, International Journal of Oral & Maxillofacial Implants 25 (2010), 63-74.
[19] Roy P, Berger S and Schmuki P. TiO2 nanotubes: synthesis and applications, Angewandte Chemie International Edition 50 (2011), 2904-2939.
[20] Brammer KS, Frandsen CJ and Jin S. TiO2 nanotubes for bone regeneration, Trends in biotechnology 30 (2012), 315-322.
[21] Gulati K, Maher S, Findlay DM and Losic D. Titania nanotubes for orchestrating osteogenesis at the bone–implant interface, Nanomedicine 11 (2016), 1847-1864.
[22] Gulati K, Aw MS and Losic D. Drug-eluting Ti wires with titania nanotube arrays for bone fixation and reduced bone infection, Nanoscale research letters 6 (2011), 571.

[23] Ercan B, Taylor E, Alpaslan E and Webster TJ. Diameter of titanium nanotubes influences anti-bacterial efficacy, Nanotechnology 22 (2011), 295102.
[24] Zhao M, Li J, Li Y, Wang J, Zuo Y, Jiang J and Wang H. Gradient Control of the Adhesive Force between Ti/TiO2 Nanotubular Arrays Fabricated by Anodization, Scientific Reports 4 (2014), 7178.

CHAPTER 2

State of the art

2.1. Titanium dental implants

A dental implant is an artificial tooth root surgically placed into the jaw bone beneath the gum to support a dental prosthesis like an artificial crown, where natural tooth is missing (Fig. 2.1) [1]. The abutment is an additional component placed between the dental implant and the crown, and is responsible for both structures connection [2]. Dental implants have become an effective and long-term treatment option for replacing tooth loss due to decay, trauma or periodontal diseases, by restoring the patient to normal function, speech, health, and aesthetics [1, 3]. The number of dental implant procedures have been on the rise and is expected to boost in the upcoming years due to increased life expectancy and the high success rates of dental implant therapies [2, 4].

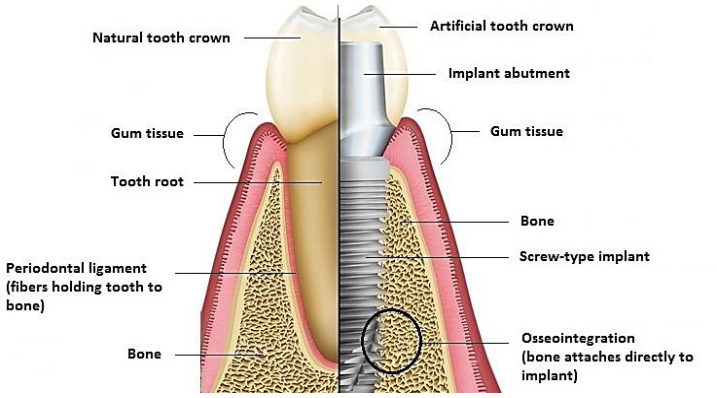

Fig. 2.1. Schematic representation of a natural tooth (at left) and an endosseous dental implant attached to bone (at right). Adapted from [5, 6].

Nowadays, endosseous dental implants shaped with a screw design are the most commonly used in dentistry, and are placed within a drilled space inside bone. The screw design is the one generally used due to the additional immediate fixation that a threaded implant may provide [4, 7, 8]. These implant systems became a revolutionary advancement in dentistry after the discovery of Per-Ingvar Brånemark (1929 - 2014), who is recognized as the father of modern implantology. He and his colleagues found that titanium (Ti) screws inserted into bone promoted the in-growth of bone tissue into the threads and crevices of Ti surfaces, without any sign of fibrous tissue formation [9], a process that they have finally named as “osseointegration” [10]. In the mid 1960´s, these implants were successfully implanted in humans by Brånemark [11], and the ones placed in his first 34-year-old patient, have lasted for more than 40 years [4]. The use of Ti for dental implants was approved by US Food and Drug Administration (FDA) in 1982 [4], and since then implant therapies have undergone a remarkable evolution.

In fact, commercially pure Ti and its alloys are the metallic materials most widely used for dental implants [2]. These are characterized by high strength and excellent ductility ensuring

high resistance to fracture, and therefore favoring long-term load bearing compared to ceramics and polymers [12]. In addition to low density (4.5 g/cm^3) and high mechanical resistance, Ti display superior biocompatibility and excellent corrosion resistance [2, 13, 14]. These properties are associated with the ability of Ti to spontaneously form a stable and adherent TiO_2 thin film in its surface, typically with less than 10 nm, named as passive film, when exposed to oxidizing conditions [2].

2.2. Understanding the failure mechanisms of titanium-based implants

2.2.1. Poor osseointegration and bone resorption

Brånemark originally described the concept of osseointegration as *"a direct structural and functional connection between ordered living bone and the surface of a load-carrying implant"* [15]. This is a process dependent on the establishment of a mechanically solid interface with complete fusion between dental implant surface and the surrounding bone tissue [16-20]. The clinical success of a dental implant is dependent on its early happening [20], however, poor osseointegration is one of the most frequent causes of failure in implant dentistry [21].

The human skeleton has a hierarchical structure including macroscale, microscale, sub-microscale, nanoscale, and sub-nanoscale, as illustrated in Fig. 2.2. This is mainly composed of two types of bone tissue, namely cortical or compact bone (3 – 12 % porosity), and trabecular or cancellous bone (50 – 90 % porosity) [22-24]. In general, bone tissue is constituted by osteoblasts, osteoclasts, and osteocytes. Moreover, mesenchymal stem cells (MSCs) are also found in bone and adjacent tissues and play a fundamental role in bone healing and remodeling [19, 25]. The extracellular matrix (ECM) of bone is composed by a hard matrix consisting of organic matter, mainly type-I collagen, and inorganic components composed mostly of calcium and phosphate that laid down in the form of hydroxyapatite (HA) crystals [26].

At the time of dental implant insertion into bone, it becomes fractured and a milieu of biologically active proteins chemoattractive towards MSCs trigger their migration to the site of injury [27]. Once at the area of damage, MSC adhesion is one of the initial critical stages to subsequent proliferation and differentiation into osteoblasts, which are the producers of bony tissue, and therefore this process plays a fundamental role in the establishment of a strong bone-implant contact [28-30]. The regenerative capacity of bone is also secured by the presence of osteoclasts, since these are bone resorbing cells that function in conjunction with osteoblasts. Osteocytes play also a key role by detecting strain/microfractures in bone, and transducing this information to osteoblasts and osteoclasts, to induce bone healing and remodeling [23].

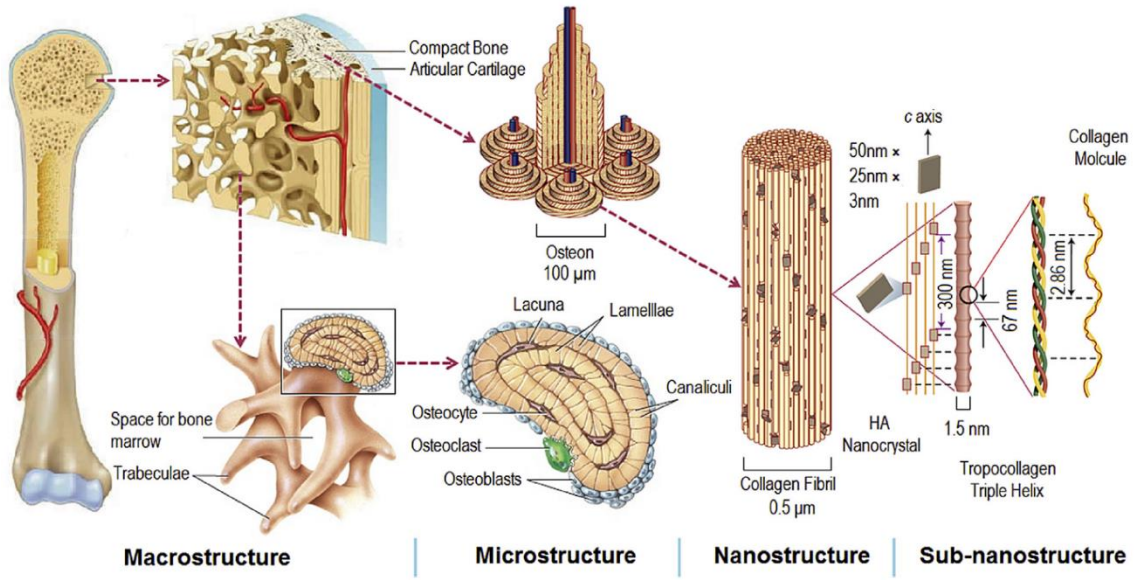

Fig. 2.2. Hierarchical structural organization of bone [31].

The series of events taking place on implant surface at the time of insertion are complex. Following the immediate binding of water molecules, proteins are adsorbed to implant surface within a few seconds to hours after implantation. These proteins come first from blood and tissue fluids and later from the cellular activity. The exact mixture of the initial adsorbed proteins and their conformation, orientation, and composition, are strongly controlled by implant surface features (e.g. topography, morphology and chemistry), and these proteins modulate the subsequent cellular adhesion process [17, 25, 32]. The initial cell adhesion is mediated through integrin receptors present in the cell membrane surface [33]. The bonding between integrins and surface protein functional groups controls the activation of intracellular signaling cascades controlling cell adhesion, cell shape, proliferation, migration, differentiation, and survival [34, 35]. Hence, the success of osseointegration is dependent on protein adsorption and the subsequent steps of cell adhesion, proliferation, differentiation, as well as on the production of ECM by osteoblasts and its mineralization.

Stress shielding is one of the main problems resulting from the mismatch of mechanical properties between bone and Ti-based implants [36]. This effect takes place because, when *in vivo* stress is applied, it is preferentially transferred to the material with high elastic modulus (i.e. Ti implant), thereby inhibiting normal stress transfer to the surrounding bone tissue. Therefore, bone becomes insufficiently loaded resulting in periprosthetic loss, which may induce to implant failure, as already reported in clinical practice [37, 38]. Implants made out of Ti are usually much stiffer than natural bones what may lead to stress shielding effect and subsequently to bone resorption, and ultimately end up in failure. Cortical bone has an elastic modulus ranging from 3 to 30 GPa, while trabecular bone has significantly lower modulus of 0.02

– 2 GPa. The most current implant materials have much higher modulus than those of bones, e.g. pure Ti and Ti-6Al-4V alloy have an elastic modulus of around 102 – 166 GPa [2, 31, 39]. Periprosthetic osteolysis (bone resorption) may be also induced by chronic inflammation of peri-implant tissues, thereby compromising osseointegration process. Inflammatory reactions are generally activated in response to fragments released from the implanted material, and these are mediated via activation of immune system cells, provoking peri-implant bone loss [2, 40].

To sum up, the clinical success of implantation procedure is largely dependent on the initial primary stability provided by the amount, quality, and distribution of bone tissue around the implant site. Some of the key factors compromising the success of bone-implant integration may be summarized as follows [2, 17, 41-47]: 1) implant material; 2) design characteristics; 3) state of the host bed (i.e. status of the bone concerned with its quantity and quality); 4) implant loading conditions; 5) implant surface features; 6) surgical technique; 7) microbial adhesion/colonization; 8) release of wear particles/metal ions from the metallic implant; and 9) mismatch of mechanical properties between bone and implant material.

2.2.2. Infection

The occurrence of infection after dental implant insertion is a response to microbial (e.g. bacterial or fungal) contamination and is generally accompanied by an inflammatory response [48, 49]. Bacterial colonization may take place at the time of the surgery, or even afterwards, from remote sources where bacteria are seeded at the vicinities of the implants [50, 51]. Micro-gaps and retentive areas at dental implant interfaces are known as the most susceptible for bacterial colonization [2]. In average, biomaterials-associated infections occur in approximately 0.5 – 6 % [47], and this is also one of the main causes of dental implants failure [17, 50, 52].

Immediately after implantation, the implant surface coated with ECM proteins like fibronectin, fibrinogen, albumin, vitronectin and collagen, function as a substrate for bacteria adhesion, subsequent colonization, and biofilm formation [2, 53]. Bacterial adhesion is the first and the most critical step leading to infection [2]. It is believed that the adhesion process is mediated by molecules present on bacteria membrane called as “adhesins”. However, far less is known about the ability and mechanisms of surface sensing by bacteria than eukaryotic cells [54]. After adhesion, bacterial colonization and biofilm formation on implant surface may induce to peri-implantitis [48], which is considered an inflammatory process that affects the function of surrounding tissues of an endosseous implant. Infected tissues with bacteria or their products, may trigger an immune response that can subsequently lead to periprosthetic resorption of bone, and ultimately to implant loosening [40, 55]. As a consequence of colonization and inflammation, bacterial cells and leucocytes may release lactic acid provoking

corrosion of Ti surfaces, which may further enhance the inflammatory response and the risk of failure [56, 57]. Dental implant-related infections are generally caused by *Staphylococcus aureus (S. aureus)*, which is present in oral cavity [53]. Furthermore, according to previous studies, infected and failing implants show greater proportions of periodontal pathogens such as *Peptostreptococcus micros (P. micros)* and *Prevotella intermedia (P. intermedia)* [7, 58].

In addition to all the above mentioned complications, bacterial adhesion and colonization on implant surface may also compromise the process of bone-implant integration. When an implant is simultaneously in contact with bacteria and bone cells it is expected that a competition takes place between them in adhesion to surface, a process known as "race of the surface" [17, 47]. Thus, it is believed that the poor osseointegration after implantation, can be also related to the presence of bacterial species at implant/bone interface.

2.2.3. Corrosion and tribocorrosion

Corrosion stands for the material degradation when placed in a hostile electrolytic environment, as a result of electrochemical (oxidation/reduction) processes taking place at its surface [59, 60]. This phenomenon is of high relevance for metallic implants inserted in the human body, since the electrolytic environment that they face might be highly corrosive [14].

Despite the high corrosion resistance of Ti-based materials, the protective passive film on their surface might not withstand the electrochemical attack when under particular aggressive *in vivo* conditions and be degraded, resulting in the liberation of metallic ions. The chemical environment of blood plasma is highly aggressive, essentially due to the presence of chloride ions (Cl^-) and their ability to induce localized corrosion [14, 61]. In particular, the presence of Cl^-, F^-, and H^+ in saliva, are the main responsible for dental implants corrosion [62]. Variations in the pH values are known to significantly influence the corrosion behavior of Ti. After surgery, the pH near the implant varies typically from 5.3 to 5.6, and afterwards, it is normally kept at 7. However, this value may varies from 3 – 9 due to several factors [14]. Beyond the environmental conditions, the corrosion behavior of an implanted material is also influenced by factors such as the material itself and its chemical composition, microstructure, and surface features [61, 63].

The negative effect of fluoride and acidic-fluoride salivary solutions on the corrosion behavior of Ti and its alloys was reported by Schiff *et al.* [64]. Accordingly, Souza *et al.* [62] also described the enhanced corrosion degradation of Ti-based materials in fluoridated medium as found in the oral cavity. Additionally, Barão *et al.* [13] observed that the pH level of artificial saliva (AS) influences the corrosion behavior of Ti and Ti-6Al-4V alloy, so that a lower pH accelerates the corrosion rate and kinetics. The electrochemical performance of Ti has been also

investigated in the presence of proteins once these constitute body fluids, and in particular saliva, at a concentration of around 200 – 500 mg/dl [65]. Takemoto *et al.* [65] reported that the corrosion of Ti was suppressed in a medium containing both fluoride and albumin, most likely due to the formation of a protective albumin film on Ti surface. The presence of bacterial colonies of *Streptococcus mutans (S. mutans)* on Ti surfaces was also found to negatively influence the corrosion resistance of Ti, as demonstrated by Souza *et al.* [57]. Beyond bacteria, the negative influence of human cells on the corrosion behavior of Ti was reported by Cadoshch *et al.* [66]. As a consequence of corrosion of Ti alloys, Khan *et al.* [63] observed that the hardness of the surface oxides was reduced. Therefore, one must be aware that the degradation of Ti-based materials takes place accompanied by the liberation, and possibly accumulation, of corrosion products in peri-implant tissues, which may consequently induce to detrimental biological complications and mitigate the survival of dental implants [13, 59]. Beyond loss of peri-implant tissue functionality, the degradation of a metallic implant by corrosion may result in its mass loss and mechanical integrity [2].

Dental implant surface interfaces with bone tissue during the moment of insertion, and during its whole lifetime through the formation of a mechanically solid interface between both (osseointegration). Thus, a tribological pair is established at implant surface/bone tissue interface. **Tribology** is the science and technology of contacting surfaces in relative motion, and deals with relevant aspects related to friction, wear, and lubrication [60]. Biological fluids are expected to be always part of dental implant surface/bone tissue interface, therefore degradation of dental implant material is expected to occur simultaneously by corrosion and wear mechanisms. **Tribocorrosion** is an emergent field that studies the influence of chemical, electrochemical and/or biological factors on the friction and wear behavior of materials surfaces in a tribological contact, and undergoing a relative movement [60].

Material degradation due to the simultaneous action of mechanical wear and electrochemical corrosion is a result of a complex synergism between both, as described in equation (1). This explains that the total material degradation by tribocorrosion (W) differs from the sum of material removed separately by corrosion (W_{corr}) or mechanical wear (W_{mechan}) [60, 67].

$$W = W_{corr} + W_{mechan} + W_{synerg} \quad (1)$$

W_{synerg} is the extra material degradation resulting from the synergism between wear and corrosion, and this is highly dependent on the characteristics of the contacting materials, the composition of the liquid environment, as well as on the properties of wear and corrosion

products. In fact, the presence of a corrosive environment may amplify the material degradation by wear, while wear may induce to an augmented corrosion rate [2].

Although in general the synergism results in an amplified material degradation, sometimes it also brings benefits to the system through the formation of self-lubricating and self-healing films [2, 68]. As a result of tribo-electrochemical interactions, thick and compact oxide layers can be formed in the contact area decreasing the overall degradation [2]. Furthermore, other mechanisms have been highlighted to explain the synergistic phenomenon in corrosion-wear processes: the release of wear debris that can speed up or reduce wear; the establishment of a galvanic coupling between worn/unworn areas, and also between both contacting materials; the accumulation of dissolved species in the environmental medium that may turn it more aggressive; the work-hardening of the materials in the contact area as a result of mechanical loading, which can alter the kinetics of electrochemical reactions [68].

Two body and three body wear mechanisms are common in tribocorrosion systems involving two surfaces under sliding contact. The first is related to an environment where debris do not exist, while the latter concerns to the presence of debris between both contacting surfaces [69, 70]. In the case of a passive metal such as Ti, the rubbing action may degrade the passive film (depassivation), and induce the formation of debris mainly consisting of hard oxides, which can act as third body particles in the tribocontact and induce abrasion on the bare material [71-73]. Alternatively, these particles may be ejected from the contact, be spread on the metallic material surface (first body), or form a transfer film on the inert counter material (second body) [70].

The degradation mechanisms of a material in a tribocorrosion system are complex and dependent on four main types of parameters:

- **Materials:** The properties of the materials involved in the tribological contact are of main importance, including the ones of the wear debris released from the contacting surfaces. The reactivity of the wear debris with the corrosive environment can modify the mechanical conditions prevailing in the contact. The hardness and ductility are known to influence significantly the wear resistance of a material, as well as the topography and chemical composition. For example, rougher topographies may induce to a concentration of load in the higher surface asperities and result in high contact pressures, which may subsequently induce the formation of third body particles and enhance material degradation. Furthermore, the mechanical properties of the oxide films formed during tribo-electrochemical interactions may also be determining in materials degradation. Naturally formed passive films also play a strong influence on the tribocorrosion performance of metallic materials [2, 69, 70, 74].
- **Mechanical/operational:** The rate of the tribo-electrochemical reactions is dependent on

mechanical aspects such as the applied contact pressure and the frequency of load application. Furthermore, the contact geometry and type of contact like sliding, fretting, rolling or impact, are also of main relevance for a given metal-environment pair. Sliding and fretting contacts are the most common configurations taking place in osseointegrated implants [69, 75].

- **Electrochemical:** The electrochemical properties also determine the tribocorrosion performance of metallic materials. The applied potential, ohmic resistance, active dissolution rate, passive film growth, and repassivation kinetics of the material, play a fundamental role [69]. The kinetics of repassivation gives important information on the electrochemical characteristics of the contact area, e.g. the formation of oxide films during mechanical solicitations, and provides information for a better understanding on the tribocorrosion mechanisms governing material degradation.
- **Solution/Environmental:** the properties of the electrolyte in contact with the material surface such as the viscosity, conductivity, pH, composition, and temperature, are also of paramount importance. Acidic solutions and electrolytes containing fluoride ions are known to significantly influence the tribocorrosion behavior of Ti-based materials, as demonstrated in previous works [13, 45, 56, 62, 76]. Studies have also shown that the existence of proteins, bone cells, and bacterial biofilms, in the environnement in contact with Ti-based surfaces, also play a major role on their tribocorrosion performances [45, 71, 77-81].

Endosseous Ti dental implants can be subjected to tribocorrosive conditions at the moment of implantation, through sliding wear between the implant surface and the surrounding bone tissue, in the presence of corrosive biological fluids. On the other hand, once osseointegration have successfully been achieved, small amplitude oscillatory movements of the order of micrometers (fretting) may take place at implant/bone interface, through transmission of mastication loads [45, 69, 75]. This become an issue of high clinical relevance once Ti-based materials display poor fretting and sliding wear resistance, ascribed to the poor mechanical integrity of the TiO_2 surface passive film, or to the plastic deformation of Ti surface and subsurface layers [45, 71, 82]. Therefore, metallic ions and solid wear debris may be released as a consequence of material degradation by tribocorrosion, inducing to peri-implant inflammatory reactions and aseptic osteolysis [82-84]. Olmedo *et al.* [85] reported 2 clinical cases of reactive lesions of tissues surrounding dental implants, where metal-like particles were histologically observed and attributed to a corrosion process. As reviewed by Cobelli *et al.* [84], the inflammatory response generated by wear particles is mediated by the resident or infiltrating osteoclasts, macrophages, and dendritic cells in the peri-implant tissue, as illustrated in Fig. 2.3. While small wear particles (< 10 µm) are phagocytosed, larger debris (> 20 µm) provoke fusion

of macrophages and giant cell formation. Activated cells release inflammatory cytokines and chemokines to recruit other cells, which contribute to further inflammation and increased periprosthetic osteolysis. The release of wear debris may also compromise bone-forming cell functions. For example, Ribeiro *et al.* [86] observed modification on human osteoblast behavior after internalization of TiO_2 nanoparticles. Furthermore, Wang *et al.* [87] reported that the exposure of wear debris to hMSCs reduced their viability and differentiation into functional osteoblasts.

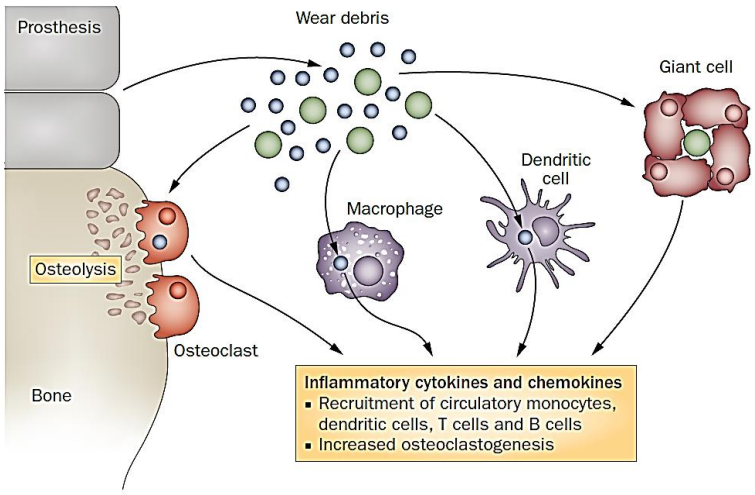

Fig. 2.3. Schematic illustration of periprosthetic inflammation and aseptic osteolysis [84].

Degradation of dental implant materials by corrosion and tribocorrosion processes is feasible, and this is an issue of high clinical significance. One must be expected that tribocorrosion processes taking place at the moment of implantation, may seriously compromise the osseointegration process. Degradation and inflammatory processes may also contribute to the loss of mechanical integrity, influencing the magnitude of micromovements at implant/bone interface, therefore compromising the long-term health of peri-implant tissues as well as the biomechanical stability of the implant [2, 88, 89]. Wear debris resulting from tribocorrosion, besides trigger locally aggressive biological reactions at peri-implant tissues, can go into bloodstream and subsequently be disseminated for human organs, leading to adverse effects at a systemic level, and therefore presenting serious risks for human health [90].

2.3. Modification of titanium implant surfaces from micron- to nano-scale: towards improved dental implant therapies

From the first implants placed by Per-Ingvar Brånemark, dental implant surfaces have undergone an enormous evolution. The demand for new and innovative strategies aiming the

synthesis of efficient implant surfaces has attracted the attention of worldwide researchers, both from academia and industry, as a strategy to mitigate failure of dental implant systems.

2.3.1. Improvement of biological responses

The modification of Ti surface features through the creation of micron- to nano-textured surfaces with physicochemical features more compatible with human cells has been adopted as a strategy to improve biological responses. Several surfaces modification techniques have been applied to modify the morphological and topographical surface features, namely sandblasting, acid etching, plasma spraying, and anodization [20, 91, 92].

Implant surface topography is known to influence cell adhesion, migration, cytoskeleton organization, proliferation, differentiation, and ECM protein expression [92-94]. Anselme and Bigerelle [91] demonstrated that the adhesion strength of osteoblasts was enhanced on rough surfaces obtained by electro-erosion, sandblasting, or acid etching, as compared to smooth Ti surfaces after polishing and machining. The authors emphasized that human osteoblasts are more sensitive to the organization and morphology of the roughness than to its amplitude. On the other hand, Jayaraman *et al.* [92] observed an improved adhesion of osteoblast-like cells on Ti-grooved in relation to sandblasted and acid-etched Ti surfaces. An experimental study with Ti microimplants in humans demonstrated the improved bone-implant contact of TiO_2 blasted Ti implants, when compared to machined [95]. TiOblast and SLA implants are good examples of commercially available rough implant surfaces [20, 96].

Various attempts have been made for the development of surfaces mimicking the hierarchical structure of bone, which varies from micro- to nano-scale structures [54]. Zhao *et al.* [97, 98] observed that the conjunction of micro and nano-topographies on Ti surfaces had a synergistic role on multiple cell functions, through the enhancement of multiple osteoblast functionalities, as compared to micro-textured surfaces. Furthermore, micro/nano-textured surfaces showed enhanced ability to induce MSC osteogenic differentiation. The benefit of a hierarchical micro/nano-topography on promoting MSC adhesion was also demonstrated by Zhang et al [99]. This approach has been already implemented in clinical available implants since, as reported by Wennernerg *et al.* [96], different companies have already introduced remarkable nano-topographical cues in well-known implants such as TiOblast, SLA, and Nanotite implants, aiming to induce enhanced osseointegration.

At the micron- and nano-scales hierarchical structures of bone, aggregated type-I collagen molecules and HA crystals form the reinforced collagen fibrils, the universal building elements of both cortical and trabecular bones, providing them flexibility, strength, and toughness. Type-I collagen is a triple helix molecule with ~ 1.5 nm diameter and ~ 300 nm length, and plate-

shaped HA crystals have 50 x 25 nm in size and 1.5 – 4 nm thick (Fig. 2.2) [31]. Therefore, bone is considered a nanostructured material and efforts have been made to synthesize bone-inspired nano-topographies to achieve enhanced cell responses [100].

As referred above, proteins from bio-fluids firstly adsorbed on implant surfaces, mediates the subsequent cell adhesion via integrin receptors present in cell membrane surface [33]. During cell adhesion process, integrin receptors cluster together when their spacing is smaller than 70 nm, and recruit specific cytoplasmic proteins to form a complex known as a focal contact [54, 101]. Focal adhesion complexes are mobile nanometer scale building blocks (size of integrin: 8 – 12 nm) and their formation and function can be influenced by surface topography and chemistry on that scale [54, 101]. Cell adhesion is mediated via focal contact complexes by activation of several intracellular signaling cascades controlling cell adhesion, cytoskeleton organization, proliferation, migration, differentiation, survival signaling, and energy metabolism [34]. Cell filopodia are actin-rich plasma-membrane protrusions that play a fundamental role in cell migration, and can sense nano-topographical features as high as 8 nm [101, 102].

Based on the above information, a strong correlation exists between the sizes of ECM bone components and cellular sensing organelles, which interplay with each other to modulate cell functions. In the last decades, great efforts have been devoted for the development of new nanostructured Ti-based surfaces, and on the study of their effect on cellular responses. It has been widely reported that nanostructured Ti surfaces positively modulate cell responses *in vitro* and *in vivo*, highlighting their enormous potential to improve osseointegration [103-110].

Besides topography, the modification of the chemical properties of implant surfaces has demonstrated potential to further improve implant anchorage in bone by rendering the implant surface bioactivity [20]. The coating of Ti-based implant surfaces with HA or calcium phosphates is a common method to achieve enhanced bone tissue ingrowth and vascularization by mimicking the mineral composition of natural bone [100, 111]. Nanostructured calcium-phosphorous nanomaterials have also recently emerged as promising biomimetic and bioactive biomaterials capable of directing cell behavior and cell fate, and enhancing tissue formation *in vivo* [112]. The incorporation of other inorganic elements such as strontium (Sr), silicon (Si), zinc (Zn), and silver (Ag), have been also widely adopted to modulate cell functionalities [111]. In particular, the inclusion of Zn on Ti surfaces, separately or together with calcium phosphate, has been reported to improve MSCs and osteoblast functions [113-115], and simultaneously, display antibacterial activity [116, 117].

2.3.2. Impairment of microbial functions

The modification of Ti surface features have been implemented by several approaches to

acquire antimicrobial properties and minimize implant-related infections. As observed for eukaryotic cells, the modification of the morphological, topographical and physicochemical features of Ti surfaces also influences bacterial functions [118]. Compared to smooth surfaces, micron-roughened substrates have shown potential to enhance the adhesion and growth of infectious bacteria [119, 120]. Furthermore, the inclusion of antimicrobial peptides on Ti surfaces, as well as the incorporation of inorganic bioactive elements such as Ag and Zn, have evinced excellent antibacterial activity against several pathogens involved in dental and orthopedic implants failure [121-124].

Nanotechnology has offered an opportunity for the discovery of antimicrobial compounds as well the use of nano-functionalization surface techniques to create new antimicrobial implant surfaces [48, 50, 125-129]. Surface functionalization of biomaterials with antibacterial properties has been achieved by coating, impregnation, or embedding nanomaterials [125, 130, 131]. Lellouche *et al.* [125] demonstrated the antibiofilm activity of surfaces coated with magnesium fluoride nanoparticles. Furthermore, Cao *et al.* [50] concluded that silver nanoparticles embedded in Ti were highly effective in inhibiting the growth of both *S. aureus* and *Escherichia coli*, while enhancing the proliferation of osteoblast-like cells. In addition, Puckett *et al.* [132] showed that nanorough Ti surfaces produced by electron beam evaporation, decreased the adherence of different species of bacteria, namely *S. aureus*, *S. epidermidis,* and *Pseudomonas aeruginosa* (*P. aeruginosa),* when compared to conventional smooth Ti. Nanostructured surfaces that display opposing behaviors for human cells and bacteria are of particular interest [133, 134], as they demonstrate that the material could be designed to enhance osteoblast functions while decrease bacteria adhesion.

2.3.3. Enhancement of tribocorrosion resistance

As previously described, the tribocorrosion behavior of metallic biomaterials is dependent on several parameters. The formation of Ti oxides by anodization in electrolytes composed of bioactive elements, has been reported as a very promising method either to enhance cell functionalities or to improve the tribocorrosion performance of Ti surfaces [135-140]. Alves *et al.* [136] fabricated porous anodic oxide surfaces by anodization of Ti in an electrolyte composed of calcium acetate (CA) and β-glycerophosphate (β-GP), and concluded that the concentration of CA influenced the crystallographic structure of the resulting oxide. The authors found that the oxides with higher Ca/P and rutile/anatase ratios displayed an improved tribocorrosion behavior, and hypothesized that the increased hardness of these films was the main factor that influenced the degradation behavior of the materials. Following, Oliveira *et al.* [135] also synthesized porous oxide films by anodization of Ti surfaces in an electrolyte containing CA, β-

GP and magnesium acetate (MA) for further incorporation of magnesium (Mg) in the structure of the films, along with Ca and P. The authors found out that the addition of Mg supported the formation of rutile which improved the tribocorrosion properties of the surfaces. The outcomes of the studies performed by Marques *et al.* [140] are in good agreement with the previously reported results, as concerns the relation established between CA concentration and the formation of harder oxides, due to the higher rutile/anatase ratio achieved after anodization. Interestingly, the authors also observed an improvement on the tribocorrosion resistance of the harder anodic oxide films enriched with Ca and P, and additionally, they observed that the inclusion of silver (Ag) nanoparticles in the anodizing electrolyte induced to further improvements. The anodic oxide films containing Ca and P and enriched with Ag nanoparticles, beyond have displayed an improved tribocorrosion behavior, also enhanced human MSCs functions.

As concerns the tribocorrosion behavior of functionalized Ti surfaces at a nano-scale level, the studies are still very limited in literature. In 2010, Faghihi *et al.* [141] studied the tribocorrosion behavior of nanostructured Ti surfaces processed by high-pressure torsion and discovered that nanostructured samples showed superior performance under the action of both wear and corrosion, when compared to coarse-grained samples.

Based on the above mentioned studies, the wear-corrosion behavior of Ti was found dependent on the surface characteristics of Ti, which were influenced by the processing conditions. Anodization appears as a very promising approach for the development of tribocorrosion resistant oxide films with variable chemical features, which may be tailored to achieve improved biological performances. However, despite the wide range of surface modification strategies already implemented to improve the performance of Ti implants, the research on the effect of those treatments on their simultaneous degradation by corrosion and wear, is still lacking.

2.4. Decoration of titanium implant surfaces with TiO_2 nanotubes by anodization: impact on osseointegration, infection and long-term stability

2.4.1. Synthesis of TiO_2 nanotubes by anodization

Among various nanostructured materials, the decoration of Ti-based surfaces with well-aligned TiO_2 nanotubes (NTs) has received special attention. The unique morphological and physicochemical properties of TiO_2 nanotubular structures, make them potential candidates for several applications such as photocatalysis, sensors, solar cells, self-cleaning materials,

biomedical implants, and even cancer thermotherapy [142-144]. However, the present work is focused on TiO_2 NTs for biomedical applications, as respects dental and orthopedic implants.

Several methods exist for TiO_2 NTs synthesis [142, 145], however, anodization has emerged as one of the most effective due to its versatility, easy operation, and commercial feasibility [142, 146]. This technique is already widely used in industry to fabricate large-scale low-cost protective oxide coatings [146]. Briefly, anodization is an electrochemical process that relies on the application of a predetermined current or voltage between Ti material (anode) and an unreactive/inert material (cathode, e.g. platinum and graphite), previously immersed in a conductive solution. When polarized, a flux of electrons is generated between both materials, and the oxide film is grown in Ti surface through oxidation reactions, along with field-driven ion diffusion [100, 143, 146]. The anodization setup for synthesis of TiO_2 NTs is illustrated in Fig. 2.4a. This process is commonly carried out by applying a constant voltage of 1 – 30 V in aqueous electrolytes, or 5 – 150 V in non-aqueous electrolytes, containing 0.1 – 1 wt.% fluoride ions (F^-) [143]. The mechanisms of TiO_2 NTs growth by anodization in a fluoride containing electrolyte, have been conventionally accepted as a result of a field assisted dissolution process consisting of three main stages: 1) the oxidation of Ti metal involving Ti^{4+} ions formation; 2) the growth of an oxide film in Ti surface, through recombination of Ti^{4+} and O^{2-} ions (provided by deprotonation of H_2O or OH^-) moving under the action of the electric field; 3) the local chemical dissolution of the growing oxide by fluoride ions and subsequently pore nucleation, with formation of water-soluble $[TiF_6]^{2-}$ species [100, 142, 143, 146-148]. This process assumes that nanotube growth takes place through the balance established between the formation of the oxide film and its enhanced dissolution at the base of the pores/tubes, where the electric field is stronger, as schematically depicted in Fig. 2.4b [147].

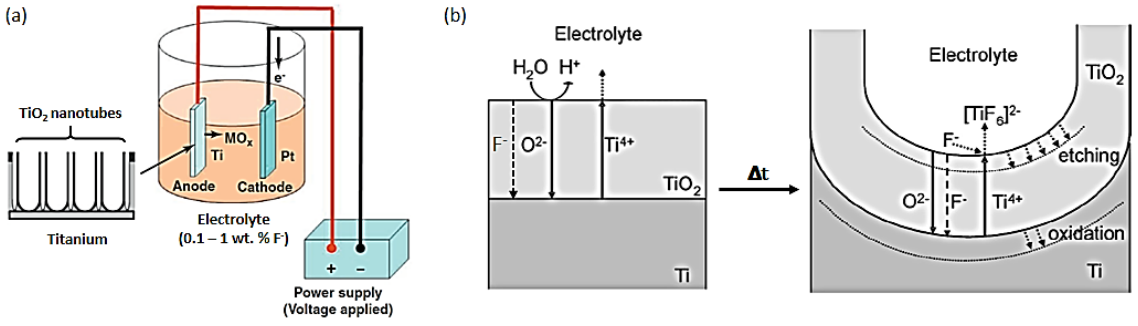

Fig. 2.4. (a) Anodization setup for synthesis of TiO_2 NTs in a fluoride containing electrolyte. In (b) the mechanisms underlying nanotube growth evolution by anodization are shown. Adapted from [143, 148, 149].

The synthesis of the first organized porous anodic oxides in Ti were reported by Zwilling and co-workers in 1999. The outcomes of their work showed that nano-porosity was formed by

anodization of Ti and Ti-6Al-4V in chromic acid solution with hydrofluoric acid, whose distribution was dependent on processing conditions [150, 151]. Two-year after, in 2001, Gong *et al.* [152] fabricated well aligned and organized oxide NTs by anodization of Ti in an aqueous solution containing hydrofluoric acid. Since then, several approaches using fluorinated acidic electrolytes corroborated these findings [153, 154], and significant improvements have been achieved in this field.

The resulting features of TiO_2 NTs, namely morphology, chemistry, and length, may vary over a wide range according to the processing anodization parameters, such as the applied voltage, duration, and electrolyte composition. As reviewed by Roy *et al.* [143], anodization time and etching rate define tube length, while nanotube diameter is controlled linearly by the applied voltage. In general, thinner films are produced in acidic electrolytes as compared to neutral, mostly ascribed to the faster dissolution rate of the oxide in a lower pH solution [142]. Accordingly, Macak *et al.* [155] reported that by using a neutral NaF-based electrolyte, significantly thicker porous layers were obtained than in acidic solution. Notwithstanding, Beranek *et al.* [154] observed that the self-ordering level of nanotubular structures produced in H_2SO_4/HF electrolyte, was favored by longer anodization duration. Furthermore, Shankar *et al.* [156] showed that by using non-aqueous organic electrolytes containing fluoride ions, such as ethylene glycol, highly ordered TiO_2 nanotube arrays up to 220 μm in length were grown, and depending on the anodization voltage, the inner pore diameters ranged from 20 to 150 nm. A remarkable advance has been reported by Han *et al.* [157], who fabricated TiO_2 nanotube arrays with enhanced self-ordering level by multistep anodic oxidation of Ti in an organic electrolyte containing fluoride ions, and this methodology has been widely adopted for self-templating anodization processes [158-160].

2.4.2. TiO_2 nanotubes: influence on cellular and microbial functions

Nanotubular structures made out of TiO_2 have demonstrated unique morphological and physicochemical features with potential to stimulate implant-bone integration, either *in vitro* or *in vivo,* by modulating osteoblasts and hMSCs functions such as adhesion, proliferation, and differentiation [161-163], when compared to conventional Ti surfaces. TiO_2 is a well-known biocompatible material, and when organized in highly-ordered nanotubular structures present high hydrophilicity, which is known to benefit initial protein adsorption and subsequent cell-material interactions [164, 165]. The high negative surface charge density at the sharp walls of TiO_2 NTs are believed to promote adsorption of ECM proteins and integrin-mediated adsorption of cells to these regions [33]. Beyond improved cell functionalities have been reported for the first generation of NTs fabricated in fluorinated aqueous electrolytes [105, 166], the most recent

studies have adopted to fabricate NTs in organic systems. In particular, anodization in ethylene glycol electrolytes containing ammonium fluoride have been widely reported, due to the production of longer nanotubes with improved self-ordering level, when compared to aqueous solutions [143, 167]. Generally, the structure of TiO_2 NTs grown by conventional anodization is amorphous, however, it can become crystalline (e.g. anatase or a mixture of anatase and rutile) by thermal treatments at 280 – 800 °C, for 2 – 3 h. Although this method is currently used to achieve enhanced surface bio-functionality, it is not standardized yet [143, 168].

The influence of nanotube diameter on cellular responses has been demonstrated by several studies, however, controversial results are found in literature in regards the optimal size range to improve cell functions. In this context, Park *et al.* [35] observed that TiO_2 nanotube diameters ranging from 15 – 100 nm, significantly influenced MSCs adhesion, growth, and differentiation. Diameters of 15 – 30 nm were found the most effective for accelerated integrin clustering/focal adhesion complex formation, which is known to control cell functions. On the other hand, diameters larger than 50 nm impaired cell functions and induced cell apoptosis, while NTs of 100 nm diameter almost completely prevented integrin clustering. As proposed by the authors, the mechanisms governing nanotube diameter-dependent cellular responses are illustrated in Fig. 2.5. Similar results were reported by Bauer *et al.* [169] for MSCs adhered on ZrO_2 and TiO_2 NTs, emphasizing that focal adhesion complex formation is being modulated by nanotube morphology, regardless of the material. Therefore, nanotube diameters modulate the formation of focal adhesion complexes, and subsequently cell functions [149]. It is believed that this phenomenon is related with the higher number of protein aggregates formed in NTs of 15 – 30 nm diameter, when compared to NTs of 70 – 100 nm [170].

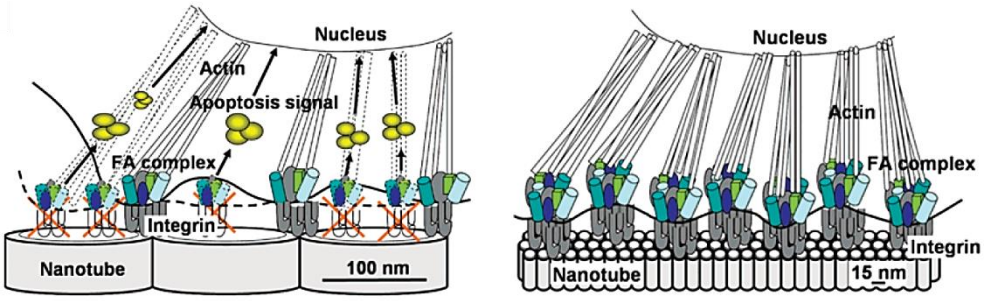

Fig. 2.5. Hypothetical mechanisms for integrin assembly into focal contacts in nanotubes with 100 nm (left side) and 15 nm diameter (right side) [35].

Controversially to Park's and Bauer's findings, Oh *et al.* [170] observed a noticeable change in hMSCs differentiation in larger nanotubes. According to Oh's findings, NTs of 70 – 100 nm diameter elicited a dramatic stem cell elongation, which induced cytoskeleton stress and selective differentiation towards osteoblast phenotype. Similar results were described by Brammer *et al.* [171] for osteoblasts, with NTs of 30 nm diameter promoting the highest degree

of adhesion, while 70 – 100 nm diameters inducing extremely elongated cell morphology and significantly higher alkaline phosphatase (ALP) synthesis. In a separate study, Zhao *et al.* [98] reported that TiO_2 NTs of 80 nm diameter displayed the best performance, by promoting simultaneously MSC proliferation and osteogenic differentiation. The authors explained that this behavior was related with the increased cytoskeletal stress of MSCs. The high cytoskeleton stress of cells adhered on larger NTs may modulate mechanotransduction events, triggering intracellular signaling pathways, and subsequently controlling differentiation process [98, 149, 172]. Furthermore, Wang *et al.* [162] reported a significant increase in bone-implant contact and gene expression levels in bone attached to TiO_2 NTs, especially those with 70 nm diameter.

TiO_2 NTs have demonstrated ability, not only to control bone-forming cell functions, but also other types of cells that might have a major role in osseointegration process such as, osteoclasts, endothelial cells, and immune system cells (e.g. macrophages) [173, 174]. Rajyalakshmi *et al.* [175] observed a significantly reduced density of macrophages adhered on TiO_2 NTs of 60 – 70 nm diameter, when compared to conventional Ti surfaces, emphasizing their potential for osseointegrated implants applications.

An additional exciting feature of TiO_2 NTs is their ability to prevent microbial adhesion and colonization, and therefore to avoid implant-related infections, which may end up in failure [176-178]. As demonstrated by Ercan *et al.* [178], nanotube diameter is also a crucial factor for determining the antibacterial efficacy of nanotubular systems. The authors studied the antibacterial ability of TiO_2 NTs with controlled diameters of 20, 40, 60, and 80 nm, followed by heat treatment or not, against *S. epidermidis* and *S. aureus.* As the main outcome of this study, heat treated TiO_2 NTs of 80 nm diameter produced the most robust antimicrobial effect. As concluded, Ti surface features including chemistry, crystallinity, nanotube size, and hydrophilicity, significantly influenced the responses of both pathogens. The higher antibacterial activity of crystalline NTs was also demonstrated by Li *et al.* [177], who also concluded that the antibacterial activity of the NTs was independent on their lengths. The effective antibacterial activity of anatase/rutile TiO_2 NTs exposed to ultraviolet light irradiation was also observed by Shi *et al.* [176], and the mechanism behind was ascribed to oxidative stress induced by TiO_2 NTs. Interestingly, Beltrán-Partida *et al.* [179] described that cross sectioning of fungal cells adhered on TiO_2 NTs revealed less nano-contacts with inferior spread, when compared to control metallic surface, suggesting a down-regulation of microbial adhesion ability on nanostructured morphology.

2.4.3. Electrochemical stability of TiO_2 nanotubes

The electrochemical degradation of TiO_2 NTs in electrolytes mimicking the existing body

fluids have been widely reported. In general, TiO_2 NTs display an improved corrosion resistance as compared to Ti-based surfaces [180, 181]. Demestrescu *et al.* [182] studied the electrochemical behavior of TiO_2 NTs in Fusayama's artificial saliva. The authors concluded that very low corrosion current densities were recorded for TiO_2 NTs due to a strong passive oxide film formation. Electrochemical impedance spectroscopy (EIS) results indicated that TiO_2 NTs consisted of a bi-layered oxide made up of an inner barrier layer associated to high impedance and responsible for corrosion protection, and a porous outer layer (NTs) of lower impedance. Similar results were reported by Yu *et al.* [183], who studied the *in vitro* corrosion behavior of TiO_2 NTs immersed in phosphate buffered saline (PBS) and Dulbecco's minimum essential medium supplemented with 10 % of fetal calf serum (D-FCS). The results showed that the NTs displayed a lower active electrochemical state, higher corrosion resistance of the inner barrier layer, and lower passive current in both test solutions, when compared to smooth Ti. Additionally, the corrosion resistance of TiO_2 NTs in D-FCS was higher than in PBS due to surface protein adsorption, which formed aggregates in NTs of 30 nm diameter.

2.4.4. Functionalization of TiO_2 nanotubes

Beyond the good biocompatibility, improved cell functions, and antibacterial activity provided by conventional TiO_2 NTs, there is still room for improvements. These structures have increasingly captured the attention of researchers, and recent advances have been achieved as regards their multi-functionalization. A special attention is being devoted to the construction of systems tailored for enhancing osteogenesis at the implant-bone interface, to minimize the risk of infection, or even both simultaneously.

Bio-functionalization of TiO_2 NTs may be easily achieved by conventional techniques already used for surface modification of biomaterials. An additional particularity of TiO_2 NTs is their potential to behave as a platform for drug-eluting and local delivery, due to their excellent controllable dimensions, surfaces chemistry and large surface-to-volume ratio. Easily by changing the nanotube diameter, wall thickness, and length, the kinetics of specific drugs can be adjustable to achieve stable and controlled release [184-186]. An interesting approach for the construction of a sustained drug delivery system was reported by Hu *et al.* [187]. After synthesis of TiO_2 NTs of 110 nm diameter and their loading with bone morphogenetic protein 2 (BMP-2), the authors covered the system with multilayered coatings of gelatin/chitosan, which effectively controlled BMP-2 delivery and induced MSC differentiation into osteoblasts, as schematically illustrated in Fig. 2.6. Recently, a similar approach was reported by Lai *et al.* [188], who fabricated TiO_2 NTs filled with simvastatin and coated with gelatin/chitosan multilayers. The bio-functionalized NTs displayed controlled drug release and also a great potential for

improving osteoblast differentiation, while at the same time inhibiting the activation of osteoclasts.

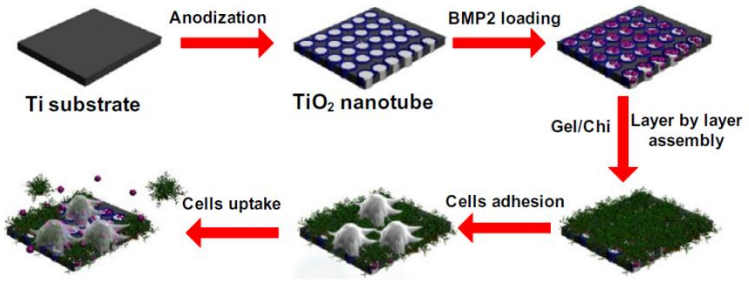

Fig. 2.6. Schematic illustration of the fabrication of TiO_2 NTs loaded with BMP-2 and cellular responses [187].

The modification of TiO_2 nanotube features by coating them with hydroxyapatite (HA) has been employed to upregulate cell functions and further achieve enhanced osseointegration, due to its biocompatibility and similarity to the chemical composition of the bone tissue [168]. Chen *et al.* [189] introduced nanoscale calcium phosphate (CaP) into well-ordered TiO_2 NTs by ultrasonification-assisted electrochemical deposition. The CaP-NTs induced to the adsorption of a greater amount of protein, and when immersed in PBS, displayed enhanced bioactivity as observed by the increased hydroxyapatite formation. Additionally, CaP-NTs enhanced cell adhesion, proliferation, and differentiation, owing the combined effects of nanoscale topography, morphology, chemical composition, and hydrophilicity. A step forward, aiming to address, simultaneously, the lack of tissue integration and infection problems, Huo *et al.* [190] incorporated Zn in TiO_2 NTs by hydrothermal treatment in Zn containing solutions. The authors observed good intrinsic antibacterial activity against *S. aureus*, and simultaneously, an excellent osteogenesis inducing ability through activation of specific intracellular signaling pathways involved in cell differentiation. Furthermore, Cheng *et al.* [191] loaded TiO_2 NTs with Sr and Ag by hydrothermal treatment to provide them combined osteoconductive and antimicrobial properties. The release of Ag provided antibacterial activity without citotoxicity, while the inclusion of Sr enhanced the initial cell adhesion, migration, and proliferation of pre-osteoblast MC3T3-E1 cells. Additionally, the release of Sr also induced to up-regulation of osteogenesis-related genes expression and mineralization.

In fact, TiO_2 NTs may behave as effective bio-selective surfaces by incorporation of different elements in its structure, hence inhibiting bacterial functions and concomitantly promoting osteoblast responses. In accordance with the available literature, the approaches for tailoring TiO_2 NTs with multiple functionalities are plentiful: NTs loading with growth factors like BMP-2 [192, 193]; functional peptide coatings as RGD peptide [121, 194, 195]; vitamins like vitamin D [196]; antibiotics such as gentamicin and vancomycin [129, 197, 198]; anti-

inflammatory drugs like sodium naproxen, quercetin and indomethacin [52, 199, 200]; incorporation of nanoparticles as gold and silver [201-204]; implantation of bioactive inorganic elements such as calcium, phosphorous, zinc, silver, palladium, strontium and silicon [12, 189, 205-212].

2.4.5. Mechanical properties, degradation mechanisms and adhesion strength of TiO_2 nanotubes

The growth of TiO_2 NTs in Ti surfaces has demonstrated potential to reduce stress shielding effect, in accordance with their mechanical properties determined by nanoindentation. An elastic modulus of 4 – 43 GPa has been determined for TiO_2 nanotubular structures [213-215], which is much closer to that of natural bone (i.e. 0.02 – 30 GPa) [22, 31, 216], when compared to Ti (i.e. 102 – 166 GPa) [2, 39].

The mechanical behavior of TiO_2 NTs was studied by Xu *et al.* [215] by nanoindentation. In summary, the authors observed that TiO_2 NTs break as long as the indentation depth increases, inducing bending and fracture of the surrounding NTs and formation of smaller fragments which become compacted. Furthermore, Crawford *et al.* [213] observed that TiO_2 NTs inelastically deform by tube crushing in the immediate neighborhood of the indenter tip, accompanied by local densification. Also, Patel et al. [217] studied the mechanical stability of TiO_2 NTs grown in Ti-6Al-4V surfaces by pullout test into a simulant bone, and observed that the film maintained their structural integrity during the insertion and pullout test. However, these studies still provide very limited information to predict the *in vivo* degradation mechanisms that TiO_2 NTs might undergo, when submitted to tribocorrosive actions.

Recently, it has been reported that TiO_2 NTs are prone to peeling off from the Ti substrate due to poor adhesion strength between them [218-220], and some efforts have been made to understand this phenomenon. In general, poor adhesion strength is believed to be assisted by two main mechanisms: 1) dissolution of a nano-thick fluoride rich layer formed beneath the NTs after anodization [218, 221], and 2) hydrogen-assisted cracking mechanism at Ti/NTs interface [220]. To improve the adhesion strength of the NTs to Ti substrate, a few efforts have been made. For example, Xiong *et al.* [222] annealed NTs and found that the adhesion strength was improved with the annealing time. Furthermore, Yu *et al.* [218] reported, for the first time, the employment of an extra anodization step in a fluoride-free electrolyte. The additional anodization in an organic electrolyte composed of 5 wt. % H_2PO_4, resulted in the formation of a 200 nm thick compact layer near the nanotube bottoms, which induced to a significant improvement in the adhesion strength. Nevertheless, the study of the tribo-electrochemical performance of TiO_2 NTs was not undertaken, neither before nor after adhesion strengthening

treatments. Furthermore, in all the above mentioned studies, no information is provided on the characteristics of the interface between TiO_2 NTs and the Ti substrate, which would provide a better insight on the mechanisms governing TiO_2 NTs adhesion. Both the understanding of the stripping mechanisms and the seeking for novel methodologies to overcome this issue are of supreme importance, otherwise their widespread applications may be entirely compromised.

As shown in the previous section, a great effort has been devoted in the last years for the construction of effective TiO_2 nanotubular systems aimed to improve osseointegration, and concomitantly, to reduce infection-related failures of dental implants. Beyond the promising features of the recently developed systems, their applicability in practice is determined by the adhesion of the TiO_2 nanotubular film to the Ti substrate. Based on the aforementioned implications of an endossoeus implant degradation by tribocorrosion, the adhesion failure of TiO_2 NTs at the moment of implantation, or even afterwards, will lead most probably to severe and painful peri-implant inflammatory reactions, which may ultimately lead to implant loosening. Up to now, no information is found in literature as regards the performance of TiO_2 NTs when submitted simultaneously to wear and corrosion solicitations, which are known to happen in real conditions. These studies are of fundamental importance, not only because of the high probability of adhesion failure of those nanotubular systems developed up to now, but also because of their high clinical relevance, since implant degradation *in vivo* can seriously compromise osseointegration or even its long-term stability. Therefore, the creation of fundamental knowledge in this area is required for the development of tribocorrosion resistant nanotubular platforms through integrated approaches which aim simultaneously minimize the risk of infection and enhance bone-implant integration.

References

[1] Oshida Y, Tuna EB, Aktören O and Gençay K. Dental implant systems, International journal of molecular sciences 11 (2010), 1580-1678.

[2] Cruz HV, Souza JCM, Henriques M and Rocha LA. Tribocorrosion and bio-tribocorrosion in the oral environment: the case of dental implants, in: Davim JP (Eds.), Biomedical tribology, Nova Science Publishers, 2011, pp. 1-30.

[3] Babbush CA, Hahn JA, Krauser JT and Rosenlicht JL. Dental implants: the art and science, Elsevier Health Sciences, 2010.

[4] Gaviria L, Salcido JP, Guda T and Ong JL. Current trends in dental implants, Journal of the Korean Association of Oral and Maxillofacial Surgeons 40 (2014), 50-60.

[5] Abai S. Implant Considerations in the Esthetic Zone. Accessed on February 24, 2017. Available from: http://glidewelldental.com/education/inclusive-dental-implant-magazine/volume-4-issue-1/implant-considerations-in-the-esthetic-zone/.

[6] Taylor TD. Dental Implants: Are They for Me?. Accessed on February 24, 2017. Available from: http://dentalimplants.uchc.edu/about/surgery_osseointegration.html.

[7] Pye AD, Lockhart DE, Dawson MP, Murray CA and Smith AJ. A review of dental implants and infection, Journal of Hospital Infection 72 (2009), 104-110.

[8] Iacono VJ. Dental implants in periodontal therapy, Journal of periodontology 71 (2000), 1934-1942.

[9] Brånemark PI, Breine U, Adell R, Hansson BO, Lindström J and Ohlsson Å. Intra-osseous anchorage of dental prostheses: I. Experimental studies, Scandinavian journal of plastic and reconstructive surgery 3 (1969), 81-100.

[10] Branemark P-I. Osseointegration and its experimental background, The Journal of prosthetic dentistry 50 (1983), 399-410.
[11] Adell R, Lekholm U, Rockler B and Brånemark PI. A 15-year study of osseointegrated implants in the treatment of the edentulous jaw, International journal of oral surgery 10 (1981), 387-416.
[12] Zhao L, Wang H, Huo K, Zhang X, Wang W, Zhang Y, Wu Z and Chu PK. The osteogenic activity of strontium loaded titania nanotube arrays on titanium substrates, Biomaterials 34 (2013), 19-29.
[13] Barão VAR, Mathew MT, Assunção WG, Yuan JCC, Wimmer MA and Sukotjo C. Stability of cp-Ti and Ti-6Al-4V alloy for dental implants as a function of saliva pH–an electrochemical study, Clinical oral implants research 23 (2012), 1055-1062.
[14] Manivasagam G, Dhinasekaran D and Rajamanickam A. Biomedical implants: Corrosion and its prevention-a review, Recent patents on corrosion science 2 (2010), 40-54.
[15] Bränemark PI, Zarb GA and Albrektsson T. Introduction to osseointegration, in Tissue Integrated Prostheses: Osseointegration in Clinical Dentistry, Chicago: Quintessence, 1985, pp. 11-76.
[16] Novaes AB, Jr., de Souza SL, de Barros RR, Pereira KK, Iezzi G and Piattelli A. Influence of implant surfaces on osseointegration, Brazilian Dental Journal 21 (2010), 471-481.
[17] Neoh KG, Hu X, Zheng D and Kang ET. Balancing osteoblast functions and bacterial adhesion on functionalized titanium surfaces, Biomaterials 33 (2012), 2813-2822.
[18] Anselme K. Osteoblast adhesion on biomaterials, Biomaterials 21 (2000), 667-681.
[19] Albrektsson T and Johansson C. Osteoinduction, osteoconduction and osseointegration, European Spine Journal 10 Suppl 2 (2001), S96-101.
[20] Le Guehennec L, Soueidan A, Layrolle P and Amouriq Y. Surface treatments of titanium dental implants for rapid osseointegration, Dental Materials 23 (2007), 844-854.
[21] Tomisa AP, Launey ME, Lee JS, Mankani MH, Wegst UG and Saiz E. Nanotechnology approaches to improve dental implants, The International Journal of Oral & Maxillofacial Implants 26 Suppl (2011), 25-44; discussion 45-29.
[22] Rho J-Y, Kuhn-Spearing L and Zioupos P. Mechanical properties and the hierarchical structure of bone, Medical Engineering & Physics 20 (1998), 92-102.
[23] Ralston SH. Bone structure and metabolism, Medicine 41 (2013), 581-585.
[24] Mour M, Das D, Winkler T, Hoenig E, Mielke G, Morlock MM and Schilling AF. Advances in Porous Biomaterials for Dental and Orthopaedic Applications, Materials 3 (2010), 2947-2974.
[25] Chug A, Shukla S, Mahesh L and Jadwani S. Osseointegration—Molecular events at the bone–implant interface: A review, Journal of Oral and Maxillofacial Surgery, Medicine, and Pathology 25 (2013), 1-4.
[26] Saladin KS. Bone Tissue, in Anatomy & Physiology: The Unity of Form and Function, McGraw-Hill Companies, 2003, pp. 217-242.
[27] Zheng X, Zhou F, Gu Y, Duan X and Mo A. Effect of Different Titanium Surfaces on Maturation of Murine Bone Marrow-Derived Dendritic Cells, Scientific Reports 7 (2017), 41945.
[28] Bigerelle M, Anselme K, Noël B, Ruderman I, Hardouin P and Iost A. Improvement in the morphology of Ti-based surfaces: a new process to increase in vitro human osteoblast response, Biomaterials 23 (2002), 1563-1577.
[29] Le Guehennec L, Lopez-Heredia MA, Enkel B, Weiss P, Amouriq Y and Layrolle P. Osteoblastic cell behaviour on different titanium implant surfaces, Acta Biomaterialia 4 (2008), 535-543.
[30] Park S-J, Bae S-B, Kim S-K, Eom T-G and Song S-I. Effect of implant surface microtopography by hydroxyapatite grit-blasting on adhesion, proliferation, and differentiation of osteoblast-like cell line, MG-63, Journal of the Korean Association of Oral and Maxillofacial Surgeons 37 (2011), 214-224.
[31] Wang X, Xu S, Zhou S, Xu W, Leary M, Choong P, Qian M, Brandt M and Xie YM. Topological design and additive manufacturing of porous metals for bone scaffolds and orthopaedic implants: a review, Biomaterials 83 (2016), 127-141.
[32] Singhatanadgit W. Biological Responses to New Advanced Surface Modifications of Endosseous Medical Implants, Bone and Tissue Regeneration Insights 2 (2009), 1-11.
[33] Kulkarni M, Mazare A, Gongadze E, Perutkova Š, Kralj-Iglič V, Milošev I, Schmuki P, Iglič A and Mozetič M. Titanium nanostructures for biomedical applications, Nanotechnology 26 (2015), 062002.
[34] Zambuzzi WF, Coelho PG, Alves GG and Granjeiro JM. Intracellular signal transduction as a factor in the development of "smart" biomaterials for bone tissue engineering, Biotechnology and bioengineering 108 (2011), 1246-1250.
[35] Park J, Bauer S, von der Mark K and Schmuki P. Nanosize and vitality: TiO2 nanotube diameter directs cell fate, Nano letters 7 (2007), 1686-1691.
[36] Oh I-H, Nomura N, Masahashi N and Hanada S. Mechanical properties of porous titanium compacts prepared by powder sintering, Scripta Materialia 49 (2003), 1197-1202.
[37] Noyama Y, Miura T, Ishimoto T, Itaya T, Niinomi M and Nakano T. Bone loss and reduced bone quality of the human femur after total hip arthroplasty under stress-shielding effects by titanium-based implant, Materials Transactions 53 (2012), 565-570.
[38] Torcasio A, van Lenthe GH and Van Oosterwyck H. The importance of loading frequency, rate and vibration for enhancing bone adaptation and implant osseointegration, European Cells and Materials 16 (2008), 56-68.

[39] Soares P, Mikowski A, Lepienski CM, Santos E, Soares GA and Kuromoto NK. Hardness and elastic modulus of TiO2 anodic films measured by instrumented indentation, Journal of Biomedical Materials Research Part B: Applied Biomaterials 84 (2008), 524-530.
[40] Tang L and Eaton JW. Inflammatory responses to biomaterials, American journal of clinical pathology 103 (1995), 466-471.
[41] Valles G, Perez C, Bore A, Martin-Saavedra F, Saldana L and Vilaboa N. Simvastatin prevents the induction of interleukin-6 gene expression by titanium particles in human osteoblastic cells, Acta Biomaterialia 9 (2013), 4916-4925.
[42] Saldaña L and Vilaboa N. Effects of micrometric titanium particles on osteoblast attachment and cytoskeleton architecture, Acta Biomaterialia 6 (2010), 1649-1660.
[43] Khan SN, Ramachandran M, Senthil Kumar S, Krishnan V and Sundaram R. Osseointegration and more–A review of literature, Indian Journal of Dentistry 3 (2012), 72-76.
[44] Stanford CM. Surface modification of biomedical and dental implants and the processes of inflammation, wound healing and bone formation, International journal of molecular sciences 11 (2010), 354-369.
[45] Souza JCM, Barbosa SL, Ariza E, Celis JP and Rocha LA. Simultaneous degradation by corrosion and wear of titanium in artificial saliva containing fluorides, Wear 292–293 (2012), 82-88.
[46] Imai Y, Yokoyama A, Yamamoto S, Obata T, Iizuka T, Kohgo T and Shindoh M. Peri-implant Tissue after Osseointegration in Diabetes in Rat Maxilla, Journal of Oral Biosciences 48 (2006), 54-61.
[47] Subbiahdoss G, Kuijer R, Grijpma DW, van der Mei HC and Busscher HJ. Microbial biofilm growth vs. tissue integration: "The race for the surface" experimentally studied, Acta Biomaterialia 5 (2009), 1399-1404.
[48] Liao J, Anchun M, Zhu Z and Quan Y. Antibacterial titanium plate deposited by silver nanoparticles exhibits cell compatibility, International Journal of Nanomedicine 5 (2010), 337-342.
[49] Quirynen M, De Soete M and Van Steenberghe D. Infectious risks for oral implants: a review of the literature, Clinical oral implants research 13 (2002), 1-19.
[50] Cao HL, Liu XY, Meng FH and Chu PK. Biological actions of silver nanoparticles embedded in titanium controlled by micro-galvanic effects, Biomaterials 32 (2011), 693-705.
[51] Lee D-W, Yun Y-P, Park K and Kim SE. Gentamicin and bone morphogenic protein-2 (BMP-2)-delivering heparinized-titanium implant with enhanced antibacterial activity and osteointegration, Bone 50 (2012), 974-982.
[52] Gulati K, Ramakrishnan S, Aw MS, Atkins GJ, Findlay DM and Losic D. Biocompatible polymer coating of titania nanotube arrays for improved drug elution and osteoblast adhesion, Acta Biomaterialia 8 (2012), 449-456.
[53] Harris LG and Richards RG. Staphylococci and implant surfaces: a review, Injury 37 (2006), S3-S14.
[54] Anselme K, Davidson P, Popa AM, Giazzon M, Liley M and Ploux L. The interaction of cells and bacteria with surfaces structured at the nanometre scale, Acta Biomaterialia 6 (2010), 3824-3846.
[55] Tosi MF. Innate immune responses to infection, Journal of Allergy and Clinical Immunology 116 (2005), 241-249.
[56] Mabilleau G, Bourdon S, Joly-Guillou ML, Filmon R, Baslé MF and Chappard D. Influence of fluoride, hydrogen peroxide and lactic acid on the corrosion resistance of commercially pure titanium, Acta Biomaterialia 2 (2006), 121-129.
[57] Souza JCM, Ponthiaux P, Henriques M, Oliveira R, Teughels W, Celis J-P and Rocha LA. Corrosion behaviour of titanium in the presence of Streptococcus mutans, Journal of Dentistry 41 (2013), 528-534.
[58] Norowski PA and Bumgardner JD. Biomaterial and Antibiotic Strategies for Peri-implantitis, Journal of Biomedical Materials Research Part B-Applied Biomaterials 88B (2009), 530-543.
[59] Adya N, Alam M, Ravindranath T, Mubeen A and Saluja B. Corrosion in titanium dental implants: literature review, The Journal of Indian Prosthodontic Society 5 (2005), 126-131.
[60] Celis J-P and Ponthiaux P. Testing tribocorrosion of passivating materials supporting research and industrial innovation: Handbook, Maney Publishing, 2012.
[61] Virtanen S, Milošev I, Gomez-Barrena E, Trebše R, Salo J and Konttinen YT. Special modes of corrosion under physiological and simulated physiological conditions, Acta Biomaterialia 4 (2008), 468-476.
[62] Souza JCM, Barbosa SL, Ariza EA, Henriques M, Teughels W, Ponthiaux P, Celis J-P and Rocha LA. How do titanium and Ti6Al4V corrode in fluoridated medium as found in the oral cavity? An in vitro study, Materials Science and Engineering: C 47 (2015), 384-393.
[63] Khan MA, Williams RL and Williams DF. The corrosion behaviour of Ti–6Al–4V, Ti–6Al–7Nb and Ti–13Nb–13Zr in protein solutions, Biomaterials 20 (1999), 631-637.
[64] Schiff N, Grosgogeat B, Lissac M and Dalard F. Influence of fluoride content and pH on the corrosion resistance of titanium and its alloys, Biomaterials 23 (2002), 1995-2002.
[65] Takemoto S, Hattori M, Yoshinari M, Kawada E and Oda Y. Corrosion behavior and surface characterization of titanium in solution containing fluoride and albumin, Biomaterials 26 (2005), 829-837.
[66] Cadosch D, Al-Mushaiqri MS, Gautschi OP, Meagher J, Simmen HP and Filgueira L. Biocorrosion and uptake of titanium by human osteoclasts, Journal of Biomedical Materials Research Part A 95 (2010), 1004-1010.
[67] Celis JP, Ponthiaux P and Wenger F. Tribo-corrosion of materials: interplay between chemical, electrochemical, and mechanical reactivity of surfaces, Wear 261 (2006), 939-946.
[68] Ponthiaux P, Wenger F and Celis J-P. Tribocorrosion: Material behavior under combined conditions of corrosion and mechanical loading, INTECH Open Access Publisher, 2012.

[69] Mathew MT, Srinivasa Pai P, Pourzal R, Fischer A and Wimmer MA. Significance of tribocorrosion in biomedical applications: overview and current status, Advances in tribology 2009 (2010).
[70] Landolt D, Mischler S, Stemp M and Barril S. Third body effects and material fluxes in tribocorrosion systems involving a sliding contact, Wear 256 (2004), 517-524.
[71] Vieira AC, Ribeiro AR, Rocha LA and Celis JP. Influence of pH and corrosion inhibitors on the tribocorrosion of titanium in artificial saliva, Wear 261 (2006), 994-1001.
[72] de Souza GB, de Lima GG, Kuromoto NK, Soares P, Lepienski CM, Foerster CE and Mikowski A. Tribo-mechanical characterization of rough, porous and bioactive Ti anodic layers, Journal of the Mechanical Behavior of Biomedical Materials 4 (2011), 796-806.
[73] Diomidis N, Celis JP, Ponthiaux P and Wenger F. A methodology for the assessment of the tribocorrosion of passivating metallic materials, Lubrication Science 21 (2009), 53-67.
[74] Rocha LA, Oliveira F, Cruz HV, Sukotjo C and Mathew MT. Bio-tribocorrosion in dental applications, in: Yan Y (Eds.), Bio-Tribocorrosion in Biomaterials and Medical Implants, Woodhead Publishing, 2013, pp. 223-249.
[75] Zhu MH, Cai ZB, Li W, Yu HY and Zhou ZR. Fretting in prosthetic devices related to human body, Tribology International 42 (2009), 1360-1364.
[76] Mathew MT, Abbey S, Hallab NJ, Hall DJ, Sukotjo C and Wimmer MA. Influence of pH on the tribocorrosion behavior of CpTi in the oral environment: synergistic interactions of wear and corrosion, Journal of Biomedical Materials Research Part B-Applied Biomaterials 100B (2012), 1662-1671.
[77] Souza JC, Henriques M, Oliveira R, Teughels W, Celis JP and Rocha LA. Do oral biofilms influence the wear and corrosion behavior of titanium?, Biofouling 26 (2010), 471-478.
[78] Mathew MT, Barão VA, Yuan JC-C, Assunção WG, Sukotjo C and Wimmer MA. What is the role of lipopolysaccharide on the tribocorrosive behavior of titanium?, Journal of the Mechanical Behavior of Biomedical Materials 8 (2012), 71-85.
[79] Runa MJ, Mathew MT, Fernandes MH and Rocha LA. First insight on the impact of an osteoblastic layer on the bio-tribocorrosion performance of Ti6Al4V hip implants, Acta Biomaterialia 12 (2015), 341-351.
[80] Runa MJ, Mathew MT and Rocha LA. Tribocorrosion response of the Ti6Al4V alloys commonly used in femoral stems, Tribology International 68 (2013), 85-93.
[81] Cruz HV, Henriques M, Teughels W, Celis J-P and Rocha LA. Combined Influence of fluoride and biofilms on the biotribocorrosion behavior of titanium used for dental applications, Journal of Bio-and Tribo-Corrosion 1 (2015), 1-12.
[82] Long M and Rack HJ. Friction and surface behavior of selected titanium alloys during reciprocating-sliding motion, Wear 249 (2001), 157-167.
[83] Song H-J, Kim M-K, Jung G-C, Vang M-S and Park Y-J. The effects of spark anodizing treatment of pure titanium metals and titanium alloys on corrosion characteristics, Surface and Coatings Technology 201 (2007), 8738-8745.
[84] Cobelli N, Scharf B, Crisi GM, Hardin J and Santambrogio L. Mediators of the inflammatory response to joint replacement devices, Nature Reviews Rheumatology 7 (2011), 600-608.
[85] Olmedo DG, Paparella ML, Brandizzi D and Cabrini RL. Reactive lesions of peri-implant mucosa associated with titanium dental implants: a report of 2 cases, International Journal of Oral and Maxillofacial Surgery 39 (2010), 503-507.
[86] Ribeiro AR, Gemini-Piperni S, Travassos R, Lemgruber L, Silva RC, Rossi AL, Farina M, Anselme K, Shokuhfar T, et al. Trojan-like internalization of anatase titanium dioxide nanoparticles by human osteoblast cells, Scientific Reports 6 (2016), 23615.
[87] Wang ML, Nesti LJ, Tuli R, Lazatin J, Danielson KG, Sharkey PF and Tuan RS. Titanium particles suppress expression of osteoblastic phenotype in human mesenchymal stem cells, Journal of Orthopaedic Research 20 (2002), 1175-1184.
[88] do Nascimento C, Barbosa RES, Issa JPM, Watanabe E, Ito IY and Albuquerque Junior RF. Bacterial leakage along the implant–abutment interface of premachined or cast components, International Journal of Oral and Maxillofacial Surgery 37 (2008), 177-180.
[89] Saidin S, Abdul Kadir MR, Sulaiman E and Abu Kasim NH. Effects of different implant–abutment connections on micromotion and stress distribution: Prediction of microgap formation, Journal of Dentistry 40 (2012), 467-474.
[90] Jacobs JJ, Hallab NJ, Urban RM and Wimmer MA. Wear particles, Journal of bone & joint surgery 88 Suppl 2 (2006), 99-102.
[91] Anselme K and Bigerelle M. Topography effects of pure titanium substrates on human osteoblast long-term adhesion, Acta Biomaterialia 1 (2005), 211-222.
[92] Jayaraman M, Meyer U, Bühner M, Joos U and Wiesmann H-P. Influence of titanium surfaces on attachment of osteoblast-like cells in vitro, Biomaterials 25 (2004), 625-631.
[93] Kim EJ, Boehm CA, Mata A, Fleischman AJ, Muschler GF and Roy S. Post microtextures accelerate cell proliferation and osteogenesis, Acta Biomaterialia 6 (2010), 160-169.
[94] Hamilton DW, Wong KS and Brunette DM. Microfabricated discontinuous-edge surface topographies influence osteoblast adhesion, migration, cytoskeletal organization, and proliferation and enhance matrix and mineral deposition in vitro, Calcified tissue international 78 (2006), 314-325.
[95] Ivanoff CJ, Widmark G, Hallgren C, Sennerby L and Wennerberg A. Histologic evaluation of the bone integration of TiO2 blasted and turned titanium microimplants in humans, Clinical oral implants research 12 (2001), 128-134.

[96] Wennerberg A and Albrektsson T. On implant surfaces: a review of current knowledge and opinions, International Journal of Oral & Maxillofacial Implants 25 (2010), 63-74.
[97] Zhao L, Mei S, Chu PK, Zhang Y and Wu Z. The influence of hierarchical hybrid micro/nano-textured titanium surface with titania nanotubes on osteoblast functions, Biomaterials 31 (2010), 5072-5082.
[98] Zhao L, Liu L, Wu Z, Zhang Y and Chu PK. Effects of micropitted/nanotubular titania topographies on bone mesenchymal stem cell osteogenic differentiation, Biomaterials 33 (2012), 2629-2641.
[99] Zhang W, Wang G, Liu Y, Zhao X, Zou D, Zhu C, Jin Y, Huang Q, Sun J, et al. The synergistic effect of hierarchical micro/nano-topography and bioactive ions for enhanced osseointegration, Biomaterials 34 (2013), 3184-3195.
[100] Yao C and Webster TJ. Anodization: a promising nano-modification technique of titanium implants for orthopedic applications, Journal of nanoscience and nanotechnology 6 (2006), 2682-2692.
[101] Nguyen AT, Sathe SR and Yim EKF. From nano to micro: topographical scale and its impact on cell adhesion, morphology and contact guidance, Journal of Physics: Condensed Matter 28 (2016), 183001.
[102] Mattila PK and Lappalainen P. Filopodia: molecular architecture and cellular functions, Nature reviews Molecular cell biology 9 (2008), 446-454.
[103] Webster TJ and Ejiofor JU. Increased osteoblast adhesion on nanophase metals: Ti, Ti6Al4V, and CoCrMo, Biomaterials 25 (2004), 4731-4739.
[104] Palin E, Liu H and Webster TJ. Mimicking the nanofeatures of bone increases bone-forming cell adhesion and proliferation, Nanotechnology 16 (2005), 1828.
[105] Yao C, Slamovich EB and Webster TJ. Enhanced osteoblast functions on anodized titanium with nanotube-like structures, Journal of Biomedical Materials Research Part A 85 (2008), 157-166.
[106] Mendonça G, Mendonça DBS, Simões LGP, Araújo AL, Leite ER, Duarte WR, Aragão FJL and Cooper LF. The effects of implant surface nanoscale features on osteoblast-specific gene expression, Biomaterials 30 (2009), 4053-4062.
[107] Raimondo T, Puckett S and Webster TJ. Greater osteoblast and endothelial cell adhesion on nanostructured polyethylene and titanium, International Journal of Nanomedicine 5 (2010), 647-652.
[108] Thalji G, Gretzer C and Cooper LF. Comparative molecular assessment of early osseointegration in implant-adherent cells, Bone 52 (2013), 444-453.
[109] Mendonça G, Mendonça DBS, Simões LGP, Araújo AL, Leite ER, Golin AL, Aragão FJL and Cooper LF. Nanostructured implant surface effect on osteoblast gene expression and bone-to-implant contact in vivo, Materials Science and Engineering: C 31 (2011), 1809-1818.
[110] Chiang C-Y, Chiou S-H, Yang W-E, Hsu M-L, Yung M-C, Tsai M-L, Chen L-K and Huang H-H. Formation of TiO2 nano-network on titanium surface increases the human cell growth, Dental Materials 25 (2009), 1022-1029.
[111] Surmenev RA, Surmeneva MA and Ivanova AA. Significance of calcium phosphate coatings for the enhancement of new bone osteogenesis–A review, Acta Biomaterialia 10 (2014), 557-579.
[112] Wang P, Zhao L, Liu J, Weir MD, Zhou X and Xu HHK. Bone tissue engineering via nanostructured calcium phosphate biomaterials and stem cells, Bone research 2 (2014).
[113] Wang X, Ito A, Sogo Y, Li X and Oyane A. Zinc-containing apatite layers on external fixation rods promoting cell activity, Acta Biomaterialia 6 (2010), 962-968.
[114] Qiao Y, Zhang W, Tian P, Meng F, Zhu H, Jiang X, Liu X and Chu PK. Stimulation of bone growth following zinc incorporation into biomaterials, Biomaterials 35 (2014), 6882-6897.
[115] Ito A, Kawamura H, Otsuka M, Ikeuchi M, Ohgushi H, Ishikawa K, Onuma K, Kanzaki N, Sogo Y, et al. Zinc-releasing calcium phosphate for stimulating bone formation, Materials Science and Engineering: C 22 (2002), 21-25.
[116] Hu H, Zhang W, Qiao Y, Jiang X, Liu X and Ding C. Antibacterial activity and increased bone marrow stem cell functions of Zn-incorporated TiO2 coatings on titanium, Acta Biomaterialia 8 (2012), 904-915.
[117] Jin G, Cao H, Qiao Y, Meng F, Zhu H and Liu X. Osteogenic activity and antibacterial effect of zinc ion implanted titanium, Colloids and Surfaces B: Biointerfaces 117 (2014), 158-165.
[118] Campoccia D, Montanaro L and Arciola CR. A review of the biomaterials technologies for infection-resistant surfaces, Biomaterials 34 (2013), 8533-8554.
[119] Wu Y, Zitelli JP, TenHuisen KS, Yu X and Libera MR. Differential response of Staphylococci and osteoblasts to varying titanium surface roughness, Biomaterials 32 (2011), 951-960.
[120] Whitehead KA, Colligon J and Verran J. Retention of microbial cells in substratum surface features of micrometer and sub-micrometer dimensions, Colloids and Surfaces B: Biointerfaces 41 (2005), 129-138.
[121] Holmberg KV, Abdolhosseini M, Li Y, Chen X, Gorr S-U and Aparicio C. Bio-inspired stable antimicrobial peptide coatings for dental applications, Acta Biomaterialia 9 (2013), 8224-8231.
[122] Ewald A, Glückermann SK, Thull R and Gbureck U. Antimicrobial titanium/silver PVD coatings on titanium, Biomedical engineering online 5 (2006), 22.
[123] Petrini P, Arciola CR, Pezzali I, Bozzini S, Montanaro L, Tanzi MC, Speziale P and Visai L. Antibacterial activity of zinc modified titanium oxide surface, The International journal of artificial organs 29 (2006), 434-442.
[124] Jin G, Qin H, Cao H, Qian S, Zhao Y, Peng X, Zhang X, Liu X and Chu PK. Synergistic effects of dual Zn/Ag ion implantation in osteogenic activity and antibacterial ability of titanium, Biomaterials 35 (2014), 7699-7713.
[125] Lellouche J, Kahana E, Elias S, Gedanken A and Banin E. Antibiofilm activity of nanosized magnesium fluoride, Biomaterials 30 (2009), 5969-5978.
[126] Vargas-Reus MA, Memarzadeh K, Huang J, Ren GG and Allaker RP. Antimicrobial activity of nanoparticulate metal oxides against peri-implantitis pathogens, International Journal of Antimicrobial Agents 40 (2012), 135-139.

[127] Al-Hazmi F, Alnowaiser F, Al-Ghamdi AA, Al-Ghamdi AA, Aly MM, Al-Tuwirqi RM and El-Tantawy F. A new large – Scale synthesis of magnesium oxide nanowires: Structural and antibacterial properties, Superlattices and Microstructures 52 (2012), 200-209.
[128] Lellouche J, Friedman A, Lellouche J-P, Gedanken A and Banin E. Improved antibacterial and antibiofilm activity of magnesium fluoride nanoparticles obtained by water-based ultrasound chemistry, Nanomedicine: Nanotechnology, Biology and Medicine 8 (2012), 702-711.
[129] Moseke C, Hage F, Vorndran E and Gbureck U. TiO2 nanotube arrays deposited on Ti substrate by anodic oxidation and their potential as a long-term drug delivery system for antimicrobial agents, Applied Surface Science 258 (2012), 5399-5404.
[130] Huang H-L, Chang Y-Y, Lai M-C, Lin C-R, Lai C-H and Shieh T-M. Antibacterial TaN-Ag coatings on titanium dental implants, Surface and Coatings Technology 205 (2010), 1636-1641.
[131] Shinonaga Y and Arita K. Antibacterial effect of acrylic dental devices after surface modification by fluorine and silver dual-ion implantation, Acta Biomaterialia 8 (2012), 1388-1393.
[132] Puckett SD, Taylor E, Raimondo T and Webster TJ. The relationship between the nanostructure of titanium surfaces and bacterial attachment, Biomaterials 31 (2010), 706-713.
[133] Colon G, Ward BC and Webster TJ. Increased osteoblast and decreased Staphylococcus epidermidis functions on nanophase ZnO and TiO2, Journal of Biomedical Materials Research Part A 78 (2006), 595-604.
[134] Ploux L, Anselme K, Dirani A, Ponche A, Soppera O and Roucoules V. Opposite responses of cells and bacteria to micro/nanopatterned surfaces prepared by pulsed plasma polymerization and UV-irradiation, Langmuir 25 (2009), 8161-8169.
[135] Oliveira FG, Ribeiro AR, Perez G, Archanjo BS, Gouvea CP, Araújo JR, Campos APC, Kuznetsov A, Almeida CM, et al. Understanding growth mechanisms and tribocorrosion behaviour of porous TiO2 anodic films containing calcium, phosphorous and magnesium, Applied Surface Science 341 (2015), 1-12.
[136] Alves AC, Oliveira F, Wenger F, Ponthiaux P, Celis J-P and Rocha LA. Tribocorrosion behaviour of anodic treated titanium surfaces intended for dental implants, Journal of Physics D: Applied Physics 46 (2013), 404001.
[137] Marques IdSV, Alfaro MF, Da Cruz NC, Mesquita MF, Takoudis C, Sukotjo C, Mathew MT and Barão VAR. Tribocorrosion behavior of biofunctional titanium oxide films produced by micro-arc oxidation: Synergism and mechanisms, Journal of the Mechanical Behavior of Biomedical Materials 60 (2016), 8-21.
[138] Alves SA, Bayón R, Igartua A, Saénz de Viteri V and Rocha LA. Tribocorrosion behaviour of anodic titanium oxide films produced by plasma electrolytic oxidation for dental implants, Lubrication Science 26 (2014), 500-513.
[139] Alves S, Bayón R, de Viteri VS, Garcia M, Igartua A, Fernandes M and Rocha L. Tribocorrosion behavior of calcium- and phosphorous-enriched titanium oxide films and study of osteoblast interactions for dental implants, Journal of Bio-and Tribo-Corrosion 1 (2015), 23.
[140] Marques IdSV, Alfaro MF, Saito MT, da Cruz NC, Takoudis C, Landers R, Mesquita MF, Nociti Junior FH, Mathew MT, et al. Biomimetic coatings enhance tribocorrosion behavior and cell responses of commercially pure titanium surfaces, Biointerphases 11 (2016), 031008.
[141] Faghihi S, Li D and Szpunar JA. Tribocorrosion behaviour of nanostructured titanium substrates processed by high-pressure torsion, Nanotechnology 21 (2010), 485703.
[142] Indira K, Mudali UK, Nishimura T and Rajendran N. A review on TiO2 nanotubes: influence of anodization parameters, formation mechanism, properties, corrosion behavior, and biomedical applications, Journal of Bio- and Tribo-Corrosion 1 (2015), 28.
[143] Roy P, Berger S and Schmuki P. TiO2 nanotubes: synthesis and applications, Angewandte Chemie International Edition 50 (2011), 2904-2939.
[144] Lee C, Hong C, Kim H, Kang J and Zheng HM. TiO2 nanotubes as a therapeutic agent for cancer thermotherapy, Photochemistry and photobiology 86 (2010), 981-989.
[145] Ge M, Li Q, Cao C, Huang J, Li S, Zhang S, Chen Z, Zhang K, Al-Deyab SS, et al. One-dimensional TiO2 Nanotube Photocatalysts for Solar Water Splitting, Advanced Science (2016).
[146] Rao BM, Torabi A and Varghese OK. Anodically grown functional oxide nanotubes and applications, MRS Communications 6 (2016), 375-396.
[147] Regonini D, Bowen CR, Jaroenworaluck A and Stevens R. A review of growth mechanism, structure and crystallinity of anodized TiO2 nanotubes, Materials Science and Engineering: R: Reports 74 (2013), 377-406.
[148] Macak JM, Tsuchiya H, Ghicov A, Yasuda K, Hahn R, Bauer S and Schmuki P. TiO2 nanotubes: self-organized electrochemical formation, properties and applications, Current Opinion in Solid State and Materials Science 11 (2007), 3-18.
[149] Brammer KS, Frandsen CJ and Jin S. TiO2 nanotubes for bone regeneration, Trends in biotechnology 30 (2012), 315-322.
[150] Zwilling V, Darque-Ceretti E, Boutry-Forveille A, David D, Perrin M-Y and Aucouturier M. Structure and physicochemistry of anodic oxide films on titanium and TA6V alloy, Surface and Interface Analysis 27 (1999), 629-637.
[151] Zwilling V, Aucouturier M and Darque-Ceretti E. Anodic oxidation of titanium and TA6V alloy in chromic media. An electrochemical approach, Electrochimica Acta 45 (1999), 921-929.
[152] Gong D, Grimes CA, Varghese OK, Hu W, Singh RS, Chen Z and Dickey EC. Titanium oxide nanotube arrays prepared by anodic oxidation, Journal of Materials Research 16 (2001), 3331-3334.

[153] Byung-Gwan LEE, Jin-Wook C, Seong-Eun LEE, Jeong Y-S, Han-Jun OH and Choong-Soo CHI. Formation behavior of anodic TiO2 nanotubes in fluoride containing electrolytes, Transactions of Nonferrous Metals Society of China 19 (2009), 842-845.
[154] Beranek R, Hildebrand H and Schmuki P. Self-organized porous titanium oxide prepared in H2SO4/HF electrolytes, Electrochemical and solid-state letters 6 (2003), B12-B14.
[155] Macak JM, Sirotna K and Schmuki P. Self-organized porous titanium oxide prepared in Na2SO4/NaF electrolytes, Electrochimica Acta 50 (2005), 3679-3684.
[156] Shankar K, Mor GK, Prakasam HE, Yoriya S, Paulose M, Varghese OK and Grimes CA. Highly-ordered TiO2 nanotube arrays up to 220 µm in length: use in water photoelectrolysis and dye-sensitized solar cells, Nanotechnology 18 (2007), 065707.
[157] Han SC, Doh JM, Yoon JK, Kim GH, Byun JY, Han SH, Hong KT and Kwun SI. Highly ordered self-organized TiO2 nanotube arrays prepared by a multi-step anodic oxidation process, Metals and Materials International 15 (2009), 493-499.
[158] Sulka GD, Kapusta-Kołodziej J, Brzózka A and Jaskuła M. Fabrication of nanoporous TiO2 by electrochemical anodization, Electrochimica Acta 55 (2010), 4359-4367.
[159] Ali G, Chen C, Yoo SH, Kum JM and Cho SO. Fabrication of complete titania nanoporous structures via electrochemical anodization of Ti, Nanoscale research letters 6 (2011), 332.
[160] Peighambardoust N-S and Nasirpouri F. Manipulating morphology, pore geometry and ordering degree of TiO2 nanotube arrays by anodic oxidation, Surface and Coatings Technology 235 (2013), 727-734.
[161] Popat KC, Leoni L, Grimes CA and Desai TA. Influence of engineered titania nanotubular surfaces on bone cells, Biomaterials 28 (2007), 3188-3197.
[162] Wang N, Li H, Lü W, Li J, Wang J, Zhang Z and Liu Y. Effects of TiO2 nanotubes with different diameters on gene expression and osseointegration of implants in minipigs, Biomaterials 32 (2011), 6900-6911.
[163] Salou L, Hoornaert A, Louarn G and Layrolle P. Enhanced osseointegration of titanium implants with nanostructured surfaces: An experimental study in rabbits, Acta Biomaterialia 11 (2015), 494-502.
[164] Lai Y, Lin L, Pan F, Huang J, Song R, Huang Y, Lin C, Fuchs H and Chi L. Bioinspired patterning with extreme wettability contrast on TiO2 nanotube array surface: a versatile platform for biomedical applications, Small 9 (2013), 2945-2953.
[165] Hamlekhan A, Butt A, Patel S, Royhman D, Takoudis C, Sukotjo C, Yuan J, Jursich G, Mathew MT, et al. Fabrication of anti-aging TiO2 nanotubes on biomedical Ti alloys, PLoS One 9 (2014), e96213.
[166] Oh S, Daraio C, Chen LH, Pisanic TR, Finones RR and Jin S. Significantly accelerated osteoblast cell growth on aligned TiO2 nanotubes, Journal of Biomedical Materials Research Part A 78 (2006), 97-103.
[167] Wan J, Yan X, Ding J, Wang M and Hu K. Self-organized highly ordered TiO2 nanotubes in organic aqueous system, Materials characterization 60 (2009), 1534-1540.
[168] Gulati K, Maher S, Findlay DM and Losic D. Titania nanotubes for orchestrating osteogenesis at the bone–implant interface, Nanomedicine 11 (2016), 1847-1864.
[169] Bauer S, Park J, Faltenbacher J, Berger S, von der Mark K and Schmuki P. Size selective behavior of mesenchymal stem cells on ZrO2 and TiO2 nanotube arrays, Integrative Biology 1 (2009), 525-532.
[170] Oh S, Brammer KS, Li YSJ, Teng D, Engler AJ, Chien S and Jin S. Stem cell fate dictated solely by altered nanotube dimension, Proceedings of the National Academy of Sciences 106 (2009), 2130-2135.
[171] Brammer KS, Oh S, Cobb CJ, Bjursten LM, van der Heyde H and Jin S. Improved bone-forming functionality on diameter-controlled TiO2 nanotube surface, Acta Biomaterialia 5 (2009), 3215-3223.
[172] Katsumi A, Orr AW, Tzima E and Schwartz MA. Integrins in mechanotransduction, Journal of Biological Chemistry 279 (2004), 12001-12004.
[173] Brammer KS, Oh S, Gallagher JO and Jin S. Enhanced cellular mobility guided by TiO2 nanotube surfaces, Nano letters 8 (2008), 786-793.
[174] Park J, Bauer S, Schlegel KA, Neukam FW, von der Mark K and Schmuki P. TiO2 nanotube surfaces: 15 nm—an optimal length scale of surface topography for cell adhesion and differentiation, Small 5 (2009), 666-671.
[175] Rajyalakshmi A, Ercan B, Balasubramanian K and Webster TJ. Reduced adhesion of macrophages on anodized titanium with select nanotube surface features, International Journal of Nanomedicine 6 (2011), 1765-1771.
[176] Shi X, Xu Q, Tian A, Tian Y, Xue X, Sun H, Yang H and Dong C. Antibacterial activities of TiO 2 nanotubes on Porphyromonas gingivalis, RSC Advances 5 (2015), 34237-34242.
[177] Li H, Cui Q, Feng B, Wang J, Lu X and Weng J. Antibacterial activity of TiO2 nanotubes: influence of crystal phase, morphology and Ag deposition, Applied Surface Science 284 (2013), 179-183.
[178] Ercan B, Taylor E, Alpaslan E and Webster TJ. Diameter of titanium nanotubes influences anti-bacterial efficacy, Nanotechnology 22 (2011), 295102.
[179] Beltrán-Partida E, Valdez-Salas B, Curiel-Álvarez M, Castillo-Uribe S, Escamilla A and Nedev N. Enhanced antifungal activity by disinfected titanium dioxide nanotubes via reduced nano-adhesion bonds, Materials Science and Engineering: C.
[180] Grotberg J, Hamlekhan A, Butt A, Patel S, Royhman D, Shokuhfar T, Sukotjo C, Takoudis C and Mathew MT. Thermally oxidized titania nanotubes enhance the corrosion resistance of Ti6Al4V, Materials Science and Engineering: C 59 (2016), 677-689.

[181] Yu W-q, Qiu J, Xu L and Zhang F-q. Corrosion behaviors of TiO2 nanotube layers on titanium in Hank's solution, Biomedical Materials 4 (2009), 065012.
[182] Demetrescu I, Pirvu C and Mitran V. Effect of nano-topographical features of Ti/TiO 2 electrode surface on cell response and electrochemical stability in artificial saliva, Bioelectrochemistry 79 (2010), 122-129.
[183] Yu W-q, Qiu J and Zhang F-q. In vitro corrosion study of different TiO2 nanotube layers on titanium in solution with serum proteins, Colloids and Surfaces B: Biointerfaces 84 (2011), 400-405.
[184] Wu S, Weng Z, Liu X, Yeung KWK and Chu P. Functionalized TiO2 based nanomaterials for biomedical applications, Advanced Functional Materials 24 (2014), 5464-5481.
[185] Hamlekhan A, Sinha-Ray S, Takoudis C, Mathew MT, Sukotjo C, Yarin AL and Shokuhfar T. Fabrication of drug eluting implants: study of drug release mechanism from titanium dioxide nanotubes, Journal of Physics D: Applied Physics 48 (2015), 275401.
[186] Popat KC, Eltgroth M, LaTempa TJ, Grimes CA and Desai TA. Titania Nanotubes: A Novel Platform for Drug-Eluting Coatings for Medical Implants?, Small 3 (2007), 1878-1881.
[187] Hu Y, Cai K, Luo Z, Xu D, Xie D, Huang Y, Yang W and Liu P. TiO 2 nanotubes as drug nanoreservoirs for the regulation of mobility and differentiation of mesenchymal stem cells, Acta Biomaterialia 8 (2012), 439-448.
[188] Lai M, Jin Z, Yang X, Wang H and Xu K. The controlled release of simvastatin from TiO2 nanotubes to promote osteoblast differentiation and inhibit osteoclast resorption, Applied Surface Science 396 (2017), 1741-1751.
[189] Chen J, Zhang Z, Ouyang J, Chen X, Xu Z and Sun X. Bioactivity and osteogenic cell response of TiO2 nanotubes coupled with nanoscale calcium phosphate via ultrasonification-assisted electrochemical deposition, Applied Surface Science 305 (2014), 24-32.
[190] Huo K, Zhang X, Wang H, Zhao L, Liu X and Chu PK. Osteogenic activity and antibacterial effects on titanium surfaces modified with Zn-incorporated nanotube arrays, Biomaterials 34 (2013), 3467-3478.
[191] Cheng H, Xiong W, Fang Z, Guan H, Wu W, Li Y, Zhang Y, Alvarez MM, Gao B, et al. Strontium (Sr) and silver (Ag) loaded nanotubular structures with combined osteoinductive and antimicrobial activities, Acta Biomaterialia 31 (2016), 388-400.
[192] Park J, Bauer S, Pittrof A, Killian MS, Schmuki P and von der Mark K. Synergistic control of mesenchymal stem cell differentiation by nanoscale surface geometry and immobilized growth factors on TiO2 nanotubes, Small 8 (2012), 98-107.
[193] Lai M, Cai K, Zhao L, Chen X, Hou Y and Yang Z. Surface functionalization of TiO2 nanotubes with bone morphogenetic protein 2 and its synergistic effect on the differentiation of mesenchymal stem cells, Biomacromolecules 12 (2011), 1097-1105.
[194] Cao X, Yu W-q, Qiu J, Zhao Y-f, Zhang Y-l and Zhang F-q. RGD peptide immobilized on TiO2 nanotubes for increased bone marrow stromal cells adhesion and osteogenic gene expression, Journal of Materials Science: Materials in Medicine 23 (2012), 527-536.
[195] Lai M, Jin Z and Su Z. Surface modification of TiO2 nanotubes with osteogenic growth peptide to enhance osteoblast differentiation, Materials Science and Engineering: C 73 (2017), 490-497.
[196] Patel S, Sukotjo C, Takoudis C, Mathew M, Amirouche F, Friedrich C and Shokuhfar T. Corrosion property of vitamin D loaded nanotubes for bio-implants application in an in vitro environment, Frontiers in Bioengineering and Biotechnology, Conference Abstract: 10th World Biomaterials Congress (2016).
[197] Popat KC, Eltgroth M, LaTempa TJ, Grimes CA and Desai TA. Decreased Staphylococcus epidermis adhesion and increased osteoblast functionality on antibiotic-loaded titania nanotubes, Biomaterials 28 (2007), 4880-4888.
[198] Gulati K, Aw MS and Losic D. Drug-eluting Ti wires with titania nanotube arrays for bone fixation and reduced bone infection, Nanoscale research letters 6 (2011), 571.
[199] Shokuhfar T, Sinha-Ray S, Sukotjo C and Yarin AL. Intercalation of anti-inflammatory drug molecules within TiO2 nanotubes, RSC Advances 3 (2013), 17380-17386.
[200] Mohan L, Anandan C and Rajendran N. Drug release characteristics of quercetin-loaded TiO2 nanotubes coated with chitosan, International Journal of Biological Macromolecules 93, Part B (2016), 1633-1638.
[201] Chen Y, Gao A, Bai L, Wang Y, Wang X, Zhang X, Huang X, Hang R, Tang B, et al. Antibacterial, osteogenic, and angiogenic activities of SrTiO3 nanotubes embedded with Ag2O nanoparticles, Materials Science and Engineering: C 75 (2017), 1049-1058.
[202] Cheng H, Li Y, Huo K, Gao B and Xiong W. Long-lasting in vivo and in vitro antibacterial ability of nanostructured titania coating incorporated with silver nanoparticles, Journal of Biomedical Materials Research Part A 102 (2014), 3488-3499.
[203] Gao A, Hang R, Huang X, Zhao L, Zhang X, Wang L, Tang B, Ma S and Chu PK. The effects of titania nanotubes with embedded silver oxide nanoparticles on bacteria and osteoblasts, Biomaterials 35 (2014), 4223-4235.
[204] Yang T, Qian S, Qiao Y and Liu X. Cytocompatibility and antibacterial activity of titania nanotubes incorporated with gold nanoparticles, Colloids and Surfaces B: Biointerfaces 145 (2016), 597-606.
[205] Bai L, Wu R, Wang Y, Wang X, Zhang X, Huang X, Qin L, Hang R, Zhao L, et al. Osteogenic and angiogenic activities of silicon-incorporated TiO2 nanotube arrays, Journal of Materials Chemistry B 4 (2016), 5548-5559.
[206] Mei S, Wang H, Wang W, Tong L, Pan H, Ruan C, Ma Q, Liu M, Yang H, et al. Antibacterial effects and biocompatibility of titanium surfaces with graded silver incorporation in titania nanotubes, Biomaterials 35 (2014), 4255-4265.

[207] Kodama A, Bauer S, Komatsu A, Asoh H, Ono S and Schmuki P. Bioactivation of titanium surfaces using coatings of TiO2 nanotubes rapidly pre-loaded with synthetic hydroxyapatite, Acta Biomaterialia 5 (2009), 2322-2330.
[208] Roguska A, Pisarek M, Andrzejczuk M, Dolata M, Lewandowska M and Janik-Czachor M. Characterization of a calcium phosphate–TiO2 nanotube composite layer for biomedical applications, Materials Science and Engineering: C 31 (2011), 906-914.
[209] Parcharoen Y, Kajitvichyanukul P, Sirivisoot S and Termsuksawad P. Hydroxyapatite electrodeposition on anodized titanium nanotubes for orthopedic applications, Applied Surface Science 311 (2014), 54-61.
[210] Huang Y, Zhang X, Zhang H, Qiao H, Zhang X, Jia T, Han S, Gao Y, Xiao H, et al. Fabrication of silver- and strontium-doped hydroxyapatite/TiO2 nanotube bilayer coatings for enhancing bactericidal effect and osteoinductivity, Ceramics International 43 (2017), 992-1007.
[211] Xin Y, Jiang J, Huo K, Hu T and Chu PK. Bioactive SrTiO3 nanotube arrays: strontium delivery platform on Ti-based osteoporotic bone implants, ACS nano 3 (2009), 3228-3234.
[212] Svensson S, Suska F, Emanuelsson L, Palmquist A, Norlindh B, Trobos M, Bäckros H, Persson L, Rydja G, et al. Osseointegration of titanium with an antimicrobial nanostructured noble metal coating, Nanomedicine: Nanotechnology, Biology and Medicine 9 (2013), 1048-1056.
[213] Crawford G, Chawla N and Houston J. Nanomechanics of biocompatible TiO2 nanotubes by interfacial force microscopy (IFM), Journal of the Mechanical Behavior of Biomedical Materials 2 (2009), 580-587.
[214] Crawford GA, Chawla N, Das K, Bose S and Bandyopadhyay A. Microstructure and deformation behavior of biocompatible TiO2 nanotubes on titanium substrate, Acta Biomaterialia 3 (2007), 359-367.
[215] Xu YN, Liu MN, Wang MC, Oloyede A, Bell JM and Yan C. Nanoindentation study of the mechanical behavior of TiO2 nanotube arrays, Journal of Applied Physics 118 (2015), 145301.
[216] Rho J-Y, Tsui TY and Pharr GM. Elastic properties of human cortical and trabecular lamellar bone measured by nanoindentation, Biomaterials 18 (1997), 1325-1330.
[217] Patel S, Solitro GF, Sukotjo C, Takoudis C, Mathew MT, Amirouche F and Shokuhfar T. Nanotopography and surface stress analysis of Ti6Al4V bioimplant: an alternative design for stability, JOM 67 (2015), 2518-2533.
[218] Yu D, Zhu X, Xu Z, Zhong X, Gui Q, Song Y, Zhang S, Chen X and Li D. Facile method to enhance the adhesion of TiO2 nanotube arrays to Ti substrate, ACS applied materials & interfaces 6 (2014), 8001-8005.
[219] Ouyang HM, Fei GT, Zhang Y, Su H, Jin Z, Xu SH and De Zhang L. Large scale free-standing open-ended TiO 2 nanotube arrays: stress-induced self-detachment and in situ pore opening, Journal of Materials Chemistry C 1 (2013), 7498-7506.
[220] Zhao M, Li J, Li Y, Wang J, Zuo Y, Jiang J and Wang H. Gradient Control of the Adhesive Force between Ti/TiO2 Nanotubular Arrays Fabricated by Anodization, Scientific Reports 4 (2014).
[221] Miraghaei S, Ashrafizadeh F, Raeissi K, Santamaria M and Di Quarto F. An Electrochemical Investigation on the Adhesion of As-Formed Anodic TiO2 Nanotubes Grown in Organic Solvents, Electrochemical and solid-state letters 14 (2011), K8-K11.
[222] Xiong J, Wang X, Li Y and Hodgson PD. Interfacial chemistry and adhesion between titanium dioxide nanotube layers and titanium substrates, The Journal of Physical Chemistry C 115 (2011), 4768-4772.

CHAPTER 3

Synthesis of calcium-phosphorous doped TiO_2 nanotubes by anodization and reverse polarization: a promising strategy for an efficient biofunctional implant surface

Published in Applied Surface Science, 399 (2017) 682 – 701

Synthesis of calcium-phosphorous doped TiO_2 nanotubes by anodization and reverse polarization: a promising strategy for an efficient biofunctional implant surface

Sofia A. Alves[1,2*], Sweetu B. Patel[2,3], Cortino Sukotjo[2,4], Mathew T. Mathew[2,5,6], Paulo N. Filho[7,8], Jean-Pierre Celis[9], Luís A. Rocha[1,7,8], Tolou Shokuhfar[2,3,10]

[1]*CMEMS – Center of MicroElectroMechanical Systems, Department of Mechanical Engineering, University of Minho, 4800-058 Guimarães, Portugal*
[2]*IBTN/US – American Branch of the Institute of Biomaterials, Tribocorrosion and Nanomedicine, UIC College of Dentistry, 60612 Chicago, IL, USA*
[3]*Department of Mechanical Engineering, Michigan Technological University, 49931 Houghton, MI, USA*
[4]*Departmenmt of Restorative Dentistry, University of Illinois at Chicago, 60612 Chicago, IL, USA*
[5]*Department of Orthopedic Surgery, Rush University Medical Center, 60612 Chicago, IL, USA*
[6]*Department of Biomedical science, UIC school of Medicine at Rockford, 61107 Rockford, IL, USA*
[7]*IBTN/Br – Brazilian Branch of the Institute of Biomaterials, Tribocorrosion and Nanomedicine, UNESP – Universidade Estadual Paulista, Faculdade de Ciências, 17033-360 Bauru, São Paulo, Brazil*
[8]*Faculdade de Ciências, Departamento de Física, UNESP – Universidade Estadual Paulista, 17033-360 Bauru, São Paulo, Brasil*
[9]*Department of Materials Engineering, KU Leuven, 3001 Leuven, Belgium*
[10]*Department of Bioengineering, University of Illinois at Chicago, 60607 Chicago, IL, USA*
**e-mail:sofiafonso@msn.com*

Abstract

The modification of surface features such as nano-morphology/topography and chemistry have been employed in the attempt to design titanium oxide surfaces able to overcome the current dental implants failures. The main goal of this study is the synthesis of bone-like structured titanium dioxide (TiO_2) nanotubes enriched with Calcium and Phosphorous able to enhance osteoblastic cell functions and, simultaneously, display an improved corrosion behavior. To achieve the main goal, TiO_2 nanotubes were synthetized and doped with Calcium and Phosphorous by means of a novel methodology which relied, firstly, on the synthesis of TiO_2 nanotubes by anodization of titanium in an organic electrolyte followed by reverse polarization and/or anodization, in an aqueous electrolyte. Results show that hydrophilic bone-like structured TiO2 nanotubes were successfully synthesized presenting a highly ordered nano-morphology characterized by non-uniform diameters. The chemical analysis of such nanotubes confirmed the presence of $CaCO_3$, $Ca_3(PO_4)_2$, $CaHPO_4$ and CaO compounds. The nanotube surfaces submitted to reverse polarization, presented an improved cell adhesion and proliferation compared to smooth titanium. Furthermore, these surfaces displayed a significantly lower passive current in artificial saliva, and so, potential to minimize their bio-degradation through corrosion processes. This study addresses a very simple and promising multidisciplinary approach bringing new insights for the development of novel methodologies to improve the outcome of osseointegrated implants.

Keywords: Bio-functionalization; Anodization; Reverse polarization; TiO_2 nanotubes; Calcium-phosphorous surface; Osseointegrated implants.

3.1. Introduction

Dental implants are widely used to replace tooth loss due to decay, trauma or periodontal diseases [1]. Additionally, market demand has been increasing within the past years, both due to the aging of the population and to the success that dental implant therapies have reached [2], improving the life quality of people. However, a significant number of dental implant failures (1 – 20%) have still been described [3], which is the subject of main concern since revision surgeries are painful to patients and very expensive to companies. The growing demand along with the high failure rates further increase the interest on the improvement of quality, efficiency and lifetime of dental implants.

Commercially pure titanium (cp-Ti) and its alloys are the metallic materials most commonly used in dental implants due to their superior biocompatibility, mechanical properties and high corrosion resistance [4-8]. However, despite the outstanding properties, implant failures are often caused by the lack of a stable implant anchorage provided by direct bone-to-implant contact (i.e. osseointegration) [9]. Also, the release of metallic wear debris and corrosion products to implant surroundings, is a main problem.

Aiming to overcome the current difficulties, researchers have been working worldwide on the improvement of implant surface features through multidisciplinary approaches. Over the past years, it has been widely reported that implant surface topography, morphology, chemical composition and surface energy have a critical influence on cell adhesion, proliferation, differentiation and osteoblastic extracellular matrix expression [10-13], which are cellular functions dictating the success rate of osseointegration [14-17]. Therefore, surface modification treatments have been carried out in a concentrated effort to construct suitable biomimetic interfacial microenvironments able to improve cell-materials interactions generating bone in a faster and improved osseointegration process [2, 18-21]. In particular, special attention is being devoted to the modification of Ti features at a nanoscale level by mimicking the micro/nanostructures of natural bone [3, 18-20, 22]. Among the various surface modification techniques, electrochemical anodization of Ti has usually been used to synthesize biologically-inspired nanostructures [23, 24]. In particular, vertically aligned TiO_2 nanotubes created on Ti, have become increasingly popular to enhance adhesion, growth and accelerate the osteo-differentiation of mesenchymal stem cells [18]. Oh *et al.* [25] indicated that the presence of nanotube structures on Ti produced an interlocked cell structure created due to the improved adhesion of osteoblasts to nanotubular Ti oxide film, with the filopodia of the growing cells going

into the nanotube pores. Furthermore, such nanotubular Ti structure led to a significant acceleration in the growth rate of osteoblasts cells by up to 400 %. Beyond the excellent osteoblast adhesion and proliferation promoted by TiO_2 nanotubes, these structures have been suggested as a way to avoid the formation of fibrous tissue [20]. The occurrence of metallic implant corrosion is also an issue of main importance. Despite the high corrosion resistance of Ti materials, they are not inert to corrosive attack in presence of the aggressive biological environment [26, 27]. Corrosion ions/products may be released from the metallic implant to surroundings tissues, causing inflammation and local toxicity, resulting in tissue damage, implant loosening and need of a new surgery [18, 28-30]. Thus, the design of implant surfaces able to resist to corrosion attack is also an issue of main significance and, electrochemical anodization appears as a very promising way to address it. It is known that implant surface features significantly influence the electrochemical stability of the metallic implant when in contact with simulated body fluids. Very interestingly, in particular, TiO_2 nanotubes have also shown potential to prevent long term implant failure due to bio-corrosion [30, 31]. This behavior is related to the anodization of Ti which is characterized by the growth of a compact oxide film on its surface formed through a natural and intrinsic chemical bond between the oxide and Ti substrate [20, 32].

In an attempt to develop new strategies for the construction of biomimetic systems, various modifications have already been employed to TiO_2 nanotubes through thermal oxidation, coating deposition, hydrothermal treatments in saturated solutions for nanotube doping and drug-loading [10, 33]. Beyond the wide number of treatments already employed, no one has explored anodization as a possible way to modify the nanotube features and provide them multiple functionalities. Electrochemical anodization is a very versatile technique which allows the handling of the chemistry of the native TiO_2 layer by the incorporation of species such as calcium (Ca) and phosphorus (P), natively present in bone [34]. The benefits of Ca- and P-enriched Ti surfaces by anodization have already been demonstrated both *in vitro* by improving cell attachment, adhesion, and proliferation and *in vivo*, by accelerating the primary osteogenic response [13, 35, 36]. Additionally, Ca- and P-based Ti surfaces synthesized by anodization, have shown improved corrosion and wear resistant properties than untreated Ti [37-40].

In the present study, reverse polarization and electrochemical anodization of TiO_2 nanotubes were explored as a new strategy for the synthesis of multifunctional implant surfaces that can enhance osteoblastic cell functions and simultaneously, minimize their degradation by corrosion. To achieve this goal, bone-like structured TiO_2 nanotubes were synthetized and doped with Ca and P (Ca/P-doped TiO_2 nanotubes) by reverse polarization and/or anodization processes in an aqueous electrolyte containing Ca and P (Ca/P-electrolyte). Ca/P-doped

nanotubes were deeply characterized regarding their surface features as well as their biological and electrochemical properties.

3.2. Experimental details

3.2.1. Surface pre-treatment

Discs of commercially pure titanium (cp-Ti) grade 2 (American Society for Testing of Materials – Grade 2) (MacMaster-carr, IL, USA) of 15 mm diameter and 2 mm thickness were used as substrates used in this study. Firstly, the samples were ground with a series of silicon carbide (SiC) sandpapers #240, #320, #400, #600 and #800 (Carbimet 2, Buehler, Lake Bluff, IL, USA). Afterwards, the TexMet polishing cloth (TexMet Polishing Cloth, Beuhler, Lake Bluff, IL, USA) with diamond paste (MetaDi 9-micron, Beuhler, Lake Bluff, IL, USA) and lubricant fluid (MetaDi Fluid, Beuhler, Lake Bluff, IL, USA), followed by the Chemomet polishing cloth (Chemomet, Buheler, Lake Bluff, IL, USA) with colloidal silica polishing suspension (MasterMed, Buehler, Lake Bluff, IL, USA), were used to polish cp-Ti surfaces until mirror finishing. Lastly, all the samples were ultrasonically cleaned in ethanol (10 min), distilled (DI) water (5 min) and finally, they were dried at room temperature. These smooth cp-Ti samples were used as a control group in the present study and they were named as Ti.

3.2.2. Synthesis of well-ordered TiO_2 nanotubes

The nanotubes were obtained by anodization using a two-electrode set-up with Ti samples and a graphite rod as the working and counter electrodes, respectively. Both electrodes were connected to a power supply (Keithley 2400 SourceMeter, Cleveland, OH, USA) and immersed in an electrolyte constituted by Ethylene Glycol (EG) (Ethylene Glycol, Fisher Scientific, Pittsburgh, PA, USA), 0.3 wt. % ammonium fluoride (NH_4F) (Ammonium Fluoride, Sigma-Aldrich, St. Louis, MO, USA)) and 3 vol. % DI water. The distance between the working and the counter electrode was approximately 2 cm, and the electrolyte was continuously stirred at room temperature (22 to 24 ^oC). The nanotubes were produced by a two-step anodizing process. The first anodization was carried out upon Ti surfaces at a constant voltage of 60 V for 1 h. The resulting nanotubes were then removed by ultrasonication in isopropanol for 15 min and afterwards these substrates were rinsed in DI water and dried in air. The second anodizing step was then performed on these surfaces for 30 min under the same conditions, leading to the growth of well-ordered nanotubes named as NT. After this final step, NT surfaces were immediately gently rinsed with DI water and dried at room temperature.

3.2.3. Bio-functionalization of well-ordered TiO_2 nanotubes with Ca and P

TiO_2 nanotubes were submitted to functionalization treatments by reverse polarization and/or anodization, aiming at the incorporation of Ca and P species in its structure. In a first approach, the NT surfaces were used as the working electrode, and a graphite rod was the counter electrode. A constant voltage of 100 V was applied for 30 min between both electrodes immersed in an electrolyte composed of 0.35 M calcium acetate (CaA) (Calcium acetate monohydrate, Sigma-Aldrich, St. Louis, MO, USA) and 0.04 M β-glycerolphosphate (β-GP) (β-glycerolphosphate disodium salt pentahydrate, Sigma-Aldrich, St. Louis, MO, USA), named as Ca/P-electrolyte. These specimens were named as NT-Ca/P. As a second approach, aiming to improve the bioactivity of TiO_2 nanotubes, a reverse polarization step was also carried out. For that, right before the anodization in the Ca/P-electrolyte, the polarity of the electrodes was inverted. By this way, NT samples became the cathode and graphite rod became the anode. Reverse polarization was applied during 10 s at 20 V. After this time, the polarity of the electrodes was inverted again, and a constant voltage of 100 V was applied for 30 min with the samples immersed in the same electrolyte. These samples were named as NT-RP-Ca/P. The nanotubular samples subjected to functionalization treatments in Ca/P-electrolyte were named as Ca/P-doped nanotubes.

3.2.4. Surface characterization

The morphology of Ti, NT, NT-Ca/P and NT-RP-Ca/P surfaces was analyzed by Field Emission Scanning Electron Microscopy (FESEM) (JSM-6320F, JEOL, Musashino 3-chome Akishima Tokyo, Japan). For imaging, the different groups of samples were mounted on an aluminum stub with double sided conductive carbon tape. FESEM images from the top of the surfaces were obtained with 10,000 X and 40,000 X magnifications. The morphology of the cross-sections of the different groups of samples was also characterized by FESEM. Before FESEM observations, the cross-sections were polished using the standard metallographic preparation protocol described in section 2.1. The FESEM images were obtained with magnification of 5,000 X. From FESEM pictures, nanotube features such as diameter, wall thickness, and the length were measured using ImageJ software.

The surface topography of the samples was assessed via White-light Interferometry (NewView 6300, Zygo Corporation, Middlefield, Connecticut, USA). The average roughness (R_a) was measured, and a 3D profile of each surface was generated using an imaging analysis tool (Metropro 8.1.5), which is associated with the interferometer. The R_a values were calculated from a minimum of three independent measurements.

The elemental composition of the different groups of surfaces was determined by Energy-dispersive X-ray spectroscopy (EDS) using a JEOL JSM-6320F detector incorporated into the FESEM system. Furthermore, the binding states of the elements detected on nanotubular surfaces were investigated by X-ray Photoelectron Spectroscopy (XPS) by using Kratos AXIS-165 surface analysis system. To find out the functional groups present on Ti surfaces after functionalization treatments, Fourier Transform Infrared Spectroscopy (FTIR, Nicolet, Madison, WI, USA) was carried out. The range of FTIR spectra was of 4000 cm^{-1} to 400 cm^{-1} with 1 cm^{-1} resolution and 512 scans. Ti samples were used as a control.

Finally, water contact angle (WCA) measurements of the different groups of surfaces were performed by the sessile drop method using a contact angle measurement apparatus (CA Goniometer, Rame'-Hart NRL, Succasunna, NJ, USA) equipped with a camera imaging system. Prior to WCA measurements, the samples were cleaned with DI water followed by N_2 gas drying, at room temperature. For WCA, a 5 µl droplet of DI water was suspended on the surface using a micro-syringe (Hamilton, Reno, NV, USA). Pictures were collected from the camera, and the contact angle between the droplet and the substrate surface was calculated by ImageJ software. The WCA measurements were performed in triplicate, within a maximum period of 48 hours after nanotubular surfaces fabrication.

3.2.5. Electrochemical studies

Potentiodynamic studies were carried out in artificial saliva (AS) at 37 °C. The composition of AS is described elsewhere [41]. The samples were fixed in an electrochemical cell with the desired surface facing upwards. For these experiments, a three-electrode setup was used where the Ti samples were the working electrode, graphite was the counter electrode, and a saturated calomel electrode (SCE, 0.244 V *vs.* SHE) the reference electrode. Firstly, the samples were immersed AS (volume = 10 mL) for 3600 s for open circuit potential (OCP) stabilization. Afterwards, potentiodynamic polarization tests were carried out from -0.8 V until 1.8 V *vs.* SCE. The scan rate used for potentiodynamic polarization was 2 mVs^{-1}. The corrosion parameter evaluated from potentiodynamic polarization scan was the passive current (I_{pass}), which was determined from current measurements within the passivation region of the potentiodynamic scan. The experiments were carried out in triplicate for each group.

The electrochemical measurements were carried out with a potentiostat (Gamry Instrument, Reference 600) coupled to the framework software (Gamry Instrument) for monitoring the electrochemical data.

3.2.6. Biological characterization of Ca/P-doped TiO_2 nanotubes

3.2.6.1. Cell culture

MG-63 human osteosarcoma cells (ATCC number CRL-1427™) were used for cell-material interactions studies. MG-63 cells were cultured in standard plates (Treated cell culture dish, Falcon, Corning, NY, USA) in Dulbecco's High Glucose Modified Eagles Medium (DMEM High Glucose, HyClone, GE Healthcare Life Sciences, UT, USA). The culture medium was supplemented with 10 % (V/V) of Fetal Bovine Serum (FBS, Gibco, Life Technologies, NY, USA) and 1 % (V/V) of antibiotic (Anti-Anti, Gibco, Life Technologies, NY, USA) in a humidified atmosphere with 5 % carbon dioxide (CO_2), at 37 ˚C. The culture medium was changed every three days. At 80 % confluence, the adherent cells were enzymatically detached from the bottom of the culture dishes using 0.05 % (1X) trypsin (HyClone, GE Healthcare Life Sciences, UT, USA) and counted in a hemocytometer (Bright-Line, Hausser Scientific, PA, USA).

Before cell culture, all the materials were sterilized by immersion in ethanol 70 % (V/V) for 30 min and placed into standard 24-well culture plates (Falcon, Corning, NY, USA). Furthermore, it is important to highlight that *in vitro* studies were conducted in samples with the maximum of one week of aging, to avoid its effect on surface wettability.

3.2.6.2. Cell morphology

The morphology of adhered MG-63 cells on materials surface was observed by FESEM. For this, one mL of MG-63 cell suspension (2 x 10^4 cell/mL) was seeded on Ti, NT, NT-Ca/P and NT-RP-Ca/P samples, which were placed into 24-well culture plates. After one and six days of incubation at 37 ˚C in a 5 % CO_2 humidified atmosphere, the morphology of MG-63 cells was observed by FESEM. During incubation period, the culture medium was changed every three days. For FESEM observation, firstly, the cells were washed in phosphate-buffered saline (PBS, HyClone, GE Healthcare Life Sciences, UT, USA) and fixed with 2 % glutaraldehyde in sodium cacodylate buffer, pH 7.4 (Electron Microscopy Sciences, Pennsylvania, USA). Then, the cells were dehydrated using graded ethanol solutions from 35 % (V/V) to 100 % (V/V) followed by immersion in 100 % (V/V) hexamethyldisilazane (HMDS). The samples lasted 10 min in each ethanol and HMDS solution. Finally, the samples were placed onto an aluminum stub and sputter coated with gold. Then, the samples were observed by FESEM (JSM-6320F, JEOL, Musashino 3-chome Akishima Tokyo) with the acceleration voltage of 10 kV.

The cell morphology was also investigated by fluorescence microscopy. For this purpose, Ti, NT, NT-Ca/P and NT-RP-Ca/P samples were placed in 24-well culture plates and 1 mL of MG-63 cell suspension (2 x 10^4 cell/mL) was cultured on each surface. After one and six days of culture, MG-63 cells were labeled for actin filaments of cytoskeleton and nucleus, for

subsequent observation in the fluorescence microscope. For this, the cells were washed in PBS and fixed with a solution of 3.7 % (V/V) formaldehyde (Ricca Chemical Company, TX, USA) in PBS for 20 minutes. Afterwards, cells were washed in PBS and permeabilized with 0.1 % triton-X (Triton X-100, Fisher Scientific, Pittsburgh, PA, USA) in PBS, for 15 minutes. Then, 1 mL of PBS was added to each well and, ActinRed™ 555 ReadyProbes™ reagent (Molecular Probes, Life Technologies, NY, USA) was added to each well according to manufacturer instructions, for actin filaments labeling. After cytoskeleton staining, cells were washed in PBS and NucBlue Fixed Cell Stain ReadyProbes™ reagent (Molecular Probes, Life Technologies, NY, USA) was added to each well, according to manufacturer instructions. Finally, cells were washed with PBS solution and maintained in this solution for fluorescence microscopy observation.

3.2.6.3. Metabolic activity

Firstly, Ti, NT, NT-Ca/P and NT-RP-Ca/P samples were placed in 24-well culture plates (triplicates were used per condition). Afterwards, 1 mL of MG-63 cell suspension (4×10^4 cell/mL) was seeded on the surface of each sample and additionally, the cells were also cultured on the wells of the culture plates, for cell viability control. Then, the culture plates were placed in a 5 % CO_2 atmosphere at 37 °C for one and six days. The culture medium was changed every three days.

After each incubation period, the cellular metabolic activity was evaluated by measuring the mitochondrial dehydrogenase activity through MTT (3-(4,5-dimethyl-2-thiazolyl)-2,5-diphenyl-2H-tetrazolium bromide) reduction assay. The MTT assay allows the assessment of living and metabolically active cells by their reduction activity of the yellow MTT into soluble purple formazan product by mitochondrial dehydrogenase [11, 15, 42]. After one and six days of culture, the cells were incubated with MTT (0.5 mg/mL, Sigma-Aldrich, MO, USA) for 4 hours at 37 °C. The formazan crystals were solubilized in Dimethyl Sulfoxide (DMSO, Fisher Scientific, PA, USA) and the absorbance (Abs) was measured at λ = 570 nm and λ = 690 nm (background) on a microplate reader spectrometer (SpectraMax Plus 384 Microplate reader, Molecular Devices, CA, USA).

3.2.7. Statistical analysis

The results were expressed as means $\pm$ standard deviations (SD). The assays were performed in triplicate and, the minimum of three points was assessed on each sample. The statistical tool SigmaStat 3.5 (Systat Software, San Jose, CA, USA) was used for statistical analysis with $p < 0.05$ considered as being statistically significant and $p < 0.01$ considered highly significant. One-Way ANOVA was used to determine the differences between the different

groups of surfaces. Tukey HSD post hoc analysis was used for pair-wise comparisons between groups.

3.3. Results

3.3.1. Characterization of Ca/P-doped TiO_2 nanotubes

3.3.1.1. Morphology of TiO_2 nanotubular films

The substrates for nanotube growth were obtained by mechanical polishing of cp-Ti surfaces until mirror finishing (Fig. 3.1a). The synthesis of nanotubular films comprised of two-step anodization process. Upon first anodization step and ultrasonication, a nano-patterned surface with a concave morphology was formed as shown in Fig. 3.1b. Afterwards, these nano-imprints were used as the template for the second anodization step, resulting in the formation of NT surfaces characterized by well-defined and well-organized nanotube arrays, as depicted in Fig. 3.1c. Lower and higher magnification FESEM pictures show the presence of uniformly distributed nanotubes with non-uniform diameters along the surface area. It is also observed that NT surfaces are characterized by the absence of cracks. The morphology of the bottom of the nanotubes is depicted in Fig. 3.1d. The hexagonal packing density of nanotube arrays shows their high self-ordering level. As described in section 2.3, NT surfaces were subjected to anodization and reverse polarization treatments in a Ca/P-electrolyte, aiming the incorporation of the bioactive elements into nanotube structure. After these treatments, NT-Ca/P and NT-RP-Ca/P samples were synthesized, and their surface morphology is depicted in Figs. 3.2a and b, respectively. No differences in morphology were observed. From observation of Fig. 3.1c, Fig. 3.2a and Fig. 3.2b, it is clear that the morphological features on NT, NT-Ca/P and NT-RP-Ca/P surfaces, are similar. From these figures, diameter and wall-thickness were measured, and the results are depicted in Table 3.1. NT samples are characterized by nanotubes with an inner diameter of 74.1 $\pm$ 13.7 nm and a wall-thickness of 19 ± 4.6 nm. Similar values were found for nanotubes in NT-Ca/P (67.2 ± 13.4 nm diameter, 17.9 ± 3.7 nm wall-thickness) and NT-RP-Ca/P (59.8 ± 12.3 nm diameter, 18.5 ± 3.2 nm wall-thickness) samples.

Nanotubes vertically oriented from Ti substrate were produced, as shown in Fig. 3.3a. The inset arrow in the figure shows the growing direction of the nanotubes and delimits their length. The FESEM cross sectional images representative of the length of the nanotubular films present on NT, NT-Ca/P and NT-RP-Ca/P samples are depicted in Figs. 3.3b, c and d, respectively. The average values of the film thickness measured from FESEM images are shown in Table 3.1. Similar values of thickness were found for nanotubes on NT (12 ± 0.4 µm length) and NT-Ca/P (13 ± 1.6 µm length) samples. On the other hand, as observed in Fig. 3.3d, the length of the

nanotubular film on NT-RP-Ca/P samples was significantly lower, reaching 5.5 ± 0.1 µm (Table 3.1).

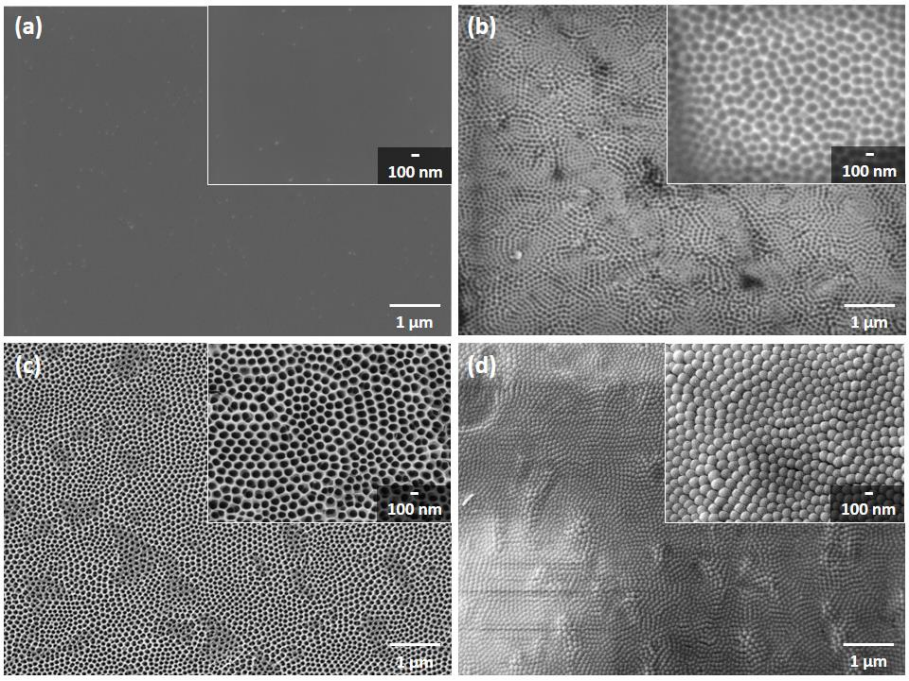

Fig. 3.1. FESEM micrographs of (a) Ti smooth and (b) nanopatterned Ti surfaces as a consequence of nanotube detachment after the first anodizing step. In (c) the FESEM image of well ordered TiO_2 nanotubes synthesised after the second anodizing step (NT surface) is shown, and finally, (d) the bottom morphology of the highly ordered nanotube arrays present on NT surfaces is observed. Higher magnification pictures are shown in the right upper corner of individual pictures.

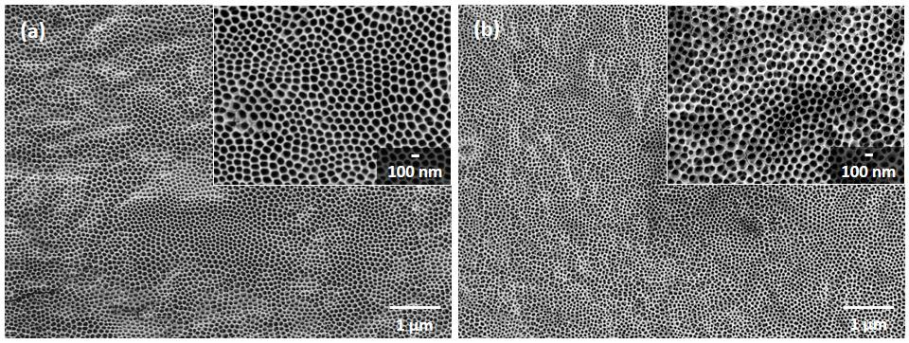

Fig. 3.2. FESEM micrographs showing the morphology of the highly ordered TiO_2 nanotubes present on (a) NT-Ca/P and (b) NT-RP-Ca/P surfaces. Higher magnification pictures are shown in the right upper corner of individual pictures.

Table 3.1. Diameter, wall-thickness and length of TiO_2 nanotube arrays on NT, NT-Ca/P and NT-RP-Ca/P samples.

Group	NT diameter (nm ± SD)	NT wall-thickness (nm ± SD)	NT length (µm ± SD)
NT	74.1 ± 13.7	19 ± 4.6	12 ± 0.4
NT-Ca/P	67.2 ± 13.4	17.9 ± 3.7	13 ± 1.6
NT-RP-Ca/P	59.8 ± 12.3	18.5 ± 3.2	5.5 ± 0.1*

(*) significantly different from NT and NT-Ca/P; $p < 0.001$.

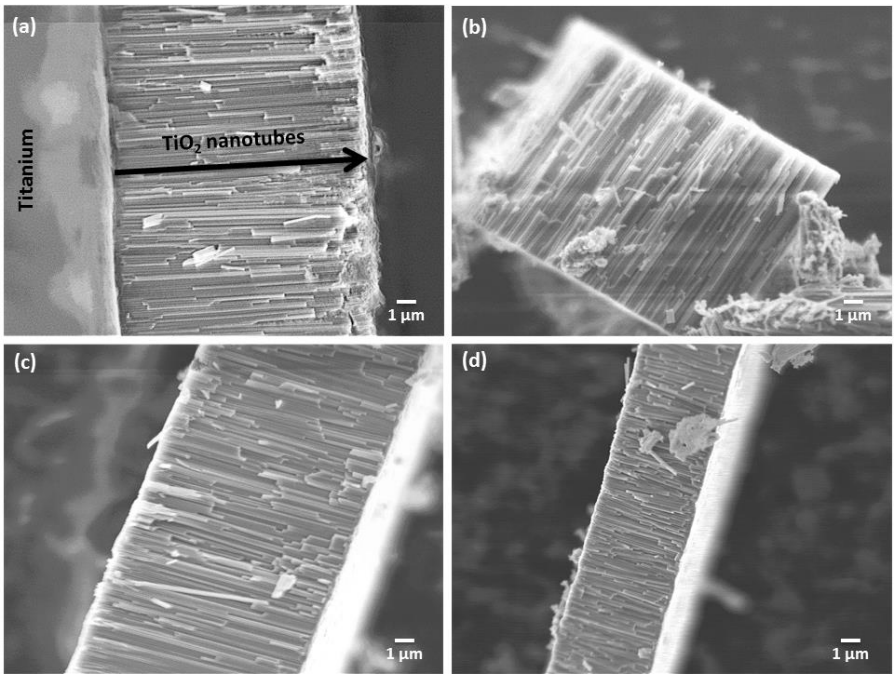

Fig. 3.3. Cross sectional FESEM image representative of TiO_2 nanotubes grown vertically oriented from Ti substrate. The inset indicates the growing direction of the nanotubes and and delimits their length. The length of the nanotubes is observed by FESEM images for (b) NT, (c) NT-Ca/P and (d) NT-RP-Ca/P samples.

3.3.1.2. Roughness

Average roughness (R_a) measurements of nanotubular films were extracted from three-dimensional (3D) surface topographies obtained from WLI. The 3D images of Ti, NT, NT-Ca/P and NT-RP-Ca/P samples are shown in Fig. 3.4 and the correspondent R_a values depicted in Table 3.2. It is clear from 3D images depicted in Figs. 3.4a and b that the surface topography of Ti is significantly different from NT surface as a result of the growth of a micron-length nanotubular film on Ti. These differences are reflected in the significant increase of the R_a values from 0.05 ± 0.01 µm to 7.40 ± 0.13 µm (Table 3.2). The 3D image of NT-Ca/P (Fig. 3.4c) as well its R_a value of 7.33 ± 0.47 µm (Table 3.2), show that they present similar topographical features to NT surfaces. On the other hand, the 3D image representative of NT-RP-Ca/P surfaces (Fig. 3.4d) shows that the reverse polarization step induced to a different film topography characterized by a significant lower R_a value (5.67 ± 0.10 µm). In general, a high surface uniformity of the nano-arrays grown from Ti was noticed.

Table 3.2. Average roughness (R_a) of Ti, NT, NT-Ca/P and NT-RP-Ca/P surfaces measured by WLI.

Group	Average roughness (R_a) (µm ± SD)
Ti	0.05 ± 0.01
NT	7.40 ± 0.13*
NT-Ca/P	7.33 ± 0.47*
NT-RP-Ca/P	5.67 ± 0.10$^{*\#}$

(*) significantly different from Ti; (#) significantly different from NT and NT-Ca/P; $p < 0.001$.

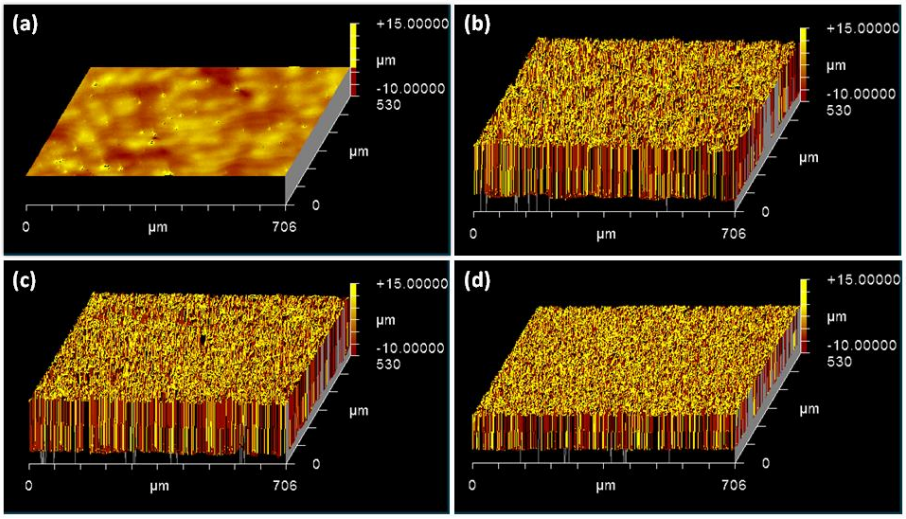

Fig. 3.4. Tridimensional topographies of (a) Ti, (b) NT, (d) NT-Ca/P and (e) NT-RP-Ca/P samples obtained from WLI measurements.

3.3.1.3. Chemical composition

The EDS spectra acquired from Ti and NT surfaces are shown in Fig. 3.5a and b, respectively. It is observed that after two-step anodization process, Oxygen (O) and Fluorine (F) were present on NT surfaces, beyond Ti and Carbon (C), elements that were also detected on Ti substrate. From EDS spectra of NT-Ca/P and NT-RP-Ca/P shown respectively in Figs. 3.5c and d, Ca and P elements were also detected in addition to the previously detected elements.

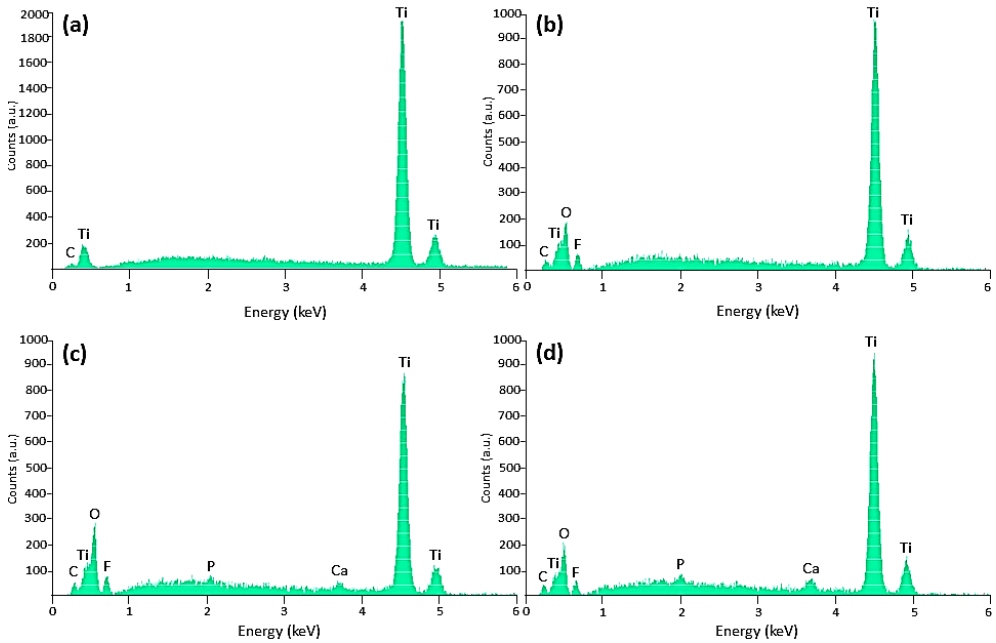

Fig. 3.5. EDS spectra of (a) Ti, (b) NT, (d) NT-Ca/P and (e) NT-RP-Ca/P samples.

The binding states of the chemical elements detected on nanotubular surfaces were studied by XPS. Chemical elements such as C 1s, Ti 2p, O 1s and F 1s were detected on NT

surfaces and the presence of Ca 2p and P 2p was confirmed on NT-Ca/P and NT-RP-Ca/P surfaces. Aiming to study the binding states of the detected elements, their individual spectra were deconvoluted into their components. C 1s peak at 284.6 eV was used as a reference binding energy for calibration [43] and a nonlinear (Shirley) background correction method was used for electron backgroung correction, which is the most commonly accepted and widely used [44]. The XPS individual spectra of the detected elements on NT, NT-Ca/P and NT-RP-Ca/P surfaces are shown in Fig. 3.6, 3.7 and 3.8, respectively. The deconvoluted peaks are shown in the individual spectra of the detected elements as well as the information obtained from deconvolution with reference to the subpeak binding energy and the possible chemical compound assigned to it, atomic percentage (at. %) and also to the chi square values (χ^2) associated to the deconvolution of each spectrum.

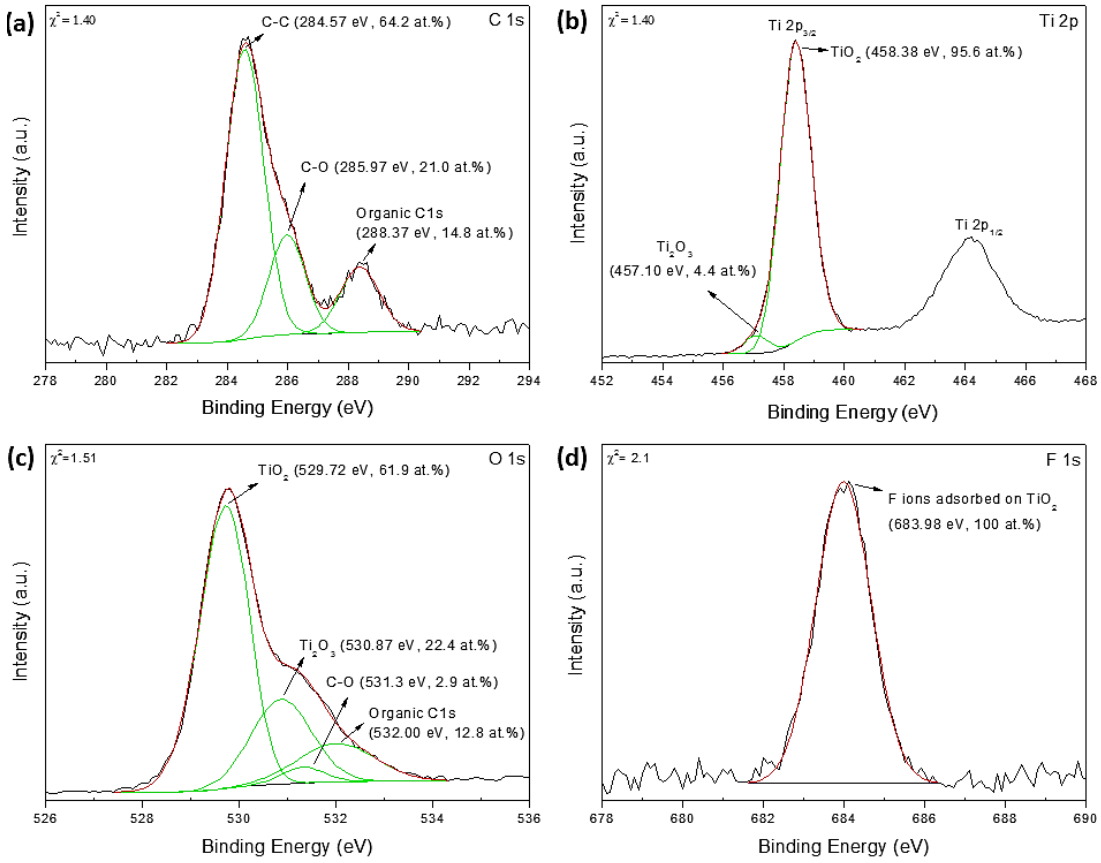

Fig. 3.6. High resolution XPS spectra of deconvoluted (a) C 1s, (b) Ti 2p, (c) O 1s and (d) F 1s elements detected on NT surface. The information obtained from deconvolution is shown in each individual spectrum with reference to the subpeak binding energy and the possible chemical compound assigned to it, atomic percentage (at. %) and also to the chi square values (χ2) associated to the deconvolution of the spectrum.

The presence of C-C and C-O groups and also organic C 1s was detected on all the nanotubular surfaces at similar binding energies, as shown in Figs. 3.6, 3.7 and 3.8. TiO_2 and Ti_2O_3 were present on all the surfaces, with a significantly higher at. % detected for TiO_2. Besides,

the presence of F ions adsorbed to TiO_2 nanotubes was found on all the groups. After functionalization processes through anodization of NT surfaces in the Ca/P-electrolyte, these were characterized also by the presence of CaF_2 and $CaCO_3$ compounds. Furthermore, $Ca_3(PO_4)_2$ and/or $CaHPO_4$ compounds were also found on NT-Ca/P and NT-RP-Ca/P surfaces. Interestingly, CaO appeared only on NT-RP-Ca/P surfaces, which means, when NT surfaces were submitted to reverse polarization process for 10 s, immediately before anodization in the Ca/P-electrolyte.

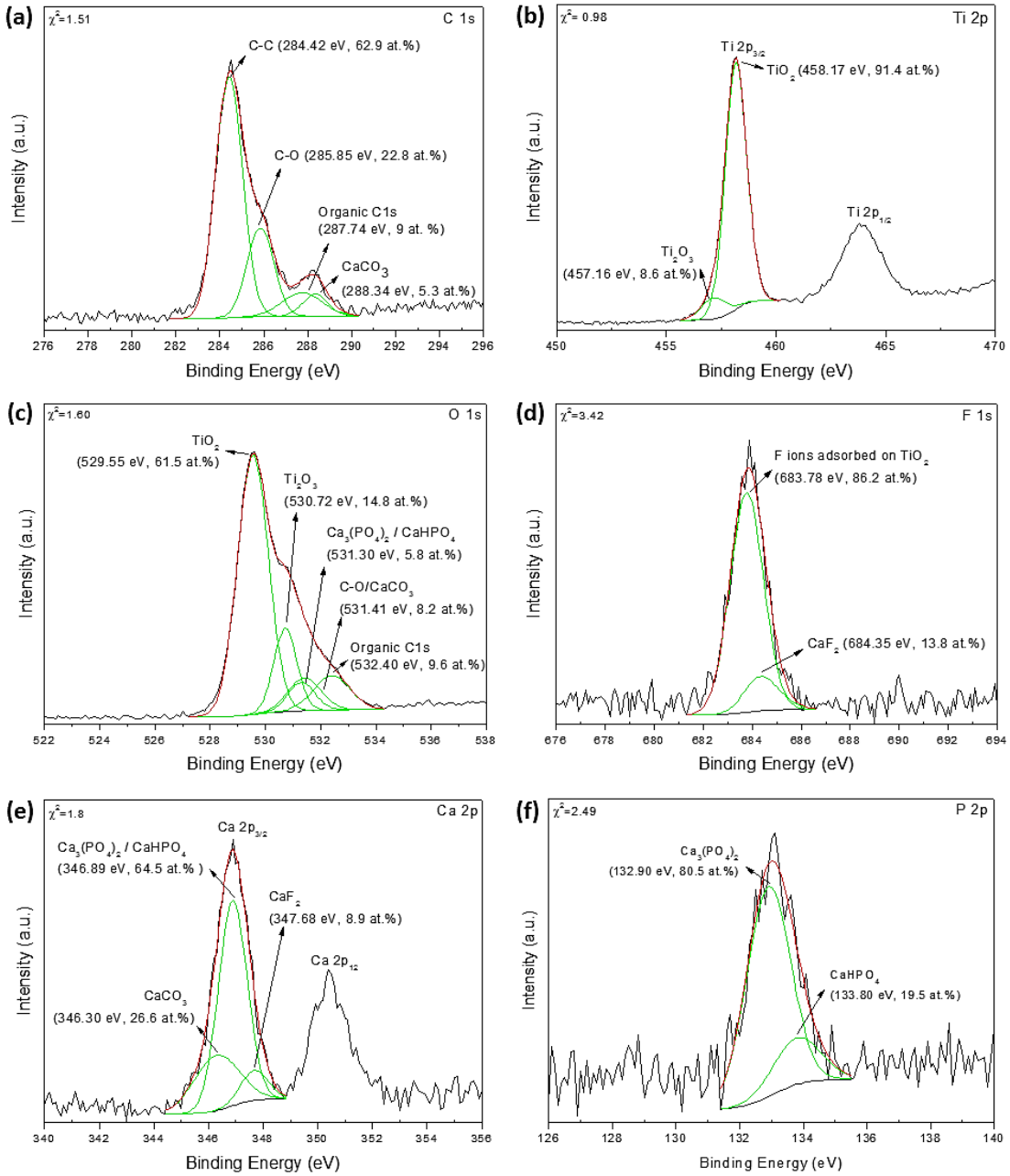

Fig. 3.7. High resolution XPS spectra of deconvoluted (a) C 1s, (b) Ti 2p, (c) O 1s, (d) F 1s, (e) Ca 2p and (f) P 2p elements detected on NT-Ca/P surface. The information obtained from deconvolution is shown in each individual spectrum with reference to the subpeak binding energy and the possible chemical compound assigned to it, atomic percentage (at. %) and also to the chi square values (χ2) associated to the deconvolution of the spectrum.

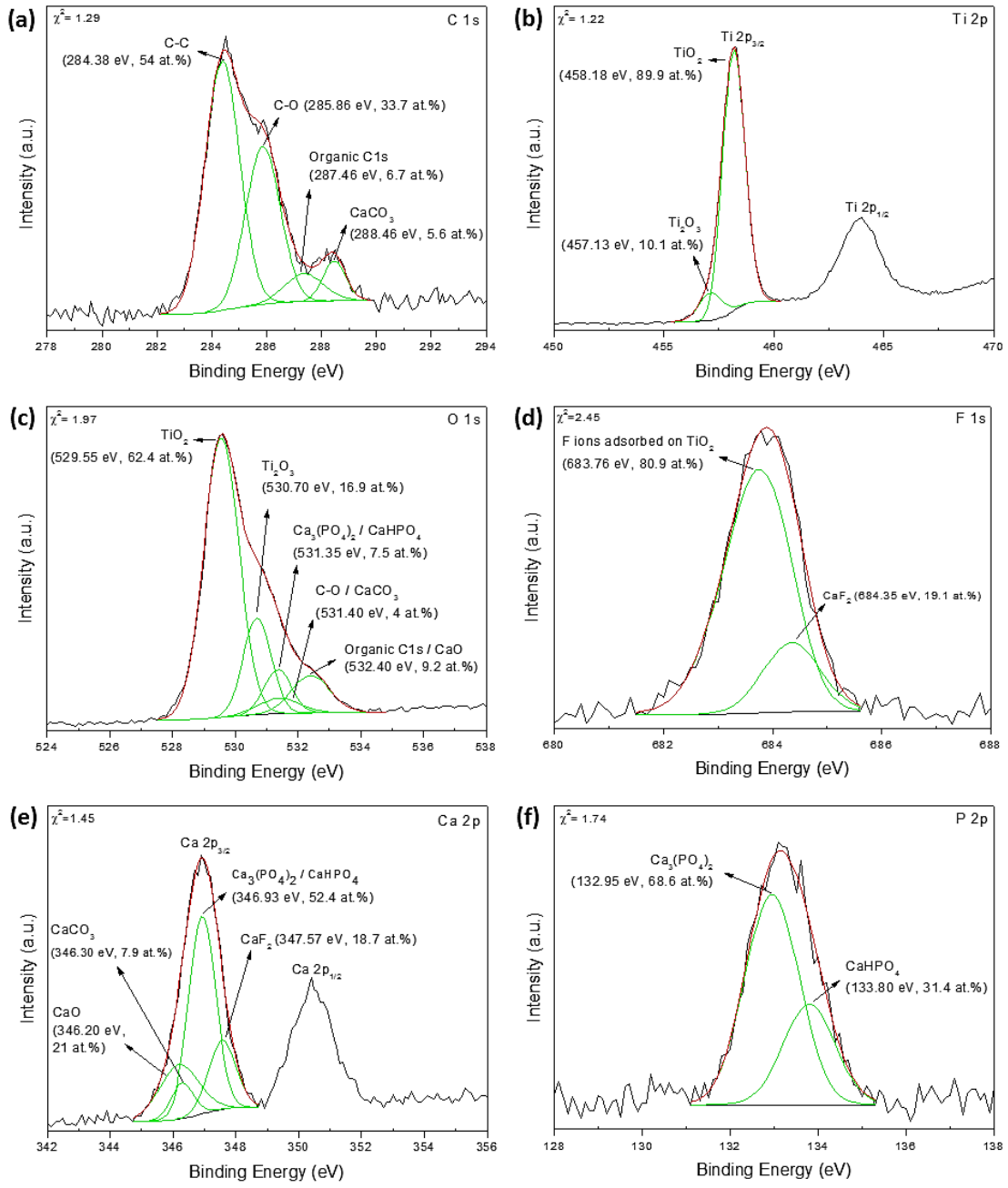

Fig. 3.8. High resolution XPS spectra of deconvoluted (a) C 1s, (b) Ti 2p, (c) O 1s, (d) F 1s, (e) Ca 2p and (f) P 2p elements detected on NT-RP-Ca/P surface. The information obtained from deconvolution is shown in each individual spectrum with reference to the subpeak binding energy and the possible chemical compound assigned to it, atomic percentage (at. %) and also to the chi square values (χ2) associated to the deconvolution of the spectrum.

The FTIR spectra of NT, NT-Ca/P and NT-RP-Ca/P surfaces are shown in Fig. 3.9. In all FTIR spectra H_2O (~ 3600-3800 cm^{-1}) and gas phase carbon dioxide (CO_2) absorption bands (~ 2200-2400 cm^{-1}) were detected, which resulted due to the residual air in the FTIR purging chamber [45-47]. Furthermore, the absorption band from ~ 3000-3500 cm^{-1}, is possibly attributed to fundamental stretching vibration of H_2O and OH groups [48-54]. The presence of CH_2 stretching modes was noticed at 2937.2 cm^{-1} and 2870.5 cm^{-1} for NT, NT-Ca/P and NT-RP-Ca/P surfaces. The region comprised between 1200-1900 cm^{-1} consists of the superposition of various

absorption bands. The absorption peaks at this region can be assigned to the bond stretch of NH_4^+ and adsorbed NH_3 on TiO_2 from the electrolyte [45]. Moreover, IR bands in the spectral range of 1300-1700 cm^{-1} may be an indicator of the presence of molecularly adsorbed O_2, CO_2, and CO molecules on TiO_2 [48]. The region between ~ 600-1200 cm^{-1} is also characterized by the superimposition of different absorption bands. According to different studies, this region is generally assigned to the presence of Ti-O, Ti-OH and TiO_2 [44, 45, 47]. Absorption peaks at 1018.5 cm^{-1} and 1086.4 cm^{-1} can be assigned to the presence of PO_4^{3-} groups on NT-Ca/P and NT-RP-Ca/P surfaces [55]. The absorption band at 1030.9 cm^{-1} may be related either to the presence of Ti-OH vibrations and PO_4^{3-} groups [45, 56, 57]. Finally, the presence of PO_4^{3-} groups can also be assigned to the absorption peak that appears at 972.2 cm^{-1} [56].

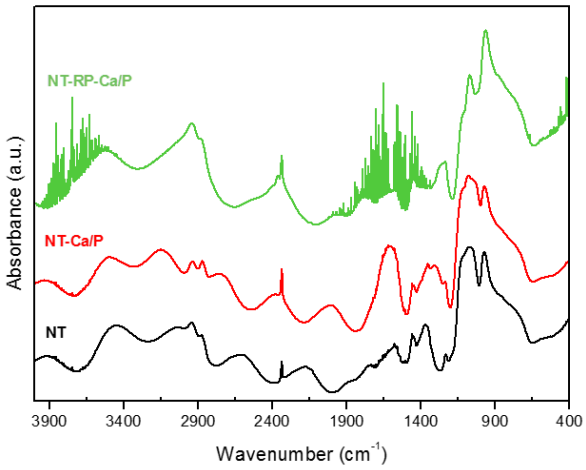

Fig. 3.9. FTIR spectra of NT, NT-Ca/P, and NT-RP-Ca/P surfaces. The different groups of surfaces are properly identified in the figure.

3.3.1.4. Wettability

The wettability of Ti and nanotubular surfaces was investigated by WCA measurements, and the results are depicted in Table 3.3. The WCA measured for polished Ti was of 45 ± 3.1 °, indicating that this surface is hydrophilic (WCA < 90 °) [58]. After anodization of Ti, the hydrophilicity of the surface was enhanced as shown by the significant decrease in the WCA measured for NT surfaces to 14.3 ± 2.2 ° ($p < 0.001$). The WCA measured for NT-Ca/P and NT-RP-Ca/P surfaces were 11.8 ± 2.8 ° and 10.5 ± 3.0 °, respectively. These values are similar to the ones measured on NT surfaces and significantly lower than WCA of Ti ($p < 0.001$).

Table 3.3. WCA measured on Ti, NT, NT-Ca/P and NT-RP-Ca/P surfaces.

Group	WCA (° ± SD)
Ti	45.4 ± 3.1
NT	14.3 ± 2.2 *
NT-Ca/P	11.8 ± 2.8 *
NT-RP-Ca/P	10.5 ± 3.0 *

(*) significantly different from Ti; $p < 0.001$.

3.3.2. Electrochemical studies

The potentiodynamic polarization curves of Ti, NT, NT-Ca/P and NT-RP-Ca/P surfaces are depicted in Fig. 3.10 and the current values extracted from the passivation region of these curves (I_{pass}), are listed in Table 3.4. The nanotubular surfaces exhibit a passive region extended over a wide potential range and display a fast and effective passivation behavior as compared to Ti, which is probably related to the effective blockage of the current provided by nanotubular films properties. The I_{pass} was similar for Ti and NT surfaces, however, NT-Ca/P and NT-RP-Ca/P surfaces revealed significantly lower I_{pass} values (Table 3.4), suggesting a higher corrosion resistance property [59].

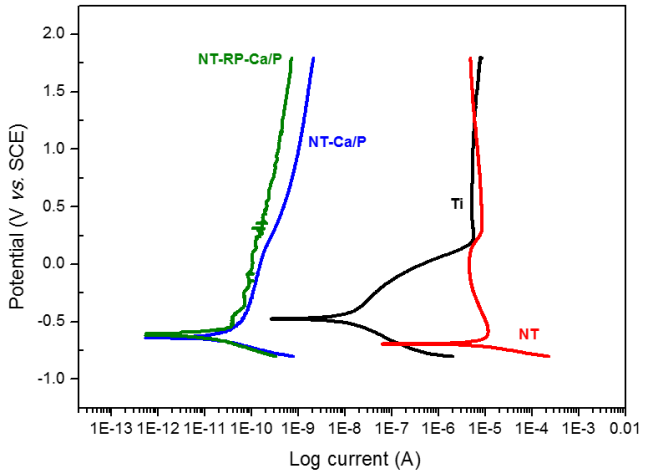

Fig. 3.10. Potentiodynamic polarization curves of Ti, NT, NT-Ca/P and NT-RP-Ca/P samples immersed in AS at 37 ˚C. Surface area exposed to AS: 0.4 cm^2; potential scan rate: 2 mVs^{-1}; potential scan from −0.8 to +1.8 V *vs.* SCE. The different groups of samples are properly identified in the figure.

Table 3.4. Passive current (I_{pass}) values measured from potentiodynamic polarization curves of Ti, NT, NT-Ca/P and NT-RP-Ca/P samples immersed in AS at 37 ˚C.

Group	I_{pass} (A)
Ti	$5.47 \times 10^{-6} \pm 1.79 \times 10^{-7}$
NT	$6.86 \times 10^{-6} \pm 1.59 \times 10^{-6}$
NT-Ca/P	$2.88 \times 10^{-10} \pm 3.59 \times 10^{-11}$*
NT-RP-Ca/P	$1.10 \times 10^{-9} \pm 4.40 \times 10^{-7}$*

(*) significantly different from Ti and NT; $p < 0.001$.

3.3.3. Biological characterization of Ca/P-doped TiO_2 nanotubes

3.3.3.1. Morphology of MG-63 cells

MG-63 cells adhered on Ti, NT, NT-Ca/P and NT-RP-Ca/P surfaces were imaged by FESEM aiming to access their morphology as well as their interaction with materials surface. In Fig. 3.11 the correspondent FESEM micrographs are shown, after one and six days of incubation. As observed in Fig. 3.11 (a1, b1, c1 and d1) cells adhere on the materials surface after one day of incubation, presenting different morphologies. Cells adhered on Ti surfaces (Fig. 3.11 a1) seem

less spread than the ones adhered on nanotubular surfaces (Figs. 3.11 b1, c1 and d1). The cells on nanotubular surfaces present a spreader morphology, and they are interconnected. It should be noticed that at this time point, the osteoblastic cells adhered on materials surface present filopodia forming adhesion points at the surface and establishing cell-cell contact as demonstrated by the inserts included in higher magnification FESEM micrographs. After six days of incubation, there is an increased number of adhered cells as observed on each different group in Fig. 3.11 (a2, b2, c2 and d2). At day six the materials surface is covered by an abundant cell layer, and all the cells seem well spread and interconnected.

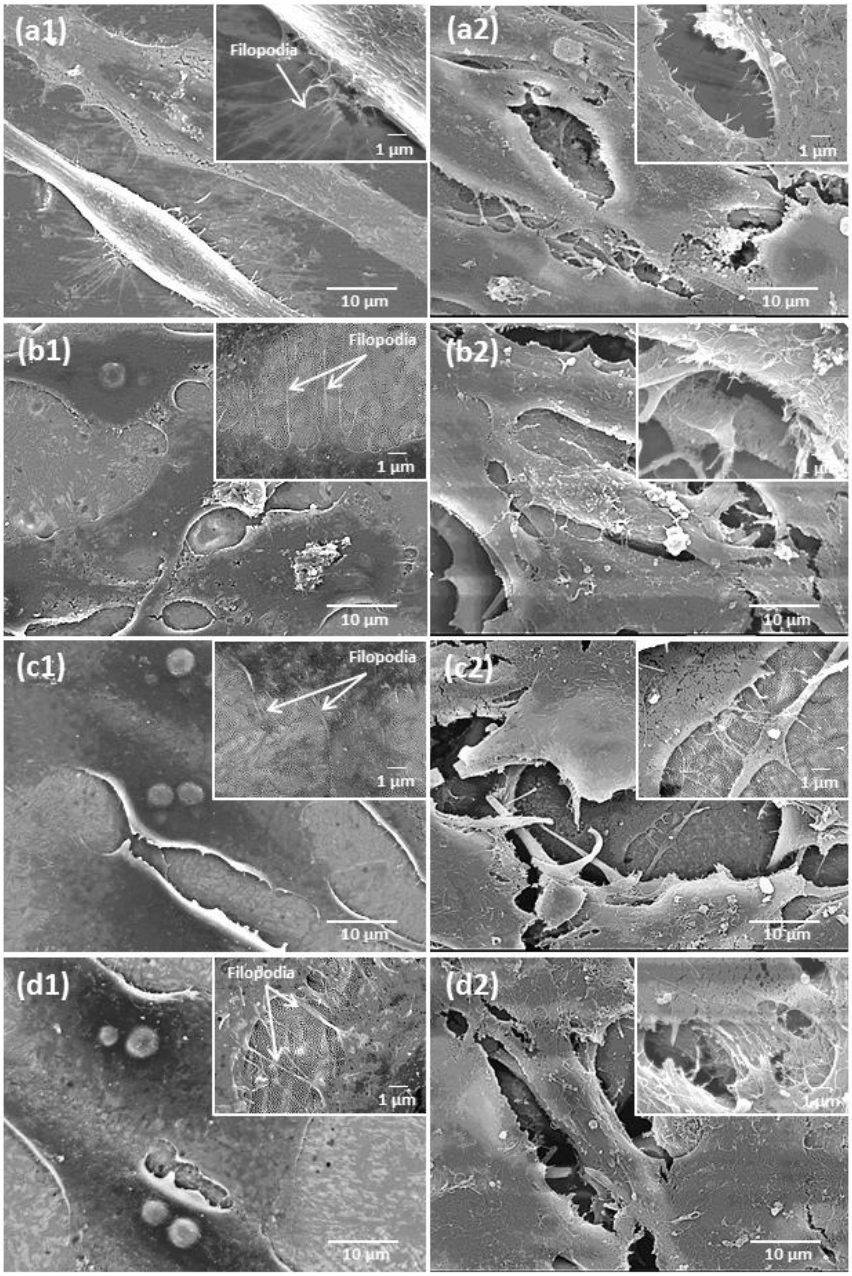

Fig. 3.11. FESEM micrographs of MG-63 cells cultured on Ti, NT, NT-Ca/P and NT-RP-Ca/P surfaces after one and six days of incubation: MG-63 cells on (a1) Ti, (b1) NT, (c1) NT-Ca/P and (d1) NT-RP-Ca/P surfaces – day one ; MG-63 cells on (a2) Ti, (b2) NT, (c2) NT-Ca/P and (d2) NT-RP-Ca/P surfaces – day six.

Fluorescence microscopy images of MG-63 cells adhered on Ti, NT, NT-Ca/P and NT-RP-Ca/P surfaces, after one and six days of incubation, are depicted in Fig. 3.12. After one day of culture (Figs. 3.12 a1, b1, c1 and d1), the cells already adhered on materials surface, and a similar number of cells seems to be present on all the groups. At this time point, adhered cells present spherical, spread and elongated morphologies. In general, cell-to-cell contact is observed to a large extent. After six days of culture, there is an increase in the number of the adhered cells except for NT-Ca/P surfaces as shown in Fig. 3.12 (a2, b2, c2 and d2). In Fig. 3.12 c2 it is observed that MG-63 cells are more scarcely distributed presenting a less spread morphology along NT-Ca/P surfaces as compared to the other groups.

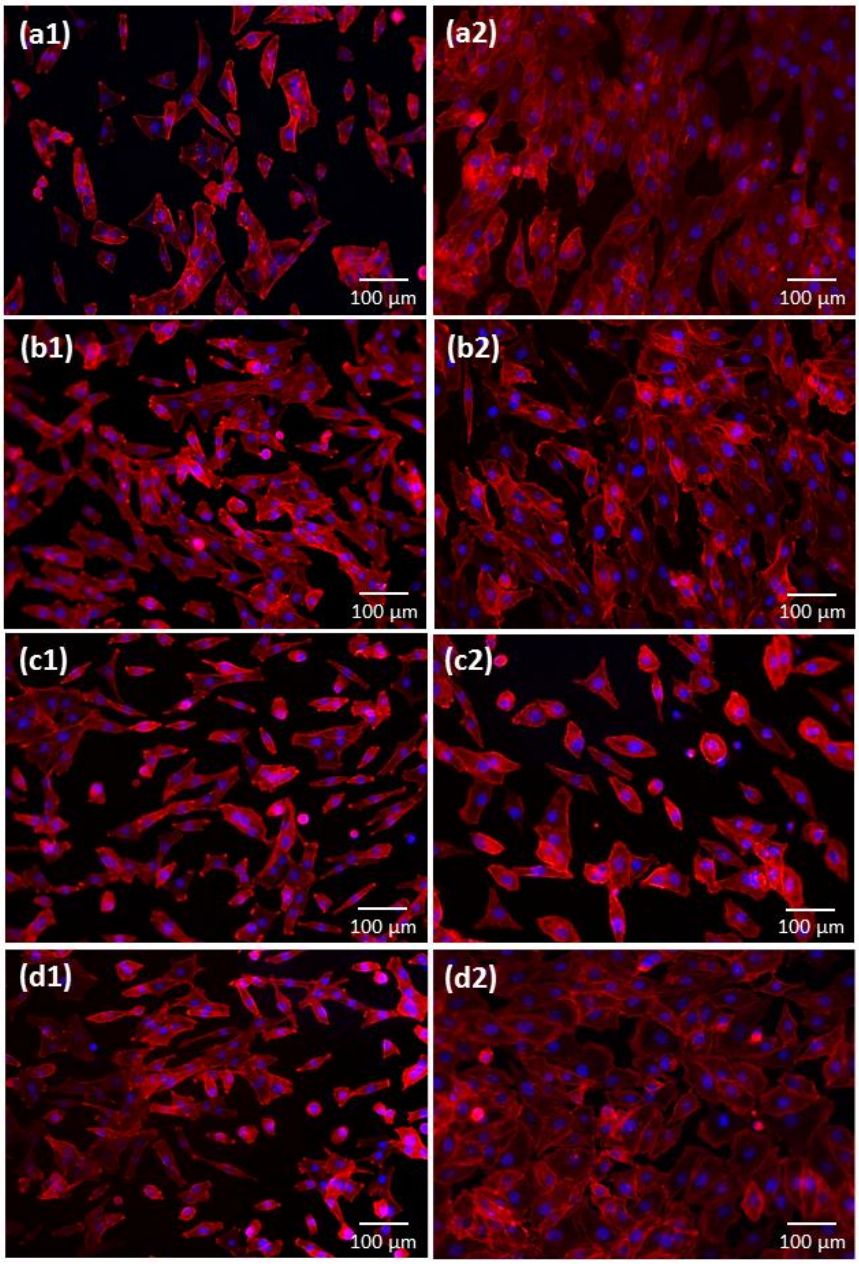

Fig. 3.12. Fluorescence microscopy images of MG-63 cells cultured on Ti, NT, NT-Ca/P and NT-RP-Ca/P surfaces after one and six days of incubation: MG-63 cells on (a1) Ti, (b1) NT, (c1) NT-Ca/P and (d1) NT-RP-Ca/P surfaces – day one ; MG-63 cells on (a2) Ti, (b2) NT, (c2) NT-Ca/P and (d2) NT-RP-Ca/P surfaces – day six.

3.3.3.2. Metabolic activity of MG-63 cells

The metabolic activity of MG-63 cells seeded on Ti, NT, NT-Ca/P and NT-RP-Ca/P surfaces was investigated by MTT reduction assay after one and six days of incubation and the correspondent absorbance values are shown in Fig. 3.13. Once MTT reduction is attributed to mitochondrial succinate dehydrogenase redox activity, the absorbance values are proportional to cell metabolism, and therefore, cell viability. Additionally, an increase in cell viability is an indicator of cell proliferation [11, 60].

At day one of culture, MG-63 cells present a similar metabolic activity level as shown by the similar absorbance values depicted for all the groups (Fig. 3.13). At day six, the absorbance values significantly increased for all the materials, suggesting that the metabolic activity increased and that cells proliferated with time. However, remarkable differences are observed between the different groups. At this time point, the cells cultured on NT-RP-Ca/P present significantly higher metabolic activity than NT-Ca/P and Ti, and similar to NT surfaces.

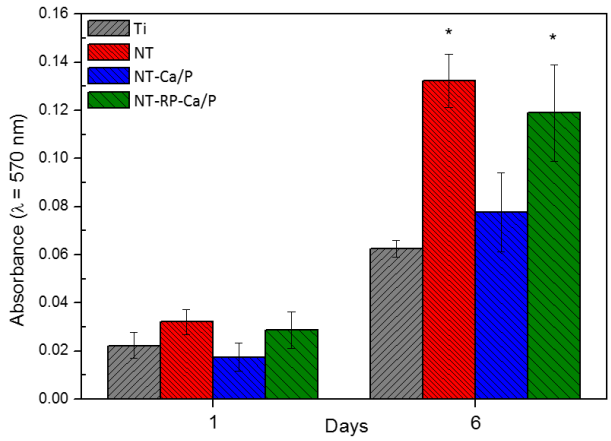

Fig. 3.13. Metabolic activity of MG-63 cells cultured on Ti, NT, NT-Ca/P and NT-RP-Ca/P surfaces after one and six days of incubation. At day six: (*), significantly different from Ti and NT-Ca/P; $p < 0.05$.

3.4. Discussion

3.4.1. Morphological and topographical features of Ca/P-doped TiO_2 nanotubes

It is commonly accepted that the mechanism for nanotube formation by anodization in a fluoride-containing electrolyte is based on a field-assisted dissolution process consisting of two main stages: 1) the anodic oxidation of Ti metal to form a passive Ti oxide film on its surface by the recombination of Ti^{4+}, O^{2-} and OH^- ions, moving under the action of an electric field and, 2) the local chemical dissolution of the growing oxide by fluoride ions (F^-) and pore formation [24, 61-63]. This process assumes that the growth of nanotubes is ensured by the balance between the formation of a oxide barrier film at the metal-oxide interface and, the field-enhanced dissolution at the base of the pores/tubes, where the electric field is stronger [63].

It is already documented in literature that the self-ordering of TiO_2 nanotubes is improved after multi-step anodic oxidation processes [64]. As stated by Serikov *et al.* [65] the repeated anodization of titanium, is one way of structuring the surface, removing contaminants and increasing the adhesion of the synthesized nanotubes. Based on this knowledge, in this study, nanotubular structures were synthesized using a two-step anodization process. Firstly, the nanotubes were produced by anodization of Ti polished surfaces (Fig. 3.1a). After this step, the nanotube layer grown from Ti was intentionally ultrasonically peeled off aiming at the formation of a nano-patterned surface presenting concave dimples (Fig. 3.1b), the common shape of the nanotube bottom [64]. These hemispheric nano-imprints were used as the template for the second anodizing step, once they acted as nucleation sites for the initial pore formation [66, 67] required for the growth of highly ordered nanotube arrays. The surface produced after the second anodizing step was named as NT and it is characterized by well-defined and well-organized nanotubes as shown in lower and higher magnification FESEM pictures in Fig. 3.1c. On the NT surface the absence of cracks and the presence of uniformly distributed nanotubes with non-uniform diameters along the surface area are noticed.

From nanotube bottom morphology depicted in Fig. 3.1d the hexagonal packing density of nanotube arrays is clearly appearing, which allows the evaluation of the self-ordering of the nanotubular film produced. Han *et al.* [64] synthesized well-ordered TiO_2 nanotubes by a multi-step anodic oxidation process carried out at 50 V for 5 hrs, in EG electrolyte containing 0.25 wt.% NH_4F. The authors concluded that the hexagonal packing density of the TiO_2 nanotubes was significantly improved after the multi-step anodic oxidation. These authors also reported that the area densities of the hexagonal TiO_2 arrays increased approximately three times from the first to the second anodic oxidation step. According to Sulka *et al.* [68] in an ideally arranged triangular lattice, each pore should be surrounded by six neighboring pores. When looking at Fig. 3.1d, it is observed that nanotube arrays with hexagonally packed arrangement are present over a large surface area. From the above discussed results, the morphological features of the nanotubes are highly dependent on the morphology of the nano-patterned substrates from where they were grown.

The morphological and surface topographical features of osseointegrated implants play a significant role on the mechanical stability of the implant once allocated into bone as well as on the healing and osseointegration processes. In the natural bone tissue, a non-uniform porosity due to the existence of cortical (3-12 % porosity, pore sizes: 10-500 μm) and trabecular bones (50-90 % porosity, pore sizes: 0.2-1 mm) is noticed. Interestingly, NT surfaces are also characterized by non-uniform pore diameters, varying at a nano-scale level and presenting a very similar morphology when compared to the structure of natural bone. Considering that

natural bone is a nanostructured material [69] and bone tissue response is mainly dictated by processes controlled at the nanoscale level [32], it is hypothesized that mimicking the microstructure of bone at a nano-scale level is an interesting approach for the development of a novel surface able to improve the performance of osseointegrated implants. Furthermore, in the attempt to develop a new strategy for obtaining biomimetic systems mimicking the natural extracellular microenvironments, the functionalization of TiO_2 nanotubes with elements natively present in natural bone, namely, Ca and P, was carried out using anodization of NT surfaces in an electrolyte composed of CaA and β-GP (Ca/P-electrolyte). Using this process, the incorporation of bioactive elements present in the anodizing solution into nanotube structure was aimed. As described in section 2.3, a cathodic polarization step was also applied to NT samples, right before the anodizing process in the Ca/P-electrolyte. With this the cathodic polarization step, it was intended to direct Ca^{2+} ions to NT surface for further incorporation of these elements into nanotube structure. After the anodizing processes carried out in both conditions, NT-Ca/P and NT-RP-Ca/P samples were synthesized, and their surface morphologies are depicted in Figs. 3.2a and b, respectively. Well-ordered and opened nanotubes, cleared of any aggregations are observed in both cases. From observation of Fig. 3.1c and Fig. 3.2, it is clear that NT, NT-Ca/P and NT-RP-Ca/P samples display similar morphological features, as confirmed by diameter and wall thickness measurements reported in Table 3.1. The novelty of this method and what distinguishes it from other bio-functionalization processes commonly reported in literature [10, 33], lies on the usage of NT samples as the cathode and, immediately after, as the anode, in the electrochemical cell.

It has been reported that cell fate is determined by the TiO_2 nanotube sizes *in vitro*, but optimum scale is still controversial. Wang *et al.* [6] reported that a significant increase in bone implant contact and gene expression levels was found in the bone attached to TiO_2 nanotubes, especially with 70 nm diameter. On the other hand, Park *et al.* [4] demonstrated that adhesion, proliferation, migration and differentiation of MSCs was maximally induced on 15 nm nanotubes, but prevented on 100 nm. In our study, non-uniform pore diameter ranging at a nano-scale level between 45 and 90 nm were formed, with potential to improve cell-materials interactions.

The representative picture of the nanotubes grown vertically oriented from the Ti substrate is shown in Fig. 3.3a. As observed from cross sectional images representative of the length of NT and NT-Ca/P nanotubular films (Fig. 3.3b and 3.3c, respectively), and from the correspondent values in Table 3.1, nanotubes with similar thickness were formed. These results indicate that the second anodizing process did not influence the length of the nanotubular film present on NT surfaces. On the other hand, the length of NT-RP-Ca/P nanotubes was significantly lower (Fig. 3.3d) what might be attributed to the reverse polarization step applied on the NT

samples during 10 s in the Ca/P-electrolyte. For reverse polarization step, the polarity of the electrodes was inverted. By this way, NT samples became the cathode and the graphite rod, the anode. According to Abellán *et al.* [70], the passive titanium oxide film might undergo different processes when submitted to cathodic polarization: various stages of oxide reduction up to oxide dissolution, the adsorption and absorption of hydrogen, hydrogen evolution, and oxygen reduction. It has been reported that when a titanium electrode covered with TiO_2 film is polarized in the potential range where hydrogen evolution reaction takes place, a decrease in film thickness occurs. This phenomenon is produced by the partial reduction of the Ti^{4+} present in TiO_2 film to Ti^{3+} in oxy-hydroxi species [71]. The cathodic potential of -0.6 V *vs. SCE* is considered as the potential that can render the protective oxide ineffective as a barrier by reducing it from TiO_2 to TiOOH. In the present work the cathodic cell potential of 20 V was applied to NT samples for 10 s. After this process, there was a significant decrease in the thickness of the nanotubular film. It is believed that the reactions which cause the thinning phenomenon of the film involved a high level of chemical dissolution of the TiO_2 nanotubular film due to the high cathodic potential applied during the process. Most probably, the dissolution occurred due to the reduction of TiO_2 nanotubes into oxy-hydroxi species [71, 72], which may be dissolved in the electrolyte or precipitate at the top of the film [71].

The average roughness (R_a) of nanotubular films was extracted from three-dimensional (3D) surface topographies obtained from WLI. A high level of uniformity of the nano-arrays growth from Ti is noticed from the 3D images (Fig. 3.4). These images reflect the phenomenon of film thinning by reverse polarization step. The significantly lower thickness of nanotubes is reflected on 3D image of NT-RP-Ca/P sample (Fig. 3.4d) and also on the correspondent R_a value (Table 3.2), which is significantly lower than the ones measured for NT and NT-Ca/P surfaces.

3.4.2. Chemical and physico-chemical features

After the two step anodization process, Ti, O, and F were detected on NT surfaces by EDS (Fig. 3.5b) and XPS (Fig. 3.6). The existence of these elements on NT surfaces is related to growth of an oxide film via anodization of Ti in a F-containing electrolyte. During anodization of Ti, its oxidation takes place with release of Ti^{4+} ions and electrons. The anodic potential applied during the process controls the rate of ion migration within the metal/electrolyte interface. The Ti^{4+} ions can be consumed for the film development by their recombination with OH^- and O^{2-} species provided by the field-assisted water dissociation, and/or field-assisted driven from the Ti substrate towards the electrolyte [63, 73]. This can result in the formation of oxide (i.e. TiO_2) or hydrated oxide (i.e. $Ti(OH)_4$). The fluorine ions present in the electrolyte can chemically dissolve both the hydrated and oxide layers, or react with Ti^{4+} ions [63, 73]. For NT-Ca/P and NT-RP-Ca/P

surfaces, Ca and P elements were also detected by EDS (Figs. 3.5c and d) and XPS (Figs. 3.7 and 3.8). This shows that after anodization processes carried out in the Ca/P-electrolyte, bioactive elements were successfully incorporated in nanotubular surfaces.

To investigate the chemical compounds possibly assigned to the detected elements, the individual XPS spectrum of each element was resolved into their components by curve fitting.

Fig. 3.6a shows the deconvolution of C 1s main peak on NT surface into three subpeaks characterizing the chemical states of carbon. The sub-peak at 284.57 eV is generally assigned to the presence of adventitious carbon [74-76] inevitable adsorbed from the atmosphere while the C 1s subpeaks at 285.97 eV and 288.37 eV may be related to C-O bonds and organic C 1s, respectively [76-78]. Carbon was also detected on TiO_2 nanotube arrays synthesized by Han *et al.* [64] at similar anodizing conditions of the present study. The authors explained that carbon was associated to species such as hydrocarbon (C-H), hydroxyl (C-OH) and carboxyl (O=C-OH) groups. This is in good agreement with FTIR results with IR bands in the spectral range of 1300-1700 cm^{-1} as an indicator of the presence of molecularly adsorbed CO groups on TiO_2 (Fig. 3.9). The deconvolution of the high resolution spectra of Ti $2p_{3/2}$ and O 1s confirms the presence of TiO_2 by the contributions found at 458.38 eV (Fig. 3.6b) and 529.72 eV (Fig. 3.6c), respectively. These peaks are characteristic of Ti $2p_{3/2}$ and O 1s in TiO_2 as already reported in previous studies [44, 74, 75, 79-83]. A characteristic band for TiO_2 was also found in FTIR spectrum in the region between ~ 600-1200 cm^{-1} (Fig. 3.9). As shown in Fig. 3.6b the subpeak energy found for Ti $2p_{3/2}$ at 457.10 eV [54, 74] is possibly related to Ti_2O_3 what is in accordance with the subpeak found for O 1s at 530.87 eV (Fig. 3.6d). Notwithstanding that, from curve fitting analysis of Ti $2p_{3/2}$ and O 1s main peaks, it is observed that the main contribution is coming from TiO_2. From Fig. 3.6d it is possible to identify a peak for F 1s at 683.98 eV, which is assigned to adsorbed fluoride ions on TiO_2 [44, 84].

In Fig. 3.7a it is observed that C 1s was detected in NT-Ca/P samples at four different binding states namely at 284.42 eV (C-C groups), 285.85 eV (C-O groups), 287.74 (Organic C 1s), and finally, at 288.34 eV, which is possibly assigned to the presence of $CaCO_3$ [85]. Ti $2p_{3/2}$ components were found at 458.17 eV (TiO_2) and 457.16 eV (Ti_2O_3) as observed in Fig. 3.7b, and the O 1s binding energies for TiO_2 and Ti_2O_3 were detected at 529.55 eV and 530.30 eV, respectively (Fig. 3.7c). The O 1s and Ca $2p_{3/2}$ core levels for $CaCO_3$ were found at 531.41 eV (Fig. 3.7c) and 346.3 eV (Fig. 3.7e), respectively [52]. Adsorbed fluoride ions on TiO_2 were detected at 683.78 eV (Fig. 3.7d). The anodization of TiO_2 nanotubes in Ca/P-electrolyte allowed the nanotubular surface enrichment with Ca and P elements. The Ca $2p_{3/2}$ peak detected at 346.89 eV (Fig. 3.7e), in agreement with P 1s peak at 132.9 eV (Fig. 3.7f), are most probably related to the presence of $Ca_3(PO_4)_2$ compounds on TiO_2 nanotubes [52, 86]. Moreover, the energy found

at 346. 30 eV may be also related with the presence of $CaHPO_4$ species, which were confirmed by the existence of a contribution for P 2p at 133.80 eV [52]. Furthermore, the O 1s binding energy at 531.3 eV (Fig. 3.7c) is corroborating the presence of $Ca_3(PO_4)_2/CaHPO_4$ species [52]. The presence of PO_4^{3-} groups can also be proved by the absorption peaks found in FTIR spectrum at 972.2 cm^{-1}, 1018.5 cm^{-1} and 1086.4 cm^{-1} (Fig. 3.9). Most likely, during anodization in Ca/P-electrolyte, Ca^{2+} ions reacted with negatively charged PO_4^{3-} and CO_3^{2-} to form the Ca-based compounds above mentioned. Finally, it is believed that anodization of nanotubes leads to the formation of CaF_2 species as found by energies detected for Ca $2p_{3/2}$ and F 1s at 347.68 eV (Fig. 3.7e) and 684.35 eV (Fig. 3.7d), respectively [87]. C 1s species similar to those detected on NT-Ca/P were found also on NT-RP-Ca/P surfaces at similar binding energies (Fig. 3.8a). Once again, a high percentage of TiO_2 was detected in Ti $2p_{3/2}$ and O 1s spectra at 458.18 eV (Fig. 3.8b) and 529.55 eV (Fig. 3.8c), respectively. Ti_2O_3 was found in a lower at. % in Ti $2p_{3/2}$ spectrum at 457.13 eV (Fig. 3.8b) and at 530.7 eV in O1s spectrum (Fig. 3.8c). NT-RP-Ca/P surfaces were submitted to a reverse polarization step during 10 s in the Ca/P-electrolyte, in which, afterwards, they were immediately anodized at 100 V for 30 min. As observed in Fig. 3.7 and 3.8, similar compounds were detected on NT-RP-Ca/P comparing to NT-Ca/P surfaces, such as $CaCO_3$, $Ca_3(PO_4)_2/CaHPO_4$ and CaF_2. However, it should be noticed that an additional peak was found in Ca $2p_{3/2}$ spectrum at 346.20 eV (Fig. 3.8e) and it is most likely assigned to the presence of an additional chemical compound formed, namely, CaO. The O 1s core level for CaO was observed at 532.4 eV (Fig. 3.8c). These results indicate that reverse polarization is a promising treatment to be applied before anodization process leading possibly to the formation of additional compounds on materials surface, in this case, CaO on NT-RP-Ca/P surface.

The surface wettability is influenced by the surface characteristics such as surface roughness, chemistry and surface free energy [45, 88-91]. Different elements are characterized by different surface energies, and so, the surface wettability depends on the surface energy of the elements. The higher the surface energy is, the higher the wetting [45, 91]. In the present study, the hydrophilicity was enhanced after anodization of Ti as shown by the significant decrease in the WCA measured on Ti compared to NT surfaces (Table 3.3). This means that once a water droplet gets in contact with NT surfaces it completely expands on the entire surface. The hydrophilic character of these nanotubular structures is most probably related to the presence of OH groups adsorbed on its surface [92]. It is believed that the O 1s binding energy found for NT surfaces at around 531 eV (Fig. 3.6c) may be also assigned to OH groups adsorbed on TiO_2. Regonini *et al.* [75] after XPS analysis of TiO_2 nanotubular films synthesized by anodization, reported a certain degree of hydration in the oxide due to a signal typical of OH groups at 531.4 eV. TiO_2 nanotube arrays with OH groups adsorbed on its surface were also

formed by Han *et al.* [64]. In agreement, absorption band from ~ 3000-3500 cm^{-1} found in FTIR spectrum (Fig. 3.9), is possibly attributed to fundamental stretching vibration of H_2O and OH groups. Earlier studies have focused on understanding the wettability behavior of titanium oxide nanotube surfaces. It has been reported that nanotubular films produced on Ti and Ti-alloys in EG-based electrolytes display superhydrophilic behavior [45, 93]. Yoriya *et al.* [93] fabricated titania nanotubular films characterized by WCA of 13.8 ± 2.2 º and stated that this was a clear indication of the superhydrophilic behaviour of the nanotube layer. In the present work, the WCA measured for NT-Ca/P and NT-RP-Ca/P surfaces were 11.8 ± 2.8 º and 10.5 ± 3.0 º, respectively (Table 3.3). These values are similar to the ones measured for NT surfaces and keep significantly lower than WCA of Ti. These results indicate that, beyond functionalization treatments of NT surfaces have influenced surface chemistry, their hydrophilic behavior remained unchanged. This feature may be of upmost importance once surface wettability plays a crucial role in cell adhesion, since this phase involves physicochemical linkages between cells and surfaces [16, 29]. Besides, changes on surface wettability can lead to alterations in the adsorption of conditioning molecules influencing the cell attachment [29]. According to several studies, cells attach more efficiently to hydrophilic surfaces when compared to hydrophobic ones [16, 29, 94].

3.4.3. Corrosion behavior

The high corrosion resistance of Ti results from the growth of a protective TiO_2 film on its surface (2-6 nm thickness) [95]. However, this nano-thick passive layer is not inert to corrosive attack when subjected to aggressive biological conditions [23] (e.g. pH variation, presence of fluorides and surface wear). As a consequence of corrosion, metal ions may be released from a metallic implant to its vicinity impairing bone cell functions and triggering an immune response that can ultimately lead to periprosthetic resorption of bone and loosening of the implant [18, 25, 34]. Beyond metal ions accumulation in bone adjacent to implants, they have also been found to be localized in blood or serum, urine and other organs [96]. Thus, the study of how Ca/P-doped TiO_2 nanotubes behave when submitted to corrosive conditions is of upmost importance.

The electrochemical behavior of Ti, NT, NT-Ca/P and NT-RP-Ca/P samples was investigated in artificial saliva (AS) at 37 ˚C by potentiodynamic polarization. The electrochemical stability was assessed by the current values measured in the passive region (I_{pass}) of potentiodynamic polarization curves, whose values are shown in Table 3.4. The potentiodynamic polarization curves observed in Fig. 3.10 show that NT, NT-Ca/P and NT-RP-Ca/P samples exhibit a passive region extending over a wide potential range when compared to Ti surfaces. In general, all the

nanotubular surfaces display a fast and effective passivation behavior, which may be related to the properties of the barrier layer formed at titanium/nanotubes interface during anodization process. The same trend was observed by Grotberg *et al.* [30] for nanotubes grown from Ti6Al4V substrates. Yu *et al.* [31] also studied the corrosion behavior of TiO_2 nanotube layers in Hank's solution and they concluded that the I_{pass} density was significantly influenced by Ti oxide nanotubes grown by anodization. Electrochemical Impedance Spectroscopy (EIS) results confirmed the better corrosion resistance of Ti nanotubes because of a thicker barrier layer present on nanotubular films than on smooth Ti. The passive layer grown during anodization process plays the main role in corrosion restricting the movement of metal ions from the metallic surface to the surrounding solution [97]. Likewise, Demestrescu *et al.* [98] studied the effect of nano-topographical features of Ti/TiO_2 electrode surface on its electrochemical stability in Fusayama's AS. From EIS and potentiodynamic studies, the authors concluded that very low corrosion current densities were recorded on TiO_2 nanotubes due to a strong passive oxide film formation. The EIS results indicated that TiO_2 nanotube surface consisted of a bi-layered oxide made up of an inner barrier layer associated to high impedance and responsible for corrosion protection, and a porous outer layer (nanotubes) of lower impedance.

Beyond the faster passivation behavior of NT samples, similar I_{pass} values were found for smooth Ti, as observed in Fig. 3.10 and confirmed by the I_{pass} values reported in Table 3.4. However, after Ca- and P-enrichment of NT surfaces by anodization and reverse polarization processes, significantly lower I_{pass} values were found for NT-Ca/P and NT-RP-Ca/P samples (Fig. 3.10, Table 3.4) suggesting that they display superior corrosion resistance ability. From NT-Ca/P and NT-RP-Ca/P polarization curves, it is believed that this abrupt decrease in the I_{pass} values is related to the barrier layer at titanium/nanotubes interface, whose properties might have been changed during the anodization of NT surfaces in the Ca/P-electrolyte. During the second anodization process it is hypothesized that the diffusion of anionic oxygen species occurs through the nanotubes and the already existing passive layer, and reacts with Ti ions liberated from the titanium substrate to form a compact oxide film providing superior corrosion resistance. Recently, Yu *et al.* [99] reported on a method to enhance the adhesion of TiO_2 arrays to Ti substrate by employing an additional anodization of nanotubes in a fluoride-free organic electrolyte constituted of H_3PO_4 and EG. The additional anodization resulted in about 200 nm thick compact layer near the nanotube bottoms and scratch test demonstrated that this layer leads to a more than threefold increase of the adhesion strength between the nanotubes and the substrate. It is important to highlight that the morphological features of all the nanotubular surfaces remained unaltered after corrosion assays, as confirmed by FESEM observation of the surface area exposed to AS (results not shown).

From the results obtained it appears that the lowering on the I_{pass} values is not affected by the reverse polarization step, which led to the significant reduction of the nanotube length as discussed in section 3.4.1, and so, it is also independent of nanotube length. Furthermore, all the nanotubular surfaces are superhydrophilic and characterized by similar values of WCA, and so, it seems that I_{pass} values are also independent on this feature. This indicates that the barrier layer formed at titanium/nanotube interface is the main cause for the significant I_{pass} lowering. The characterization of the newly formed titanium/nanotubes interface after anodization of nanotubes in Ca/P-electrolyte regarding compact layer morphology, thickness and elemental composition is of upmost importance. This knowledge will allow to predict the mechanisms behind the barrier layer formation and to understand the properties responsible for the improved corrosion resistance of Ca/P-doped TiO_2 nanotubes.

3.4.4. Adhesion and proliferation of MG-63 cells

Ideally, the biological fixation between an implant surface and the surrounding bone should occur ensuring the establishment of a mechanically solid interface without fibrous tissue formation [33, 35, 100], however, this is still one of the main challenges that researchers aim to overcome [32]. This present study uses a novel surface functionalization strategy to provide a biomimetic surface. The new adopted methodology aims to tailor more effective bone-integrating surfaces by mimicking the morphology of natural bone at a nano-scale level, as well as its composition through the enrichment of the TiO_2 nanotubes with Ca and P species.

From the results described in section 3.3.6.1, all the nanotubular surfaces influenced the cell responses regarding cell adhesion and proliferation. In accordance with FESEM observation of MG-63 cells after one day of incubation (Figs. 3.11 a1, b1, c1 and d1), the cells adhered on TiO_2 nanotube surfaces presented a spreader morphology with filopodia forming adhesion points and promoting cell-cell contact through cytoplasmic extensions, compared to smooth Ti. Moreover, the metabolic activity of cells measured by MTT assay after six days of culture (Fig. 13), suggests that NT surfaces induced to a significantly higher proliferation of MG-63 cells than smooth Ti [101, 102]. These outcomes may be related to the more rapid adhesion and spreading of osteoblastic cells on NT surfaces as also observed by Oh *et al.* [102]. Cell adhesion is one of the critical initial stages to subsequent proliferation of osteoblastic cells producers of bony tissue, playing a crucial role in the establishment of a high bone-implant contact [9, 11, 103].

Cell-substrate adhesion is based on membrane integrins (8-12 nm), which are essential for the formation of focal adhesion points with the implant surface [104]. Integrins can translate the attachment of external ligands (e.g. fibronectin and vitronectin) to internal information that induces adhesion, spreading, cell migration, growth and differentiation [105]. It has been

already shown that TiO_2 nanotubes influence cell proliferation, migration and differentiation resulting from integrin clustering and focal contact formation [104], and these responses depend on nanotube features such as diameter and wall thickness. However, the cell response to different TiO_2 nanotube diameters is still controversial in literature. Nanotubes with 15 – 30 nm promote cell adhesion and proliferation and, on the other hand, nanotubes with 70 – 100 nm are believed to induce a greater bone forming ability [105]. Brammer *et al.* [101] prepared various sizes (30 – 100 nm diameter) of TiO_2 nanotubes on Ti substrates by anodization, and investigated the osteoblast cellular behavior in response to these different nanotube sizes. The experimental data indicated that a substantially increased elongation of the cells when cultured on 100 nm diameter nanotubes was achieved with cell differentiation ability, when compared to flat Ti. In the present work, TiO_2 nanotubes with diameter ranging from 45 – 90 nm and a wall thickness from 14 – 24 nm were produced. The improved cell adhesion and proliferation of MG-63 cells adhered on NT surfaces is probably related with these nanofeatures of the tubes that influence cell adhesion process through integrin receptors, as mentioned previously. Furthermore, it has been reported that cells adhere better on hydrophilic surfaces and with functional groups such as OH^- [106], which are characteristics of NT surfaces when compared to Ti. Additionally, F ions adsorbed on NT surfaces, may be stimulating initial cell attachment [104]. Thus, it is believed that the surface features of NT surfaces as morphology and chemistry are beneficial for the initial protein adsorption and subsequent cell adhesion process when compared to smooth Ti.

Different behaviors regarding cell adhesion quality and proliferation were observed for osteoblastic cells seeded on NT-Ca/P and NT-RP-Ca/P surfaces. After six days of culture, osteoblastic cells seeded on NT-RP-Ca/P surfaces presented a spreader and more stretched morphology compared to the ones on NT-Ca/P surfaces (Fig. 3.12 d2 *vs* Fig. 3.12 c2) as well as an enhanced metabolic activity (Fig. 3.13). In Figs. 3.12 d1 and d2 it is observed that there is an increased number of adhered cells on NT-RP-Ca/P surfaces through the culture time. However, the same behavior is not observed on NT-Ca/P surfaces (Figs. 12 c1 and c2), where there is not an increase on the amount of MG-63 cells, which in turns are more scarcely distributed presenting a rounder morphology. The MTT results are in good agreement with these observations, showing a significantly lower metabolic activity of the adhered cells on NT-Ca/P compared to NT-RP-Ca/P surfaces, suggesting a lower proliferation. Cell to cell contacts are quite observed on NT-RP-Ca/P surfaces through filopodia, which are also observed traveling along the nanotubes. The differences on cellular responses found between NT-Ca/P and NT-RP-Ca/P surfaces are most probably related to their chemical features, which were changed after reverse polarization step. As known from literature, surface chemistry plays an important role in cell

adhesion because it influences short-term adhesion, which is a step that involves adsorption and rearrangement of proteins [106]. From chemical analysis of NT-RP-Ca/P surfaces it was found the presence of $Ca_3(PO_4)_2$/$CaHPO_4$, CaF_2, $CaCO_3$ and CaO species. These compounds were also found on NT-Ca/P surfaces with the exception of CaO. According to the findings by Dorner-Reisel *et al.* [107], an alteration of the biological acceptance of Diamond-Like Carbon (DLC) films was induced by CaO incorporation. In accordance with the authors, the DLC doping with CaO led to an improvement on cell morphology and viability. In the present study, the formation of CaO may be acting as a determining factor, influencing the initial adherence of proteins on the surface, and consequently, the cell adhesion and proliferation. However, further studies must be carried out to confirm this hypothesis.

From the results above discussed, it appears that the anodization of nanotubes in Ca/P-electrolyte is modulating cell responses and that reverse polarization is a very promising strategy for the design of new osseointegrative surfaces. The reverse polarization step before anodization in the Ca/P-electrolyte helps to recover the biological functions of cells adhered on NT surfaces regarding metabolic cell activity and cell adhesion. This suggests that beyond morphological/topographical features, cells seem to respond to chemical properties of TiO_2 nanotubes. Further studies still need to be carried out aiming to understand better the mechanisms governing cell adhesion and proliferation on these surfaces. Furthermore, cell differentiation studies would be also of fundamental importance to perform, aiming to understand if Ca/P-doped TiO_2 nanotubes have potential to modulate osteogenesis.

3.5. Conclusions

The synthesis of biocompatible Ca/P-doped TiO_2 nanotubes was successfully achieved with improved electrochemical behavior in AS. The main conclusions of this investigation are as follows:

- Highly ordered TiO_2 nanotubes were synthesized by two-step anodizing treatments. The nanotubes are characterized by non-uniform diameters varying at a nano-scale level from 50-90 nm, presenting a very similar morphology when compared to the micron structure of natural bone.

- Reverse polarization of highly ordered TiO_2 nanotubes in a Ca/P-electrolyte, followed by anodization in the same electrolyte, leads to a nanotubular film enriched with bioactive elements namely, Ca and P. The functionalization treatment by reverse polarization before anodization does not affect the morphology of the nanotubes, however, it influences their chemical properties.

- Reverse polarization in Ca/P-electrolyte improves the biocompatibility of Ca/P-doped

TiO_2. By this novel approach, the chemistry of TiO_2 nanotubes may be modified without compromising the desired surface morphological features.

- Ca/P-doped TiO_2 nanotubes display a significantly lower passive current than NT and smooth Ti samples in AS at 37 °C. The anodization of TiO_2 nanotubes in Ca/P-electrolyte seems to be a promising and simple approach to improve the electrochemical stability of metallic implants and avoid their degradation by corrosion.

The present study brings up a novel methodology that relies on the bio-functionalization of TiO_2 nanotubes by the conjugation of reverse polarization and anodization processes in a Ca/P-electrolyte. This new strategy allows the synthesis of bone-like structured TiO_2 nanotubes enriched with bioactive elements, able to enhance osteoblastic cell functions and simultaneously, to minimize their degradation by corrosion. This study addresses a very promising and simple approach providing new insights for the further development of novel methodologies to improve the outcome of dental and orthopedic implants.

Acknowledgements

This work made use of the facilities at the Electron Microscopy Service (Research Resource Center, UIC). The authors would like to thank the financial support provided by the Department of Bioengineering of the University of Illinois at Chicago; the National Science Foundation for the DMR Grant # 1564950 and NSF Grant #1067424; the Portuguese Foundation for Science and Technology for the doctoral grant (Ref. SFRH/BD/88517/2012); the National Council for Scientific and Technological Development for the grant (Ref. 490761/2013-5); and the Coordination for the Improvement of Higher Education Personnel for the financial support (Ref. 99999.008666/2014-08).

References

[1] Oshida Y, Tuna EB, Aktören O, Gençay K. Dental implant systems, International journal of molecular sciences 11 (2010), 1580-1678.
[2] Norowski PA, Bumgardner JD. Biomaterial and antibiotic strategies for peri-implantitis: A review, Journal of Biomedical Materials Research Part B: Applied Biomaterials 88B (2009), 530-543.
[3] Taylor TD. Prosthodontic problems and limitations associated with osseointegration, The Journal of Prosthetic Dentistry 79 (1998), 74-78.
[4] Park J, Bauer S, Schlegel KA, Neukam FW, von der Mark K, Schmuki P. TiO2 nanotube surfaces: 15 nm—an optimal length scale of surface topography for cell adhesion and differentiation, Small 5 (2009), 666-671.
[5] Vieira AC, Ribeiro AR, Rocha LA, Celis JP. Influence of pH and corrosion inhibitors on the tribocorrosion of titanium in artificial saliva, Wear 261 (2006), 994-1001.
[6] Wang N, Li H, Lü W, Li J, Wang J, Zhang Z, Liu Y. Effects of TiO2 nanotubes with different diameters on gene expression and osseointegration of implants in minipigs, Biomaterials 32 (2011), 6900-6911.
[7] Kane R, Ma PX. Mimicking the nanostructure of bone matrix to regenerate bone, Materials Today 16 (2013), 418-423.
[8] Ibrahim N, Parsa A, Hassan B, van der Stelt P, Wismeijer D. Diagnostic imaging of trabecular bone microstructure for oral implants: a literature review, Dentomaxillofacial Radiology 42 (2013), 20120075.
[9] Indira K, Mudali UK, Rajendran N. Corrosion behavior of electrochemically assembled nanoporous titania for

biomedical applications, Ceramics International 39 (2013), 959-967.
[10] Zhao L, Wang H, Huo K, Zhang X, Wang W, Zhang Y, Wu Z, Chu PK. The osteogenic activity of strontium loaded titania nanotube arrays on titanium substrates, Biomaterials 34 (2013), 19-29.
[11] Le Guehennec L, Lopez-Heredia MA, Enkel B, Weiss P, Amouriq Y, Layrolle P. Osteoblastic cell behaviour on different titanium implant surfaces, Acta Biomaterialia 4 (2008), 535-543.
[12] Surmenev RA, Surmeneva MA, Ivanova AA. Significance of calcium phosphate coatings for the enhancement of new bone osteogenesis–A review, Acta Biomaterialia 10 (2014), 557-579.
[13] Ribeiro A, Oliveira F, Boldrini L, Leite P, Falagan-Lotsch P, Linhares A, Zambuzzi W, Fragneaud B, Campos A, et al. Micro-arc oxidation as a tool to develop multifunctional calcium-rich surfaces for dental implant applications, Materials Science and Engineering: C 54 (2015), 196-206.
[14] Cao H, Qin H, Zhao Y, Jin G, Lu T, Meng F, Zhang X, Liu X. Nano-thick calcium oxide armed titanium: boosts bone cells against methicillin-resistant Staphylococcus aureus, Scientific reports 6 (2016).
[15] Demetrescu I, Pirvu C, Mitran V. Effect of nano-topographical features of Ti/TiO2 electrode surface on cell response and electrochemical stability in artificial saliva, Bioelectrochemistry 79 (2010), 122-129.
[16] Das K, Bose S, Bandyopadhyay A. Surface modifications and cell-materials interactions with anodized Ti, Acta Biomaterialia 3 (2007), 573-585.
[17] Klinge B, Hultin M, Berglundh T. Peri-implantitis, Dent Clin North Am 49 (2005), 661-676, vii-viii.
[18] Song H-J, Kim M-K, Jung G-C, Vang M-S, Park Y-J. The effects of spark anodizing treatment of pure titanium metals and titanium alloys on corrosion characteristics, Surface and Coatings Technology 201 (2007), 8738-8745.
[19] Gulati K, Ramakrishnan S, Aw MS, Atkins GJ, Findlay DM, Losic D. Biocompatible polymer coating of titania nanotube arrays for improved drug elution and osteoblast adhesion, Acta Biomaterialia 8 (2012), 449-456.
[20] Crawford GA, Chawla N, Houston JE. Nanomechanics of biocompatible TiO2 nanotubes by Interfacial Force Microscopy (IFM), Journal of the Mechanical Behavior of Biomedical Materials 2 (2009), 580-587.
[21] Minagar S, Berndt CC, Wang J, Ivanova E, Wen C. A review of the application of anodization for the fabrication of nanotubes on metal implant surfaces, Acta Biomaterialia 8 (2012), 2875-2888.
[22] Albrektsson T, Johansson C. Osteoinduction, osteoconduction and osseointegration, European Spine Journal 10 Suppl 2 (2001), S96-101.
[23] Mathew MT, Barão VA, Yuan JC-C, Assunção WG, Sukotjo C, Wimmer MA. What is the role of lipopolysaccharide on the tribocorrosive behavior of titanium?, Journal of the Mechanical Behavior of Biomedical Materials 8 (2012), 71-85.
[24] Liu X, Chu PK, Ding C. Surface nano-functionalization of biomaterials, Materials Science and Engineering: R: Reports 70 (2010), 275-302.
[25] Faghihi S, Li D, Szpunar JA. Tribocorrosion behaviour of nanostructured titanium substrates processed by high-pressure torsion, Nanotechnology 21 (2010), 485703.
[26] Le Guehennec L, Soueidan A, Layrolle P, Amouriq Y. Surface treatments of titanium dental implants for rapid osseointegration, Dental materials 23 (2007), 844-854.
[27] Jayaraman M, Meyer U, Bühner M, Joos U, Wiesmann H-P. Influence of titanium surfaces on attachment of osteoblast-like cells in vitro, Biomaterials 25 (2004), 625-631.
[28] de Souza GB, de Lima GG, Kuromoto NK, Soares P, Lepienski CM, Foerster CE, Mikowski A. Tribo-mechanical characterization of rough, porous and bioactive Ti anodic layers, Journal of the Mechanical Behavior of Biomedical Materials 4 (2011), 796-806.
[29] Zhu X, Chen J, Scheideler L, Reichl R, Geis-Gerstorfer J. Effects of topography and composition of titanium surface oxides on osteoblast responses, Biomaterials 25 (2004), 4087-4103.
[30] Grotberg J, Hamlekhan A, Butt A, Patel S, Royhman D, Shokuhfar T, Sukotjo C, Takoudis C, Mathew MT. Thermally oxidized titania nanotubes enhance the corrosion resistance of Ti6Al4V, Materials Science and Engineering: C 59 (2016), 677-689.
[31] Yu W-q, Qiu J, Xu L, Zhang F-q. Corrosion behaviors of TiO2 nanotube layers on titanium in Hank's solution, Biomedical Materials 4 (2009), 065012.
[32] Monsees TK, Barth K, Tippelt S, Heidel K, Gorbunov A, Pompe W, Funk RH. Effects of different titanium alloys and nanosize surface patterning on adhesion, differentiation, and orientation of osteoblast-like cells, Cells Tissues Organs 180 (2005), 81-95.
[33] Anselme K. Osteoblast adhesion on biomaterials, Biomaterials 21 (2000), 667-681.
[34] Cobelli N, Scharf B, Crisi GM, Hardin J, Santambrogio L. Mediators of the inflammatory response to joint replacement devices, Nature Reviews Rheumatology 7 (2011), 600-608.
[35] Novaes AB, Jr., de Souza SL, de Barros RR, Pereira KK, Iezzi G, Piattelli A. Influence of implant surfaces on osseointegration, Brazilian Dental Journal 21 (2010), 471-481.
[36] Cheng Z, Zhang F, He F, Zhang L, Guo C, Zhao S, Yang G. Osseointegration of titanium implants with a roughened surface containing hydride ion in a rabbit model, Oral Surgery, Oral Medicine, Oral Pathology, Oral Radiology, and Endodontology 110 (2010), e5-12.
[37] Mendonca G, Mendonca DB, Simoes LG, Araujo AL, Leite ER, Duarte WR, Aragao FJ, Cooper LF. The effects of implant surface nanoscale features on osteoblast-specific gene expression, Biomaterials 30 (2009), 4053-4062.
[38] Brammer KS, Frandsen CJ, Jin S. TiO2 nanotubes for bone regeneration, Trends in Biotechnology 30 (2012), 315-322.

[39] Minagar S, Li Y, Berndt CC, Wen C. The influence of titania–zirconia–zirconium titanate nanotube characteristics on osteoblast cell adhesion, Acta Biomaterialia 12 (2015), 281-289.
[40] Alves S, Bayón R, de Viteri VS, Garcia M, Igartua A, Fernandes M, Rocha L. Tribocorrosion Behavior of Calcium- and Phosphorous-Enriched Titanium Oxide Films and Study of Osteoblast Interactions for Dental Implants, Journal of Bio-and Tribo-Corrosion 1 (2015), 1-21.
[41] Fusayama T, Katayori T, Nomoto S. Corrosion of Gold and Amalgam Placed in Contact with Each Other, Journal of Dental Research 42 (1963), 1183-1197.
[42] Komasa S, Taguchi Y, Nishida H, Tanaka M, Kawazoe T. Bioactivity of nanostructure on titanium surface modified by chemical processing at room temperature, Journal of Prosthodontic Research 56 (2012), 170-177.
[43] Dementjev A, De Graaf A, Van de Sanden M, Maslakov K, Naumkin A, Serov A. X-ray photoelectron spectroscopy reference data for identification of the C3N4 phase in carbon–nitrogen films, Diamond and Related Materials 9 (2000), 1904-1907.
[44] Antony RP, Mathews T, Dash S, Tyagi AK, Raj B. X-ray photoelectron spectroscopic studies of anodically synthesized self aligned TiO2 nanotube arrays and the effect of electrochemical parameters on tube morphology, Materials Chemistry and Physics 132 (2012), 957-966.
[45] Patel SB, Hamlekhan A, Royhman D, Butt A, Yuan J, Shokuhfar T, Sukotjo C, Mathew MT, Jursich G, et al. Enhancing surface characteristics of Ti–6Al–4V for bio-implants using integrated anodization and thermal oxidation, Journal of Materials Chemistry B 2 (2014), 3597-3608.
[46] Yates D. Infrared studies of the surface hydroxyl groups on titanium dioxide, and of the chemisorption of carbon monoxide and carbon dioxide, The Journal of Physical Chemistry 65 (1961), 746-753.
[47] Hamlekhan A, Butt A, Patel S, Royhman D, Takoudis C, Sukotjo C, Yuan J, Jursich G, Mathew MT, et al. Fabrication of Anti-Aging TiO2 Nanotubes on Biomedical Ti Alloys, PloS one 9 (2014), e96213.
[48] Bezrodna T, Puchkovska G, Shymanovska V, Baran J, Ratajczak H. IR-analysis of H-bonded H2O on the pure TiO2 surface, Journal of Molecular Structure 700 (2004), 175-181.
[49] Vasconcelos DCL, Nunes EHM, Gasparon M, Vasconcelos WL. Infrared spectroscopy of titania sol-gel coatings on 316L stainless steel, Materials Sciences and Applications 2 (2011), 1375.
[50] Becker I, Hofmann I, Müller FA. Preparation of bioactive sodium titanate ceramics, Journal of the European Ceramic Society 27 (2007), 4547-4553.
[51] Chen X-B, Li Y-C, Plessis JD, Hodgson PD, Wen Ce. Influence of calcium ion deposition on apatite-inducing ability of porous titanium for biomedical applications, Acta Biomaterialia 5 (2009), 1808-1820.
[52] Roguska A, Pisarek M, Andrzejczuk M, Dolata M, Lewandowska M, Janik-Czachor M. Characterization of a calcium phosphate–TiO2 nanotube composite layer for biomedical applications, Materials Science and Engineering: C 31 (2011), 906-914.
[53] Goudarzi M, Batmanghelich F, Afshar A, Dolati A, Mortazavi G. Development of electrophoretically deposited hydroxyapatite coatings on anodized nanotubular TiO2 structures: Corrosion and sintering temperature, Applied Surface Science 301 (2014), 250-257.
[54] Pisarek M, Roguska A, Marcon L, Andrzejczuk M. Biomimetic and Electrodeposited Calcium-Phosphates Coatings on Ti-Formation, Surface Characterization, Biological Response: INTECH Open Access Publisher, 2012.
[55] Yajing Y, Qiongqiong D, Yong H, Han S, Pang X. Magnesium substituted hydroxyapatite coating on titanium with nanotublar TiO2 intermediate layer via electrochemical deposition, Applied Surface Science 305 (2014), 77-85.
[56] Berzina-Cimdina L, Borodajenko N. Research of calcium phosphates using Fourier transform infrared spectroscopy, Infrared Spectroscopy Materials Science, Engineering and Technology, Edited by Theophile Theophanides (2012), 123-149.
[57] Roguska A, Hiromoto S, Yamamoto A, Woźniak MJ, Pisarek M, Lewandowska M. Collagen immobilization on 316L stainless steel surface with cathodic deposition of calcium phosphate, Applied Surface Science 257 (2011), 5037-5045.
[58] Wang S, Liu Y, Zhang C, Liao Z, Liu W. The improvement of wettability, biotribological behavior and corrosion resistance of titanium alloy pretreated by thermal oxidation, Tribology International 79 (2014), 174-182.
[59] Saji VS, Choe HC, Brantley WA. An electrochemical study on self-ordered nanoporous and nanotubular oxide on Ti–35Nb–5Ta–7Zr alloy for biomedical applications, Acta Biomaterialia 5 (2009), 2303-2310.
[60] Takahashi S, Abe T, Gotoh J, Fukuuchi Y. Substrate-dependence of reduction of MTT: a tetrazolium dye differs in cultured astroglia and neurons, Neurochemistry International 40 (2002), 441-448.
[61] Fojt J, Moravec H, Joska L. Nanostructuring of Titanium for Medical Applications, Nanocon 2010, 2nd International Conference (2010), 209-213.
[62] Grigorescu S, Pruna V, Titorencu I, Jinga VV, Mazare A, Schmuki P, Demetrescu I. The two step nanotube formation on TiZr as scaffolds for cell growth, Bioelectrochemistry 98 (2014), 39-45.
[63] Regonini D, Bowen CR, Jaroenworaluck A, Stevens R. A review of growth mechanism, structure and crystallinity of anodized TiO2 nanotubes, Materials Science and Engineering: R: Reports 74 (2013), 377-406.
[64] Han S, Doh J, Yoon J, Kim G, Byun J, Han S, Hong K, Kwun S. Highly ordered self-organized TiO2 nanotube arrays prepared by a multi-step anodic oxidation process, Metals and Materials International 15 (2009), 493-499.
[65] Serikov T, Ibrayev NK, Gladkova V. Synthesis and investigation of the geometric characteristics of titanium dioxide nanotubes, IOP Conference Series: Materials Science and Engineering: IOP Publishing, 2015, pp. 012121.
[66] Sulka GD, Kapusta-Kołodziej J, Brzózka A, Jaskuła M. Anodic growth of TiO2 nanopore arrays at various

temperatures, Electrochimica Acta 104 (2013), 526-535.
[67] Grigorescu S, Ungureanu C, Kirchgeorg R, Schmuki P, Demetrescu I. Various sized nanotubes on TiZr for antibacterial surfaces, Applied Surface Science 270 (2013), 190-196.
[68] Sulka G, Stroobants S, Moshchalkov V, Borghs G, Celis J-P. Effect of tensile stress on growth of self-organized nanostructures on anodized aluminum, Journal of The Electrochemical Society 151 (2004), B260-B264.
[69] Hu Y, Cai KY, Luo Z, Xu DW, Xie DC, Huang YR, Yang WH, Liu P. TiO2 nanotubes as drug nanoreservoirs for the regulation of mobility and differentiation of mesenchymal stem cells, Acta Biomaterialia 8 (2012), 439-448.
[70] Peláez Abellán E, Rocha-Souza L, Guastaldi A. Cathodic behaviour of anodized titanium in simulated physiological, Latin American applied research 41 (2011), 199-203.
[71] Torresi R, Camara O, De Pauli C. Influence of the hydrogen evolution reaction on the anodic titanium oxide film properties, Electrochimica Acta 32 (1987), 1357-1363.
[72] Vezvaie M, Noël J, Tun Z, Shoesmith D. Hydrogen Absorption into Titanium under Cathodic Polarization: An In-Situ Neutron Reflectometry and EIS Study, Journal of The Electrochemical Society 160 (2013), C414-C422.
[73] Kowalski D, Kim D, Schmuki P. TiO2 nanotubes, nanochannels and mesosponge: Self-organized formation and applications, Nano Today 8 (2013), 235-264.
[74] Roguska A, Pisarek M, Andrzejczuk M, Dolata M, Lewandowska M, Janik-Czachor M. Characterization of a calcium phosphate–TiO 2 nanotube composite layer for biomedical applications, Materials Science and Engineering: C 31 (2011), 906-914.
[75] Regonini D, Jaroenworaluck A, Stevens R, Bowen CR. Effect of heat treatment on the properties and structure of TiO2 nanotubes: phase composition and chemical composition, Surface and interface analysis 42 (2010), 139-144.
[76] Shin H, Jung J, Kim S, Lee W. XPS Analysis on Chemical Properties of Calcium Phosphate Thin Films and Osteoblastic HOS Cell Responses, Journal of Industrial and Engineering Chemistry 12 (2006), 476-483.
[77] Jensen H, Soloviev A, Li Z, Søgaard EG. XPS and FTIR investigation of the surface properties of different prepared titania nano-powders, Applied Surface Science 246 (2005), 239-249.
[78] Mangrulkar PA, Kamble SP, Joshi MM, Meshram JS, Labhsetwar NK, Rayalu SS. Photocatalytic degradation of phenolics by N-doped mesoporous titania under solar radiation, International Journal of Photoenergy 2012 (2011).
[79] Raja K, Gandhi T, Misra M. Effect of water content of ethylene glycol as electrolyte for synthesis of ordered titania nanotubes, Electrochemistry communications 9 (2007), 1069-1076.
[80] Grimes CA, Mor GK. Material Properties of TiO2 Nanotube Arrays: Structural, Elemental, Mechanical, Optical and Electrical, TiO2 Nanotube Arrays: Springer, 2009, pp. 67-113.
[81] Indira K, Mudali UK, Rajendran N. In-vitro biocompatibility and corrosion resistance of strontium incorporated TiO2 nanotube arrays for orthopaedic applications, Journal of biomaterials applications 29 (2014), 113-129.
[82] Hang R, Liu Y, Liu S, Bai L, Gao A, Zhang X, Huang X, Tang B, Chu PK. Size-dependent corrosion behavior and cytocompatibility of Ni–Ti–O nanotubes prepared by anodization of biomedical NiTi alloy, Corrosion Science (2015).
[83] Sreekantan S, Saharudin KA, Lockman Z, Tzu TW. Fast-rate formation of TiO2 nanotube arrays in an organic bath and their applications in photocatalysis, Nanotechnology 21 (2010), 365603.
[84] Neoh KG, Hu X, Zheng D, Kang ET. Balancing osteoblast functions and bacterial adhesion on functionalized titanium surfaces, Biomaterials 33 (2012), 2813-2822.
[85] Raliya R, Som A, Shetty N, Reed N, Achilefu S, Biswas P. Nano-antacids enhance pH neutralization beyond their bulk counterparts: synthesis and characterization, RSC Advances 6 (2016), 54331-54335.
[86] Bigerelle M, Anselme K, Noël B, Ruderman I, Hardouin P, Iost A. Improvement in the morphology of Ti-based surfaces: a new process to increase in vitro human osteoblast response, Biomaterials 23 (2002), 1563-1577.
[87] Fu W, Ding S, Wang Y, Wu L, Zhang D, Pan Z, Wang R, Zhang Z, Qiu S. F, Ca co-doped TiO2 nanocrystals with enhanced photocatalytic activity, Dalton Transactions 43 (2014), 16160-16163.
[88] Rupp F, Scheideler L, Rehbein D, Axmann D, Geis-Gerstorfer J. Roughness induced dynamic changes of wettability of acid etched titanium implant modifications, Biomaterials 25 (2004), 1429-1438.
[89] Lim YJ, Oshida Y, Andres CJ, Barco MT. Surface characterizations of variously treated titanium materials, The International journal of oral & maxillofacial implants 16 (2000), 333-342.
[90] Bhushan B, Chae Jung Y. Wetting study of patterned surfaces for superhydrophobicity, Ultramicroscopy 107 (2007), 1033-1041.
[91] Rupp F, Gittens RA, Scheideler L, Marmur A, Boyan BD, Schwartz Z, Geis-Gerstorfer J. A review on the wettability of dental implant surfaces I: Theoretical and experimental aspects, Acta Biomaterialia 10 (2014), 2894-2906.
[92] Shin DH, Shokuhfar T, Choi CK, Lee S-H, Friedrich C. Wettability changes of TiO2 nanotube surfaces, Nanotechnology 22 (2011), 315704.
[93] Yoriya S, Kittimeteeworakul W, Punprasert N. Effect of anodization parameters on morphologies of TiO2 nanotube arrays and their surface properties, Journal of Chemistry and Chemical Engineering 6 (2012), 686-691.
[94] Artzi Z, Nemcovsky CE, Tal H, Weinberg E, Weinreb M, Prasad H, Rohrer MD, Kozlovsky A. Clinical and histomorphometric observations around dual acid-etched and calcium phosphate nanometer deposited-surface implants, International Journal of Oral & Maxillofacial Implants 26 (2011), 893-901.
[95] Yang L, Chinthapenta V, Li Q, Stout D, Liang A, Sheldon BW, Webster TJ. Understanding osteoblast responses to stiff nanotopographies through experiments and computational simulations, Journal of Biomedical Materials

Research Part A 97 (2011), 375-382.
[96] Sun ZL, Wataha JC, Hanks CT. Effects of metal ions on osteoblastlike cell metabolism and differentiation, gene expression 11 (1997), 12.
[97] Yu X, Li Y, Wlodarski W, Kandasamy S, Kalantar-zadeh K. Fabrication of nanostructured TiO2 by anodization: A comparison between electrolytes and substrates, Sensors and Actuators B: Chemical 130 (2008), 25-31.
[98] Demetrescu I, Pirvu C, Mitran V. Effect of nano-topographical features of Ti/TiO 2 electrode surface on cell response and electrochemical stability in artificial saliva, Bioelectrochemistry 79 (2010), 122-129.
[99] Yu D, Zhu X, Xu Z, Zhong X, Gui Q, Song Y, Zhang S, Chen X, Li D. Facile method to enhance the adhesion of TiO2 nanotube arrays to Ti substrate, ACS applied materials & interfaces 6 (2014), 8001-8005.
[100] Kaneco S, Chen Y, Westerhoff P, Crittenden JC. Fabrication of uniform size titanium oxide nanotubes: Impact of current density and solution conditions, Scripta Materialia 56 (2007), 373-376.
[101] Ravanetti F, Borghetti P, De Angelis E, Chiesa R, Martini FM, Gabbi C, Cacchioli A. In vitro cellular response and in vivo primary osteointegration of electrochemically modified titanium, Acta Biomaterialia 6 (2010), 1014-1024.
[102] Tomisa AP, Launey ME, Lee JS, Mankani MH, Wegst UG, Saiz E. Nanotechnology approaches to improve dental implants, Int J Oral Maxillofac Implants 26 Suppl (2011), 25-44; discussion 45-29.
[103] Oh S, Daraio C, Chen L-H, Pisanic TR, Fiñones RR, Jin S. Significantly accelerated osteoblast cell growth on aligned TiO2 nanotubes, Journal of Biomedical Materials Research Part A 78A (2006), 97-103.
[104] Park S-J, Bae S-B, Kim S-K, Eom T-G, Song S-I. Effect of implant surface microtopography by hydroxyapatite grit-blasting on adhesion, proliferation, and differentiation of osteoblast-like cell line, MG-63, Journal of the Korean Association of Oral and Maxillofacial Surgeons 37 (2011), 214-224.
[105] Jackson MJ, Ahmed W. Anodization: a promising nano-modification technique of titanium implants for orthopedic applications, in: Mark JJ, Waqar A (Eds.), Surface Engineered Surgical Tools and Medical Devices. 1 ed: Springer, 2007, pp. 21-47.
[106] He J, Zhou W, Zhou X, Zhong X, Zhang X, Wan P, Zhu B, Chen W. The anatase phase of nanotopography titania plays an important role on osteoblast cell morphology and proliferation, Journal of Materials Science: Materials in Medicine 19 (2008), 3465-3472.
[107] Dorner-Reisel A, Schürer C, Nischan C, Seidel O, Müller E. Diamond-like carbon: alteration of the biological acceptance due to Ca–O incorporation, Thin Solid Films 420 (2002), 263-268.

CHAPTER 4

A first insight on the bio-functionalization mechanisms of TiO_2 nanotubes with calcium, phosphorous and zinc by reverse polarization anodization

Under revision for publication in Surface and Coatings Technology

A first insight on the bio-functionalization mechanisms of TiO_2 nanotubes with calcium, phosphorous and zinc by reverse polarization anodization

Sofia A. Alves[1,2], André L. Rossi[3], Ana R. Ribeiro[2,4,5], Jacques Werckmann[2,6], Jean-Pierre Celis[7], Luís A. Rocha[1,2,8*], Tolou Shokuhfar[9,10*]

[1]*CMEMS – Center of MicroElectroMechanical Systems, Department of Mechanical Engineering, University of Minho, Azurém, 4800-058 Guimarães, Portugal*
[2]*IBTN/BR – Brazilian Branch of the Institute of Biomaterials, Tribocorrosion and Nanomedicine, Faculty of Sciences, UNESP – Universidade Estadual Paulista, 17033-360 Bauru, São Paulo, Brazil*
[3]*Brazilian Center for Research in Physics, 22290-180 Rio de Janeiro, Brazil*
[4]*Directory of Life Sciences Applied Metrology, National Institute of Metrology, Quality and Technology, 25250-020 Duque de Caxias – RJ, Brazil*
[5]*Postgraduate Program in Translational Biomedicine, University of Grande Rio, 25070-000 Duque de Caxias – RJ, Brazil*
[6]*Institute of Biomedical Sciences, UFRJ – Federal University of Rio de Janeiro, 21941-901 Rio de Janeiro Brazil*
[7]*Department of Materials Engineering, KU Leuven, 3001 Leuven, Belgium*
[8]*Faculdade de Ciências, Departamento de Física, UNESP – Universidade Estadual Paulista, 17033-360 Bauru, São Paulo, Brasil*
[9]*Department of Bioengineering, University of Illinois at Chicago, 60607 Chicago, Illinois, USA*
[10]*IBTN/US – American Branch of the Institute of Biomaterials, Tribocorrosion and Nanomedicine, University of Illinois at Chicago, 60612 Chicago, Illinois, USA*
**e-mail: lrocha@fc.unesp.br; tolou@uic.edu*

Abstract

The decoration of titanium (Ti) implant surfaces with bio-functionalized TiO_2 nanotubes is a very promising way to simultaneously improve osseointegration and avoid infection as the next generation of dental and orthopedic implants. Nevertheless, it has been reported that nanotubular films are prone to peeling off from the Ti substrate due to the poor interfacial adhesion. The knowledge on the interfacial properties of such interface, although not well explored, is crucial for understanding the mechanisms behind the poor adhesion problem of these films and to further achieve an easy and effective solution to solve it.

This paper is focused on the bio-functionalization of TiO_2 nanotubular films with zinc (Zn) as an antimicrobial and bone healing agent, together with two major constituents of the mineral phase of bone, namely calcium (Ca) and phosphorous (P). The main aim is, for the first time, the thorough characterization of the interface between TiO_2 nanotubes and the Ti substrate, along with the better understanding of the bio-functionalization mechanisms of TiO_2 nanotubes and their influence on the interfacial features of the films.

TiO_2 nanotubes were successfully synthesized by two-step anodization and their bio-functionalization with Ca, P and Zn was achieved by reverse polarization and anodization treatments. The in-depth characterization of the morphological and chemical features of TiO_2 nanotubes was carried out along their length by scanning transmission electron microscopy (STEM) and energy dispersive X-ray spectroscopy (EDS), before and after bio-functionalization

treatments. STEM images showed that the interface between conventional TiO_2 nanotubes and Ti is non-continuous due to the existence of a hollow space. However, STEM images of bio-functionalized TiO_2 nanotubes evidenced an interface with different features, due to the formation of an interfacial nano-thick oxide film as a consequence of anodization, with a thickness comprised between 230 – 250 nm.

The results presented in this work may inspire the emergence of novel surface treatment strategies seeking the long-term performance of metallic-modified osseointegrated implants.

Keywords: TiO_2 nanotubes; Interface; Reverse polarization; Anodization; Osseointegrated implants.

4.1. Introduction

Dental implants require the use of materials that beyond fulfilling requirements such as mechanical, chemical and physical properties, must provide excellent biocompatibility and avoid foreign body responses [1, 2]. Along with the discovery of Ti implants, introduced by Brånemark in 1964, revealing the ability of titanium (Ti) to induce osseointegration, the exploration of this material for use in dentistry and orthopedic fields has undergone a global boom [1]. In fact, nowadays, Ti-based materials represent the most widely used in dental and orthopedic fields, owing to their good mechanical properties, excellent biocompatibility and high corrosion resistance, resulting from the spontaneous formation of a thin (of 3 – 10 nm in thickness) and stable titanium dioxide (TiO_2) film on its surface [1, 3, 4].

In spite of the high success rate that Ti-based dental implant therapies have reached to replace tooth loss due to trauma or periodontal diseases, a significant number of failures have still been reported to be comprised between 1 – 20 % [3, 5, 6]. Dental implant failures are generally ascribed both to biological (e.g. bacterial infection and inadequate implant-to-bone contact) and biomechanical factors (e.g. occlusal overloading leading to fracture and/or damage of dental implant material) [5, 7]. Despite the good biocompatibility of Ti, insufficient osteogenic activity and the lack of antimicrobial properties are the main factors leading to delayed osseointegration and complicated bacterial infections, which may conduce to implant failures, essentially in patients with complex pathologies [4, 8-11]. Aiming to overcome the current bone-loss and infection related complications, several studies have been devoted to functionalization of Ti implant surfaces by modifying their features regarding morphology, topography and chemistry [12-15] .

Nanotechnology has emerged in the last years as an exciting and successful way to engineer Ti surfaces with nanoscale features for fast integration with bone that is also

considered a nanostructured composite matrix [16-19]. Studies have shown that the decoration of Ti-based materials with TiO_2 nanotubes through electrochemical anodization, is a simple and effective way to promote cellular functions, which may be ascribed to their unique morphological, physical and chemical properties [20-23]. The benefits of bio-functionalization of conventional TiO_2 nanotubes have been demonstrated through *in vitro* and *in vivo* studies, as they have led to an enhancement on osteoblastic cell functions [24-28], ability to impair bacterial adhesion [29-32] or even both, simultaneously [33, 34]. Apart the outstanding properties that bio-functionalized TiO_2 nanotubes have revealed for osseointegrated implants applications [35, 36], it has been reported that these films are prone to peeling off from the Ti substrate due to the poor interfacial adhesion between them [37]. This might have catastrophic consequences since, during and after implantation, osseointegrated implants are exposed to tribological and tribocorrosive conditions, which may induce to film degradation accompanied by the release of wear debris and corrosion products to implant surroundings, triggering harmful biological effects and ending up in implant failure [38-45].

A few studies have been reported seeking to understand the poor adhesion of TiO_2 nanotubes to Ti substrate. In accordance with Miraghaei *et al.* [46] TiO_2 nanotubes detach easily from the substrate due to the dissolution of a fluoride-rich layer existing between the tubes and Ti. Moreover, a hydrogen-assisted crack mechanism induced by the existence of Ti-H and hydrogen blisters in the bottom layer of the nanotubes was proposed by Zhao *et al.* [47]. The beneficial effect of anodization of TiO_2 nanotubes on their adhesion strength to Ti was reported by Yu *et al.* [37], which was ascribed to the formation of a compact layer near the nanotube bottom. However, the characteristics of Ti/TiO_2 film interface before and after anodization, were not reported. The knowledge of the characteristics of Ti/TiO_2 nanotubes interface is still very limited in literature, which is an issue of crucial importance to well-understand the poor adhesion problem of these films and to further achieve an effective solution to solve it.A new methodology for TiO_2 nanotubes bio-functionalization trough reverse polarization and anodization processes was described by our group in a previous work [48]. Biocompatible calcium-phosphorous doped TiO_2 nanotubes were synthesized displaying superior corrosion behavior than conventional nanotubes. The focus of the present contribution is on the bio-functionalization of the calcium-phosphorous doped TiO_2 nanotubes with zinc, through the previously reported methodology [48]. The main aim relies, for the first time, on the in-depth morphological and chemical characterization of the TiO_2 nanotubes along their length, with special focus at the interface region, before and after bio-functionalization treatments. A first

insight on the bio-functionalization mechanisms of TiO_2 nanotubes by reverse polarization and anodization processes is presented.

4.2. Materials and methods

4.2.1. Surface pre-treatment

Commercially pure titanium (cp-Ti grade 2) (American Society for Testing of Materials – Grade 2) (MacMaster-carr, IL, USA) rods cut into discs of 15 mm diameter and 2 mm thickness were the substrates used in this study. A series of silicon carbide (SiC) sandpapers #240, #320, #400, #600 and #800 were used to ground cp-Ti surfaces followed by their polishing with alumina suspension untill achieve a mirror finishing. After polishing, the Ti samples were ultrasonically cleaned in ethanol (10 min) and distilled (DI) water (5 min), followed by drying at room temperature.

4.2.2. Synthesis of TiO_2 nanotubes by two-step anodization

Titanium dioxide (TiO_2) nanotubes were synthesized by two-step anodization of Ti in an optimized electrolyte constituted of ethylene glycol (EG), 0.3 wt. % ammonium fluoride (NH_4F) (VETEC, Xerém, Rio de Janeiro, Brazil) and 3 vol. % DI water. The electrolyte was continuously stirred (150 rpm) at room temperature (22 to 24 ^oC). The anodic treatments were conducted using a dc power supply (KEYSIGHT, N5751A) set at 60 V with a limiting current of 2.5 A.

Firstly, Ti polished samples (anode) and a graphite rod (cathode) were immersed in the EG-based electrolyte separated at a fixed distance of around 2 cm, and a voltage of 60 V was applied for 1 h. The resulting nanotubes grown from Ti through this first anodization step, were intentionally removed by ultrasonication in isopropanol for 15 min followed by cleaning in DI water for 5 min. Secondly, the resulting nanopatterned Ti surfaces were anodized at the previous conditions for 30 min. The second anodization step resulted in the growth of self-ordered TiO_2 nanotube arrays, which were named as NT. Immediately after the second anodization step, NT samples were rinsed with DI water and dried at room temperature.

4.2.3. Bio-functionalization of TiO_2 nanotubes with calcium, phosphorous and zinc by reverse polarization and anodization

The TiO_2 nanotubular samples were bio-functionalized by reverse polarization and anodization processes, aiming the doping of nanotubes with calcium (Ca), phosphorous (P) and zinc (Zn) elements. Cathodic and anodic treatments were performed in an aqueous electrolyte constituted of calcium acetate (CaA) (Calcium acetate monohydrate, VETEC, Xerém, Rio de Janeiro, Brazil) and β-glycerolphosphate (β-GP) (β-glycerolphosphate disodium salt

pentahydrate, Sigma-Aldrich, St. Louis, MO, USA) as the source of Ca and P, respectively, and this electrolyte was named as Ca/P-based electrolyte. The concentrations of CaA and β-GP were established in accordance with the methodology described in a previous work [48]. Zinc acetate (Zinc acetate dihydrate, Sigma-Aldrich, St. Louis, MO, USA) at a concentration of 0.35 M was added to the previous Ca/P-based electrolyte aiming the additional incorporation of Zn in the nanotubular structure, and this solution was named as Ca/P/Zn-based electrolyte.

The reverse polarization and anodization treatments were conducted using a dc power supply (KEYSIGHT, N5751A) set with a limiting current of 2.5 A. NT samples were reverse polarized at 20 V for 30 s in the Ca/P-based electrolyte, followed by anodization in the same electrolyte for 30 min at 100 V. These samples were named as NT-Ca/P. Additionally, NT samples were treated in the Ca/P/Zn-based electrolyte, at the previous reverse polarization and anodization conditions, and were named as NT-Ca/P/Zn. All the reverse polarization and anodization treatments were carried out under magnetic stirring at 200 rpm.

4.2.4. Characterization of TiO_2 nanotubular films

TiO_2 nanotubular samples before and after bio-functionalization treatments were mounted on a stub with double sided conductive carbon tape, and their morphology was analyzed by scanning electron microscopy (SEM) using a FEI Helios NanoLab 650. This instrument was equipped with a detector for energy dispersive X-ray spectroscopy (EDS). EDS spectra and elemental maps were acquired to evaluate the chemical composition of the nanotubular samples and the distribution of the elements.

For a better understanding of the bio-functionalization mechanisms of TiO_2 nanotubes, the morphological and chemical features of the nanotubes were evaluated along their length. For this purpose, thin cross-sections of the nanotubular films (around 100 nm thick) were obtained in a dual beam instrument equipped with focused ion beam (FIB) (TESCAN LYRA 3) operated with gallium (Ga) ion source. A thin gold (Au) layer was previously deposited to the film surface to improve the electrical conductivity. A platinum (Pt) layer of 1 µm was locally deposited in situ using a gas injection system and 1 nA Ga^+ ion current accelerated at 30 keV. Initial etching was performed with 5 and 2 nA at 30 keV. The lamella was then transferred to a cupper (Cu) transmission electron microscopy (TEM) grid using a nanomanipulator and Pt deposition. Thinning was performed in 3 steps to obtain a lamella of ~ 100 nm: 1) 1 nA/30 keV; 2) 0.1 nA/10 keV; 3) 10 pA/5 keV. A final step was accomplished with 3 keV to reduce the damaged layer produced during the thinning process.

FIB cross-sections were investigated by TEM and dark-field scanning transmission electron microscopy (STEM-DF) using a JEOL 2100F operating at an accelerating voltage of 200 kV. EDS spectra and elemental maps were obtained in the same instrument with an EDS detector (Noran Seven), in STEM mode. Selected area electron diffraction patterns were obtained to investigate the crystallinity of the anodic oxide films.

4.3. Results

4.3.1. Surface characterization

Well-defined and well-organized TiO_2 nanotube arrays were fabricated by two-step anodization in a fluoride (F^-) containing electrolyte, whose surface morphology is depicted in Fig. 4.1a. These samples are mainly composed of Carbon (C), Ti, Oxygen (O) and Fluorine (F) as observed in the correspondent EDS spectrum in Fig. 4.1b. As demonstrated by XPS studies carried out in a previous work [48], NT surfaces are composed of Ti and O mainly as TiO_2.

TiO_2 nanotubular samples were submitted to cathodic and anodic treatments aiming their functionalization with bioactive elements, namely calcium (Ca), phosphorous (P) and zinc (Zn). For this purpose, NT samples were reverse polarized in a Ca/P-based electrolyte and, immediately after, anodized in the same solution. The surface morphology of NT-Ca/P samples is shown in Fig. 4.1c, and the correspondent EDS spectrum shows the presence of Ca and P elements (Fig. 4.1d). To achieve the incorporation of Zn, together with Ca and P, NT samples were submitted to reverse polarization and anodization processes in a Ca/P/Zn-based electrolyte, and the morphology of the fabricated nanotubes is shown in Fig. 4.1e. The presence of Zn is confirmed by the EDS spectrum shown in Fig. 4.1f. No significant differences are observed on the nanotube surface morphology before and after bio-functionalization treatments.

The EDS elemental maps in Fig. 4.2a show the homogeneous distribution of Ti, O and F along the surface of NT, NT-Ca/P and NT-Ca/P/Zn samples. The elemental maps of Ca and P extracted from NT-Ca/P samples are shown in Fig. 4.2b, while in Fig. 4.2c the elemental distribution of Ca, P and Zn on NT-Ca/P/Zn samples is depicted.

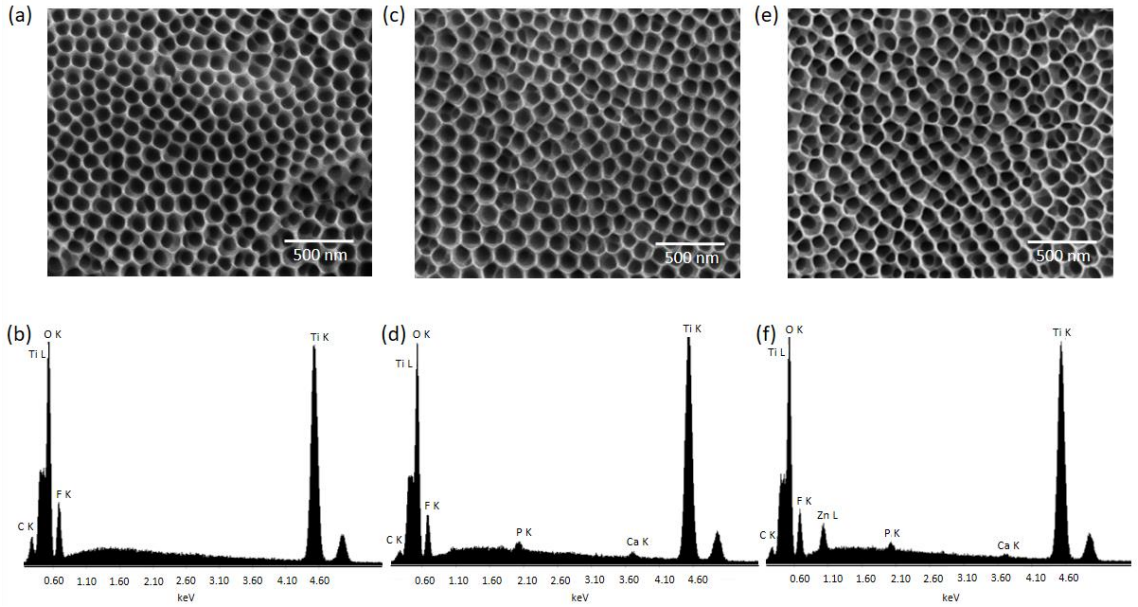

Fig. 4.1. SEM micrographs and EDS spectra showing the surface morphology and elemental composition of (a) and (b) NT; (c) and (d) NT-Ca/P; (e) and (f) NT-Ca/P/Zn samples.

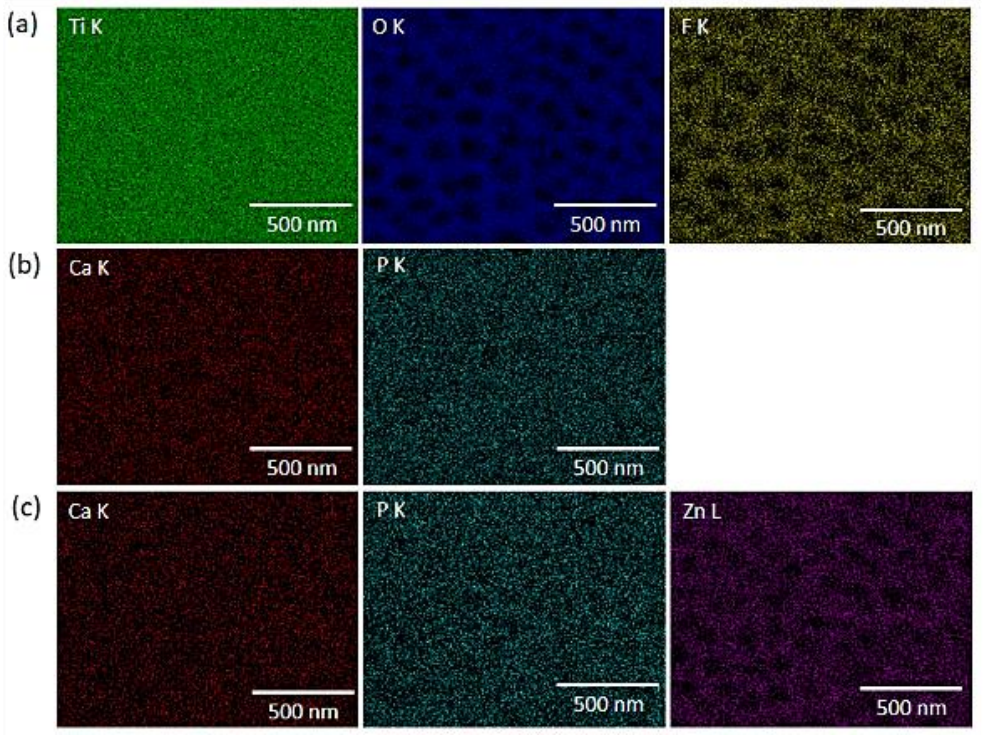

Fig. 4.2. (a) Elemental maps representative of Ti K, O K and F K extracted from NT, NT-Ca/P and NT-Ca/P/Zn samples. In (b) the elemental maps of Ca K and P K obtained from NT-Ca/P samples are depicted, while in (c) are presented the maps for Ca K, P K and Zn L elements acquired from NT-Ca/P/Zn samples. The elemental maps were obtained from the samples shown in Fig. 4.1.

4.3.2. Cross-sectional characterization of nanotubular films

Thin cross-sectional slices of the nanotubular films with approximately 100 nm thickness were obtained by FIB, then imaged by TEM and STEM and analyzed by EDS. The general overview

of TiO_2 nanotubes produced by two-step anodization is depicted in Fig. 4.3a. From this TEM image the thickness of the film was measured as 6.1 ± 0.1 µm. In Fig. 4.3b a higher magnification STEM-DF image representative of the cross-sectional view of TiO_2 nanotubes in the top region of the film is shown. The region from which the magnified image was taken is indicated by the inset square in Fig. 4.3a named as A1. From this image the wall and the hollow part of the nanotubes can be observed and, in general, the tubes are well aligned and present a uniform morphology. Furthermore, the insertion in this image shows the electron diffraction pattern composed of diffuse rings indicating an amorphous nature of TiO_2 nanotubes for this region of the film. To study the elemental distribution along the nanotubular films thickness, STEM-EDS elemental maps of Ti, O and F were acquired in the upper part and at the interface region. As observed from elemental maps depicted in Fig. 4.3c - A1, representative of the upper part of TiO_2 nanotubular films, it is observed that Ti, O and F are uniformly distributed along the nanotube thickness. Similar features are observed at the interface region shown in Fig. 4.3c - A2, where the distribution of these elements is also uniform. The interface between TiO_2 nanotubes and Ti can be easily identified in the maps by the lower O and F color intensity in the area related to Ti substrate and, on the contrary, by the higher intensity of the color for Ti in this region.

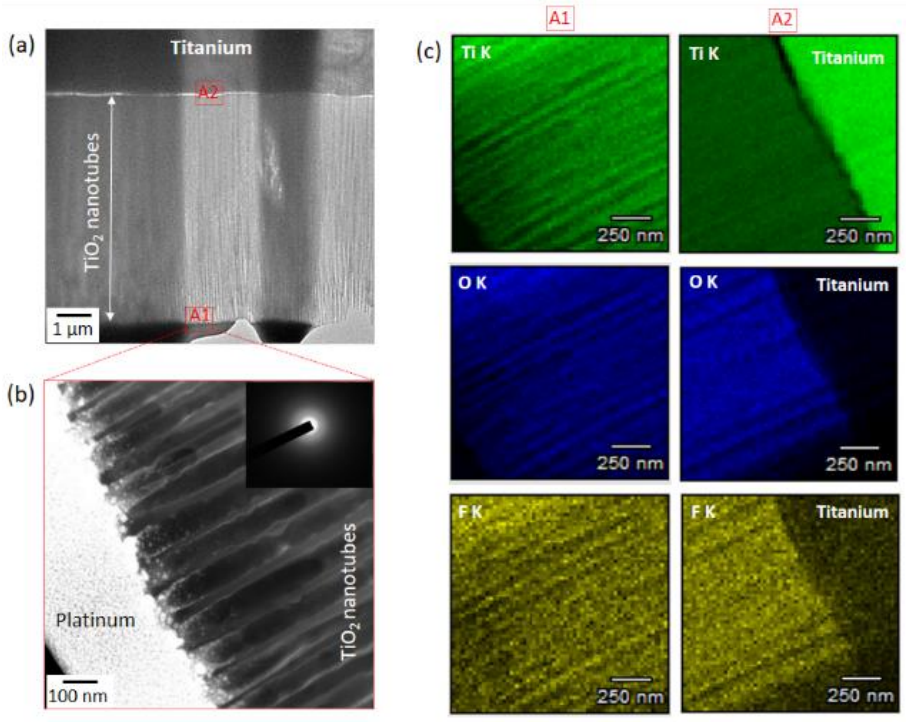

Fig. 4.3. TEM and STEM-DF images of the FIB cross-section of TiO_2 nanotubular film synthesized by two-step anodization: (a) general overview of the film; (b) upper region of the film. The inset in (b) shows the electron diffraction pattern obtained for TiO_2 film. In (c) are shown the STEM-EDS elemental maps of Ti K, O K and F K obtained from two different regions in the TiO_2 nanotubular film shown in (a): A1 – the upper region of the film; A2 – the region at the Ti/film interface.

The morphological and chemical features of TiO_2 nanotubes were also investigated after bio-functionalization treatments with Ca and P. The TEM image representative of the FIB cross-section of NT-Ca/P film is shown in Fig. 4.4a. The nanotube length, i.e the thickness of the film, was measured as 4.8 ± 0.1 µm. The upper part of the film was imaged at higher magnification as shown in Fig. 4.4b, in which well-aligned single nanotubes are clearly observed. The STEM-EDS spectrum obtained from the region indicated by the inset red square A in Fig. 4.4b, is shown in Fig. 4.4c. From this spectrum it is observed that C, Ti, O, F and Ca were detected in the superficial region of the film (until approximately 1 µm depth). Additional chemical elements such as Cu, Ga, Silicon (Si), Au and Pt were also detected in the uppermost regions of NT-Ca/P (Fig. 4.4c) film. The presence of Cu is related to the Cu grid used for TEM and STEM analyses, while the Ga is related to the Ga primary ion beam used by FIB system. Additionally, the detection of a small signal of Si is probably related with the internal fluorescence peak from Si dead layer of Si-Li detector [49]. Finally, the presence of Au and Pt are related to the Au surface coating performed before sample preparation by FIB, and to the Pt protection against Ga ions during polishing. The inset spectrum in Fig. 4.4c, with energy values comprised between 2 – 5 keV, intends to show in more detail the peak of Ca. In this spectrum, the escape peak for Ti K (Ti K - Si K = 2.77 keV) is also observed. After bio-functionalization processes in the Ca/P/Zn-based electrolyte, nanotubular films with a length of 4.6 ± 0.1 µm were produced, as shown in Fig. 4.5a. The STEM-DF image of the uppermost region of NT-Ca/P/Zn film is shown in Fig. 4.5b, from which well-ordered and single nanotubes are observed. Bright dots are Pt and Au particles that penetrated the TiO_2 nanotubes during samples preparation for FIB sectioning. The STEM-EDS spectrum acquired from the area highlighted by the inset red square in Fig. 4.5b is depicted in Fig. 4.5c. From this spectrum, elements such as C, Ti, O and F were identified, including Ca and Zn as shown by the more detailed spectrum added in the figure, with energy values comprised between 3 – 10 keV. Once again the presence of elements such as Cu, Ga, Si, Au and Pt were detected, whose source was previously explained in the above description of Fig. 4.4c. In this case, a more intense peak for Si was detected that is also probably related with the silicon carbide sandpapers used for polishing of Ti samples. Additionally, Chromium (Cr), Iron (Fe) and Cobalt (Co) were also present in the upper part of these films, which are most likely related to contamination from the metallic alligator clip used as the electrical conductive holder of Ti samples during anodization processes. It is noteworthy to highlight that additional contributions were found for both films at the elemental energy of P, which are related to Pt and Au. Therefore, it is not possible to accurately identify this element in both spectra (Fig. 4.4c and Fig. 4.5c). However, from the EDS surface spectra obtained from NT-Ca/P (Fig. 4.1d) and NT-Ca/P/Zn

(Fig. 4.1f) samples (prepared without Au and Pt), it is expected that P compounds are present in this region of the films.

For a better understanding on the elemental distribution along the length of the nanotubes in the top region of the films, STEM-EDS spectra were acquired from different regions along the STEM images depicted in Fig. 4.4b and Fig. 4.5b (results not shown). From these results the elements were found uniformly distributed along the nanotube length, and no gradient on their atomic concentration was observed. Similar results were found for STEM-EDS analysis carried out in the central part of the bio-functionalized nanotubular films (results not shown).

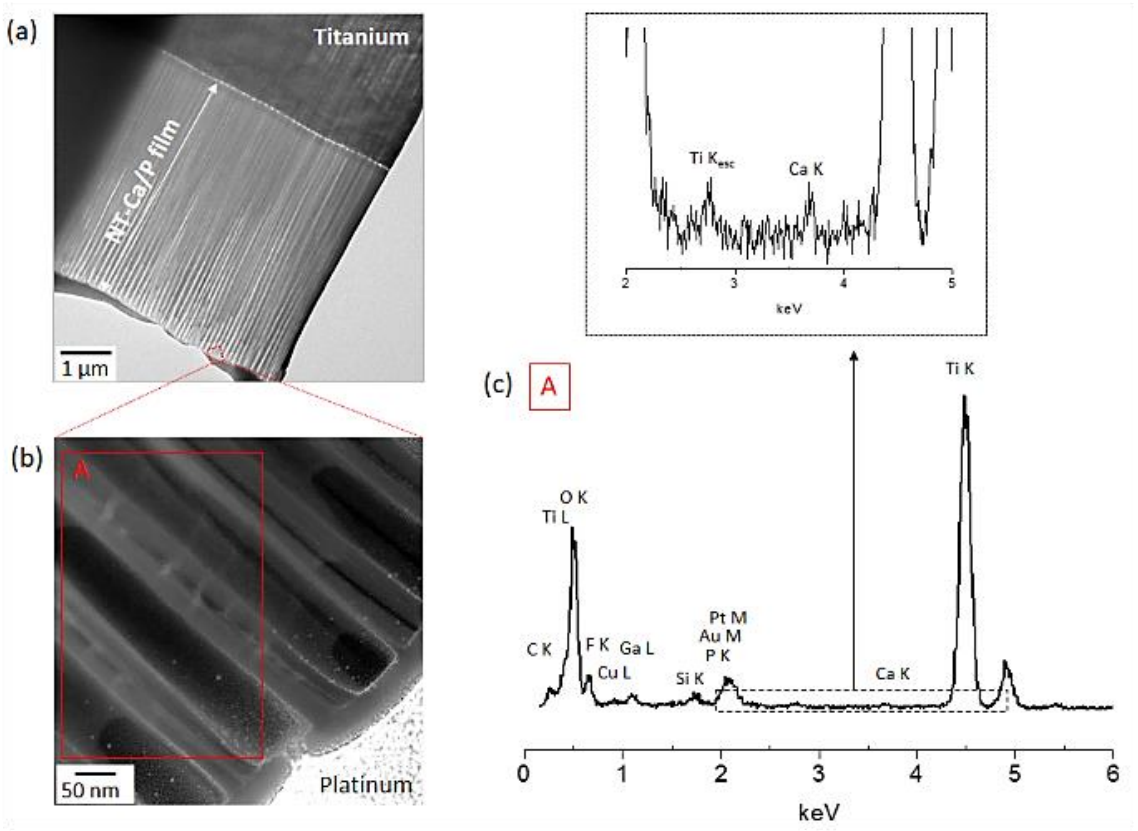

Fig. 4.4. TEM and STEM-DF images of the FIB cross-section of NT-Ca/P film: (a) TEM image showing a general overview of the film; (b) upper region of the film. In (c) the STEM-EDS spectrum obtained from the area correspondent to the inset red square A in (b) is shown. The inset spectrum in (c), with energy values comprised between 2 – 5 keV, intends to show in more detail the detected peak for Ca K.

One of the most important issues to take into consideration when a new film is being developed, is related to the characteristics of the interface between the film and the substrate, which strongly dictates the adhesion strength of the film and consequently its interfacial properties. Aiming to study the interfacial features of TiO_2 nanotubular films, before and after bio-functionalization processes, STEM-DF images were taken at the interface regions. The lower and higher magnification STEM-DF images at the interface of TiO_2 nanotubular films are shown in Fig. 4.6. The region of Ti substrate is easily identified as the brighter area contrasting with the

darker region related to TiO_2 nanotubes, as indicated in the image. A non-continuous interface is observed between TiO_2 nanotubes and the Ti substrate, as shown by the darker region appearing between TiO_2 nanotubes and Ti. This discontinuous interface characterized by a hollow space is indicated by the inset white arrow in Fig. 4.6b, and is maintained along the extension of the film with a thickness at a nanoscale range (35 ± 4.3 nm).

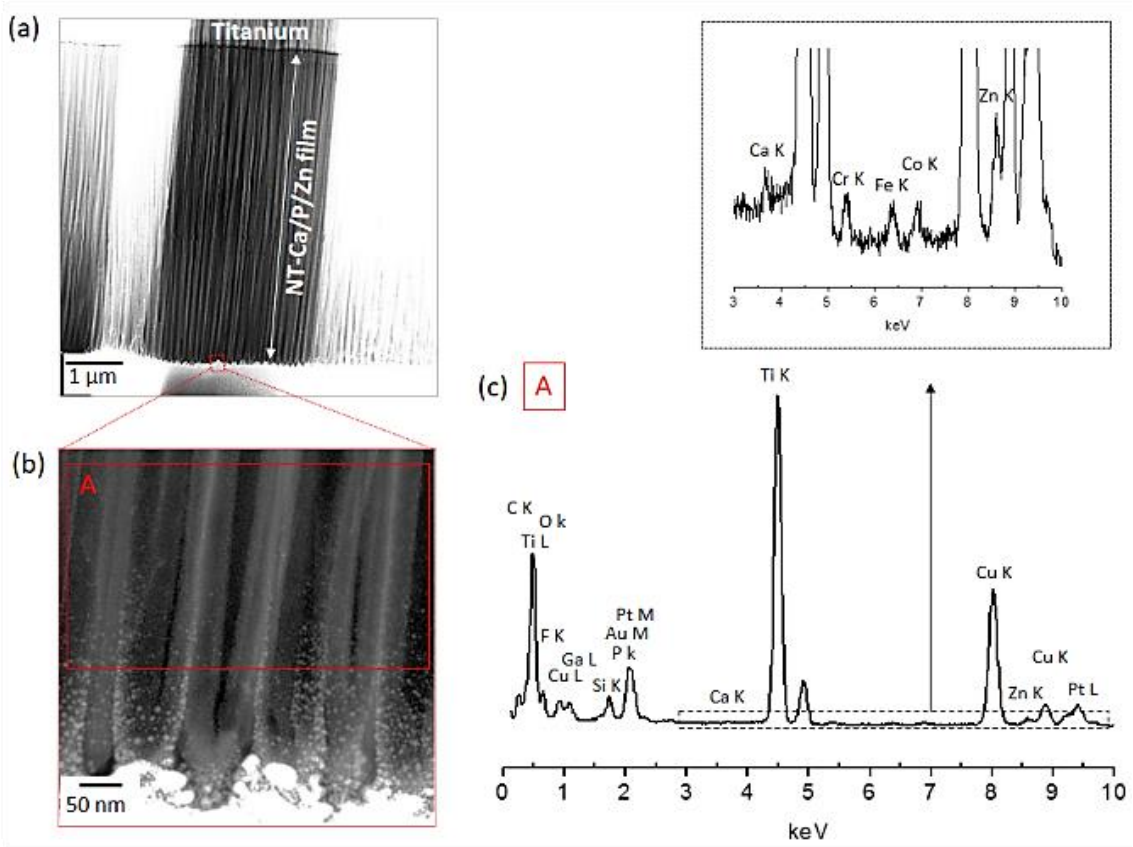

Fig. 4.5. TEM and STEM-DF images of the FIB cross-section of NT-Ca/P/Zn film: (a) general overview of the film; (b) upper region of the film. In (c) the STEM-EDS spectrum obtained from the area correspondent to the inset red square A in (b) is depicted. The inset EDS spectrum in (c), with energy values comprised between 3 – 10 keV, intends to show in more detail the detected peaks for Ca K and Zn K elements.

After bio-functionalization treatments, remarkable changes were observed at the interface, as the continuous hollow space was not observed anymore, although some defects were still present. The interface regions of NT-Ca/P and NT-Ca/P/Zn films are shown in Fig. 4.7a and b, respectively, with both films presenting an interface with similar morphological features. From higher magnification STEM-DF images shown in Fig. 4.7c and d, it is observed a porous interface characterized by the presence of an oxide film between, bellow and above the pores, suggesting the growth of an oxide film during the functionalization treatments. A second interface was found in these films, as observed from the line appearing along the films length, which is indicated with the inset white arrows in the figures. This second interface supports the hypothesis of a voltage-assisted oxide film formation, with thickness values comprised between

230 – 250 nm for both nanotubular films. NT-Ca/P and NT-Ca/P/Zn films are overall amorphous, as confirmed from electron diffraction patterns obtained from the lower, middle and upper regions of the films, characterized by broad and diffuse rings in every case (results not shown).

For a better knowledge of the differences observed at the interface region before and after bio-functionalization treatments, the current *vs.* time curves were recorded during all the anodization processes (Fig. 4.8). The current *vs.* time evolution recorded during the second step of anodization for TiO_2 nanotube formation is shown in Fig. 4.8a. This is a typical curve showing the three main stages of current achieved during anodization of Ti for nanotube formation [50]. Firstly, there is a decrease in the current values from 60 mA until approximately 15 mA. Afterwards, a slightly increase in the current is observed until 20 mA followed by a period of stabilization until the end of the anodization process. The current evolution achieved during bio-functionalization of NT samples in the Ca/P-based electrolyte is observed in Fig. 4.8b. In this curve it is shown the initial period of reverse polarization applied for 30 s, in which the current values were kept approximately at 750 mA. In the inset graph in Fig. 4.8b it is observed the evolution of the current during the anodization step carried out at 100 V for 30 min. As observed, as soon as a voltage of 100 V is applied, the current reaches the limiting value of 2.5 A for a few milliseconds, followed by a sudden decrease until approximately 0 A, a value that was kept constant until the end of the anodization period. The current *vs.* time evolution recorded during the synthesis of NT-Ca/P/Zn samples, is shown in Fig. 4.8c. In this case, during anodization, the current was kept at 2.5 A for a longer period (a few seconds), before it reaches values close to 0 A.

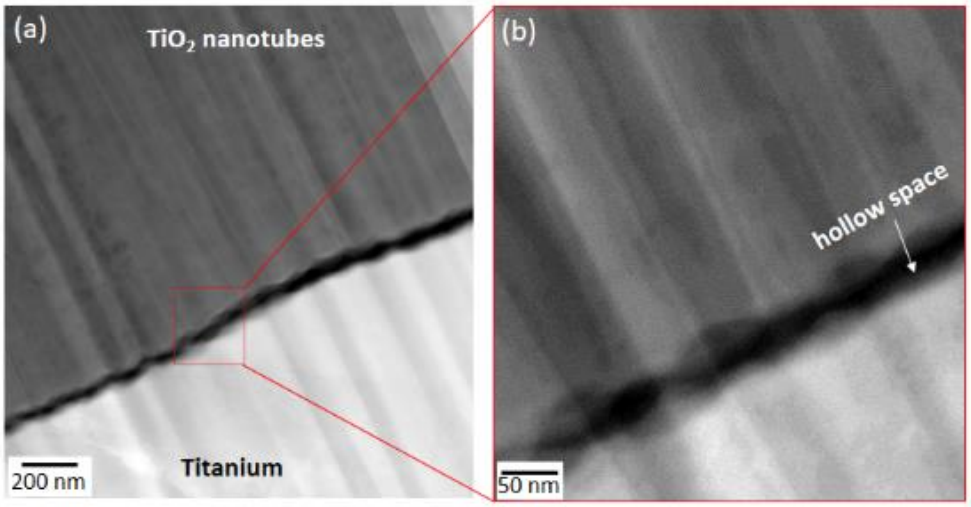

Fig. 4.6. STEM-DF images of the FIB cross-section of TiO_2 nanotubular films in the interface region at (a) lower and (b) higher magnifications.

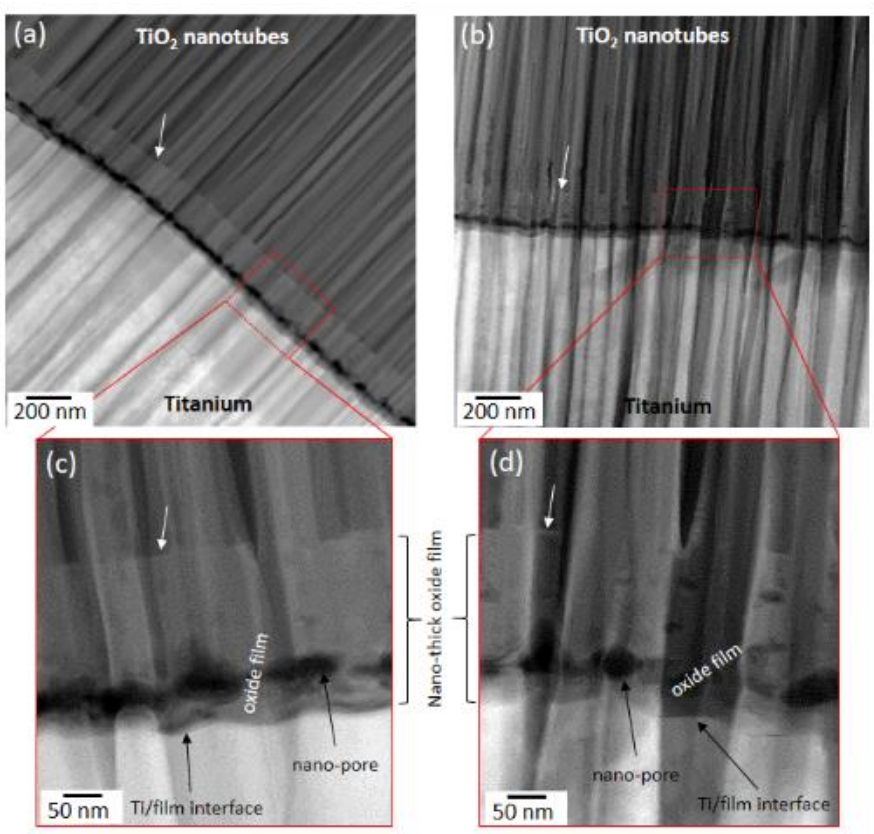

Fig. 4.7. STEM-DF images of the FIB cross-sections of (a) NT-Ca/P and (b) NT-Ca/P/Zn films in the interface region. Higher magnification images are shown in (c) and (d) for the region highlighted by inset red squares in (a) and (b), respectively. The white arrows show the interface between the nano-thick oxide films (grown during bio-functionalization processes) and TiO_2 nanotubes.

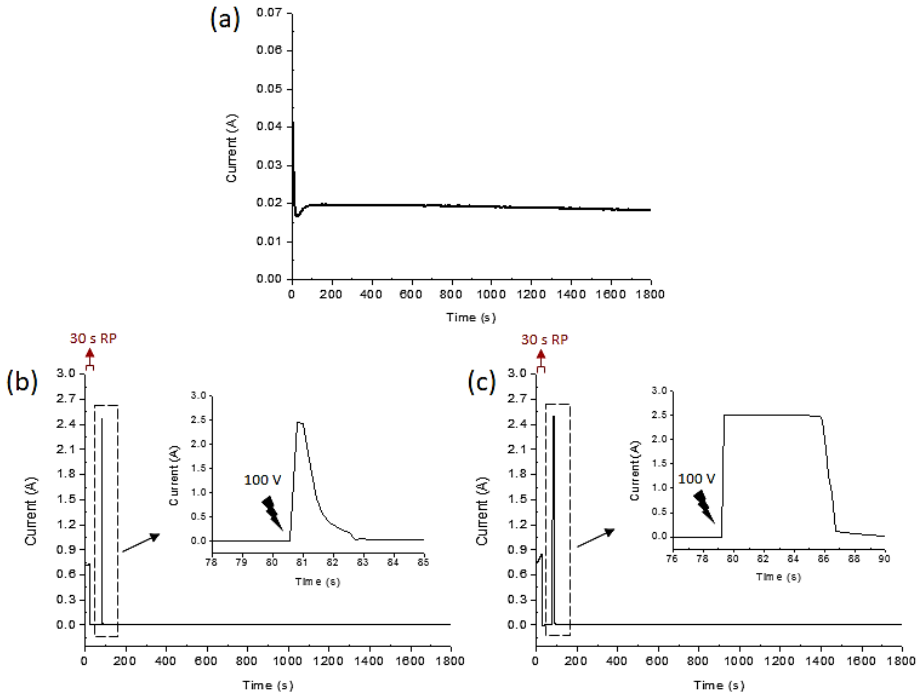

Fig. 4.8. (a) Current *vs.* time evolution during the second anodization step of nanotextured Ti for TiO_2 nanotube synthesis. The current evolutions during reverse polarization (at 20 V for 30 s) and anodization (at 100 V for 30 min) are shown for treatments carried out in the (b) Ca/P and (c) Ca/P/Zn-based electrolytes. The inset graphs in (b) and (c) intend to show in more detail the current evolution during the initial stage of anodization processes.

The chemical features of the interface of bio-functionalized films were studied aiming a better comprehension of the relation between the current *vs.* time evolution recorded during anodization, with their characteristics. For this purpose, line profile STEM-EDS analyses were carried out at the interface of NT-Ca/P films (Fig. 4.9a). The spectrum in Fig. 4.9b was extracted from the inset white square A in Fig. 4.9a and it shows the presence of Ca and P, jointly with other elements such as Ti, O, F, Ga and Si. The EDS spectra acquired from line scan analyses performed in three different spots at the interface of NT-Ca/P films is shown in Fig. 4.9c. These analyses were carried out along the uppermost part of the nano-thick film formed by anodization, as indicated by a, b and c white spots inserted in Fig. 4.9a. As it is observed, Ti, O and F were found along this line, however, there is a peak of Ca, only detected in point b, suggesting the entrapment of Ca at that site and its non-uniform distribution along the delimiting interface line. To check the Ca distribution outside and inside this interface, additional EDS analyses were carried along the points 1, 2 and 3 (shown in Fig. 4.9a), whose spectra are shown in Fig. 4.9d. The expected elements were found, namely Ti, O and F. Interestingly, the peak for Ca was also found only in point 2, evidencing the entrapment of this element at that place. Finally, the chemical features of the interface of NT-Ca/P/Zn films (Fig. 4.10a) were investigated. The general spectrum acquired from the area delimited by the inset white square in Fig. 4.10a is shown in Fig. 4.10b. The presence of the elements, such as Ti, O, F, Si, P, Ca and Zn was detected. Line scan EDS analyses were carried out at 7 specific points across the nano-thick oxide film formed by anodization (shown in Fig. 4.10a), and the correspondent acquired spectra are shown in Fig. 4.10c. The EDS analysis for each point, shows clearly the presence of P and Zn elements non-uniformly distributed across the interface. The presence of P appeared more pronounced in the intermediate zone of the film, as shown by the peaks of P found in the spots numbered from 2 – 6. Moreover, the presence of Zn was found more prominent in the spots 3 and 5. It is noteworthy to highlight that in some of the presented spectra part of the elemental peaks are not being depicted in full, once a more detailed view of the less counted peaks is aimed.

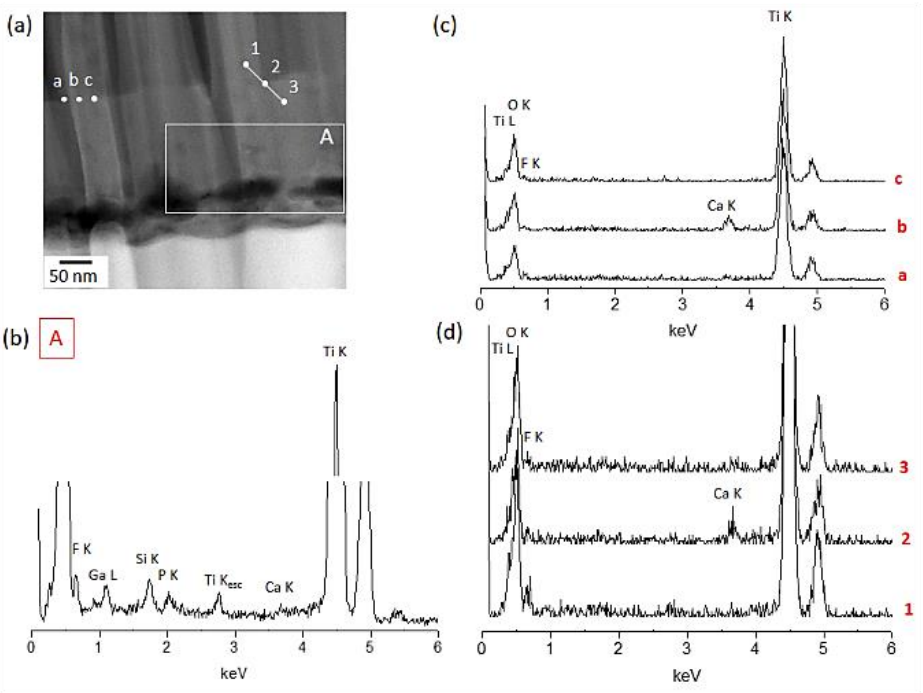

Fig. 4.9. STEM-EDS analyses in the interface region of NT-Ca/P film: (a) STEM-DF image showing the NT-Ca/P film interface, with the white insets indicating where the elemental analyses were performed; (b) EDS spectrum obtained from the region comprised in the inset red square A in (a); (c) Line scan EDS analyses along the uppermost part of the nano-thick oxide film formed by anodization, as indicated by a, b and c white spots inserted in (a); (d) Line scan EDS analyses across the uppermost part of the nano-thick oxide film, as indicated by the inset white number 1, 2 and 3 in (a).

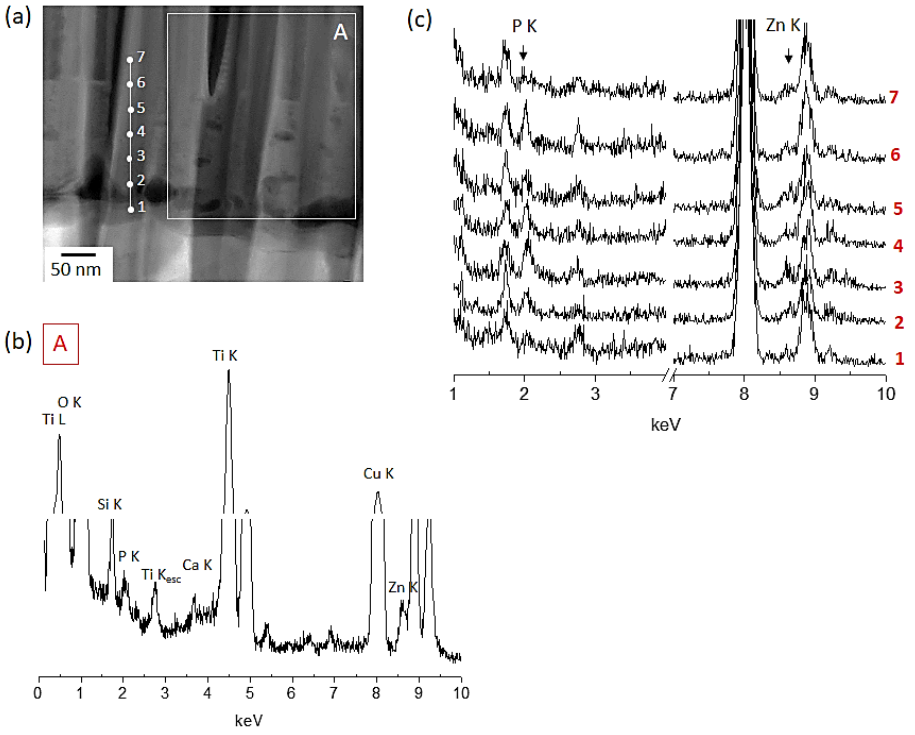

Fig. 4.10. STEM-EDS analyses in the interface region of NT-Ca/P/Zn film: (a) STEM-DF image showing the NT-Ca/P/Zn film interface, with the white insets indicating where the elemental analyses were performed; (b) EDS spectrum obtained from the region comprised by the inset white square A in (a); (c) Line scan EDS analyses along the nano-thick oxide film formed by anodization, as indicated the white spots numbered in (a) from 1 – 7.

4.4. Discussion

4.4.1. Morphological and chemical features of bio-functionalized TiO_2 nanotubes

Anodization has been extensively employed for formation of TiO_2 nanotubes [18, 19, 23, 28, 32, 35, 36, 51] and particularly, multi-step anodization of Ti in a fluoride-containing electrolyte has been investigated [52, 53] as it is known to improve the self-ordering of TiO_2 nanotubes [50]. To achieve the desired bone-inspired surface morphology observed in Fig. 4.1a, TiO_2 nanotubes were synthesized by anodization of a nano-patterned Ti surface with the nanotube bottom hemispherical morphology. These nano-imprints with nanotube bottom shape, resulted from a first anodization step of a Ti smooth surface, in which TiO_2 nanotubes were grown drilling their rounded bottom into the metallic substrate and afterwards, intentionally removed [50]. During anodization of nano-patterned Ti surfaces, it is believed that nanotubes growth is based on electric field assisted oxidation and dissolution processes, which rely on the formation of a passive Ti oxide film through the recombination of Ti^{4+}, O^{2-} and OH^- ions and the local chemical dissolution of the growing oxide by F^- ions, with the nano-imprinted dimples acting as nucleation sites for the initial pore formation [50, 54]. In this study, almost ideally hexagonally arranged nanotube arrays were grown with high self-ordering level, as demonstrated in a previous work from SEM imaging of nanotube hemispherical bottom morphology [48]. In accordance with the equifield strength model, a closed packed pore array with hemispherical bottom, tends to be formed to achieve a uniform field distribution at the pore base, and the formation of a hexagonal pore array is achieved once the self-adjustment of the pore-pore distance is reached. It is believed that the self-adjustment of the morphology of TiO_2 nanotube arrays is achieved through plastic deformation of the oxide layer to achieve a uniform field distribution [54]. This information supports that during the first and second anodization steps carried out for nanotube formation, a uniform field distribution was achieved at the bottom of each tube and that nanotube growth was based on field assisted oxidation and dissolution processes.

The synthesis of highly-ordered TiO_2 nanotube arrays presenting a bone-inspired nano-morphology was achieved. From Fig. 4.1a it is observed that this morphology is characterized by the presence of bigger and smaller pores and in some cases the formation of multiple pores inside a bigger pore is observed. This event is probably related with the nanotube formation mechanisms. Macak *et al.* [55] studied the growth phases of TiO_2 nanotubes by observation of the top surface and the cross-section of anodized Ti in an organic electrolyte containing fluoride ions. In the very first stage of the electrochemical process, the authors observed that a thin and non-porous layer was formed where localized accelerated dissolution occurred under the action of the electric field. In general, in the beginning of the anodization process some pits are

generated due to the non-homogenous dissolution rate or local dielectric breakdown at the oxide surface, acting as the starting points of pore formation [54]. From two-step anodization, it is expected that the nano-imprints generated from the first anodizing step act as nucleation sites for initial pore formation and thus, behave as an intentionally designed template to trigger localized dissolution and obtain the desired final morphology. The formation of multiple pores inside a main one is probably related with the events taking place in the beginning of the second anodization step. Possibly, the primary localized dissolution occurred in multiple sites inside the same nano-dimple, resulted from the first anodization step. Macak *et al.* [55] observed that pore nucleation events become apparent over the entire surface after 1 – 3 min of anodization, presenting a random appearance, which is maintained after 10 min of anodization [55]. Thus, it is expected that the surface morphology resulting from the primary localized dissolution is preserved over time, since during anodization, pronounced dissolution takes place at the bottom of the pores, where the electric filed is stronger, making them significantly deeper over time [54, 55]. The illustration of the different growth stages of TiO_2 nanotubes from nano-patterned Ti substrates is schematically shown in Fig. 4.11.

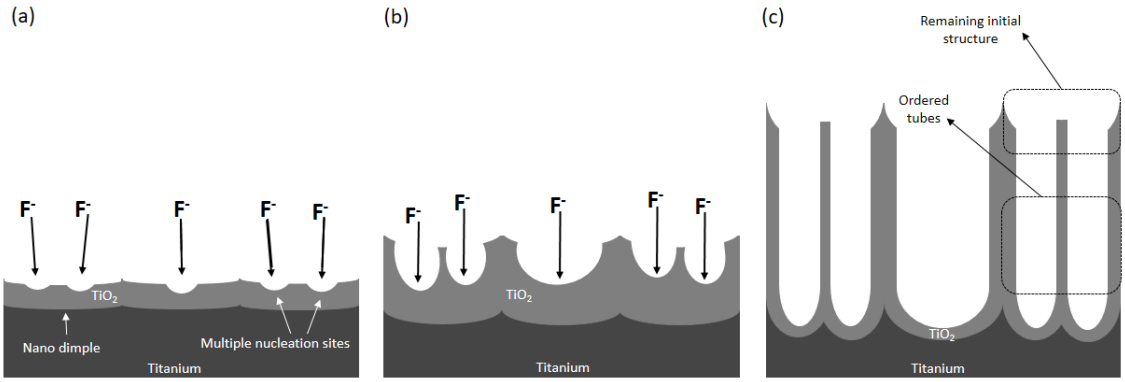

Fig. 4.11. Illustration of the different growth stages of TiO_2 nanotubes from nano-patterned Ti substrates. In (a) it is depicted the first stage during which the local chemical dissolution of the growing anodic oxide film by F^- ions takes place, with the nano-imprinted dimples acting as single or multiple nucleation sites; in (b) is shown a second stage in which the pronounced dissolution takes place at the bottom of the pores, where the electric filed is stronger; finally in (c) is depicted a later stage achieved after a long period of anodization (i.e. 30 min), after which the initial structure remains in the top region of the film while ordered tubes are underneath.

The bone-inspired TiO_2 nanotubes were doped with Ca and P, whose morphology and composition are shown in Fig. 4.1c and d, respectively. TiO_2 nanotubes were bio-functionalized using a novel methodology recently reported [48]. From previous results, biocompatible Ca/P-doped nanotube surfaces were synthesized by reverse polarization and anodization processes in a Ca/P-based electrolyte. Reverse polarization appeared as a very promising way to improve the surface biocompatibility by modifying the chemistry of the nanotubes without

compromising their morphological features. Ca and P were previously assigned to the presence of $Ca_3(PO_4)_2$/$CaHPO_4$, CaF_2, $CaCO_3$ and CaO species [48]. Beyond the lack of osseointegrative properties, Ti-based implants are also related to complicated bacterial infection due to the lack of antimicrobial properties, and so, the design of new implant surfaces with antimicrobial features is also urgently required. Recently, nano-featured surface topographies have been widely investigated as an attractive tool for reducing infection by preventing microbial adhesion at the time of implantation [56, 57]. Moreover, the surface chemistry also plays a significant role on bacteria adhesion. As demonstrated by Hu *et al.* [58] the inclusion of Zn in TiO_2 coatings by anodization improved the osteogenic differentiation of bone marrow stem cells and simultaneously, provided antibacterial activity. Therefore, the possibility of Zn incorporation on TiO_2 nanotubular structures has stimulated our interest. It was hypothesized that by changing the chemical composition of the anodization electrolyte, it would be possible to change the surface chemistry of the nanotubes, and the incorporation of Zn, without changing their morphology. To achieve this goal, zinc acetate was added to the anodization electrolyte. The presence of Zn was successfully achieved by anodization of TiO_2 nanotubes in the Ca/P/Zn-based electrolyte (Fig. 4.1f), with no differences observed on the acquired morphology (Fig. 4.1e). In general, the bioactive elements (i.e. Ca, P and Zn) are uniformly distributed along the TiO_2 nanotubular samples, as observed in EDS elemental maps shown in Fig. 4.2b and c. From O and F EDS elemental maps (Fig. 4.2a), the hollow cavity of the nanotubes is observed indicating the high self-alignment of these structures, perpendicularly oriented relatively to the Ti substrate.

TiO_2 nanotubes were grown perpendicularly oriented to the Ti substrate (Fig. 4.3a) with high self-ordering level, as observed through single nanotubes depicted in the STEM-DF image of the upper part of the film (Fig. 4.3b). EDS elemental maps taken in the upper part and at the interface region of the film show the presence of Ti, O and F along the nanotubes length (Fig. 4.3c). The morphological and chemical features of the films are related to the nanotube growing mechanisms, which are based on the establishment of an equilibrium between the oxide film formation at the Ti interface and the local chemical dissolution of the oxide by F^- ions. It has been generally accepted that a layer enriched with fluoride is formed at the oxide/metal interface during anodization. This layer can be ascribed to the twice fast migration rate of F^- compared to O^{2-} ions, resulting in a fluoride rich layer which has a thickness of a few tens of nanometers [37, 59]. The existence of this fluoride rich layer was already proved by XPS sputter profiles taken from the tube bottom side of the tubes [60]. Berger *et al.* [50] proved for the first time that TiO_2 nanotubes grown in fluoride-based ethylene glycol electrolytes form a fluoride rich layer (few nm thick) between the individual nanotubes, and this might be the reason for the detection of fluoride species all over the nanotubular layer through EDS analysis.

After bio-functionalization of TiO_2 nanotubes in both electrolytes the high level of ordering and integrity of the tubes is maintained along their length. Single nanotubes are clearly seen without any aggregates along the tube walls, they are organized in parallel to each other and perpendicularly oriented to Ti substrate from which they were grown (Fig. 4.4 and Fig. 4.5). From the EDS spectra in Fig. 4c and Fig. 4.5c it can be observed that Ti and O were detected, related with the presence of Ti oxide composing the nanotubes. The presence of F detected in both spectra indicates that bio-functionalization processes have not influenced the composition of the nanotubes regarding its F content. Beyond other techniques have been used to modify the chemical properties of Ti [61-64], reverse polarization has been revealed as a versatile approach to develop bio-functional implant surfaces for biomedical applications. Chen *et al.* [63] also used reverse polarization to introduce nanoscale calcium phosphate on TiO_2 nanotubes. The electrochemical deposition treatments were conducted in an electrolyte containing $Ca(NO_3)_2$ and $NH_4H_2PO_4$. The results indicate that β-tricalcium phosphate was formed and deposited in TiO_2 nanotube surface, inducing to an enhanced bioactivity, protein adsorption and osteogenic cell responses, by improving cellular adhesion, proliferation and differentiation.

4.4.2. Characterization of Ti/TiO_2 nanotubes interface

The bond strength between a film or a coating layer with the metallic substrate is a critical factor that influences the biomechanical stability of the implant, which is a requirement for long term implant success [38]. The adhesion strength between TiO_2 nanotubes and Ti substrate is influenced by the characteristics of the interface thus compromising many of their exciting properties and consequently, their potential use for biomedical applications. Beyond the wide range of studies reported in literature showing the promising features of these nanostructures for the design of new implant systems, little knowledge still exists on the adhesion properties of nanotubular films to the Ti substrate, and thus the ability of these structures to ensure an appropriate long term biomechanical stability. For this reason, the interfacial features of the TiO_2 nanotubular films produced by two-step anodization of Ti were investigated. After the second anodization step for TiO_2 nanotube synthesis, the presence of a non-continuous interface was found between the nanotubular film and the Ti substrate, as shown in Fig. 4.6. This interface is characterized by a hollow space that is extended over the width of the film. Although general adhesion of TiO_2 barrier layer formed by anodization of Ti is reported to be good [46, 50], a few studies have shown that TiO_2 nanotubes are susceptible to peeling off from the underlying substrate, while rinsing with water or drying, because of the poor adhesion strength of TiO_2 nanotubes to Ti [37, 46].

Aiming to understand the mechanisms underlying the TiO_2 nanotube film detachment, researchers have recently made interesting findings. Different mechanisms have been proposed for nanotube detachment, namely the water assisted dissolution of the fluoride-rich layer existing beneath the nanotubes [37, 46]. In accordance with Miraghaei *et al.* [46] TiO_2 nanotubes are detached from the substrate after immersion in aqueous solutions due to dissolution of TiF_4 layer existing between the tubes and Ti. Furthermore a hydrogen-assisted crack mechanism induced by the existence of Ti-H and hydrogen blisters in the bottom layer of the nanotubes was also reported by Zhao *et al.* [47], which may directly influence the interfacial adhesion between the nanotubes and the Ti substrate. Based on this knowledge, the existence of a hollow non-continuous interface after anodization of Ti, might be related to water assisted dissolution of a fluoride-rich layer formed underneath the nanotubes. The hollow space existing between Ti substrate and TiO_2 nanotubes bottom is of a few tens of nanometers (Fig. 4.6b), similar to the thickness reported for the fluoride-rich layer [59]. Notwithstanding, the existence of this non-continuous interface might be also related to the hydrogen assisted crack mechanism reported by Zhao *et al.* [47], since TiO_2 nanotubes were washed with distilled water after fabrication.

Researchers have recently made some efforts to improve the adhesion between TiO_2 nanotubes and Ti substrate. Zhao *et al.* [47] reported a novel method to control the detachment of TiO_2 nanotubes by their post-treatment in protic and aprotic solvents with different polarities. In accordance with the authors, the post-treatment using an organic solvent of lower polarity increases the adhesion of the tube layer, in contrast to the spontaneous detachment of the TiO_2 nanotube layer after treatment using a solvent of higher polarity. The beneficial effect of anodization of TiO_2 nanotubes on their electrochemical and photoelectrochemical responses was reported by Miraghaei *et al.* [46] due to the formation of a new barrier layer beneath them. Furthermore, Yu *et al.* [37] also employed an additional anodization step of TiO_2 nanotubes in a fluoride-free electrolyte resulting in the formation of a 200 nm thick compact layer near the nanotube bottom, which led to more than threefold increase in the adhesion strength. Recently, annealing was also a method used by Roguska *et al.* [65] to stabilize the interfacial region between Ti substrate and TiO_2 nanotubes. The authors reported that after annealing at 450^{o}C and 650^{o}C there was an increase in the thickness of the crystalline interphase region from a few up to hundred nanometers. However, no information is given about the morphology of the interface before thermal treatments. Thus, beyond the previous reports on TiO_2 nanotube film anodization have shown the formation of a nano-thick compact layer in the bottom part of the tubes with potential to improve their adhesion strength to the substrate, the morphological and chemical characterization of the newly formed film as well as of the new Ti/TiO_2 interface generated is still missing in literature. These characterization studies are of upmost relevance

since this knowledge allows the better comprehension of the adhesion phenomenon (before and after functionalization) and thus provide new insights for further improvements. Interfacial features, at a nanoscale level, may influence the performance of TiO_2 nanotubes such as electrochemical, tribo-electrochemical and mechanical, and so dictate the widespread biomedical applications of these nanostructures.

4.4.3. Understanding the bio-functionalization mechanisms of TiO_2 nanotubes by reverse polarization and anodization

The bio-functionalization of TiO_2 nanotubes was achieved by reverse polarization and anodization processes, a methodology that was previously shown to induce the formation of biocompatible and corrosion resistant Ca/P-doped TiO_2 nanotubular films [48]. The Ti/TiO_2 interface of bio-functionalized films was characterized aiming to understand the influence of reverse polarization and anodization on their features.

After bio-functionalization of TiO_2 nanotubes it is observed an interface that is not empty anymore, as a consequence of the formation of a nano-thick oxide film at the interface region of NT-Ca/P and NT-Ca/P/Zn films, which presents a nanoporous morphology (Fig. 4.7). To explain this observation current *vs.* time evolution recorded during bio-functionalization processes in the Ca/P and Ca/P/Zn-based electrolytes were considered (Fig. 4.8b and c). During anodization processes, three main stages can be identified. Firstly, once 100 V is applied, there is an increase in current values to its limiting value of 2.5 A (first stage), followed by a period during which the current drops very quickly to values near to 0 A (second stage), a stage that is kept constant until the end of the anodization process (third stage). This is the typical current *vs.* time evolution characteristic of the growth behavior of a compact oxide film on Ti by anodization in a fluoride free electrolyte [50]. A similar behavior was reported by Fernando *et al.* [66] during anodic oxidation of Ti in an electrolyte with composition similar to the one used in this study. The authors explained that the first stage of the graph (with limiting current of 2.5 A), is related to the time during which a high current contributes to the fast growth of the oxide film. As the oxide becomes thicker, its resistivity increases resulting in the decrease of the current to lower values, most likely due to the high resistivity of the newly oxide film formed that is kept constant with time. This behavior observed in Fig. 4.8b and c explains the nano-thick oxide film formation observed in Fig. 4.7, independently of the electrolyte composition. A longer duration for the first stage was achieved for anodization in the Ca/P/Zn electrolyte, probably related with its higher conductivity (Fig. 4.8c). Fernando *et al.* [66] reported that as higher this period, higher the total charge in the system is. The authors pointed out that theoretically, this would influence the total

amount of oxide grown during the process, with effects on the measured thickness and compactness of the film. Nonetheless, no significant differences were found in the thickness of the newly formed interfacial films, as in both cases, thickness ranges between 230 – 250 nm.

The study of the chemical composition of the nano-thick films formed by anodization showed that these are composed of O and Ti, including in the inter pore-areas, evidencing the growth of a Ti oxide (Fig. 4.7 c and d). Furthermore, the lighter contrast at the nano-thick oxide film region observed in STEM-DF images (Fig. 4.7), evidences the presence of a film with a higher density compared to the one in a darker area. The existence of the bioactive elements (i.e. Ca, P and Zn) at the interface region (Fig. 4.9 and Fig. 4.10) shows that the electrolyte penetrated along the film length during reverse polarization and anodization processes. Line scan EDS analyses along and across the uppermost region of the nano-thick film formed in NT-Ca/P interface (Fig. 4.9a), shows that Ca was not homogeneously distributed along the film (Fig. 4.9c) and interestingly, appeared to be entrapped on it (Fig. 4.9d). Ca entrapment at the interface is an additional indicator that the oxide film was formed during bio-functionalization processes. Line scan EDS analysis along NT-Ca/P/Zn interface evidenced a non-uniform distribution of Zn and P across the nano-thick oxide film formed. Beyond Ca has been detected in this interface (Fig. 4.10b), its presence was not identified along the line scan analyses, and this might be related with its non-uniform distribution along the film length, as discussed previously.

During reverse polarization, it is believed that positively charged ions in solution, namely Ca^{2+} and Zn^{2+} ions, are directed towards TiO_2 nanotube surface and penetrate the nanotubes towards its bottom part, as schematically illustrated in Fig. 4.12a. It is believed that during this stage, part of the Ca^{2+} and Zn^{2+} ions are adsorbed to TiO_2, and possibly Ca^{2+} ions react with F^- ions. In is noteworthy that F^- ions are present on TiO_2 nanotube wall as a result of the nanotube synthesis process. As soon as the anodization process starts, it is expected that an inversion in the electrode polarity leads to an inversion on the ions movement: those positively charged still remaining in solution, such as Ca^{2+} and Zn^{2+}, tend to move away the bottom part of the film and, on the other hand, negatively charged ions such as phosphate (PO_4^{3-}) and oxygen (O^{2-}), are directed towards the interface as illustrated in Fig. 4.12b. Simultaneously, it is expected that Ti^{4+} ions are generated at Ti surface, as a consequence of the anodic voltage applied. These ions, under the action of the electric filed, migrate through the hollow interface and the bottom part of the tubes reacting with O^{2-} ions moving in opposite direction (provided by H_2O or OH^- in the electrolyte), leading to the formation of the Ti oxide film [50]. A possible mechanism for Ca entrapment at the interface region can be ascribed to the growing of the oxide film during anodization and the simultaneous movement of positively charged Ca^{2+} ions in direction to the uppermost part of the nanotubes.

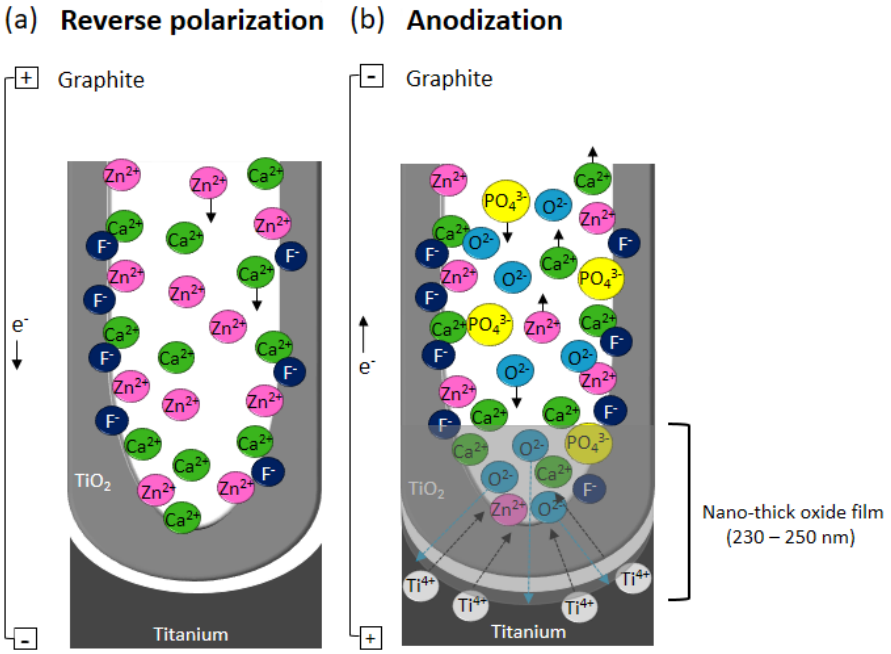

Fig. 4.12. Schematic illustration of the bio-functionalization mechanisms of TiO_2 nanotubes by (a) reverse polarization followed by (b) anodization. During anodization, Ti^{4+} ions are generated as a consequence of the polarization of Ti and they migrate across the hollow interface and the bottom part of the tubes reacting with O^{2-} ions, leading to the formation of a Ti oxide film with thickness comprised between 230 – 250 nm.

In a previous work [48], TiO_2 nanotubes displayed a significantly lower passive current in artificial saliva after bio-functionalization treatments, independently of reverse polarization step. From the findings achieved in this investigation, the formation of a nano-thick oxide film as a consequence of anodization might be the reason for the significant improvement on the electrochemical behavior of nanotubular films. These results indicate that the nano-thick oxide film display the ability to protect the Ti substrate against corrosion, thus guaranteeing good prospects for their application for osseointegrated implants.

The formation of an oxide film as a consequence of anodization in an aqueous electrolyte might influence the adhesion of the film to Ti substrate. This is an issue of main importance and therefore further adhesion tests should be conducted. Furthermore, the investigation of the mechanical properties of the bio-functionalized TiO_2 nanotubes would be also of valuable interest. The mechanical properties of the films dictate their ability to withstand to mechanical stress, and thus to resist to degradation. The investigation of the degradation behavior of TiO_2 nanotubular samples before and after bio-functionalization, should be addressed under the simultaneous action of wear and corrosion (tribocorrosion), aiming to simulate the harsh and real conditions that osseointegrated implants are submitted to. Lastly, but not the least, a deepest investigation on the biological responses to these bio-functionalized TiO_2 nanotubes is

of upmost importance. More specific biological assays must be accomplished to ensure that the surface features of these structures do not compromise the cellular functions.

4.5. Conclusions

Bioactive elements of Zn, Ca, and P were successfully incorporated in TiO_2 nanotubular structures through reverse polarization and anodization processes. Cross-sectioned bio-functionalized nanotubular films were characterized regarding morphology and chemistry with a special focus given to Ti/TiO_2 nanotubes interface. Hereafter the main outcomes of this research are highlighted:

- The incorporation of Ca, P and Zn elements in TiO_2 nanotubes was successfully achieved by reverse polarization and anodization processes, with the bioactive elements uniformly distributed along the topmost regions of the films as well along their length.
- Bio-functionalization treatments do not compromise the bone-inspired morphology of TiO_2 nanotubes, neither their high self-ordering and integrity.
- The anodization of TiO_2 nanotubes in aqueous electrolytes induces the growth of a nano-thick protective oxide film (230 – 250 nm) at the Ti/TiO_2 nanotube interface region, which appears to improve the interfacial features, suggesting a better adhesion property. This interfacial nano-thick oxide film is constituted by Ca, P and Zn, however, these elements appeared to be non-uniformly distributed across the film length, with Ca found to be entrapped on its superficial region.

Reverse polarization arises as a fundamental step to confer biocompatibility to TiO_2 nanotubes while anodization promotes the growth of a nano-thick oxide film at the Ti/TiO_2 interface, providing an improved corrosion behavior to TiO_2 nanotubes. This highlights the potential of the nano-thick film to improve the bonding strength of the nanotubular film to Ti, a critical factor determining the biomechanical stability of an implant, and so its long term success. This work brings up a first insight on the bio-functionalization mechanisms of TiO_2 nanotubular films by reverse polarization and anodization processes. This novel methodology may inspire the emergence of novel surface treatment strategies seeking the long-term performance of metallic-modified implants.

Acknowledgements

The authors would like to thank the Portuguese Foundation for Science and Technology for the doctoral grant (Ref. SFRH/BD/88517/2012) as well CNPq (Brazil - Ref. 490761/2013-5) and CAPES (Brazil - Ref. 99999.008666/2014-08) for the financial support. Also, the authors acknowledge

all the support from LABNANO/CBPF (Brazilian Center for Research in Physics) for electron microscopy analyses. Tolou Shokuhfar is especially thankful to US National Science Foundation NSF-DMR CAREER award# 1564950 for providing partial financial support.

References

[1] Navarro M, Michiardi A, Castano O, Planell J. Biomaterials in orthopaedics, Journal of the Royal Society Interface 5 (2008), 1137-1158.
[2] Bauer S, Schmuki P, von der Mark K, Park J. Engineering biocompatible implant surfaces: Part I: Materials and surfaces, Progress in Materials Science 58 (2013), 261-326.
[3] Oshida Y, Tuna EB, Aktören O, Gençay K. Dental implant systems, International journal of molecular sciences 11 (2010), 1580-1678.
[4] Neoh KG, Hu X, Zheng D, Kang ET. Balancing osteoblast functions and bacterial adhesion on functionalized titanium surfaces, Biomaterials 33 (2012), 2813-2822.
[5] Norowski PA, Bumgardner JD. Biomaterial and antibiotic strategies for peri-implantitis: A review, Journal of Biomedical Materials Research Part B: Applied Biomaterials 88B (2009), 530-543.
[6] Taylor TD. Prosthodontic problems and limitations associated with osseointegration, The Journal of Prosthetic Dentistry 79 (1998), 74-78.
[7] Porter JA, Von Fraunhofer JA. Success or failure of dental implants? A literature review with treatment considerations, General dentistry 53 (2004), 423-432; quiz 433, 446.
[8] Yu Y, Jin G, Xue Y, Wang D, Liu X, Sun J. Multifunctions of dual Zn/Mg ion co-implanted titanium on osteogenesis, angiogenesis and bacteria inhibition for dental implants, Acta Biomaterialia 49 (2016), 590-603.
[9] Subbiahdoss G, Kuijer R, Grijpma DW, van der Mei HC, Busscher HJ. Microbial biofilm growth vs. tissue integration:"The race for the surface" experimentally studied, Acta Biomaterialia 5 (2009), 1399-1404.
[10] Gulati K, Aw MS, Losic D. Drug-eluting Ti wires with titania nanotube arrays for bone fixation and reduced bone infection, Nanoscale research letters 6 (2011), 571.
[11] Svensson S, Suska F, Emanuelsson L, Palmquist A, Norlindh B, Trobos M, Bäckros H, Persson L, Rydja G, et al. Osseointegration of titanium with an antimicrobial nanostructured noble metal coating, Nanomedicine: Nanotechnology, Biology and Medicine 9 (2013), 1048-1056.
[12] Zhang W, Wang G, Liu Y, Zhao X, Zou D, Zhu C, Jin Y, Huang Q, Sun J, et al. The synergistic effect of hierarchical micro/nano-topography and bioactive ions for enhanced osseointegration, Biomaterials 34 (2013), 3184-3195.
[13] Yazici H, Fong H, Wilson B, Oren E, Amos F, Zhang H, Evans J, Snead M, Sarikaya M, et al. Biological response on a titanium implant-grade surface functionalized with modular peptides, Acta Biomaterialia 9 (2013), 5341-5352.
[14] Huang H-L, Chang Y-Y, Weng J-C, Chen Y-C, Lai C-H, Shieh T-M. Anti-bacterial performance of Zirconia coatings on Titanium implants, Thin Solid Films 528 (2013), 151-156.
[15] Jin G, Qin H, Cao H, Qiao Y, Zhao Y, Peng X, Zhang X, Liu X, Chu PK. Zn/Ag micro-galvanic couples formed on titanium and osseointegration effects in the presence of S. aureus, Biomaterials 65 (2015), 22-31.
[16] Swami N, Cui Z, Nair LS. Titania nanotubes: novel nanostructures for improved osseointegration, Journal of Heat Transfer 133 (2011), 034002.
[17] Balasundaram G, Webster TJ. Nanotechnology and biomaterials for orthopedic medical applications, Nanomedicine 1 (2006), 169-176.
[18] Friedrich CR, Kolati M, Moser T, Sukotjo C, Shokuhfar T. Survivability of TiO2 nanotubes on the surface of bone screws, Surface Innovations 2 (2014), 60-68.
[19] Bhosle S, Patel S, Taheril MM, Sukotjo C, Shokuhfar T. Electrochemical anodization of Ti-15Zr Implant: Effect of different voltage and time, Surface Innovations (2017), 1-26.
[20] Robin A, de Almeida Ribeiro MB, Rosa JL, Nakazato RZ, Silva MB. Formation of TiO2 Nanotube Layer by Anodization of Titanium in Ethylene Glycol-H2O Electrolyte, J Surf Eng Mater Adv Technol 2014 (2014).
[21] Kulkarni M, Mazare A, Park J, Gongadze E, Killian MS, Kralj S, von der Mark K, Iglič A, Schmuki P. Protein interactions with layers of TiO2 nanotube and nanopore arrays: Morphology and surface charge influence, Acta Biomaterialia 45 (2016) 357-366.
[22] Tian A, Qin X, Wu A, Zhang H, Xu Q, Xing D, Yang H, Qiu B, Xue X, et al. Nanoscale TiO2 nanotubes govern the biological behavior of human glioma and osteosarcoma cells, Int J Nanomedicine 10 (2015), 2423.
[23] Hamlekhan A, Butt A, Patel S, Royhman D, Takoudis C, Sukotjo C, Yuan J, Jursich G, Mathew MT, et al. Fabrication of anti-aging TiO2 nanotubes on biomedical Ti alloys, PLoS One 9 (2014), e96213.
[24] Lv L, Liu Y, Zhang P, Zhang X, Liu J, Chen T, Su P, Li H, Zhou Y. The nanoscale geometry of TiO2 nanotubes influences the osteogenic differentiation of human adipose-derived stem cells by modulating H3K4 trimethylation, Biomaterials 39 (2015), 193-205.

[25] Chen J, Zhang Z, Ouyang J, Chen X, Xu Z, Sun X. Bioactivity and osteogenic cell response of TiO2 nanotubes coupled with nanoscale calcium phosphate via ultrasonification-assisted electrochemical deposition, Appl Surf Sci 305 (2014), 24-32.
[26] Roguska A, Pisarek M, Andrzejczuk M, Dolata M, Lewandowska M, Janik-Czachor M. Characterization of a calcium phosphate-TiO2 nanotube composite layer for biomedical applications, Mater Sci Eng C 31 (2011), 906-914.
[27] Frandsen CJ, Brammer KS, Noh K, Johnston G, Jin S. Tantalum coating on TiO 2 nanotubes induces superior rate of matrix mineralization and osteofunctionality in human osteoblasts, Mater Sci Eng C 37 (2014), 332-341.
[28] Shokuhfar T, Hamlekhan A, Chang J-Y, Choi CK, Sukotjo C, Friedrich C. Biophysical evaluation of cells on nanotubular surfaces: the effects of atomic ordering and chemistry, International journal of nanomedicine 9 (2014), 3737.
[29] Mazare A, Totea G, Burnei C, Schmuki P, Demetrescu I, Ionita D. Corrosion, antibacterial activity and haemocompatibility of TiO2 nanotubes as a function of their annealing temperature, Corrosion Science 103 (2016), 215-222.
[30] Guo Z, Chen C, Gao Q, Li Y, Zhang L. Fabrication of silver-incorporated TiO2 nanotubes and evaluation on its antibacterial activity, Materials Letters 137 (2014), 464-467.
[31] Li H, Cui Q, Feng B, Wang J, Lu X, Weng J. Antibacterial activity of TiO2 nanotubes: influence of crystal phase, morphology and Ag deposition, Applied Surface Science 284 (2013), 179-183.
[32] Zhao Y, Xing Q, Janjanam J, He K, Long F, Low K-B, Tiwari A, Zhao F, Shahbazian-Yassar R, et al. Facile electrochemical synthesis of antimicrobial TiO2 nanotube arrays, International journal of nanomedicine 9 (2014), 5177.
[33] Zhang H, Sun Y, Tian A, Xue XX, Wang L, Alquhali A, Bai X. Improved antibacterial activity and biocompatibility on vancomycin-loaded TiO2 nanotubes: in vivo and in vitro studies, Int J Nanomedicine 8 (2013), 4379.
[34] Gulati K, Ramakrishnan S, Aw MS, Atkins GJ, Findlay DM, Losic D. Biocompatible polymer coating of titania nanotube arrays for improved drug elution and osteoblast adhesion, Acta Biomaterialia 8 (2012), 449-456.
[35] Shokuhfar T, Sinha-Ray S, Sukotjo C, Yarin AL. Intercalation of anti-inflammatory drug molecules within TiO 2 nanotubes, Rsc Advances 3 (2013), 17380-17386.
[36] Hamlekhan A, Sinha-Ray S, Takoudis C, Mathew MT, Sukotjo C, Yarin AL, Shokuhfar T. Fabrication of drug eluting implants: study of drug release mechanism from titanium dioxide nanotubes, Journal of Physics D: Applied Physics 48 (2015), 275401.
[37] Yu D, Zhu X, Xu Z, Zhong X, Gui Q, Song Y, Zhang S, Chen X, Li D. Facile method to enhance the adhesion of TiO2 nanotube arrays to Ti substrate, ACS applied materials & interfaces 6 (2014), 8001-8005.
[38] Mohseni E, Zalnezhad E, Bushroa A. Comparative investigation on the adhesion of hydroxyapatite coating on Ti–6Al–4V implant: A review paper, International Journal of Adhesion and Adhesives 48 (2014), 238-257.
[39] Velard F, Braux J, Amedee J, Laquerriere P. Inflammatory cell response to calcium phosphate biomaterial particles: an overview, Acta Biomaterialia 9 (2013), 4956-4963.
[40] Ribeiro AR, Gemini-Piperni S, Travassos R, Lemgruber L, C. Silva R, Rossi AL, Farina M, Anselme K, Shokuhfar T, et al. Trojan-Like Internalization of Anatase Titanium Dioxide Nanoparticles by Human Osteoblast Cells, Scientific reports 6 (2016), 23615.
[41] Olmedo D, Paparella M, Brandizzi D, Cabrini R. Reactive lesions of peri-implant mucosa associated with titanium dental implants: a report of 2 cases, International journal of oral and maxillofacial surgery 39 (2010), 503-507.
[42] Goodman SB, Ma T, Chiu R, Ramachandran R, Smith RL. Effects of orthopaedic wear particles on osteoprogenitor cells, Biomaterials 27 (2006), 6096-6101.
[43] Rocha L, Oliveira F, Cruz H, Sukotjo C, Mathew M. Bio-Tribocorrosion in Biomaterials and Medical Implants, In Bio-tribocorrosion in dental applications, Elsevier Inc. (2013), 223-249.
[44] Alves S, Bayón R, Igartua A, Saénz de Viteri V, Rocha L. Tribocorrosion behaviour of anodic titanium oxide films produced by plasma electrolytic oxidation for dental implants, Lubrication science 26 (2014), 500-513.
[45] Alves S, Bayón R, de Viteri VS, Garcia M, Igartua A, Fernandes M, Rocha L. Tribocorrosion Behavior of Calcium- and Phosphorous-Enriched Titanium Oxide Films and Study of Osteoblast Interactions for Dental Implants, Journal of Bio-and Tribo-Corrosion 1 (2015), 1-21.
[46] Miraghaei S, Ashrafizadeh F, Raeissi K, Santamaria M, Di Quarto F. An Electrochemical Investigation on the Adhesion of As-Formed Anodic TiO2 Nanotubes Grown in Organic Solvents, Electrochemical and Solid-State Letters 14 (2011), K8-K11.
[47] Zhao M, Li J, Li Y, Wang J, Zuo Y, Jiang J, Wang H. Gradient Control of the Adhesive Force between Ti/TiO2 Nanotubular Arrays Fabricated by Anodization, Scientific reports 4 (2014).
[48] Alves SA, Patel SB, Sukotjo C, Mathew MT, Filho PN, Celis J-P, Rocha LA, Shokuhfar T. Synthesis of calcium-phosphorous doped TiO2 nanotubes by anodization and reverse polarization: A promising strategy for an efficient biofunctional implant surface, Applied Surface Science 399 (2017), 682-701.
[49] Williams DB, Carter CB. Transmission Electron Microscopy, Springer US, 2009.
[50] Roy P, Berger S, Schmuki P. TiO2 nanotubes: synthesis and applications, Angewandte Chemie International Edition 50 (2011), 2904-2939.
[51] Patel S, Solitro GF, Sukotjo C, Takoudis C, Mathew MT, Amirouche F, Shokuhfar T. Nanotopography and surface stress analysis of Ti6Al4V bioimplant: an alternative design for stability, JOM 67 (2015), 2518-2533.

[52] Ali G, Chen C, Yoo SH, Kum JM, Cho SO. Fabrication of complete titania nanoporous structures via electrochemical anodization of Ti, Nanoscale research letters 6 (2011), 1-10.
[53] Yuan X, Zheng M, Ma L, Shen W. High-speed growth of TiO2 nanotube arrays with gradient pore diameter and ultrathin tube wall under high-field anodization, Nanotechnology 21 (2010), 405302.
[54] Su Z, Zhou W. Formation, morphology control and applications of anodic TiO2 nanotube arrays, Journal of Materials Chemistry 21 (2011), 8955-8970.
[55] Macak J, Hildebrand H, Marten-Jahns U, Schmuki P. Mechanistic aspects and growth of large diameter self-organized TiO2 nanotubes, Journal of Electroanalytical Chemistry 621 (2008), 254-266.
[56] Ercan B, Taylor E, Alpaslan E, Webster TJ. Diameter of titanium nanotubes influences anti-bacterial efficacy, Nanotechnology 22 (2011), 295102.
[57] Puckett SD, Taylor E, Raimondo T, Webster TJ. The relationship between the nanostructure of titanium surfaces and bacterial attachment, Biomaterials 31 (2010), 706-713.
[58] Hu H, Zhang W, Qiao Y, Jiang X, Liu X, Ding C. Antibacterial activity and increased bone marrow stem cell functions of Zn-incorporated TiO2 coatings on titanium, Acta Biomaterialia 8 (2012), 904-915.
[59] Berger S, Albu SP, Schmidt-Stein F, Hildebrand H, Schmuki P, Hammond JS, Paul DF, Reichlmaier S. The origin for tubular growth of TiO2 nanotubes: a fluoride rich layer between tube-walls, Surface Science 605 (2011), L57-L60.
[60] Albu SP, Ghicov A, Aldabergenova S, Drechsel P, LeClere D, Thompson GE, Macak JM, Schmuki P. Formation of Double-Walled TiO2 Nanotubes and Robust Anatase Membranes, Advanced Materials 20 (2008), 4135-4139.
[61] Gao A, Hang R, Huang X, Zhao L, Zhang X, Wang L, Tang B, Ma S, Chu PK. The effects of titania nanotubes with embedded silver oxide nanoparticles on bacteria and osteoblasts, Biomaterials 35 (2014), 4223-4235.
[62] Xie C, Li P, Liu Y, Luo F, Xiao X. Preparation of TiO2 nanotubes/mesoporous calcium silicate composites with controllable drug release, Materials Science and Engineering: C 67 (2016), 433-439.
[63] Chen J, Zhang Z, Ouyang J, Chen X, Xu Z, Sun X. Bioactivity and osteogenic cell response of TiO 2 nanotubes coupled with nanoscale calcium phosphate via ultrasonification-assisted electrochemical deposition, Applied Surface Science 305 (2014), 24-32.
[64] Zhao L, Wang H, Huo K, Cui L, Zhang W, Ni H, Zhang Y, Wu Z, Chu PK. Antibacterial nano-structured titania coating incorporated with silver nanoparticles, Biomaterials 32 (2011), 5706-5716.
[65] Roguska A, Pisarek M, Belcarz A, Marcon L, Holdynski M, Andrzejczuk M, Janik-Czachor M. Improvement of the bio-functional properties of TiO2 nanotubes, Applied Surface Science 388 (2016), 775-785.
[66] Oliveira FG, Ribeiro AR, Perez G, Archanjo BS, Gouvea CP, Araújo JR, Campos AP, Kuznetsov A, Almeida CM, et al. Understanding growth mechanisms and tribocorrosion behaviour of porous TiO 2 anodic films containing calcium, phosphorous and magnesium, Applied Surface Science 341 (2015), 1-12.

CHAPTER 5

TiO_2 nanotubes enriched with calcium, phosphorous and zinc: promising bio-selective functional surfaces for osseointegrated titanium implants

Submitted for publication in Biomaterials

TiO_2 nanotubes enriched with calcium, phosphorous and zinc: promising bio-selective functional surfaces for osseointegrated titanium implants

S.A. Alves[1,2*], A.R. Ribeiro[2,3,4,5], S. Gemini-Piperni[6], R.C. Silva[3], A.M. Saraiva[3], P.E. Leite[3], G. Perez[7], J.R. Araujo[7], B.S. Archanjo[7], M.E. Rodrigues[8], M. Henriques[8], J.-P Celis[9], T. Shokuhfar[10,11], L.A. Rocha[1,2,12], R. Borojevic[2,13], J.M. Granjeiro[2,3,14]

[1]*CMEMS – Center of MicroElectroMechanical Systems, Department of Mechanical Engineering, University of Minho, Azurém, 4800-058 Guimarães, Portugal*
[2]*IBTN/BR – Brazilian Branch of the Institute of Biomaterials, Tribocorrosion and Nanomedicine, Faculty of Sciences, UNESP – Universidade Estadual Paulista, 17033-360 Bauru, São Paulo, Brazil*
[3]*Directory of Metrology Applied to Life Sciences, National Institute of Metrology, Quality and Technology, 25250-020 Duque de Caxias – RJ, Brazil*
[4]*Postgraduate Program in Translational Biomedicine, University of Grande Rio – UNIGRANRIO, 25070-000 Duque de Caxias – RJ, Brazil*
[5]*Postgraduate Program in Biotechnology, National Institute of Metrology, Quality and Technology, 25250-020 Duque de Caxias – RJ, Brazil*
[6]*Brazilian Center for Research in Physics, 22290-180 Rio de Janeiro, Brazil*
[7]*Metrology Materials Division, National Institute of Metrology Quality and Technology, 25250-020 Duque de Caxias – RJ, Brazil*
[8]*CEB – Centre of Biological Engineering, University of Minho, Campus de Gualtar, 4710-057 Braga, Portugal*
[9]*Department of Materials Engineering, KU Leuven, 3001 Leuven, Belgium*
[10]*Department of Bioengineering, University of Illinois at Chicago, 60607 Chicago, Illinois, USA*
[11]*IBTN/US – American Branch of the Institute of Biomaterials, Tribocorrosion and Nanomedicine, University of Illinois at Chicago, 60612 Chicago, Illinois, USA*
[12]*Faculdade de Ciências, Departamento de Física, UNESP – Universidade Estadual Paulista, 17033-360 Bauru, São Paulo, Brasil*
[13]*Center of Regenerative Medicine, Faculty of Medicine of Petrópolis – FASE, 25680-120 Petrópolis – RJ, Brazil*
[14]*School of Dentistry, Fluminense Federal University, 24220-900 Niterói – RJ, Brazil*
**e-mail: sofiafonso@msn.com*

Abstract

The lack of osseointegration and implant-related infections are two major complications leading to failure of dental and orthopedic implants. Therefore, the development of effective titanium (Ti) implant surfaces able to display enhanced osteogenic activity and antimicrobial properties is a challenge, and such multifunctional surfaces have only recently been studied. In particular, titanium dioxide (TiO_2) nanotubes (NTs) have demonstrated promising features to modulate biological responses, as they may be easily tailored to achieve multiple functions. This work aims to functionalize TiO_2 NTs through a novel methodology, and to study their ability to induce osseointegration, and concomitantly, to avoid infection.

TiO_2 NTs were bio-functionalized with bone-constituting calcium (Ca), phosphorous (P), and zinc (Zn) elements, the last playing a major role in bone remodeling while exhibiting antibacterial properties. Bio-functionalization of TiO_2 NTs was achieved by reverse polarization anodization. Morphological and topographical surface features of NTs were observed through scanning electron microscopy (SEM), while surface chemistry was investigated by X-ray photoelectron spectroscopy (XPS). Biocompatibility studies were conducted with MG-63 and

human mesenchymal stem cells (hMSCs) through MTT assay. Furthermore, cell morphology and cytoskeleton organization were observed by SEM and laser scanning confocal microscopy (LSCM). The osteoblastic differentiation capacity of hMSCs was studied by real-time PCR, as well as their angiogenesis ability by measuring the total release of vascular endothelial growth factor (VEGF). Finally, viability of *Staphylococcus aureus (S. aureus)* was assessed by live/dead bacterial viability assay. Results show that TiO_2 NTs modulated cells morphology, suggesting a stronger adhesion. Moreover, hMSCs in contact with NTs, released a significantly higher amount of VEGF compared to adequate Ti controls. In particular, NTs enriched with Ca, P, and Zn, induced to significantly up-regulated levels of bone morphogenetic protein 2 (BMP-2) and osteopontin (OPN) genes of hMSCs, when compared to conventional NTs, along with the significant reduction in the number of live bacteria as compared to Ti.

In conclusion, the superimposition of TiO_2 nanotubular-textured surfaces and their enrichment with Ca, P, and Zn, is a very promising approach for the development of novel bio-selective implant surfaces able to improve osseointegration, and simultaneously, avoid infection.

Keywords: TiO_2 nanotubes; Bio-functionalization; Bio-selectivity; Osseointegration; Infection**.**

5.1. Introduction

Titanium (Ti) and its alloys are the most commonly used materials for orthopedic and dental implants applications owing their excellent mechanical properties, corrosion resistance and biocompatibility [1, 2]. The good corrosion resistance and biocompatibility of Ti-based materials, are associated with their ability to form a stable and tightly adherent TiO_2 thin film (1.5 – 10 nm in thickness) when exposed to oxygen [1, 3]. Nonetheless, the lack of a functional implant-bone interface (i.e. poor osseointegration), extensive inflammation, and bacterial infection, have been currently reported as the main causes of failure of Ti-based implants [4-7]. Implant-related infections are often the result of bacteria adhesion on implant surface during surgery [4, 8], with *S. aureus* accounting for 70 % of orthopedic implants infections [5]. Infection may lead to extensive revision surgeries, extended antibiotic treatment, tissue integration impairment, significant health care expenses, and in some cases, even death [8, 9].

It has been reported that approximately 332.000 primary hip and 719.000 primary total knee arthroplasties were performed in the US in 2010, with infection rates of 0.8 – 2.2 % [9]. Aseptic loosening, widely related to poor osseointegration, is responsible for > 70 % hip revision surgeries over the mid- and long-term [10]. As concerns dental implants, a 8-year follow up

analysis in patients with age from 21 – 78 years reported failure rates of 2 – 3 % [11], mainly associated to bone loss and/or inflammation (52.5 %), as well as implant mobility (43.4 %). Additionally, a 10-year follow up study conducted in elderly patients (≥ 65 years), reported failure rates of 8 – 9 % associated with bone loss and peri-implant inflammation [12]. The number of dental implant procedures is expected to boost in the near future, not only because life expectancy is increasingly high, but also because dental implant therapies have become progressively adopted as a treatment option for replacing missing teeth [13]. Therefore, if implant-related complications are not surmounted, the number of failures is expected to rise within the upcoming years.

The demand for new and innovative strategies aiming the synthesis of efficient implant surfaces has attracted the attention of worldwide researchers, as a strategy to mitigate failures of hip and dental implants. The modification of implant surface features has been currently adopted, and improved biological responses have been achieved through the creation of rough surfaces with an enhanced chemistry and a more compatible morphology/topography for bone cells [3, 14-16]. In particular, nanostructures have demonstrated to play a fundamental role on biological responses, by mimicking the nanoscale features of bone [3, 17, 18]. Anodization is a simple, versatile, and low-cost technique that has been widely used to fabricate TiO_2 NTs in Ti surfaces, as the next generation of dental and orthopedic implants. TiO_2 nanotubular surfaces have become increasingly recognized to enhance osteoblasts and mesenchymal stem cells (MSCs) functions, e.g. adhesion, proliferation, and differentiation [19-23], or even to reduce inflammation and impair bacterial adhesion or survival [24-27].

Functionalization attempts of TiO_2 NTs have been widely reported by immersion, electrochemical deposition, plasma spraying, sputtering, and sol-gel processes [28-31]. Beyond the promising potential to induce osseointegration and reduce infection, nanotubular surfaces can behave as effective drug delivery systems. A successful example of a drug delivery system based on TiO_2 NTs was reported by Hu et al. [32] The authors loaded TiO_2 NTs with BMP-2 and covered them with multilayered coatings of gelatin/chitosan for controlled drug release. The system demonstrated ability to promote osteoblastic differentiation of MSCs. For tailoring TiO_2 NTs with advanced functionalities, various attempts have been performed through the incorporation of a wide variety of bioactive and/or antimicrobial agents into their cavities, such as modular peptides, anti-inflammatory and/or anti-infectious drugs, as well as inorganic bioactive elements such as silver (Ag), Zn, P, and Ca [2, 28, 32-39]. In particular, Zn appears as a very interesting regulator of bone formation, since Zn^{2+} ions can regulate various intracellular signaling cascades involved in osteoblastic differentiation [40]. Previous studies have demonstrated that Zn promotes the expression of bone-related genes, as well as stimulate

osteoblast proliferation and mineralization [34, 41]. Huo *et al.* [34] produced TiO_2 NTs incorporated with Zn by hydrothermal treatment, and the amount of Zn could be adjusted by varying nanotube diameter and length. The authors concluded that the inclusion of Zn provided relevant intrinsic antibacterial properties against *S. aureus*, as well as an excellent osteogenesis inducing ability, as shown by higher alkaline phosphatase (ALP) synthesis and mineralized nodules formation by bone MSCs. The beneficial effect of Zn was also shown by Yusa *et al.* [42] after incorporation of this element on Ti surfaces. As a result of this, human dental pulp stem cells presented significantly up-regulation levels of osteoblast-related genes of runt-related transcription factor-2 (RUNX-2), collagen type-1 (COL-1), BMP-2, ALP, OPN, and VEGF.

The next generation of orthopedic and dental implants displaying both osteogenic and antibacterial properties is required to achieve improved clinical performances. In a recent work of our group [33], a novel and promising strategy for functionalization of TiO_2 NTs was reported, by incorporation of Ca and P via reverse polarization anodization processes. Bio-functionalized TiO_2 NTs displayed the ability to improve cell functions and minimize bio-degradation of Ti and conventional NTs by corrosion. In the present work, the additional incorporation of Zn into TiO_2 NTs was achieved through the previously reported methodology. In this study, the influence of bio-functionalized nanotubular surface features on osteoblast-like and hMSCs functions was studied. Beyond cell viability and adhesion ability, the aim was to study the differentiation of MSC through the expression of osteoblast-related genes (RUNX-2, ALP, COL-1, BMP-2 and OPN) and VEGF synthesis, and furthermore, the impact of bio-functionalization on the adhesion and viability of *S. aureus*. This study brings novel and important insights on the influence of the morphological, topographical and physicochemical properties of bio-functionalized TiO_2 NTs to enhance the adhesion, differentiation, as well as the release of VEGF by hMSCs, and simultaneously, to decrease bacterial viability.

5.2. Materials and Methods

5.2.1. Synthesis and characterization of bio-functionalized TiO_2 NTs

Pure Titanium (Ti, 99.7 %) foils (thickness 0.25 mm) were purchased (Sigma-Aldrich, St. Louis, MO, USA) and cut into 10 mm x 10 mm squares. These samples were chemically etched in a solution containing 10 vol. % nitric acid (HNO_3) and 2 vol. % hydrofluoric acid (HF) for 10 min. Cleaning of both groups of samples was performed in the ultrasonic bath in isopropanol (10 min) followed by distilled water (5 min), and finally dried at room temperature. Cleaned Ti samples were termed as TiP and TiE before and after chemical etching, respectively.

After chemical etching and cleaning, TiE samples were connected to an electrochemical cell with a two-electrode configuration and connected to a dc power supply (KEYSIGHT, N5751A). A graphite rod was used as the cathode and TiE samples as the anode. TiO_2 NTs were synthesized by two-step anodization of TiE samples in an optimized electrolyte constituted of ethylene glycol (EG, Sigma-Aldrich, St. Louis, MO, USA), 0.3 wt. % ammonium fluoride (NH_4F, Ammonium Fluoride, Sigma-Aldrich, St. Louis, MO, USA) and 3 vol. % distilled water. Firstly, TiE samples were anodized at 60 V for 1 h under magnetic stirring (150 rpm) followed by ultrasonic cleaning in isopropanol (15 min) and distilled water (5 min). Secondly, the resulting nanopatterned surfaces were anodized for 30 min at the previous conditions for nanotube growth. Finally, the anodized samples were cleaned in isopropanol (10 min), distilled water (5 min) and dried at room temperature. The resulting TiO_2 nanotubular samples were named as NT.

Afterwards, the bio-functionalization treatments of NT samples were performed according to a novel methodology recently reported elsewhere [33], which relies on reverse polarization and anodization treatments of TiO_2 NTs. In brief, the electrochemical treatments were conducted in an aqueous electrolyte composed of 0.35 M calcium acetate (Calcium acetate monohydrate, Sigma-Aldrich, St. Louis, MO, USA) and 0.04 M β-glycerolphosphate (β-GP) (β-glycerolphosphate disodium salt pentahydrate, Sigma-Aldrich, St. Louis, MO, USA), as the source of Ca and P respectively. For cathodic and anodic treatments, the NT samples were immersed in the Ca/P-based electrolyte under magnetic stirring (200 rpm) 2 cm away from a graphite rod. Afterwards, the surfaces were reverse polarized for 30 s, followed by anodization in the same electrolyte for 30 min at 100 V. Aiming the incorporation of Zn, 0.35 M zinc acetate (Zinc acetate dihydrate, Sigma-Aldrich, St. Louis, MO, USA) was added to the previous Ca/P-based electrolyte and bio-functionalization treatments of NT samples were conducted at the previous conditions. All the anodization processes were conducted at room temperature (22 to 24 ^{o}C). Finally, the samples were cleaned in isopropanol (10 min), distilled water (5 min) and dried at room temperature. The resulting TiO_2 NTs enriched with Ca and P were named as NT-Ca/P, while the ones containing Zn were named as NT-Ca/P/Zn.

The surface morphology and chemical composition of all samples were analyzed by Scanning Electron Microscopy (SEM, FEI Nova NanoLab 600) and Energy Dispersive X-ray Spectroscopy (EDS). EDS spectra were collected using 15 kV accelerating voltage with the samples 50° tilted, to guarantee the acquisition of more signal from TiO_2 NTs and less from Ti substrate. Chemical composition of the surfaces was further investigated by X-ray Photoelectron Spectroscopy (XPS, Escaplus system, Omicron Nanotechnology) using Mg Kα as the X-ray source at 1253.6 eV. Sputter-etch cleaning of samples was carried out operated at 1 kV and 5 mA for

20 min. High resolution spectra were acquired with a resolution of 0.08 eV at a pass energy of 40 eV. Binding energy of C 1s peak at 284.6 eV was used as the reference binding energy for calibration.

5.2.2. Biological characterization

Prior to cell culture experiments, the surfaces (including their backsides) were sterilized by 2 h immersion in ethanol 70 % (V/V) followed by 2 h of ultraviolet light irradiation, in a sterile culture hood.

5.2.2.1. Culture of human osteosarcoma MG-63 cells

Human osteosarcoma MG-63 cells (ATCC number CRL-1427™) were provided by Rio de Janeiro cell bank and were used for cell-materials interactions studies. Osteosarcoma cells (osteoblast-like cells) are derived from malignant bone tumors and are commonly used for osteoblastic models [43]. Osteoblast-like MG-63 cells in passage 105 were cultured in standard culture plates in Dulbecco's High Glucose Modified Eagles Medium (DMEM High Glucose, Lonza) supplemented with 10 % (V/V) of fetal bovine serum (FBS, Vitrocell, Embriofile) and 1 % (V/V) of penicillin-streptomycin (Sigma-Aldrich) in a humidified atmosphere with 5 % carbon dioxide (CO_2) at 37 °C. The culture medium was changed every three days. For cell culture experiments, at approximately 80 % confluence, the adherent cells were washed with phosphate buffered solution (PBS) and enzymatically detached with trypsin.

5.2.2.2. Culture of primary human mesenchymal stem cells

Although cells derived from osteosarcoma are regularly used as osteoblastic models, these are derived from malignant bone tumors consisting of cells with abnormal functionalities in regards to the gene expression profiles and extracellular proteins translation, as compared to normal osteoblasts [43].

Therefore, to better predict the influence of surface features on human healthy cells, studies were also performed with primary human mesenchymal stem cells (hMSCs). These cells are known to play a major role in bone formation and regeneration [44], therefore these studies become fundamental to strengthen our findings and predict real *in vivo* responses. In this study, hMSCs were isolated from bone marrow after surgical procedures on two adult healthy donors. The consent was obtained from all the individuals and all the procedures were approved by the ethics committee of Arthur Sá Earp Neto Faculty and Faculty of Medicine of Petrópolis (CAAE

number: 46618615.8.0000.5245). The cells were negative for mycoplasma [45] and authenticated by STR analysis [46].

Briefly, to isolate the cellular fraction, the collected bone marrow was homogenized in a vortex for three cycles of 15 s. Afterwards, it was washed in PBS and homogenized again followed by centrifugation for 15 min. After this step, the supernatant was discarded and the pellet was resuspended in Iscove's medium (Sigma-Aldrich) supplemented as follows: 20 % (V/V) FBS; 1 % (V/V) ciprofloxacin antibiotic (Isofarma); 10 % (V/V) essential amino acids; 10 % (V/V) pyruvate; 10 % (V/V) glutamine; and 10 % (V/V) vitamins. After determination of cell concentration, the cellular suspension was cultured in sterile cell culture flasks (1 x 10^7 cells/25 cm^2) with fresh supplemented Iscove's medium, and placed in the incubator at 37 °C and 5 % CO_2. After 24 h post-seeding, the culture medium was replaced for the first time, and then it was changed every two – three days. *In vitro* experiments were carried out with hMSCs at 2 – 3 passages. At approximately 80 % confluence, the adherent cells were washed with PBS and enzymatically detached with trypsin.

For osteoblastic differentiation, hMSCs were cultured with Iscove's medium supplemented with 10 mM β-Glycerolphosphate (Sigma-Aldrich), 50 µg/mL ascorbic acid-2 phosphate (Sigma-Aldrich) and 100 nM dexamethasone (Sigma-Aldrich). This supplement is currently used to stimulate the differentiation of MSCs into osteoblasts [44]. Throughout this work, Iscove's osteogenic medium was named as Iscove's OM.

5.2.2.3. Cell viability

The viability of MG-63 cells and hMSCs cultured on TiP, TiE, NT, NT-Ca/P and NT-Ca/P/Zn samples was investigated through MTT (3-(4,5-dimethyl-2-thiazolyl)-2,5-diphenyl-2H-tetrazolium bromide) reduction assay. Firstly, the samples were placed (in triplicate per test condition) in 24-well polystyrene culture places, and afterwards 2 x 10^4 cells were seeded on each sample. The cells were additionally cultured on the wells of the culture plate for cell viability control. After seeding, the cells were incubated at 37 ^oC in a 5 % CO_2 atmosphere and the culture medium was changed every two – three days. MG-63 cells and hMSCs were cultured with DMEM High Glucose and OM Iscove's culture medium, respectively. Each culture medium was supplemented as previously described.

Cell viability was evaluated after one and six days of culture. After each culture period, the cells were incubated with MTT (0.5 mg/mL, Sigma-Aldrich, MO, USA) for 4 hours at 37 °C. The MTT assay allows the assessment of metabolically active viable cells, which convert MTT into a purple colored formazan product [47]. After the incubation period the formazan was

solubilized by dimethyl sulfoxide (DMSO) and the absorbance was measured at λ = 570 nm and λ = 690 nm (background) on a microplate reader spectrometer (Infinite® 200 PRO, Tecan).

Three independent experiments were carried out for cell viability studies with MG-63 and hMSCs, and only hMSCs derived from one patient were used to conduct these tests.

5.2.2.4. Cell morphology, spreading and adhesion

Osteoblast-like MG-63 cells and hMSCs were seeded on TiP, TiE, NT, NT-Ca/P and NT-Ca/P/Zn samples for 24 h. The studies with hMSCs were carried out only with cells extracted from one single patient. For this purpose, 1 x 10^4 cells were seeded on materials surfaces, which had been previously placed into 24-well culture plates. MG-63 cells were cultured as described above. After one day of incubation, the cells were washed in PBS and fixed for 2h (room temperature) with 2.5 % (V/V) glutaraldehyde (Electron Microscopy Sciences) in 0.1 M cacodylate buffer, pH 7.4 (Electron Microscopy Sciences). Afterwards, the samples were washed three times (5 min each) in cacodylate buffer and then postfixed with 1 % (V/V) osmium tetroxide in distilled water for 1 h, in dark conditions. After washing steps in cacodylate buffer and distilled water, the cells were dehydrated in series of graded ethanol solutions of 15 %, 30 %, 50 %, 70 %, 90 % and 100 % (V/V), followed by critical point drying (Leica EM CPD030, Leica microsystems, Austria). Finally, the samples were placed onto a stub and sputter coated with carbon. The cell morphology was then observed in a FEI Magellan 400 microscope.

Morphological features of hMSCs were also investigated by laser scanning confocal microscopy by cytoskeleton staining of actin filaments and nucleus. Briefly, 1 x 10^4 hMSCs were seeded on materials surfaces for 2 h incubation period in Iscove's medium. After this time, the cells were washed in PBS and fixed with a solution of 4 % (V/V) paraformaldehyde in PBS for 20 min. Afterwards, hMSCs were washed twice in PBS (5 min each) and permeabilized with 0.1 % (V/V) Triton X-100 in PBS, for 30 minutes. After washing in PBS the cells, were incubated in 50 nM NH_4Cl in PBS for 15 min for blocking of non-specific binding sites. Then, hMSCs were incubated with Alexa Fluor® 546 Phalloidin (Molecular Probes, Life Technologies) in darkness for 60 min, and after washing twice in PBS (5 min each), the nucleus was stained with 4',6-Diamidino-2-Phenylindole, Dehydrochloride (DAPI) (Molecular Probes, Life Technologies) for 10 min. At the end, the cells were imaged using a Leica TCS SP3 confocal microscope.

5.2.2.5. Expression of osteoblast-related genes

The expression levels of osteoblast-related genes were determined by real-time quantitative polymerase chain reaction (qPCR). hMSCs were seeded (2 x 10^4 cells) on TiP, TiE, NT, NT-Ca/P and NT-Ca/P/Zn samples and incubated for 14 days in OM Iscove's. Four different

samples were used per each condition. After 14 days of incubation, the cells were washed in PBS and the total RNA was extracted using RNeasy Plus mini kit (Qiagen) in accordance with manufacturer's instructions. Afterwards, the RNA concentrations were determined by using a NanoDrop 2000c spectrophotometer (Thermo Scientific) at 260 nm (A_{260}). Only samples with A_{260}/A_{280} and A_{260}/A_{230} ratio equal or greater than 1.8 were used for the subsequent steps, since this is an indicator of absence of contamination by protein and organic compounds. After RNA extraction and quantification, first-strand cDNA was synthesized from 200 ng of RNA using SuperScript® IV First-Strand synthesis kit (Invitrogen™, Life Technologies), by following manufacturer's instructions. The qPCR experiments were carried out with a 7500 Real-Time PCR system (Applied Biosystems®) using Power SYBR® green PCR master mix (Applied Biosystems™, Life Technologies).

The relative expression of genes related to osteoblastic differentiation was determined, namely runt-related transcription factor-2 (RUNX-2), alkaline phosphatase (ALP), collagen type-1 (COL-1), bone morphogenetic protein-2 (BMP-2) and osteopontin (OPN). Their main functionalities may be summarized as follows: RUNX-2 is an essential transcription factor involved in the very early stage of osteoblast differentiation; ALP is a specific protein that displays a crucial role in osteoblast differentiation and mineralization of bone matrix; COL-1 is a key structural protein of bone matrix; BMP-2 is a protein that stimulates bone formation; and OPN is a major structural protein of bone matrix [48-52]. The nucleotide sequences of forward (F) and reverse (R) primers used for qPCR are shown in Table 5.1. The relative gene expression levels were determined based on the comparative Ct method (also known as $2^{-\Delta\Delta Ct}$) [53], and these were normalized to that of the endogenous housekeeping gene cancer susceptibility candidate 3 (CASC-3). Fold change values were determined with TiP as the reference group.

The qPCR assays were performed only for hMSCs and two independent experiments were carried out with cells obtained from each donor. Therefore, a total number of four independent tests (n = 4) were carried out.

Table 5.1. Forward (F) and reverse (R) sequences of primers used for qPCR.

Gene	Forward primer sequence (5' – 3')	Reverse primer sequence (5' – 3')
RUNX-2	TGGTTACTGTCATGGCGGGTA	TCTCAGATCGTTGAACCTTGCTA
ALP	ACTGGTACTCAGACAACGAGA	ACGTCAATGTCCCTGATGTTATG
COL-1	GAGGGCCAAGACGAAGACATC	CAGATCACGTCATCGCACAAC
BMP-2	ACTACCAGAAACGAGTGGGAA	GCATCTGTTCTCGGAAAACCT
OPN	AGACCTGACATCCAGTACCCT	GTGGGTTTCAGCACTCTGGT
CASC-3	AGCCTTCTTTCCTGCAACCA	GGTCCTGCTCCCATGTGTATATG

5.2.2.6. Alkaline phosphatase activity and matrix mineralization

In this study, human fibroblasts (hFb) and human Saos-2 osteosarcoma cells were cultured on polystyrene culture plate wells as negative and positive controls of osteoblastic

differentiation of hMSCs, respectively. Human fibroblasts were obtained from surgical procedures of a healthy donor child in accordance with a local Ethical Committee (University of Grande Rio – UNIGRANRIO, CAAE number: 46799215.1.3001.5282) and Saos-2 cells were provided by Rio de Janeiro cell bank. Saos-2 cells were used as positive control instead of MG-63 cells, because they reveal the most mature osteoblastic labelling profile [43]. Alkaline phosphatase (ALP) activity and matrix mineralization were assessed for hFb, Saos-2, and hMSCs seeded on culture plate wells (2 x 10^4 cells, in triplicate) for 14 and 21 days, respectively. It is noteworthy that hFb were cultured in Iscove's medium, Saos-2 in DMEM High Glucose medium, and hMSCs in Iscove's OM. DMEM high clucose and Iscove's culture mediums were supplemented as above described.

After 14 days of culture, the cells were washed in PBS and fixed with a solution of 4 % (V/V) paraformaldehyde in PBS for 20 min. After washing in PBS, the ALP activity was detected by incubation in a mixture of naphthol AS-MX phosphate alkaline solution with fast red violet B salt (Leukocyte Alkaline Phosphatase Kit, Sigma-Aldrich), in accordance with manufacturer's instructions. Finally, images were acquired in an inverted microscope (Zeiss, Axio Observer.D1, Germany) by using a 10 x objective. The matrix mineralization of cells was evaluated by Alizarin Red S staining (Sigma-Aldrich). Briefly, after culturing for 21 days, all the cells were washed in PBS and fixed with a solution of 4 % (V/V) paraformaldehyde in PBS for 20 min, and then washed with distilled water. Afterwards, the cells were incubated with Alizarin red S solution 1 % (wt/vol) for 30 min. Finally, the samples were washed 5x with distilled water to remove the unabsorbed dye, and images were obtained in the previous mentioned inverted microscope (10 x objective).

5.2.2.7. Analysis of VEGF secretion

hMSCs were seeded (2 x 10^4 cells) on TiP, TiE, NT, NT-Ca/P and NT-Ca/P/Zn samples and incubated for 14 days in Iscove's OM. The culture medium was changed every two days. At day 14, 1 mL of the culture medium was collected with 48 h of incubation, for detection and quantification of vascular endothelial growth factor (VEGF) produced by hMSCs in contact with the different materials. VEGF detection was performed through bead-based immunoassay with the XMap Technology (Luminex Corp, USA) by using a singleplex kit (Biorad, USA). Afterwards, washes were performed using the automated washer Bio-Plex Pro (Biorad, USA). Identification and quantification of the magnetic beads containing VEGF were performed with a Bio-Plex MAGPIX system (Biorad, USA) following manufacturer's protocol. Finally, the concentration of VEGF was quantified with xPONENT software version 4.2 (Biorad, USA). These experiments were carried out in triplicate, to guarantee the repeatability of the results.

5.2.3. Antibacterial test

The antibacterial ability of TiO_2 nanotubular surfaces was accessed using *S. aureus* as the target organism. *S. aureus* ATCC 6538 obtained from stock solid cultures were grown in Tryptic Soy Broth medium (TSB, Liofilchem) at 37 °C for approximately 24 h. Before bacterial seeding, the samples were placed inside a 24-well culture plate and all the samples were sterilized by immersion in ethanol 70 % (V/V) for 2 h inside a sterile culture hood.

Bacterial concentration was determined by measuring absorbance at 620 nm (EZ Read 800 Plus Microplate reader, Biochrom), and the cell suspension was adjusted to an optical density corresponding to the final concentration of 1 x 10^5 cell/mL.

Samples previously sterilized by immersion in ethanol 70 % (v/v) for 2 h in 24-well plates, were seeded with 1 mL of the prepared cell suspension and incubated for 2 h at 37 °C and 120 rpm. Samples were then washed twice in PBS and the viability of adherent bacteria was accessed by LIVE/DEAD® BacLight™ bacterial viability kit (Molecular Probes, Life Technologies) in accordance with manufacturer's instructions. Finally, the total number of live and dead bacteria adhered on materials surfaces was determined by fluorescence microscope (Olympus BX51, Perafita, Portugal), using a combination of the 470 to 490 nm and 530 to 55 nm optical excitation filters. A total number of 35 images were acquired for each sample, from which the number of live and dead bacteria were counted. For each testing condition, three samples were used and three independent experiments were carried out.

5.2.4. Statistical analysis

All the quantitative data were expressed as means $\pm$ standard deviations. The statistical tool SigmaStat 3.5 (Systat Software, San Jose, CA, USA) was used for statistical analysis with $p < 0.05$ considered as being statistically significant and $p < 0.01$ considered highly significant.

One-Way ANOVA was applied to determine the differences between the different groups of surfaces and Tukey HSD post hoc analysis was used for pair-wise comparisons between groups. In particular, the statistical significance in the relative gene expression of hMSCs, measured between the control group and all the others testing groups, was determine by t-student test.

5.3. Results

5.3.1. Surface characterization

In this study, smooth and micron/nano-roughened Ti surfaces (TiP and TiE) were taken as control groups, whose morphologies are depicted in Fig. 5.1a and b respectively. The morphological and chemical surface features of TiO_2 nanotubular films synthesized by two-step

anodization processes are depicted in Fig. 5.1c. A bone-inspired morphology was achieved at a nano-scale level, with NTs characterized by non-uniform diameters ranging from 50 – 90 nm, as reported in a previous study [33]. XPS studies were conducted to determine the surface chemical features of TiO_2 NTs, through which chemical elements such as Ti, Oxygen (O) and Fluorine (F) were detected. The individual XPS spectra of these elements were deconvoluted into their components aiming to study their binding states. The deconvoluted peaks are shown in the individual spectra of the elements with reference to the subpeak binding energy and the possible chemical compound assigned to it (Fig. 5.1c). The high resolution spectra of Ti $2p_{3/2}$ and O 1s confirm the presence of TiO_2 by the subpeaks found at 458.8 eV and 530 eV [36, 54, 55], respectively. The energy difference of 5.7 eV for Ti $2p_{1/2}$ and Ti $2p_{3/2}$ confirms the presence of TiO_2 [54]. Two additional contributions were found in Ti $2p_{3/2}$ spectrum, which are most likely related to the presence of Ti_2O_3 (456.9 eV) and Ti-OH (458.3 eV) compounds [56, 57]. The O 1s spectrum showed an additional subpeak at 531.4 eV assigned both to the presence of Ti_2O_3 and Ti-OH [54, 55, 58] compounds. Adsorbed fluoride (F^-) ions on TiO_2 nanotubular surfaces were also found by the F 1s peak detected at 684.6 eV [54]. EDS analysis confirmed the presence of Ti, O, F and C (Fig. 5.1f – black curve). These results are in good agreement with our previous study [33], in which XPS and EDS studies were carried out for NT surfaces.

The surface morphology of NT-Ca/P and NT-Ca/P/Zn samples is shown in Fig. 5.1d and e, respectively. No significant differences are observed on the morphological/topographical features of both bio-functionalized nanotubular surfaces compared to the non-treated ones (Fig. 5.1c). However, dissimilar chemical features were found after bio-functionalization treatments. NT-Ca/P surfaces are composed of Ca and P as shown by the individual XPS spectra of Ca 2p and P 2p in Fig. 5.1d. The Ca $2p_{3/2}$ subpeak detected at 347.6 eV, in agreement with the P 2p peak found at 132.9 eV, evidence the presence of $Ca_3(PO_4)_2$ compounds on TiO_2 NTs [36]. Furthermore, the energy found for Ca $2p_{3/2}$ subpeak may be also related to the presence of $CaHPO_4$ species, as confirmed by the P 2p subpeak found at 134.1 eV (Fig. 5.1d) [36]. Moreover, additional contributions were found in Ca $2p_{3/2}$ main peak at 346.7 eV and 348.6 eV, which might be assigned to $CaCO_3$/CaO and CaF_2 [36, 59, 60] compounds respectively. These findings are in accordance with XPS results reported in a previous work for similar NT-Ca/P surfaces [33]. The EDS spectrum obtained from NT-Ca/P samples (Fig. 5.1f – red curve) showed the presence of Ti, O, F, Ca, P, and a small amount of sodium (Na) from the anodization process. Once Na was not detected by XPS, it is probably located in deeper regions of TiO_2 NTs. As regards NT-Ca/P/Zn surfaces, Zn and P elements were detected by XPS, and the correspondent high resolution spectra are shown in Fig. 5.1e. Although the presence of Ca 2p was found insignificant on these surfaces by XPS, a small amount of Ca was detected by the EDS (Fig. 5.1f – blue curve), most

probably because it is located deep in TiO_2 NTs. Furthermore, EDS analysis also showed the presence of Ti, O, F, Zn and P. The peak for Zn $2p_{3/2}$ was found at 1021.6 eV and assigned to ZnO compounds [61], while P 2p was revealed at 133.6 eV and related to PO_4^{3-} groups adsorbed to TiO_2 NTs [36]. It is noteworthy to highlight that Ti 2p, O 1s and F 1s were also detected on NT-Ca/P and NT-Ca/P/Zn surfaces by XPS and assigned to the presence of TiO_2, Ti_2O_3 and Ti-OH, as well as F^- ions adsorbed to TiO_2 NTs (results not shown).

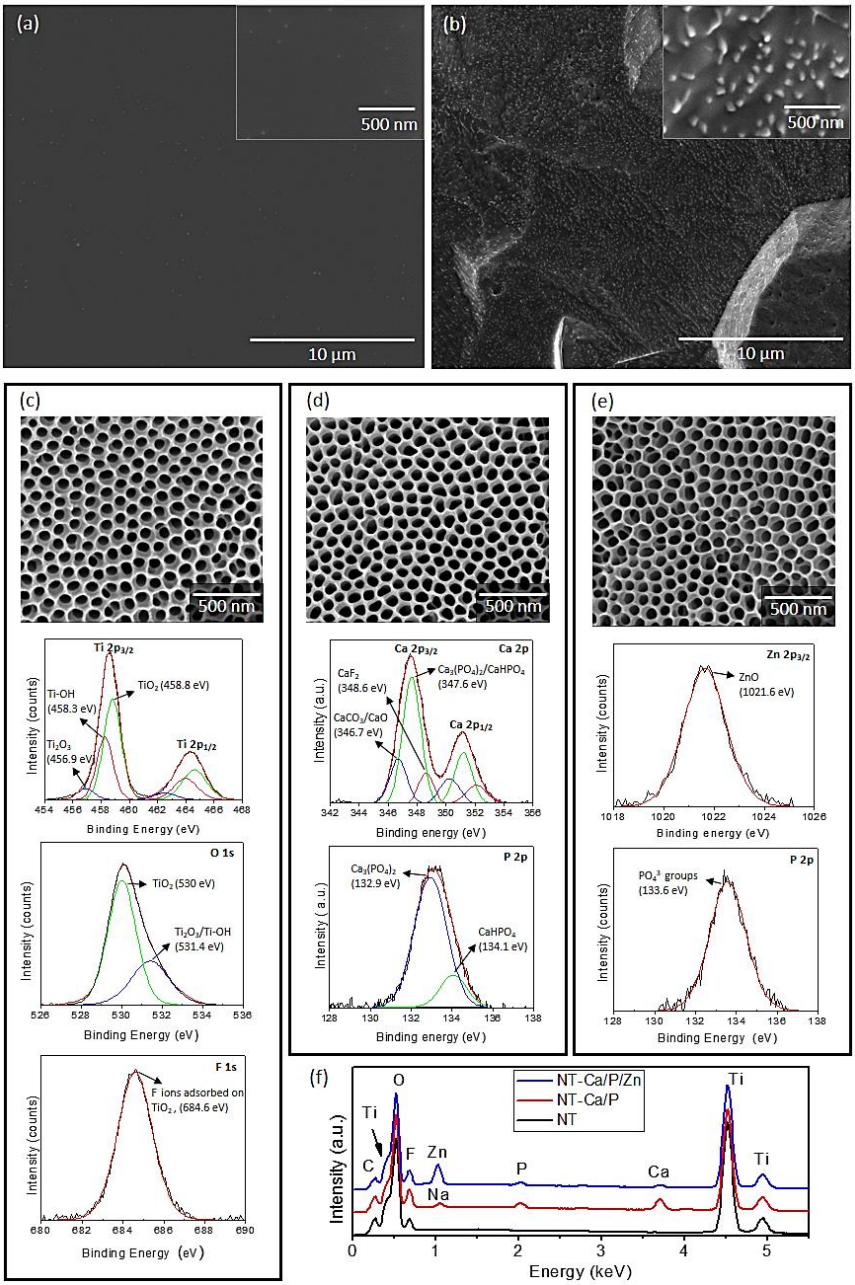

Fig. 5.1. SEM micrographs of (a) TiP, (b) TiE, (c) NT, (d) NT-Ca/P and (e) NT-Ca/P/Zn surfaces. The inset images in (a) and (b) intend to show the morphological/topographical surface features in more detail. The representative high resolution XPS spectra of deconvoluted Ti 2p, O 1s and F 1s detected on NT surfaces are shown in (c). Furthermore, the XPS spectra of Ca 2p and P 2p detected on NT-Ca/P surfaces are depicted in (d), while in (e) the XPS spectra for Zn $2p_{3/2}$ and P 2p detected on NT-Ca/P/Zn surfaces are shown. The information extracted from deconvolution is depicted in each individual spectrum in respect to the subbeak binding energy and possible chemical compound assigned to it. In (f) the EDS spectra acquired from NT, NT-Ca/P and NT-Ca/P/Zn samples are depicted.

5.3.2. Biological characterization

5.3.2.1. Viability and adhesion of MG-63 and hMSCs

The viability of MG-63 cells (human osteoblast-like osteosarcoma cell line) cultured on materials surfaces (i.e. TiP, TiE, NT, NT-Ca/P and NT-Ca/P/Zn) was investigated after one and six days of incubation, and the results are graphically represented in Fig. 5.2a. TiE surfaces were chosen also as positive control due to its well-known ability to improve osteoblast functions and by its attractiveness in clinical applications [62]. The percentage of absorbance values measured after MTT assay were converted into a percentage that was calculated in reference to TiP samples, which means that the absorbance value measured for TiP was taken as 100 %. After the first day of incubation, MG-63 osteoblast-like cells adhered on TiP and on all the nanotubular surfaces displayed a significantly inferior level of metabolic activity compared to the one on TiE surfaces. After six days of culture, as expected, a significant increase of cellular metabolic activity is observed for all groups, confirming cell proliferation throughout the culture time. Interestingly, it is observed that the metabolic activity of cells adhered on TiE and all the nanotubular surfaces, was significantly superior compared to TiP surfaces. This evidences that all the groups of treated surfaces are biocompatible.

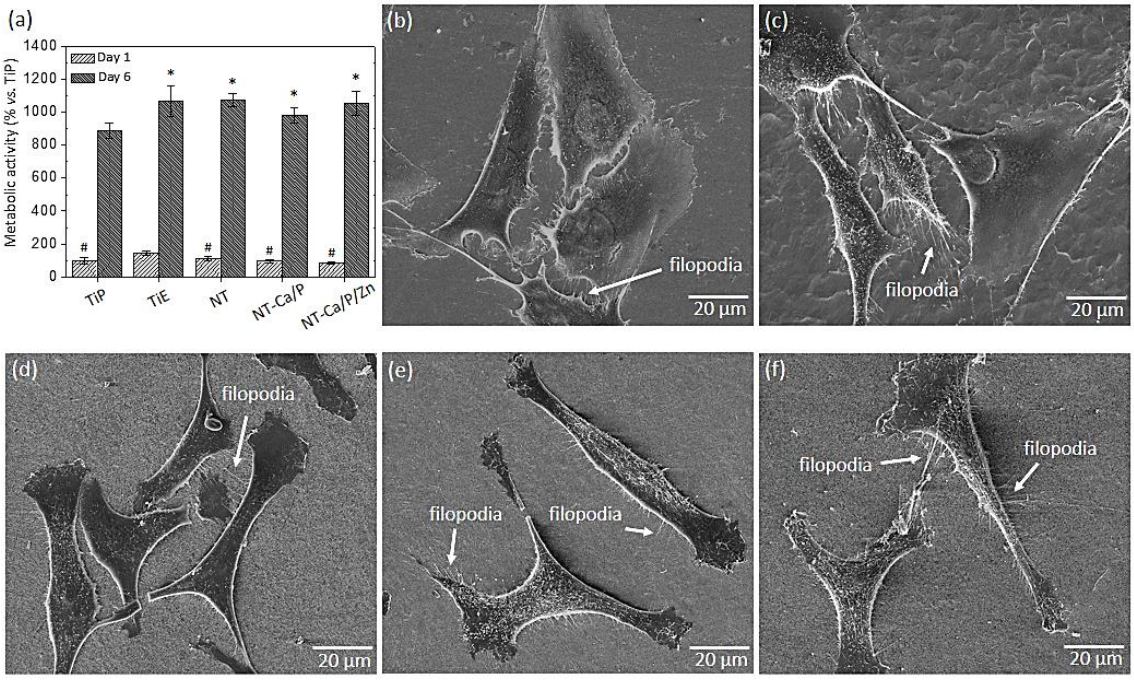

Fig. 5.2. (a) Metabolic activity of MG-63 cells cultured on TiP, TiE, NT, NT-Ca/P and NT-Ca/P/Zn samples after one and six days of incubation. SEM micrographs of MG-63 cells adhered on (b) TiP, (c) TiE, (d) NT, (e) NT-Ca/P and (f) NT-Ca/P/Zn samples after one day (24 h) of culture. Inset white arrows point to cytoplasmic protrusions of cells (filopodia). At day 1: (#) significantly different from TiE, $p < 0.05$; at day 6: (*) significantly different from TiP, $p < 0.05$.

The morphology of osteoblasts adhered on the different groups of samples was investigated after 24 h of culture, and the representative SEM micrographs are shown in Fig.

5.2b–f. Significant differences are observed between cell morphology on Ti (Fig. 5.2b and c) and nanotubular surfaces (Fig. 5.2d–f). MG-63 cells adhered on nanotubular surfaces display a stretched and elongated shape when compared with those on Ti groups, in which they exhibit spreader morphologies apparently covering a higher surface area. In all the cases, noticeable plasma membrane protrusions (filopodia) are visible evidencing cell-surface and cell-cell interactions. Interestingly, although a high density of filopodia has been found on all the surfaces, the cytoplasmic extensions presented different features: thinner and longer on Ti-based surfaces, and thicker and shorter on nanotubular surfaces, as shown in Fig. 5.3a and b respectively. These differences may be observed in more detail in Fig. 5.3c and d. Curiously, filopodia endings display a "ball-like" morphology on Ti surfaces (Fig. 5.3c) compared to the flattened filopodia shape observed on nanotubular surfaces (Fig. 5.3d).

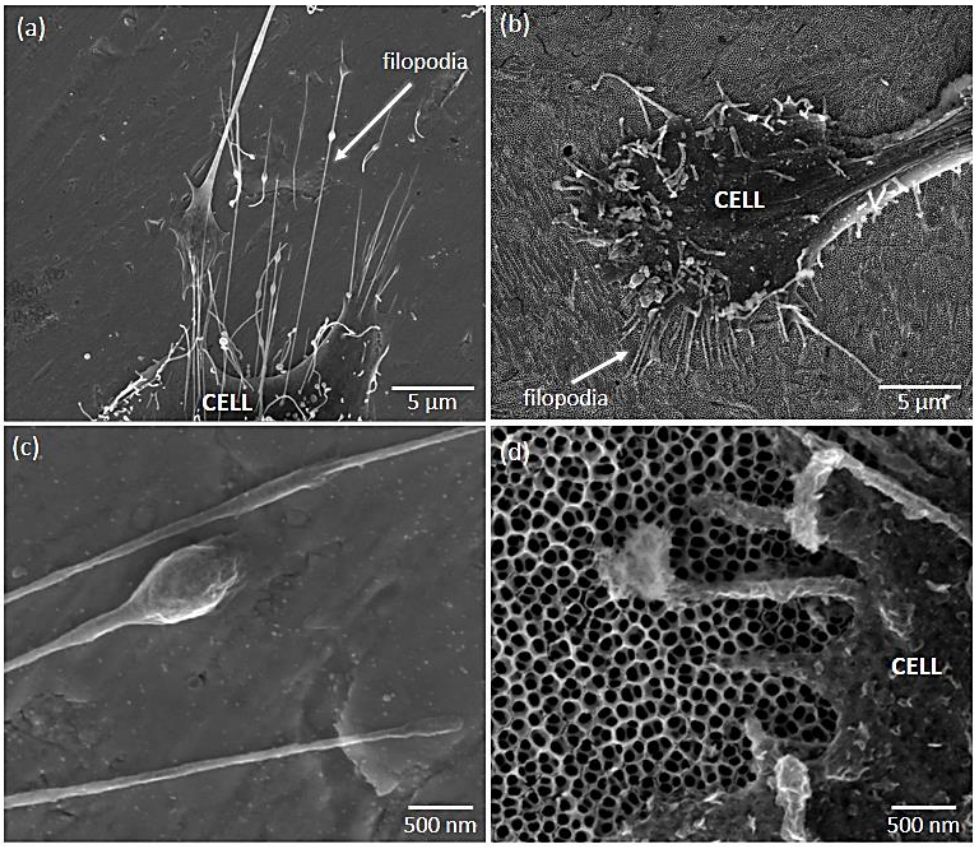

Fig. 5.3. SEM micrographs showing the differences between cytoplasmic protrusions (filopodia) of MG-63 cells adhered on (a) Ti and (b) nanotubular surfaces after one day (24 h) of culture. Inset white arrows point to filopodia. Higher magnified images of filopodia are shown in (c) and (d) for Ti and nanotubular surfaces, respectively.

The biocompatibility of treated and non-treated nanotubular surfaces was also investigated for human mesenchymal stem cells (hMSCs) by MTT assay. The percentage of absorbance values are depicted in Fig. 5.4a after cell culture in OM for one and six days. After one day of culture, a significant lower metabolic activity was measured for cells adhered on NT-

Ca/P and NT-Ca/P/Zn samples as compared to TiE, and after six days these differences were kept significant only for NT-Ca/P/Zn samples.

As regards hMSCs morphology after 24 h of adhesion, significant differences were observed for cells adhered on Ti and nanotubular samples, as previously observed for MG-63 cells. It is clearly perceived that cells adhered on nanotubular surfaces (Fig. 5.4d–f) present a more stretched and elongated morphology with filopodia interacting with nanotubular surfaces. On the other hand, the cells adhered on TiP and TiE surfaces (Fig. 5.4b and c), show a less defined morphology, and are spreader along the surface apparently covering a larger surface area. Filopodia are also observed for these cells evidencing interaction with the surface and neighboring cells.

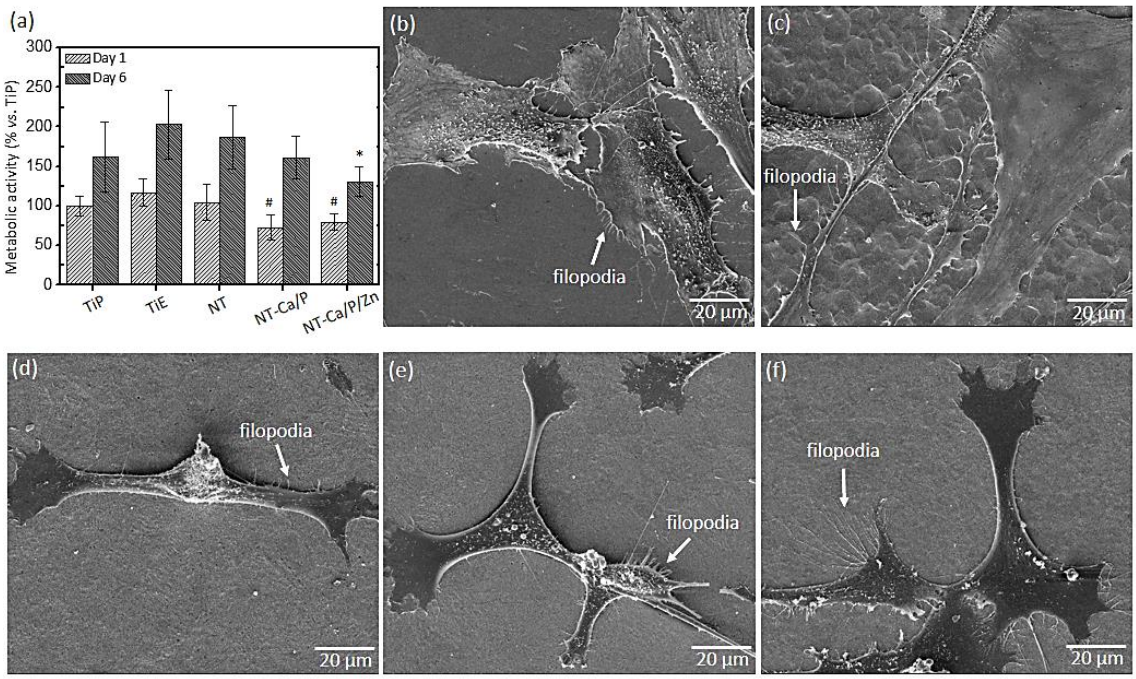

Fig. 5.4. (a) Metabolic activity of hMSCs cells cultured on TiP, TiE, NT, NT-Ca/P and NT-Ca/P/Zn samples after one and six days of incubation in OM. SEM micrographs of hMSCs cells adhered on (b) TiP, (c) TiE, (d) NT, (e) NT-Ca/P and (f) NT-Ca/P/Zn samples after one day (24 h) of culture. Inset white arrows point to cytoplasmic protrusions of cells (filopodia). At day 1: (#) significantly different from TiE, $p < 0.05$; at day 6: (*) significantly different from TiE, $p < 0.05$.

In order to understand the cytoskeleton organization of hMSCs adhered on Ti and nanotubular surfaces in an early stage of adhesion, the actin filaments were observed by confocal fluorescence microscopy and the results are shown in Fig. 5.5. As observed, clear differences are noticed between the morphology of hMSCs adhered on Ti (i.e. TiP and TiE) and nanotubular surfaces (i.e. NT, NT-Ca/P and NT-Ca/P/Zn). The cells on Ti surfaces present a rounder morphology compared to the cells adhered on nanotubular surfaces, and undergone a remarkably less stretching. On the other hand, the cells on nanotubular surfaces are already

very well stretched and elongated. This indicates that cells settled faster on TiO_2 NTs, and that they have quickly interacted and became adapted to these surfaces earlier than on Ti. The cells on all the nanotubular surfaces present a typical morphology characterized by a stretched and tinny cell body (Fig. 5.5c–e). Nevertheless, the cell endings are spreader along the surfaces compared to the main body, evidencing a higher contact and an intense interaction with the substrate through a high number of filopodia (Fig. 5.5e) and stress fibers formation, which are key signals for cell adhesion and migration [32].

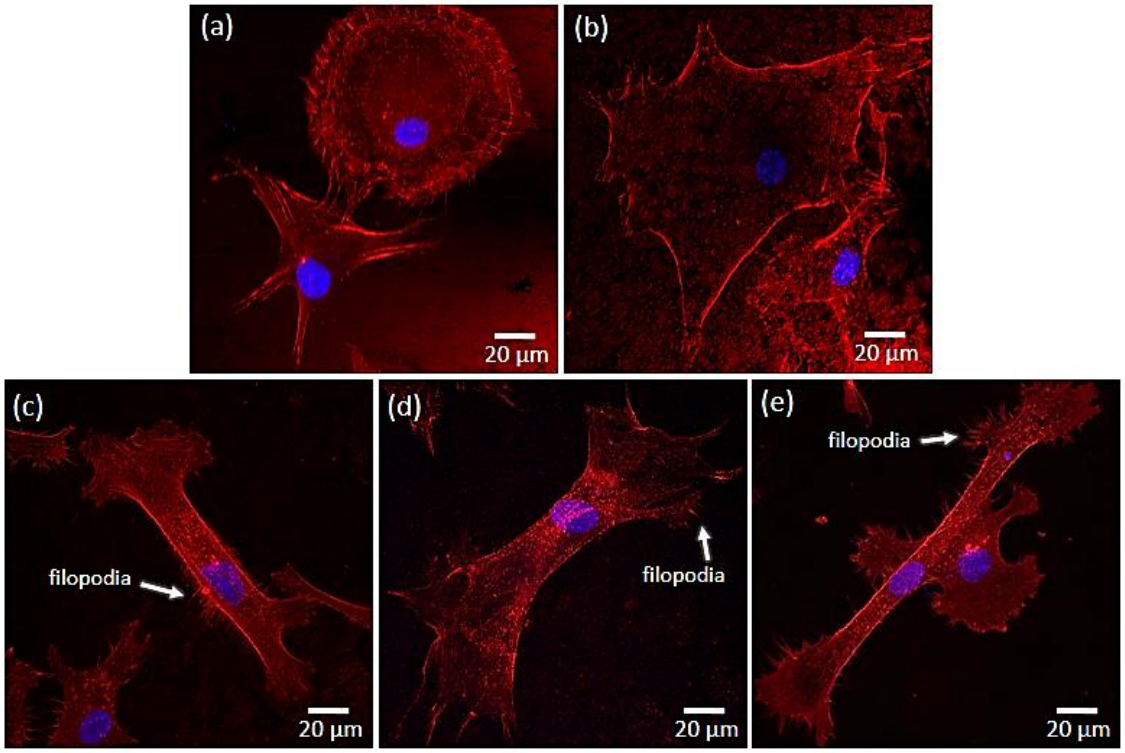

Fig. 5.5. Confocal fluorescence images showing actin cytoskeleton organization of hMSCs adhered on (a) TiP, (b) TiE, (c) NT, (d) NT-Ca/P, and (e) NT-Ca/P/Zn samples after 2h of incubation.

5.3.2.2. Osteogenic differentiation of hMSCs

To better characterize the osteoblastic phenotype of hMSCs cultured on standard culture plates in OM, primary human fibroblasts (hFb) and osteoblast-like Saos-2 cells (Saos-2) were taken as negative and positive controls, respectively. The colorimetric assay for detection of ALP was carried out after 14 days of culture for the three groups of cells, and the results are shown in Fig. 5.6. As observed in Fig. 5.6a, hFb are not producers of ALP, contrarily to Saos-2 (Fig. 5.6b), as would be expected since Saos-2 cells exhibit mature osteoblast phenotype [43]. As evidenced from Fig. 5.6c, hMSCs cultured in OM are producers of ALP after 14 days of culture, indicating that the cells have undergone osteoblastic differentiation. This was confirmed by matrix

mineralization performed after 21 days of culture for the same groups of cells, for which mineralization occurred in Saos-2 (Fig. 5.6e) and hMSCs (Fig. 5.6f), contrarily to hFb (Fig. 5.6d).

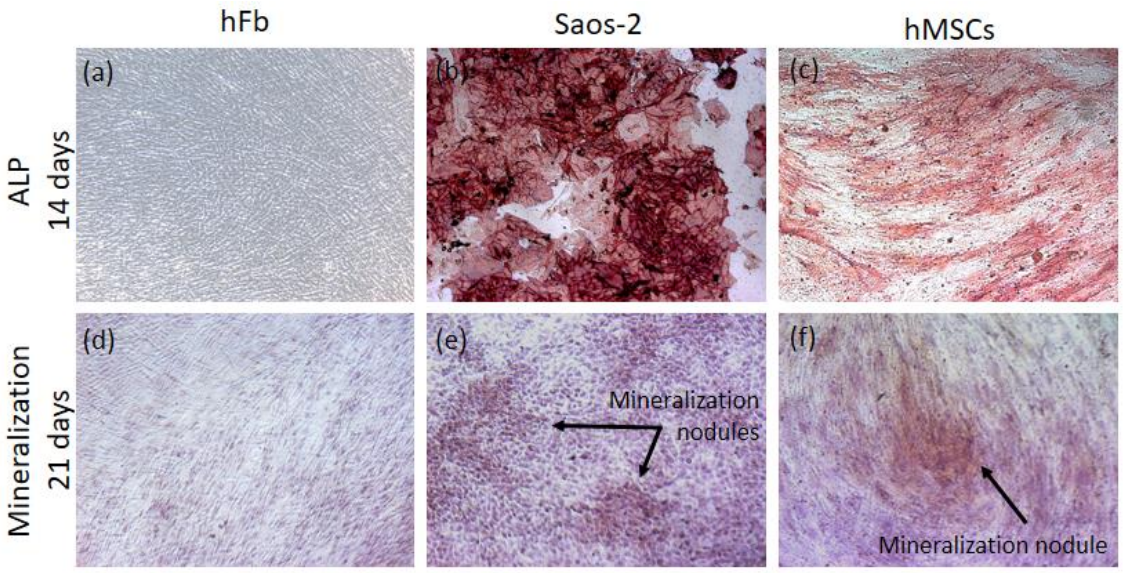

Fig. 5.6. Optical micrographs of (a) hFb, (b) Saos-2 and (c) hMSCs after colorimetric assay for detection of ALP (14 days of culture). The colorimetric assay for detection of mineralization nodules was also carried out and the optical micrographs of (d) hFb, (e) Saos-2 and (f) hMSCs are shown for 21 days of culture.

The relative expression of osteogenesis-related genes, namely runt-related transcription factor 2 (RUNX-2), alkaline phosphatase (ALP), collagen type-1 (COL-1), bone morphogenetic protein-2 (BMP-2) and osteopontin (OPN) was determined to investigate whether morphological/topographical and chemical features of Ti and nanotubular surfaces influence the osteogenic differentiation of hMSCs. The gene expression of the different targets is shown in Fig. 5.7, and the values are presented as fold changes, which were calculated in reference to the control group TiP. The results show that while no significant differences were found for the expression of RUNX-2 (Fig. 5.7a) and ALP (Fig. 5.7b) genes within the different groups, statistically significant differences were observed for COL-1 (Fig. 5.7c), BMP-2 (Fig. 5.7d) and OPN (Fig. 5.7e) genes expression.

The expression of COL-1 was significantly up-regulated in hMSCs cultured on TiE ($p < 0.01$), NT ($p < 0.05$) and NT-Ca/P/Zn ($p < 0.01$) surfaces compared to the control group TiP (Fig. 5.7c). Instead, the relative expression of BMP-2 was found significantly down-regulated for NT ($p < 0.01$), NT-Ca/P ($p < 0.01$) and NT-Ca/P/Zn ($p < 0.05$) surfaces relatively to TiP (Fig. 5.7d). Moreover, OPN gene expression was also down-regulated in hMSCs present on NT ($p < 0.01$) and NT-Ca/P ($p < 0.01$) surfaces (Fig. 5.7e). Interestingly, a clear trend of a higher expression of both BMP-2 and OPN genes for NT-Ca/P/Zn is observed, when compared to NT-Ca/P and NT samples, as observed in Fig. 5.7d and e. To further confirm this trend, the relative expression of

BMP-2 and OPN genes was determined settling NT as the reference group, and the results are shown in the insets graphs in Fig. 5.7d and e, respectively. As clearly observed, the expression of BMP-2 gene was significantly higher for NT-Ca/P ($p < 0.01$), and even more pronounced for NT-Ca/P/Zn surfaces ($p < 0.01$) compared to NT control group. Furthermore, significantly higher differences ($p < 0.05$) were also found for the relative gene expression of OPN for NT-Ca/P/Zn samples as compared to NT. The BMP-2 and OPN genes were around 3 times more expressed in hMSCs cultured on the nanotubular surfaces enriched with Zn, when compared to conventional nanotubular surfaces. It is noteworthy that significantly different ($p < 0.05$) gene expression levels of BMP-2 and OPN genes were also observed for NT-Ca/P/Zn compared to NT-Ca/P samples, with fold change values determined by taking NT-Ca/P surfaces as the reference (results not shown).

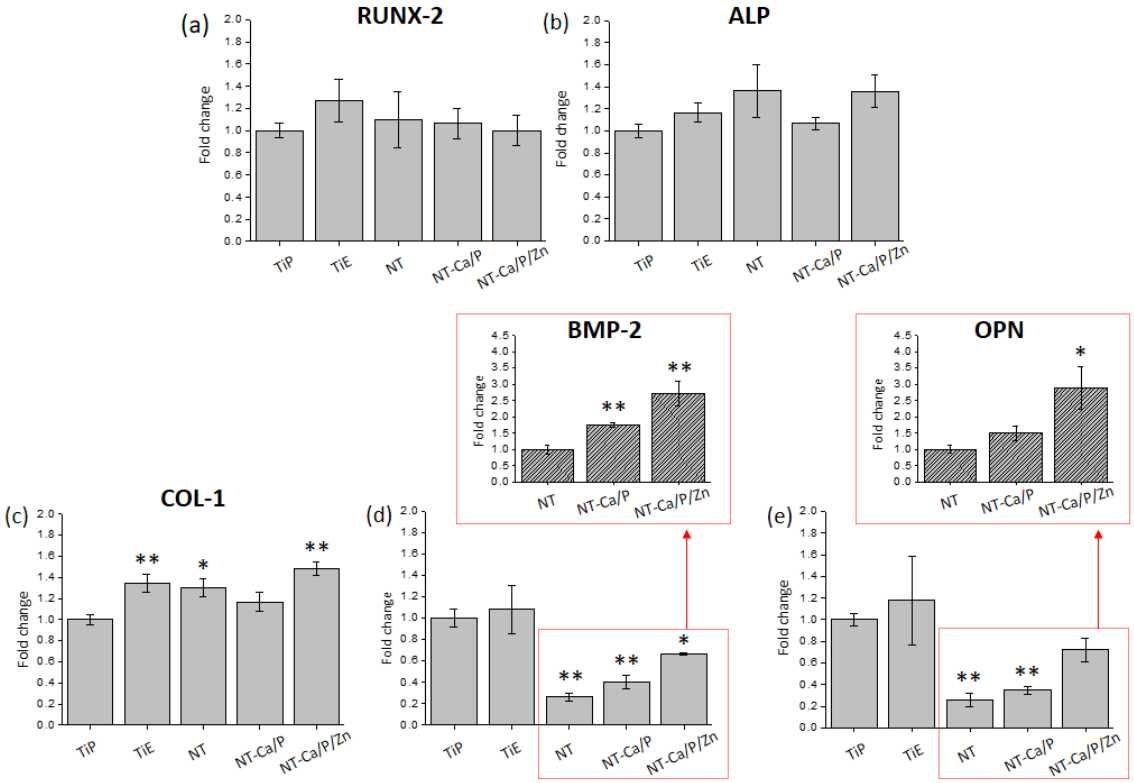

Fig. 5.7. Relative expression of (a) RUNX-2, (b) ALP, (c) COL-1, (d) BMP-2 and (e) OPN genes of hMSCs cultured on TiP, TiE, NT, NT-Ca/ and NT-Ca/P/Zn samples after 14 days of incubation in OM. Fold change values were calculated against the control TiP. (*), significantly different from TiP, $p < 0.05$; highly significantly different from TiP (**) $p < 0.01$. The insets in (d) and (e) show the relative gene expression of BMP-2 and OPN respectively, whose values were calculated with NT samples as the control group. (*), significantly different from NT, $p < 0.05$; highly significantly different from NT (**) $p < 0.01$. Gene expression levels were normalized against housekeeping gene CASC-3.

5.3.2.3. VEGF release by hMSCs

To investigate the possible role of surface characteristics on vascularization process, the quantity of vascular endothelial growth factor (VEGF) produced by hMSCS was quantified after 14 days of culture in OM, and the results are shown in Fig. 5.8. The cells in contact with NT and NT-Ca/P/Zn surfaces produced significantly higher VEGF amounts compared to the ones on TiP and TiE surfaces ($p < 0.01$). Furthermore, a significantly higher extent of VEGF was also released by cells on NT-Ca/P compared to TiE surfaces ($p < 0.01$).

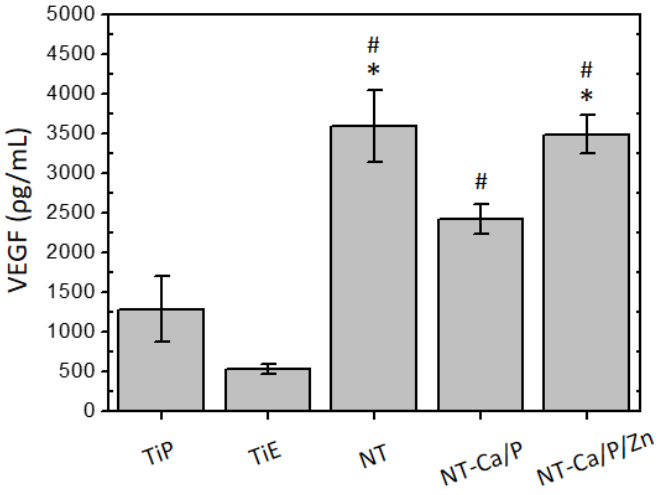

Fig. 5.8. Amount of VEGF produced by hMSCs adhered on TiP, TiE, NT, NT-Ca/P and NT-CA/P/Zn surfaces after 14 days of culture in OM. (*) significantly different from TiP, $p < 0.01$; (#) significantly different from TiE, $p < 0.01$.

5.3.3. Microbiological characterization

The influence of materials surface features on the early adhesion and viability of *S. aureus* was investigated, by counting the number of live and dead bacteria adhered to the different groups of surfaces. These results are shown in Fig. 5.9a, in which the percentage of live and dead bacteria adhered after 2h of culture is depicted for each group. The number of total live bacteria was converted into a percentage in reference to TiP samples, meaning that the total number of live bacteria counted on TiP samples was taken as 100 %. The number of live bacteria adhered on NT, NT-Ca/P and NT-Ca/P/Zn surfaces was significantly lower compared to the number on TiE samples ($p < 0.01$). On the other hand, a significantly higher number of dead bacteria was found on NT-Ca/P and NT-Ca/P/Zn surfaces, when compared to TiP and TiE. The representative images of live (green color) and dead (red color) bacteria adhered on the different groups of surfaces are shown in Fig. 5.9b–f. In agreement with the previous results, a higher number of live bacteria are observed on TiP and TiE compared to NT, NT-Ca/P and NT-Ca/P/Zn surfaces.

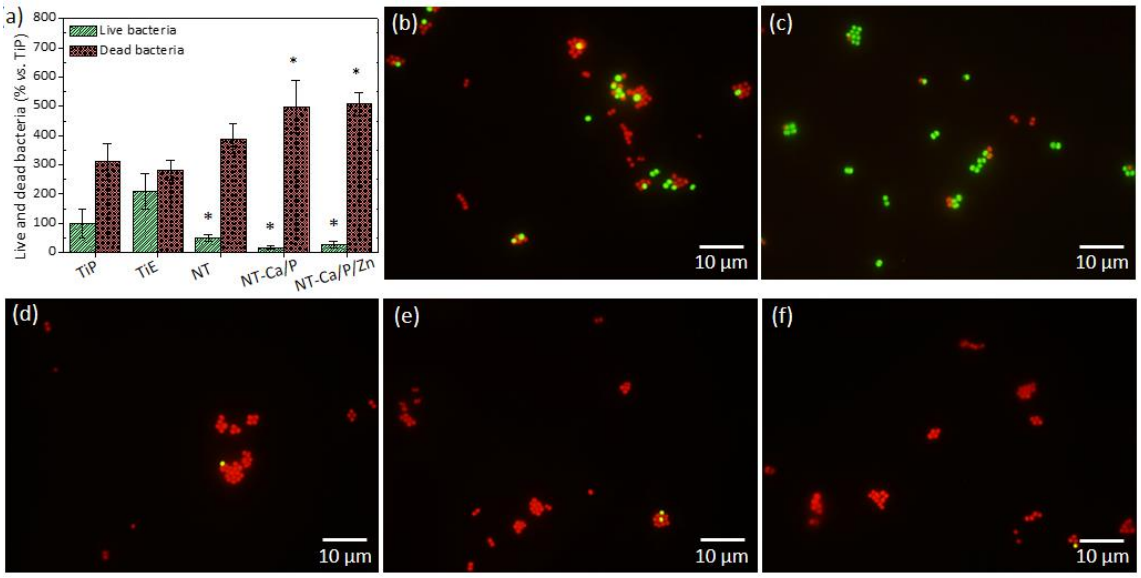

Fig. 5.9. (a) Live and dead bacteria adhered on TiP, TiE, NT, NT-Ca/P and NT-Ca/P/Zn samples after 2h of culture. The representative fluorescence images of live (green) and dead (red) adhered bacteria are shown for (b) TiP, (c) TiE, (d) NT, (e) NT-Ca/P and (f) NT-Ca/P/Zn surfaces. For live bacteria: (*) highly significantly different from TiE ($p < 0.001$); For dead bacteria: (*) highly significantly different from TiP and TiE ($p < 0.001$).

5.4. Discussion

5.4.1. Biocompatibility and adhesion ability of MG-63 and hMSCs

The benefits of the superimposition of micro- and nano-scale topographies on osteoblasts and MSCs functions such as adhesion, proliferation, and differentiation have been reported in previous studies [14, 63, 64]. Therefore, it is believed that the enhanced metabolic activity of osteoblast-like cells on TiE samples after one day of culture (Fig. 5.2a), could have been modulated by the combined micro/nano-topographical surface features (Fig. 5.1b). Zhao *et al.* [63] explained that micro/nano topographies may regulate the integrin-mediated cell adhesion process, through several intracellular signal transduction pathways [65]. Nonetheless, the promoter effect of TiE surfaces on cell viability is neither too strong nor long lasting since by day six, the metabolic activity on nanotubular samples is at the same level as that of TiE samples (Fig. 5.2a), which highlights the biocompatibility of TiO_2 NTs, before and after bio-functionalization treatments. On the other hand, Ti smooth samples keep inducing a significantly lower metabolic activity throughout the culture time, which is most likely related to the absence of either micro or nano topographical cues.

The metabolic activity of hMSCs increased with culture time for all the groups of surfaces (Fig. 5.4a), however, at a rather limited rate compared to the one observed for MG-63 cells (Fig. 5.2a). This is probably related with the low metabolic activity of primary hMSCs and their low proliferation rate, when compared to tumoral cells [66]. In addition, it is known that throughout differentiation, the proliferative potential of hMSCs decreases [67]. This also may explain the

limited proliferation rate of these cells because, as they were cultured in OM, most likely they were already undergoing a differentiation process at that time.

Both osteoblast-like cells and hMSCs presented very well stretched morphologies when adhered to nanotubular surfaces compared to those of cells on TiP and TiE surfaces (Fig. 5.2b–f and Fig. 5.4b–f). These differences may be related with the dissimilar features of Ti and nanotubular surfaces, namely their chemistry, surface energy, and nano morphology/topography. These characteristics may play, separately or together, fundamental roles on the initial protein adsorption and subsequent cell adhesion process [1, 68, 69]. Nano topographical surface features that directly correspond to the sizes of extracellular matrix (ECM) proteins, are known to modulate their initial surface adsorption. Kubo *et al.* [70] showed the benefits on adding nanonodules on Ti micro-roughened surfaces to boost their capacity of early albumin adsorption. In particular, it is known that the high negative charged density at sharp edges of TiO_2 NTs are expected to promote the adsorption of ECM proteins such as vitronectin, fibronectin, fibrinogen and albumin, which mediates the adsorption of cells to these regions trough integrin receptors present in negatively charged osteoblast membrane surface [71, 72]. Nanotubular structures are known to strongly influence the clustering of integrins into focal adhesion complexes, and further activation of intracellular signaling cascades controlling cell adhesion, cell shape, proliferation, migration, differentiation, and apoptosis [73, 74]. Although NTs diameters are known to significantly regulate the activation of integrin-mediated intracellular signaling pathways, the optimal range of nanotube diameters to improve cell functions still remains unclear. Controversial results are found in literature, for different studies carried out with 15 – 150 nm diameter NTs [21]. In the present work, TiO_2 NTs with inner diameters ranging from 50 – 90 nm and wall thickness comprised between 14 – 24 nm were synthesized [33]. It is believed that the highly stretched morphology observed for MG-63 and hMSC cells on NTs may be related with their non-uniform diameters. Integrins clustering takes place when they are distanced less than 70 nm [75], and in general, small diameter NTs are known to induce a higher extent of focal adhesion contacts transduced in a stronger cell adhesion and cytoskeleton rearrangement [71, 73, 76, 77]. Based on this knowledge, it is hypothesized that NTs with non-uniform diameters induced the adhesion of proteins in preferential areas of the surfaces, most likely at those places where the density of small-diameter tubes was higher, which consequently might have induced to focal adhesion complexes formation by clustering of integrins at those places. Through activation of intracellular signaling pathways, an increased cytoskeleton stress was probably created inducing cell stretching across the tubes. As observed in Fig. 5.3d filopodia of cells interacts with NTs by crossing them along their walls, and in general they do not penetrate inside their hollow cavity.

This may further indicate that proteins are mainly adsorbed on nanotube wall where cells adhere preferentially.

A dramatic stem cell elongation was also observed by Oh *et al.* [78] in 100 nm diameter NTs, which induced cytoskeletal stress and differentiation into osteoblasts. The high cytoskeletal tension influences stem cells shape, and their well spreading and stretching across nanotube surfaces predicts their fate towards osteoblast phenotype [21]. In fact, the high cytoskeleton tension may induce to mechanotransduction events and trigger intracellular signaling pathways, which control differentiation [21, 79]. However, in this study no correlations were found between the enhanced hMSCs stretching on NTs, and their ability to differentiate into osteoblasts, as it will be further on discussed in more detail.

Different morphologies are observed between filopodia of cells adhered on Ti-based and nanotubular surfaces. As stated by Matilla *et al.* [80], filopodia are actin-rich plasma membrane protrusions that function as sensors for cells to probe their environment, and are involved in a high number of cell responses such as cell migration and adhesion. In general, osteoblastic-like cells adhered on Ti surfaces present longer and thinner filopodia (Fig. 5.3a), and their endings display a “ball-like” shape morphology (Fig. 5.3c). On the contrary, osteoblast-like cells adhered on nanotubular surfaces show shorter and thicker filopodia (Fig. 5.3b) with flattened endings (Fig. 5.3d). This is an indicator that MG-63 cells are sensitive to nanotubular surface features, and further suggests that they are stronger adhered to these surfaces. The ability of nanotubular surfaces to strengthen cell adhesion is also suggested by the improved stretching of hMSCs adhered on NTs right after 2h of adhesion, when compared to the rounder and less stretched morpholohy of cells adhered on Ti surfaces (Fig. 5.5). Furthermore, the formation of stress fibers is also observed for hMSCs on nanotubular surfaces, essentially located in cells’ endings where well-developed lamellipodia and filopodia are found, through which generally cell spreading occurs [81]. These findings are in accordance with the study performed by Lv *et al.* [62], who also found that TiO_2 NTs promoted the early adhesion of human stem cells, by accelerating their adhesion as compared to smooth and acid-etched Ti surfaces. Also, Park *et al.* [73] demonstrated that TiO_2 NTs induced to improved MSC adhesion and spreading as compared to smooth Ti, through focal contact formation and stress fiber assembly.

5.4.2. Osteogenic differentiation and angiogenic ability of hMSCs

MSCs play a major role in bone formation and regeneration [44], and their differentiation into mature osteoblasts is comprised by different cellular stages, which are identified by specific markers [48]. Thus, the expression of a series of osteogenic specific genes are involved in

osteoblast differentiation and maturation [82], and some of those important bone markers were addressed in this study.

After 14 days of culture in OM, the expression of BMP-2 was found down-regulated in hMSCs adhered on NT, NT-Ca/P and NT-Ca/P/Zn samples, compared to TiP control (Fig. 5.7d). Interestingly, although BMP-2 regulates osteogenesis by modulating the expression of RUNX-2 [49, 83], which is known as a master regulator of osteogenic gene expression [82], no link between the down-regulation of BMP-2 and the expression of RUNX-2 was observed (Fig. 5.7a). Additionally, no correlation between the expression of ALP and COL-1 genes, and the down-regulation of BMP-2 was established (Fig. 5.7b and c). This may be related with the activation level of RUNX-2, which is not being influenced by BMP-2. RUNX-2 is an important transcriptional factor needed for the osteoblast lineage commitment, and further modulation of osteoblast differentiation, bone development, and the expression of ECM protein genes [49, 50, 82, 84]. In the earliest stage, MSCs form pre-osteoblasts that secrete ALP, an early marker of ostogenesis [49], while in a later stage mature osteoblasts secrete bone organic matrix rich in COL-1, which afterwards become mineralized through hydroxyapatite deposition [48]. The expression of ALP and COL-1 present similar levels for hMSCs cultured both on Ti and nanotubular surfaces, suggesting that osteogenic differentiation is not being compromised by surface modification treatments induced on Ti surfaces. As regards the lower expression of BMP-2 in cells cultured on nanotubular surfaces, no correlation was found with the increased cell stretching observed for these cells, as previously discribed. Studies found in literature show the reverse trend, since cell stretching stress is reported to induce osteogenic differentiation of stem cells [63, 85-87]. A possible explanation for this behavior may be related with surface chemistry, which is different for all the nanotubular surfaces as compared to Ti surfaces. The presence of fluoride ions adsorbed to TiO_2 NTs were found on all the nanotubular surfaces (Fig. 5.1c), and previous studies have reported that fluoride regulate osteoblastic differentiation [88-90]. A recent study conducted by Gandhi *et al.* [89] showed that fluoride induced chronic oxidative and inflammatory stress in osteoblast-like cells, which was highlighted to possibly hamper osteoblast differentiation. Furthermore, Zhao *et al.* [88] found that fluoride inhibited BMP-2 expression levels in rat osteoblasts. Thus, the presence of fluoride on TiO_2 nanotubular surfaces may be a possible reason for the reduced BMP-2 levels.

Remarkably, the expression levels of OPN followed the same trend of BMP-2 for NT and NT-Ca/P samples, in which OPN gene was down-regulated compared to Ti smooth and rough surfaces (Fig. 5.7d and e). This suggests that the regulation of OPN gene is being influenced by BMP-2. In fact, some reports have mentioned that BMP-2 regulates the cellular gene expression of OPN [91-93], however, the mechanisms behind still remain unclear. It is known that the BMP

signaling pathway plays multiple and crucial roles in bone formation and is involved in several stages of its development [49]. The stimulation of the differentiation of MSCs into osteoblasts through BMP-2 is mainly achieved through stimulating Smad signaling pathway. By activating Smad-1/5/8 and RUNX-2, BMP-2 regulates the expression of osteoblastic-specific genes such as OPN, a late osteogenic marker [49, 50, 83]. Yang *et al.* [93] studied the role of BMP-2 on the enhancement of RUNX-2 and OPN expression by Smad-1 and signal-related kinase (ERK) 1/2 signaling pathways, and concluded that extracellular ERK 1/2 pathway modulates BMP-2-induced OPN expression. Thus, it is believed that Smad and/or ERK 1/2 are the most probable pathways involved in the control of OPN expression by BMP-2. However, further studies must be performed to clarify this hypothesis.

Besides gene expression levels of BMP-2 and OPN have been found down-regulated in cells cultured on nanotubular surfaces compared to TiP, these genes were significantly up-regulated on TiO_2 nanotubular surfaces enriched with ZnO compounds (Fig. 5.1e), when compared to NT and NT-Ca/P surfaces (insertions in Fig. 5.7d and e). This suggests that the inclusion of Zn on TiO_2 NTs is enhancing the osteoblastic differentiation of hMSCs. It is known that Zn ions (Zn^{2+}) concentration is relatively high in bone and it has been propose to stimulate bone formation and mineralization [40]. Previous studies have demonstrated that Zn plays an important role in differentiation of osteoblasts and bone remodeling. Recently, Yusa *et al.* [42] demonstrated that Zn-modified Ti surface enhances osteoblast differentiation of dental pulp stem cells. The authors reported that Zn-Ti surfaces, beyond exhibited significantly up-regulated gene expression levels of BMP-2, OPN, RUNX-2, ALP, and COL-1, also promoted ECM mineralization. Additionally, it is suggested that the improved osteogenic-genes expression in Zn-Ti surfaces was linked to the activation of Smad-1/5/8. In particular, the enrichment of TiO_2 NTs with Zn has shown promising results by improving osseointegration both *in vitro* and *in vivo* [41]. For example, Huo *et al.* [34] reported that the incorporation of Zn on nanotube arrays showed excellent ostegenesis inducing ability through higher activity of extracellular ERK 1/2, which is one of the alternative pathways (non-Smad-dependent pathway) that regulates osteogenic differentiation of stem cells [94]. These finding are in accordance with recent discoveries reporting that Zn^{2+} ions regulate several intracellular signaling pathways including BMP-2 signaling cascade. It is believed that intracellular influx of Zn^{2+} ions is controlled by Zn transporters involved in bone homeostasis [40]. Based on these findings, it is hypothesized that Zn^{2+} ions liberated from NT-Ca/P/Zn samples reaches the intracellular environment through Zn specific transporters, and by this way may enhance the activity of intracellular signaling pathways involved in osteogenic differentiation, including Smad and/or ERK 1/2. As previously mentioned, BMP-2 is known to promote osteoblast differentiation and OPN is a mature

osteoblast marker gene recognized to play an important role in bone formation, resorption, and remodeling [42, 51]. By enhancing the BMP-2 and OPN levels, the addition of Zn on nanotubular surfaces seems be of crucial importance to act as a potent inducer of bone formation and remodeling.

As regards hMSCs adhered on nanotubular surfaces, although not statistically significant, a trend is observed for a gradual decrease in the metabolic activity of cells adhered on those bio-functionalized samples as compared to conventional NTs, both after one and six days of culture (Fig. 5.4a). A lower metabolic activity is indicator of a lower proliferation rate, and this is agreement with the interrelation found between proliferation and differentiation of cells during development of osteoblast phenotype [14]. This slight suppressive effect of metabolic activity is possibly related to hMSCs differentiation tendency found for bio-functionalized NTs, in particular those containing Zn. However, the micro/nano scale surface topography of TiE samples seems to result in an additive effect on hMSCs metabolic activity, when compared to NT-Ca/P and NT-Ca/P/Zn samples (day one), and after six days this difference become only significant for NT-Ca/P/Zn samples. Nevertheless, nanotubular samples are shown to support MSC proliferation and do not compromise their viability, as the values are never lower than that of the well-known biocompatible Ti smooth surfaces. The stronger adhesion strength of cells adhered on nanotubular surfaces may also be related with the lower proliferation rate since, as explained by Zhao *et al.* [63], as cells need to detach slightly to undergo division, a tight adhesion is expected to hamper this process.

Bone is a highly vascularized tissue, and blood vessels largely contribute for bone growth and remodeling [95, 96]. Therefore, vasculogenesis and angiogenesis processes are required for proper osseointegration. Vascular endothelial growth factor (VEGF) is among the many identified growth factors that initiates and controls angiogenesis [97]. The amount of VEGF produced by hMSCs after 14 days of incubation in OM, was found to be significantly higher for NT and NT-Ca/P/Zn surfaces compared to TiP and TiE surfaces (Fig. 5.8). Moreover, hMSCs on NT-Ca/P surfaces released a significantly higher amount of VEGF in relation to TiE, although these differences were found not significant when compared to TiP surfaces. These results may be related with the morphological/topographical and physicochemical properties of the surfaces. In previous studies, surface topography and surface energy were found to regulate the secretion of angiogenic factors by cells, partially via $\alpha_2\beta_1$ integrin signaling [97, 98]. TiO_2 nanotubular surfaces, in addition to nanotopography, are more hydrophilic (higher surface energy [62]) compared to Ti surfaces (results not shown). Thus, it is believed that both nanotopography and physicochemical features of nanotubular surfaces are influencing the synthesis of VEGF, probably mediated by integrin signaling pathways. Although not statistically

significant, there is a trend for a lower VEGF production by cells in contact with NT-Ca/P, as compared to NT and NT-Ca/P/Zn surfaces. However, no relation has been found between VEGF synthesis and the presence of Ca, which is the main difference existing between the surfaces. One must be highlighted that VEGF and BMP-2 play important roles in the communication between osteogenesis and angiogenesis [98]. In accordance with previous studies, the production of VEGF by osteoblasts is regulated by factors that stimulate osteogenesis, including BMP-2 [97, 99]. Based on this knowledge, we postulate that the lower expression level of BMP-2 gene for NT surfaces is not compromising the synthesis of VEGF.

5.4.3. Early bacterial adhesion and survival on Ti and nanotubular surfaces

In addition to complicated infections, bacterial adhesion on implant surfaces may compromise the osseointegration process [1]. In this study, the early adhesion of *S. aureus* on Ti and nanotubular surfaces was investigated. The main aim was to understand the influence of the surface features on bacterial adhesion, as well as infer on their ability to impair their viability.

In this study, a significantly higher number of live bacteria was adhered on TiE surfaces compared to NT, NT-Ca/P and NT-Ca/P/Zn surfaces (Fig. 5.9). One of the main differences between theses surfaces is the micro/nano topography of TiE surfaces. As compared to smooth surfaces, roughened substrates have demonstrated potential to enhance the adhesion and growth of infectious bacteria [15, 100-103]. Wu *et al.* [15] studied the effects of surface topography on *S. epidermidis* using clinically relevant Ti surface finishes, and they found that bacterial adhesion and growth was substantially higher on rough (0.830 µm < Ra < 11 µm) surfaces than on the Ti polished (R_a = 0.006 µm) surfaces after 24 h of culture. The observed differences were linked to the substantially higher roughness of the former surfaces at lengths scales comparable to that of bacterial colonies (several microns). Whitehead *et al.* [104] also studied the adhesion of bacteria on substrates with micrometer and sub-micrometer dimensions, and found that *S. aureus* and *Pseudomonas aeruginosa (P. aeruginosa)* were retained mainly in the largest (2 µm) surface features. On the other hand, i*n vitro* antibacterial properties of nanostructured Ti surfaces have been demonstrated by several studies [25, 105, 106]. Puckett el al. [107] examined the adhesion of *S. aureus*, *S. epidermidis*, and *P. aeruginosa* on conventional Ti (nano-smooth) and nanostructured Ti surfaces after 1 h of culture. The results indicated that nanorough Ti surfaces are the best surfaces for inhibiting bacterial adhesion. The authors explained that the decreased bacterial attachment was related with the higher surface energy of nanostructured Ti surfaces which increased fibronectin adsorption, and subsequently decreased bacteria attachment. The above mentioned studies suggest that while micron-

roughened Ti substrates show potential to enhance the adhesion and growth of bacteria, nanostructured Ti surfaces display the reverse trend.

An additional interesting outcome in this investigation is related with the remarkably higher number of dead bacteria on NT-Ca/P and NT-Ca/P/Zn surfaces, when compared to TiP and TiE surfaces. These results suggest that TiO_2 nanotubular surfaces display the ability to impair bacterial functions in respect to their viability. Ercan *et al.* [25] also found that TiO_2 nanotubular structures reduced the number of live adhering *S. epidermidis* and *S. aureus*. However, the mechanisms behind such strong bactericidal effect of TiO_2 NTs are still poorly understood, and controversial results are found in literature. Antimicrobial properties of TiO_2 NTs are reported to be related mainly to the following mechanisms: 1) formation of reactive oxygen species (ROS) in bacteria [105]; 2) disruption of bacteria membrane due to stress effects induced by NTs [25]; and 3) oxidative stress induced by photocatalytic activity of TiO_2 [106]. In fact, the topographical cues of TiO_2 NTs may be one of the reasons for the lower bacterial viability. Kang *et al.* [108] reported that bacterial cell membrane damage resulting from direct contact with single-walled carbon NTs is the probable mechanism leading to bacterial cell death. This mechanism was also addressed by Shi *et al.* [26] to explain the increased antibacterial activity of TiO_2 NTs with diameters ranging from 30 – 60 nm. The authors suggested that physical contact of bacteria with NTs could induce a punch on bacteria with cell membrane ruptures and cytoplasm outflow, leading eventually to cell apoptosis.

Beyond morphological/topographical characteristics, all the nanotubular surfaces present different chemical features as compared to Ti surfaces. These surfaces beyond TiO_2, which is also present on Ti surfaces, are composed of adsorbed fluoride ions (Fig. 5.1c), which can inhibit the metabolism and growth of bacteria. Breaker [109] reported that bacteria such as *Escherichia coli* or fungi such as *Candida albicans* cannot survive upon long exposure to fluoride approaching 250 mM, the concentration found in some fluoride toothpastes. It is believed that fluoride can affect bacterial metabolism through a set of actions and different mechanisms such as acting directly as an enzyme inhibitor [110]. Recently, Liu *et al.* [111] reported that the incorporation of fluoride ions into bioactive glasses significantly promoted the antimicrobial activity against periodontal pathogens. Thus, the mechanism behind the bactericidal activity of nanotubular surfaces compared to Ti may be also related with fluoride action by inhibiting enzymatic activity of bacteria. Furthermore, although not statistically significant, the number of live and dead bacteria adhered on NT-Ca/P surfaces was found lower and higher, respectively, when compared to bacteria adhered on NT and NT-Ca/P/Zn surfaces (Fig. 5.9), suggesting that Ca and P also may influence bacteria viability. However, further studies should be performed to better understand the simultaneous action of topographical and physicochemical features of

TiO_2 NTs, on the significant decrease and increase of live and dead adhered bacteria, respectively.

5.5. Conclusions

TiO_2 NTs enriched with Ca, P and Zn were successfully synthesized by reverse polarization anodization treatments carried out over conventional TiO_2 nanotubular surfaces. The influence of bio-functionalized TiO_2 NTs on the biological performance of MG-63 and hMSCs cells was investigated, together with their ability to display antimicrobial properties. Henceforward the main outcomes of this study are highlighted:

- Bio-functionalized TiO_2 nanotubular surfaces are biocompatible for MG-63 and hMCS cells.
- TiO_2 nanotubular surfaces modulated the morphology of MG-63 and hMSC cells: both cells presented a more stretched morphology compared to Ti smooth and rough surfaces.
- Although a high density of filopodia was found for cells adhered on Ti and nanotubular surfaces, significant differences were found between them: thinner and longer filopodia were found on Ti contrasting with thicker and shorter extensions on NTs, with these latter suggesting stronger cell-surface adhesion properties.
- The expression of BMP-2 was found down-regulated in hMSCs adhered on conventional TiO_2 NTs compared to Ti, which was reflected in a down-regulation of OPN.
- OPN gene expression is probably regulated by BMP-2 levels: the enrichment of TiO_2 nanotubular surfaces with Zn significantly enhanced the expression of BMP-2, which was reflected in the up-regulation of OPN.
- All TiO_2 nanotubular surfaces induced the release of significantly higher amount of VEGF as compared to smooth and micro/nano-roughened Ti surfaces;
- TiO_2 nanotubes, before and after bio-functionalization, presented significantly enhanced antimicrobial properties compared to Ti surfaces.

Taking together the enhanced BMP-2 and OPN expression levels along with the higher amount of VEGF produced, these results suggest that the combined effect of TiO_2 nanotubular-textured surfaces with the surface enrichment with Ca, P, and Zn, is a very promising approach to promote bone formation, remodeling and vascularization processes, thereby improving implant osseointegration. Simultaneously, these surfaces display antimicrobial properties coming up with new insights for the development of efficient bio-selective surfaces for osseointegrated implants applications.

Acknowledgements

The authors acknowledge the financial support from FCT by the doctoral grant (Ref. SFRH/BD/88517/2012), CAPES (Proc. 99999.008666/2014-08), CNPq (Proc. 490761/2013-5) and UNESP. Also, the authors would like to thank Rio de Janeiro cell bank (BCRJ, Rio de Janeiro, Brasil) for all the support provided for biological experiments, as well Fernando Almeida for technical assistance at confocal microscope in CENABIO-UFRJ (Rio de Janeiro, Brasil). Tolou Shokuhfar especially thanks to US National Science Foundation NSF-DMR CAREER award # 1564950.

References

[1] Neoh KG, Hu X, Zheng D, Kang ET. Balancing osteoblast functions and bacterial adhesion on functionalized titanium surfaces, Biomaterials 33 (2012), 2813-2822.
[2] Lee D-W, Yun Y-P, Park K, Kim SE. Gentamicin and bone morphogenic protein-2 (BMP-2)-delivering heparinized-titanium implant with enhanced antibacterial activity and osteointegration, Bone 50 (2012), 974-982.
[3] Yao C, Webster TJ. Anodization: a promising nano-modification technique of titanium implants for orthopedic applications, Journal of nanoscience and nanotechnology 6 (2006), 2682-2692.
[4] Ribeiro M, Monteiro FJ, Ferraz MP. Infection of orthopedic implants with emphasis on bacterial adhesion process and techniques used in studying bacterial-material interactions, Biomatter 2 (2012), 176-194.
[5] Raphel J, Holodniy M, Goodman SB, Heilshorn SC. Multifunctional coatings to simultaneously promote osseointegration and prevent infection of orthopaedic implants, Biomaterials 84 (2016), 301-314.
[6] Paquette DW, Brodala N, Williams RC. Risk factors for endosseous dental implant failure, Dental Clinics of North America 50 (2006), 361-374.
[7] Gulati K, Ramakrishnan S, Aw MS, Atkins GJ, Findlay DM, Losic D. Biocompatible polymer coating of titania nanotube arrays for improved drug elution and osteoblast adhesion, Acta biomaterialia 8 (2012), 449-456.
[8] Subbiahdoss G, Kuijer R, Grijpma DW, van der Mei HC, Busscher HJ. Microbial biofilm growth vs. tissue integration: "The race for the surface" experimentally studied, Acta biomaterialia 5 (2009), 1399-1404.
[9] Abt E, Hellstein JW, Lockhart PB, Mariotti AJ, Sollecito TP, Truelove EL, Armstrong S, De Rossi SS, Epstein JB, et al. American Dental Association guidance for utilizing appropriate use criteria in the management of the care of patients with orthopedic implants undergoing dental procedures, The Journal of the American Dental Association 2 (2017), 57-59.
[10] Landgraeber S, Jäger M, Jacobs JJ, Hallab NJ. The pathology of orthopedic implant failure is mediated by innate immune system cytokines, Mediators of inflammation 2014 (2014), 1-9.
[11] Schwartz-Arad D, Laviv A, Levin L. Failure causes, timing, and cluster behavior: an 8-year study of dental implants, Implant dentistry 17 (2008), 200-207.
[12] Srinivasan M, Meyer S, Mombelli A, Müller F. Dental implants in the elderly population: a systematic review and meta-analysis, Clinical oral implants research 00 (2016), 1-11.
[13] Cruz HV, Souza JCM, Henriques M, Rocha LA. Tribocorrosion and bio-tribocorrosion in the oral environment: the case of dental implants, in: Davim JP (Eds.), Biomedical Tribology, Nova Science Publishers, 2011, pp. 1-30.
[14] Gittens RA, McLachlan T, Olivares-Navarrete R, Cai Y, Berner S, Tannenbaum R, Schwartz Z, Sandhage KH, Boyan BD. The effects of combined micron-/submicron-scale surface roughness and nanoscale features on cell proliferation and differentiation, Biomaterials 32 (2011), 3395-3403.
[15] Wu Y, Zitelli JP, TenHuisen KS, Yu X, Libera MR. Differential response of Staphylococci and osteoblasts to varying titanium surface roughness, Biomaterials 32 (2011), 951-960.
[16] Alves S, Bayón R, de Viteri VS, Garcia M, Igartua A, Fernandes M, Rocha L. Tribocorrosion behavior of calcium- and phosphorous-enriched titanium oxide films and study of osteoblast interactions for dental implants, Journal of Bio-and Tribo-Corrosion 1 (2015), 23.
[17] Chiang C-Y, Chiou S-H, Yang W-E, Hsu M-L, Yung M-C, Tsai M-L, Chen L-K, Huang H-H. Formation of TiO2 nano-network on titanium surface increases the human cell growth, Dental Materials 25 (2009), 1022-1029.
[18] Svensson S, Suska F, Emanuelsson L, Palmquist A, Norlindh B, Trobos M, Bäckros H, Persson L, Rydja G, et al. Osseointegration of titanium with an antimicrobial nanostructured noble metal coating, Nanomedicine: Nanotechnology, Biology and Medicine 9 (2013), 1048-1056.
[19] Brammer KS, Frandsen CJ, Jin S. TiO2 nanotubes for bone regeneration, Trends Biotechnol 30 (2012), 315-322.
[20] Oh S, Daraio C, Chen L-H, Pisanic TR, Fiñones RR, Jin S. Significantly accelerated osteoblast cell growth on aligned TiO2 nanotubes, Journal of Biomedical Materials Research Part A 78A (2006), 97-103.
[21] Brammer KS, Frandsen CJ, Jin S. TiO2 nanotubes for bone regeneration, Trends in biotechnology 30 (2012), 315-322.

[22] Bjursten LM, Rasmusson L, Oh S, Smith GC, Brammer KS, Jin S. Titanium dioxide nanotubes enhance bone bonding in vivo, Journal of Biomedical Materials Research Part A 92 (2010), 1218-1224.
[23] Shokuhfar T, Hamlekhan A, Chang J-Y, Choi CK, Sukotjo C, Friedrich C. Biophysical evaluation of cells on nanotubular surfaces: the effects of atomic ordering and chemistry, International journal of nanomedicine 9 (2014), 3737.
[24] Rajyalakshmi A, Ercan B, Balasubramanian K, Webster TJ. Reduced adhesion of macrophages on anodized titanium with select nanotube surface features, International journal of nanomedicine 2011 (2011), 1765-1771.
[25] Ercan B, Taylor E, Alpaslan E, Webster TJ. Diameter of titanium nanotubes influences anti-bacterial efficacy, Nanotechnology 22 (2011), 295102.
[26] Shi X, Xu Q, Tian A, Tian Y, Xue X, Sun H, Yang H, Dong C. Antibacterial activities of TiO2 nanotubes on Porphyromonas gingivalis, RSC Advances 5 (2015), 34237-34242.
[27] Zhao Y, Xing Q, Janjanam J, He K, Long F, Low K-B, Tiwari A, Zhao F, Shahbazian-Yassar R, et al. Facile electrochemical synthesis of antimicrobial TiO2 nanotube arrays, International journal of nanomedicine 9 (2014), 5177.
[28] Gao A, Hang R, Huang X, Zhao L, Zhang X, Wang L, Tang B, Ma S, Chu PK. The effects of titania nanotubes with embedded silver oxide nanoparticles on bacteria and osteoblasts, Biomaterials 35 (2014), 4223-4235.
[29] Xie C, Li P, Liu Y, Luo F, Xiao X. Preparation of TiO2 nanotubes/mesoporous calcium silicate composites with controllable drug release, Materials Science and Engineering: C 67 (2016), 433-439.
[30] Chen J, Zhang Z, Ouyang J, Chen X, Xu Z, Sun X. Bioactivity and osteogenic cell response of TiO2 nanotubes coupled with nanoscale calcium phosphate via ultrasonification-assisted electrochemical deposition, Applied Surface Science 305 (2014), 24-32.
[31] Zhao L, Wang H, Huo K, Cui L, Zhang W, Ni H, Zhang Y, Wu Z, Chu PK. Antibacterial nano-structured titania coating incorporated with silver nanoparticles, Biomaterials 32 (2011), 5706-5716.
[32] Hu Y, Cai K, Luo Z, Xu D, Xie D, Huang Y, Yang W, Liu P. TiO2 nanotubes as drug nanoreservoirs for the regulation of mobility and differentiation of mesenchymal stem cells, Acta biomaterialia 8 (2012), 439-448.
[33] Alves SA, Patel SB, Sukotjo C, Mathew MT, Paulo Filho N, Celis J-P, Rocha LA, Shokuhfar T. Synthesis of calcium-phosphorous doped TiO2 nanotubes by anodization and reverse polarization: A promising strategy for an efficient biofunctional implant surface, Applied Surface Science 399 (2017), 682-701.
[34] Huo K, Zhang X, Wang H, Zhao L, Liu X, Chu PK. Osteogenic activity and antibacterial effects on titanium surfaces modified with Zn-incorporated nanotube arrays, Biomaterials 34 (2013), 3467-3478.
[35] Yazici H, Fong H, Wilson B, Oren E, Amos F, Zhang H, Evans J, Snead M, Sarikaya M, et al. Biological response on a titanium implant-grade surface functionalized with modular peptides, Acta biomaterialia 9 (2013), 5341-5352.
[36] Roguska A, Pisarek M, Andrzejczuk M, Dolata M, Lewandowska M, Janik-Czachor M. Characterization of a calcium phosphate–TiO2 nanotube composite layer for biomedical applications, Materials Science and Engineering: C 31 (2011), 906-914.
[37] Shokuhfar T, Sinha-Ray S, Sukotjo C, Yarin AL. Intercalation of anti-inflammatory drug molecules within TiO 2 nanotubes, RSC Advances 3 (2013), 17380-17386.
[38] Hamlekhan A, Sinha-Ray S, Takoudis C, Mathew MT, Sukotjo C, Yarin AL, Shokuhfar T. Fabrication of drug eluting implants: study of drug release mechanism from titanium dioxide nanotubes, Journal of Physics D: Applied Physics 48 (2015), 275401.
[39] Gulati K, Aw MS, Losic D. Drug-eluting Ti wires with titania nanotube arrays for bone fixation and reduced bone infection, Nanoscale research letters 6 (2011), 571.
[40] Fukada T, Hojyo S, Furuichi T. Zinc signal: a new player in osteobiology, Journal of bone and mineral metabolism 31 (2013), 129-135.
[41] Li Y, Xiong W, Zhang C, Gao B, Guan H, Cheng H, Fu J, Li F. Enhanced osseointegration and antibacterial action of zinc-loaded titania-nanotube-coated titanium substrates: In vitro and in vivo studies, Journal of Biomedical Materials Research Part A 102 (2014), 3939-3950.
[42] Yusa K, Yamamoto O, Takano H, Fukuda M, Iino M. Zinc-modified titanium surface enhances osteoblast differentiation of dental pulp stem cells in vitro, Scientific Reports 6 (2016), 29462.
[43] PAUTKE C, SCHIEKER M, TISCHER T, KOLK A, NETH P, MUTSCHLER W, MILZ S. Characterization of osteosarcoma cell lines MG-63, Saos-2 and U-2 OS in comparison to human osteoblasts, Anticancer research 24 (2004), 3743-3748.
[44] Kraus KH, Kirker-Head C. Mesenchymal stem cells and bone regeneration, Veterinary surgery 35 (2006), 232-242.
[45] Falagan-Lotsch P, Lopes TS, Ferreira N, Balthazar N, Monteiro AM, Borojevic R, Granjeiro JM. Performance of PCR-based and Bioluminescent assays for mycoplasma detection, Journal of microbiological methods 118 (2015), 31-36.
[46] Cosme B, Falagan-Lotsch P, Ribeiro M, Napoleão K, Granjeiro JM, Moura-Neto R. Are your results valid? Cellular authentication a need from the past, an emergency on the present, In Vitro Cellular & Developmental Biology-Animal (2017), 1-5.
[47] Riss TL, Moravec RA, Niles AL, Benink HA, Worzella TJ, Minor L. Cell viability assays, in: Sittampalam GS CN, Brimacombe K, et al. (Eds.), Assay Guidance Manual [Internet], Eli Lilly & Company and the National Center for Advancing Translational Sciences, 2015.

[48] Dirckx N, Hul M, Maes C. Osteoblast recruitment to sites of bone formation in skeletal development, homeostasis, and regeneration, Birth Defects Research Part C: Embryo Today: Reviews 99 (2013), 170-191.
[49] Beederman M, Lamplot JD, Nan G, Wang J, Liu X, Yin L, Li R, Shui W, Zhang H, et al. BMP signaling in mesenchymal stem cell differentiation and bone formation, Journal of biomedical science and engineering 6 (2013), 32.
[50] Yang J, Shi P, Tu M, Wang Y, Liu M, Fan F, Du M. Bone morphogenetic proteins: Relationship between molecular structure and their osteogenic activity, Food Science and Human Wellness 3 (2014), 127-135.
[51] Terai K, Takano-Yamamoto T, Ohba Y, Hiura K, Sugimoto M, Sato M, Kawahata H, Inaguma N, Kitamura Y, et al. Role of osteopontin in bone remodeling caused by mechanical stress, Journal of Bone and Mineral Research 14 (1999), 839-849.
[52] Rodrigues WC, da Silva Fabris AL, Hassumi JS, Gonçalves A, Sonoda CK, Okamoto R. Kinetics of gene expression of alkaline phosphatase during healing of alveolar bone in rats, British Journal of Oral and Maxillofacial Surgery 54 (2016), 531-535.
[53] Livak KJ, Schmittgen TD. Analysis of relative gene expression data using real-time quantitative PCR and the 2−ΔΔCT method, methods 25 (2001), 402-408.
[54] Antony RP, Mathews T, Dash S, Tyagi AK, Raj B. X-ray photoelectron spectroscopic studies of anodically synthesized self aligned TiO2 nanotube arrays and the effect of electrochemical parameters on tube morphology, Materials Chemistry and Physics 132 (2012), 957-966.
[55] Regonini D, Jaroenworaluck A, Stevens R, Bowen CR. Effect of heat treatment on the properties and structure of TiO2 nanotubes: phase composition and chemical composition, Surface and interface analysis 42 (2010), 139-144.
[56] Pisarek M, Roguska A, Marcon L, Andrzejczuk M. Biomimetic and electrodeposited calcium-phosphates coatings on Ti-formation, surface characterization, biological response, INTECH Open Access Publisher, 2012.
[57] Kang B-S, Sul Y-T, Oh S-J, Lee H-J, Albrektsson T. XPS, AES and SEM analysis of recent dental implants, Acta biomaterialia 5 (2009), 2222-2229.
[58] Indira K, Mudali UK, Rajendran N. In-vitro biocompatibility and corrosion resistance of strontium incorporated TiO2 nanotube arrays for orthopaedic applications, Journal of biomaterials applications 29 (2014), 113-129.
[59] Fu W, Ding S, Wang Y, Wu L, Zhang D, Pan Z, Wang R, Zhang Z, Qiu S. F, Ca co-doped TiO 2 nanocrystals with enhanced photocatalytic activity, Dalton Transactions 43 (2014), 16160-16163.
[60] Lee D-B, Hong L-S, Kim Y-J. Effect of Ca and CaO on the high temperature oxidation of AZ91D Mg alloys, Materials transactions 49 (2008), 1084-1088.
[61] Tanaka Y, Saito H, Tsutsumi Y, Doi H, Imai H, Hanawa T. Active hydroxyl groups on surface oxide film of titanium, 316L stainless steel, and cobalt-chromium-molybdenum alloy and its effect on the immobilization of poly (ethylene glycol), Materials transactions 49 (2008), 805-811.
[62] Lv L, Liu Y, Zhang P, Zhang X, Liu J, Chen T, Su P, Li H, Zhou Y. The nanoscale geometry of TiO2 nanotubes influences the osteogenic differentiation of human adipose-derived stem cells by modulating H3K4 trimethylation, Biomaterials 39 (2015), 193-205.
[63] Zhao L, Liu L, Wu Z, Zhang Y, Chu PK. Effects of micropitted/nanotubular titania topographies on bone mesenchymal stem cell osteogenic differentiation, Biomaterials 33 (2012), 2629-2641.
[64] Zhao L, Mei S, Chu PK, Zhang Y, Wu Z. The influence of hierarchical hybrid micro/nano-textured titanium surface with titania nanotubes on osteoblast functions, Biomaterials 31 (2010), 5072-5082.
[65] Kim EJ, Boehm CA, Mata A, Fleischman AJ, Muschler GF, Roy S. Post microtextures accelerate cell proliferation and osteogenesis, Acta biomaterialia 6 (2010), 160-169.
[66] Heidari B, Shirazi A, Akhondi MM, Hassanpour H, Behzadi B, Naderi MM, Sarvari A, Borjian S. Comparison of proliferative and multilineage differentiation potential of sheep mesenchymal stem cells derived from bone marrow, liver, and adipose tissue, Avicenna journal of medical biotechnology 5 (2013), 104-117.
[67] Baksh D, Song L, Tuan R. Adult mesenchymal stem cells: characterization, differentiation, and application in cell and gene therapy, Journal of cellular and molecular medicine 8 (2004), 301-316.
[68] Chug A, Shukla S, Mahesh L, Jadwani S. Osseointegration—Molecular events at the bone–implant interface: A review, Journal of Oral and Maxillofacial Surgery, Medicine, and Pathology 25 (2013), 1-4.
[69] Singhatanadgit W. Biological Responses to New Advanced Surface Modifications of Endosseous Medical Implants, Bone and Tissue Regeneration Insights 2 (2009), 1-11.
[70] Kubo K, Tsukimura N, Iwasa F, Ueno T, Saruwatari L, Aita H, Chiou W-A, Ogawa T. Cellular behavior on TiO 2 nanonodular structures in a micro-to-nanoscale hierarchy model, Biomaterials 30 (2009), 5319-5329.
[71] Kulkarni M, Mazare A, Gongadze E, Perutkova Š, Kralj-Iglič V, Milošev I, Schmuki P, Iglič A, Mozetič M. Titanium nanostructures for biomedical applications, Nanotechnology 26 (2015), 062002.
[72] Pegueroles M, Tonda-Turo C, Planell JA, Gil F-J, Aparicio C. Adsorption of fibronectin, fibrinogen, and albumin on TiO2: time-resolved kinetics, structural changes, and competition study, Biointerphases 7 (2012), 1-13.
[73] Park J, Bauer S, von der Mark K, Schmuki P. Nanosize and vitality: TiO2 nanotube diameter directs cell fate, Nano letters 7 (2007), 1686-1691.
[74] Zambuzzi WF, Coelho PG, Alves GG, Granjeiro JM. Intracellular signal transduction as a factor in the development of “smart” biomaterials for bone tissue engineering, Biotechnology and bioengineering 108 (2011), 1246-1250.
[75] Nguyen AT, Sathe SR, Yim EK. From nano to micro: topographical scale and its impact on cell adhesion, morphology and contact guidance, Journal of Physics: Condensed Matter 28 (2016), 183001.

[76] Bauer S, Park J, Faltenbacher J, Berger S, von der Mark K, Schmuki P. Size selective behavior of mesenchymal stem cells on ZrO2 and TiO2 nanotube arrays, Integrative Biology 1 (2009), 525-532.
[77] Imani R, Kabaso D, Erdani Kreft M, Gongadze E, Penič S, Eleršič K, Kos A, Veranič P, Zorec R, et al. Morphological alterations of T24 cells on flat and nanotubular TiO2 surfaces, Croatian medical journal 53 (2012), 577-585.
[78] Oh S, Brammer KS, Li YSJ, Teng D, Engler AJ, Chien S, Jin S. Stem cell fate dictated solely by altered nanotube dimension, Proceedings of the National Academy of Sciences 106 (2009), 2130-2135.
[79] Shih YRV, Tseng KF, Lai HY, Lin CH, Lee OK. Matrix stiffness regulation of integrin-mediated mechanotransduction during osteogenic differentiation of human mesenchymal stem cells, Journal of Bone and Mineral Research 26 (2011), 730-738.
[80] Mattila PK, Lappalainen P. Filopodia: molecular architecture and cellular functions, Nature reviews Molecular cell biology 9 (2008), 446-454.
[81] Tian A, Qin X, Wu A, Zhang H, Xu Q, Xing D, Yang H, Qiu B, Xue X, et al. Nanoscale TiO2 nanotubes govern the biological behavior of human glioma and osteosarcoma cells, International journal of nanomedicine 10 (2015), 2423.
[82] Zheng X, Zhou F, Gu Y, Duan X, Mo A. Effect of Different Titanium Surfaces on Maturation of Murine Bone Marrow-Derived Dendritic Cells, Scientific Reports 7 (2017), 41945.
[83] Wang Y-K, Yu X, Cohen DM, Wozniak MA, Yang MT, Gao L, Eyckmans J, Chen CS. Bone morphogenetic protein-2-induced signaling and osteogenesis is regulated by cell shape, RhoA/ROCK, and cytoskeletal tension, Stem cells and development 21 (2011), 1176-1186.
[84] Komori T. Regulation of bone development and extracellular matrix protein genes by RUNX2, Cell and tissue research 339 (2010), 189.
[85] Li R, Liang L, Dou Y, Huang Z, Mo H, Wang Y, Yu B. Mechanical strain regulates osteogenic and adipogenic differentiation of bone marrow mesenchymal stem cells, BioMed research international 2015 (2015), 1-10.
[86] Yang X, Gong P, Lin Y, Zhang L, Li X, Yuan Q, Tan Z, Wang Y, Man Y, et al. Cyclic tensile stretch modulates osteogenic differentiation of adipose-derived stem cells via the BMP-2 pathway, Archives of Medical Science 6 (2010), 152-159.
[87] Grottkau BE, Yang X, Zhang L, Ye L, Lin Y. Comparison of effects of mechanical stretching on osteogenic potential of ASCs and BMSCs, Bone research 1 (2013), 282-290.
[88] Zhao Y, Huo M, Liu Y, Xie Y, Wang J, Li Y, Wang J. EFFECTS OF FLUORIDE ON THE EXPRESSION OF BMP-2 AND SMAD1 IN RAT OSTEOBLASTS IN VITRO, Fluoride 49 (2016), 13-22.
[89] Gandhi D, Naoghare PK, Bafana A, Kannan K, Sivanesan S. Fluoride-Induced Oxidative and Inflammatory Stress in Osteosarcoma Cells: Does It Affect Bone Development Pathway?, Biological trace element research 175 (2017), 103-111.
[90] Yang C, Wang Y, Xu H. Fluoride Regulate Osteoblastic Transforming Growth Factor-β1 Signaling by Mediating Recycling of the Type I Receptor ALK5, PloS one 12 (2017), e0170674.
[91] Sun J, Li J, Li C, Yu Y. Role of bone morphogenetic protein-2 in osteogenic differentiation of mesenchymal stem cells, Molecular medicine reports 12 (2015), 4230-4237.
[92] Schwarting T, Schenk D, Frink M, Benölken M, Steindor F, Oswald M, Ruchholtz S, Lechler P. Stimulation with bone morphogenetic protein-2 (BMP-2) enhances bone–tendon integration in vitro, Connective tissue research 57 (2016), 99-112.
[93] Yang X, Meng X, Su X, Mauchley DC, Ao L, Cleveland Jr JC, Fullerton DA. Bone morphogenic protein 2 induces Runx2 and osteopontin expression in human aortic valve interstitial cells: Role of Smad1 and extracellular signal-regulated kinase 1/2, The Journal of Thoracic and Cardiovascular Surgery 138 (2009), 1008-1015.e1001.
[94] Wu M, Chen G, Li Y-P. TGF-β and BMP signaling in osteoblast, skeletal development, and bone formation, homeostasis and disease, Bone research 4 (2016), 16009.
[95] Saran U, Piperni SG, Chatterjee S. Role of angiogenesis in bone repair, Archives of biochemistry and biophysics 561 (2014), 109-117.
[96] Veeriah V, Zanniti A, Paone R, Chatterjee S, Rucci N, Teti A, Capulli M. Interleukin-1β, lipocalin 2 and nitric oxide synthase 2 are mechano-responsive mediators of mouse and human endothelial cell-osteoblast crosstalk, Scientific Reports 6 (2016).
[97] Raines AL, Olivares-Navarrete R, Wieland M, Cochran DL, Schwartz Z, Boyan BD. Regulation of angiogenesis during osseointegration by titanium surface microstructure and energy, Biomaterials 31 (2010), 4909-4917.
[98] Bai L, Wu R, Wang Y, Wang X, Zhang X, Huang X, Qin L, Hang R, Zhao L, et al. Osteogenic and angiogenic activities of silicon-incorporated TiO2 nanotube arrays, Journal of Materials Chemistry B 4 (2016), 5548-5559.
[99] Deckers MM, Van Bezooijen RL, Van Der Horst G, Hoogendam J, van der Bent C, Papapoulos SE, Löwik CW. Bone morphogenetic proteins stimulate angiogenesis through osteoblast-derived vascular endothelial growth factor A, Endocrinology 143 (2002), 1545-1553.
[100] Hori K, Matsumoto S. Bacterial adhesion: From mechanism to control, Biochemical Engineering Journal 48 (2010), 424-434.
[101] Anselme K, Davidson P, Popa A, Giazzon M, Liley M, Ploux L. The interaction of cells and bacteria with surfaces structured at the nanometre scale, Acta biomaterialia 6 (2010), 3824-3846.
[102] Han A, Tsoi JKH, Rodrigues FP, Leprince JG, Palin WM. Bacterial adhesion mechanisms on dental implant surfaces and the influencing factors, International Journal of Adhesion and Adhesives 69 (2016), 58-71.

[103] Bazaka K, Jacob MV, Crawford RJ, Ivanova EP. Plasma-assisted surface modification of organic biopolymers to prevent bacterial attachment, Acta biomaterialia 7 (2011), 2015-2028.
[104] Whitehead KA, Colligon J, Verran J. Retention of microbial cells in substratum surface features of micrometer and sub-micrometer dimensions, Colloids and Surfaces B: Biointerfaces 41 (2005), 129-138.
[105] Roguska A, Pisarek M, Belcarz A, Marcon L, Holdynski M, Andrzejczuk M, Janik-Czachor M. Improvement of the bio-functional properties of TiO2 nanotubes, Applied Surface Science 388, Part B (2016), 775-785.
[106] Li H, Cui Q, Feng B, Wang J, Lu X, Weng J. Antibacterial activity of TiO2 nanotubes: Influence of crystal phase, morphology and Ag deposition, Applied Surface Science 284 (2013), 179-183.
[107] Puckett SD, Taylor E, Raimondo T, Webster TJ. The relationship between the nanostructure of titanium surfaces and bacterial attachment, Biomaterials 31 (2010), 706-713.
[108] Kang S, Pinault M, Pfefferle LD, Elimelech M. Single-walled carbon nanotubes exhibit strong antimicrobial activity, Langmuir 23 (2007), 8670-8673.
[109] Breaker R. New insight on the response of bacteria to fluoride, Caries research 46 (2012), 78-81.
[110] Marquis RE. Antimicrobial actions of fluoride for oral bacteria, Canadian journal of microbiology 41 (1995), 955-964.
[111] Liu J, Rawlinson SC, Hill RG, Fortune F. Fluoride incorporation in high phosphate containing bioactive glasses and in vitro osteogenic, angiogenic and antibacterial effects, Dental Materials 32 (2016), e221-e237.

CHAPTER 6

Tribo-electrochemical behavior of bio-functionalized TiO_2 nanotubes in artificial saliva: understanding of degradation mechanisms

Submitted for publication in Wear

Tribo-electrochemical behavior of bio-functionalized TiO_2 nanotubes in artificial saliva: understanding of degradation mechanisms

Sofia A. Alves[1,2*], André L. Rossi[3], Ana R. Ribeiro[2,4,5], Fatih Toptan[1,6], Ana M. Pinto[1,6], Jean-Pierre Celis[7,8], Tolou Shokuhfar[9,10*], Luís A. Rocha[1,2,11*]

[1]*CMEMS – Center of MicroElectroMechanical Systems, Department of Mechanical Engineering, University of Minho, Azurém, 4800-058 Guimarães, Portugal*

[2]*IBTN/BR – Brazilian Branch of the Institute of Biomaterials, Tribocorrosion and Nanomedicine, Faculty of Sciences, UNESP – Universidade Estadual Paulista, 17033-360 Bauru, São Paulo, Brazil*

[3]*Brazilian Center for Research in Physics, 22290-180 Rio de Janeiro, Brazil*

[4]*Directory of Life Sciences Applied Metrology, National Institute of Metrology, Quality and Technology, 25250-020 Duque de Caxias – RJ, Brazil*

[5]*Postgraduate Program in Translational Biomedicine, University of Grande Rio, 25070-000 Duque de Caxias – RJ, Brazil*

[6]*Department of Mechanical Engineering, University of Minho, Azurém, 4800-058 Guimarães, Portugal*

[7]*Department of Materials Engineering, KU Leuven, 3001 Leuven, Belgium*

[8]*Falex Tribology N.V., Wingepark 23B, 3110 Rotselaar, Belgium*

[9]*Department of Bioengineering, University of Illinois at Chicago, 60607 Chicago, Illinois, USA*

[10]*IBTN/US – American Branch of the Institute of Biomaterials, Tribocorrosion and Nanomedicine, University of Illinois at Chicago, 60612 Chicago, Illinois, USA*

[11]*Faculdade de Ciências, Departamento de Física, UNESP – Universidade Estadual Paulista, 17033-360 Bauru, São Paulo, Brasil*

**e-mail: lrocha@fc.unesp.br; tolou@uic.edu*

Abstract

It has been shown that the synthesis of TiO_2 nanotubes by anodization provides outstanding properties to Ti surfaces intended for dental and orthopedic implants applications. Beyond the very well-known potential of these surfaces to improve osseointegration and avoid infection, the knowledge on the adhesion and degradation behavior of TiO_2 nanotubes under the simultaneous action of wear and corrosion is still poorly understood and these are issues of tremendous importance. The main aim of this work is to investigate, for the first time, the tribo-electrochemical degradation behavior of Ti surfaces decorated with TiO_2 nanotubes before and after bio-functionalization treatments.

Well-aligned TiO_2 nanotubes (NTs) were produced containing elements natively present in bone such as calcium (Ca) and phosphorous (P), in addition of zinc (Zn) as an antimicrobial agent and stimulator of bone formation. The synthesis of Ca/P/Zn-doped nanotubes (NT-Ca/P/Zn) was achieved by reverse polarization and anodization treatments applied to conventional TiO_2 nanotubes grown by two-step anodization. The nanotube surfaces were analyzed by scanning electron microscopy (SEM) while dark-field scanning transmission electron microscopy (STEM-DF) was used to characterize the Ti/TiO_2 nanotubular films interfaces. Tribo-electrochemical tests were conducted under reciprocating sliding conditions in artificial saliva. The open circuit potential (OCP) was monitored before, during and after sliding tests, and the coefficient of friction (COF) values were registered during rubbing action. The wear tracks

resulting from sliding tests were characterized by SEM and wear volume measurements were carried out by 2D profilometry.

The results show that the tribo-electrochemical behavior of TiO_2 nanotubes was significantly improved after bio-functionalization treatments. The higher electrochemical stability and lower mechanical degradation of these films was correlated with their improved adhesion strength to Ti substrate, which is granted by the nano-thick oxide film formed at the interface region, during bio-functionalization processes. A first insight on the degradation mechanisms taking place during tribo-electrochemical action is proposed. The outcomes of this study may contribute in a great extent for the development of new implant surfaces with improved biomechanical stability and thus contribute for the long term success of dental implants.

Keywords: TiO_2 nanotubes; Bio-functionalization; Film adhesion; Tribocorrosion; Dental implants.

6.1. Introduction

Titanium (Ti) and Ti alloys are the gold standard materials for dental implants applications mainly owing to their superior mechanical properties, biocompatibility and excellent corrosion resistance [1]. It is well documented that biocompatibility and corrosion resistance properties are mainly dictated by the formation of a well-adhering, dense and protective passive TiO_2 film (2 – 10 nm thickness) on the Ti-based materials surface when exposed to oxygen-containing environments [2-5]. However, despite the high corrosion resistance of Ti, the stability of the passive film may be modified in the presence of aggressive *in vivo* conditions, enhancing the corrosion process [6-9]. Furthermore, Ti-based materials display poor wear resistance, presenting severe adhesion wear and low abrasion resistance [9-12].

After implantation and the establishment of an adequate contact between bone and the implant surface (osseointegration), dental implants might be subjected to mechanical solicitations arising from biting forces generated during mastication. The masticatory action may induce cyclic micro-movements at the implant/bone interface and consequently to shear stresses at that place [9, 13]. This occurs in the presence of a corrosive biological environment leading to the degradation of the dental implant material simultaneously by wear and corrosion processes, a phenomenon known as tribocorrosion [14-16]. As a consequence of wear-corrosion processes taking place at implant /bone interface, wear debris and corrosion products may be released to the implant surroundings and induce to adverse biological reactions and, ultimately, lead to implant loosening [17-19]. In spite of the negative impact that tribocorrosion processes

may have on the long term biological and mechanical stability of dental implants, the development of new implant systems addressing an integrated approach, which includes wear-corrosion resistance as a pre-requisite for implant success, is still lacking.

Recent advances in the fabrication of novel coatings and nanopatterning of dental implant surfaces have been achieved and there is a strong believe that nanoscale materials will produce the new generation of implant materials [20]. In the last decades, vertically aligned TiO_2 nanotubes grown in Ti surfaces by electrochemical anodization have become increasingly popular to enhance adhesion, growth and accelerate the osteogenic differentiation of osteoblasts and mesenchymal stem cells (MSCs) [21-26]. Furthermore, these nanostructures have shown the ability to display antimicrobial properties and thus inhibit microbial infections [27-35]. Additionally, TiO_2 nanotubes possess a lower elastic modulus (36 – 43 GPa) than cp-Ti (120 – 166 GPa), which is closer to that of natural bone (11 – 30 GPa), and thus TiO_2 nanotubular structured Ti surfaces are expected to have improved biomechanical compatibility, by reducing stress shielding effect [36-39].

TiO_2 nanotubes have been functionalized through different approaches in an attempt to develop new strategies for the construction of biomimetic systems mimicking the natural extracellular micro-environments, addressing osseointegration [23, 40-42] and microbial implant-infection related issues [43, 44]. Beyond all the evidences that TiO_2 nanotubes may effectively enhance cellular functions while simultaneously decrease bacterial action [45], the study of the adhesion properties of nanotubular films to the Ti substrate as well as their degradation mechanisms by wear-corrosion processes are still missing. These topics are of main relevance since poor adhesion strength of TiO_2 films before and/or after functionalization treatments, as well as their degradation through wear and corrosion mechanisms, may strongly compromise their use for osseointegrated implants applications. The biomechanical stability must be ensured after implantation since it might influence the implant lifetime, the probability of failure and thus the quality of life for implant receiving patients.

In this work the tribo-electrochemical degradation behavior of TiO_2 nanotubes before and after bio-functionalization processes is studied, for the first time, through reciprocating sliding tests in artificial saliva. A first insight on the tribo-electrochemical degradation mechanisms of TiO_2 nanotubes was proposed, and remarkable differences were observed between conventional and bio-functionalized TiO_2 nanotubes.

6.2. Experimental section

6.2.1. Surface pre-treatment

Commercially pure titanium (cp-Ti, ASTM grade 2) rod (MacMaster-carr, IL, USA) was cut into discs of 15 mm diameter and 2 mm thickness. A series of silicon carbide (SiC) sandpapers from #240 to #1200 were used to ground cp-Ti disc surfaces followed by their polishing. The surface mirror finishing was achieved by using a polishing cloth with non-crystallizing colloidal silica suspension (MasterMet 2, Buehler, Lake Bluff, IL, USA). After polishing, the cp-Ti samples were cleaned in the ultrasonic bath in isopropanol (10 min) followed by distilled water (5 min), and finally dried at room temperature. Cp-Ti smooth surfaces were the substrates used in this study and were taken as the control group, named as Ti.

6.2.2. TiO_2 nanotubes synthesis and bio-functionalization

The synthesis of TiO_2 nanotubes relied on two-step anodization processes carried out in an organic electrolyte constituted of ethylene glycol (EG, Fluka Analytical, St. Louis, MO, USA), 0.3 wt. % ammonium fluoride (NH_4F, Ammonium Fluoride, Sigma-Aldrich, St. Louis, MO, USA) and 3 vol. % distilled water. The anodization processes were conducted at room temperature (22 to 24 ^oC) and the electrolyte was under continuous magnetic agitation (150 rpm). A DC power supply (Keysight (Agilent) Technologies N5772A) was used for the anodic treatments with a limiting current of 2.5 A.

For TiO_2 nanotube fabrication, firstly, Ti smooth samples (anode) were immersed in the EG electrolyte jointly with a graphite rod (cathode), separated at a distance of about 2 cm, and the power supply was set at 60 V for 1 h. Afterwards, the samples were ultrasonically cleaned in isopropanol (15 min) and distilled water (5 min) aiming to intentionally remove the nanotubular film grown in Ti surfaces during the first anodizing step, and create a nanopatterned Ti surface with nanotube bottom shape imprinted on it. Finally, these nanopatterned surfaces were anodized for 30 min at the previous conditions, to synthesize the TiO_2 nanotubular films with the desired morphology. At the end of the process, the samples were cleaned in isopropanol (10 min), distilled water (5 min) and dried at room temperature. The resulting Ti samples with TiO_2 nanotubes were named as NT.

The NT samples previously synthesized were bio-functionalized by following a new methodology described in a previous work [46], which relies on reverse polarization and anodization treatments. The processes were carried out in a continuously stirred (200 rpm) aqueous electrolyte composed of 0.35 M calcium acetate (Calcium acetate monohydrate, Sigma-Aldrich, St. Louis, MO, USA), 0.04 M β-glycerolphosphate (β-GP) (β-glycerolphosphate disodium

salt pentahydrate, Sigma-Aldrich, St. Louis, MO, USA) and 0.35 M zinc acetate (Zinc acetate dihydrate, Sigma-Aldrich, St. Louis, MO, USA) as the source of Calcium (Ca), Phosphorous (P) and Zinc (Zn), respectively. The cathodic and anodic treatments were conducted at room temperature (22 – 24 °C) using a DC power supply (Keysight (Agilent) Technologies N5772A) set at a limiting current of 2.5 A. For bio-functionalization of TiO_2 nanotubes, the NT samples were immersed in the aqueous electrolyte containing Ca, P and Zn elements (Ca/P/Zn-based electrolyte), distanced 2 cm from a graphite rod. Afterwards, the samples were reverse polarized for 30 s, followed by anodization in the same electrolyte for 30 min at 100 V. Finally, the samples were cleaned in isopropanol (10 min), distilled water (5 min) and dried at room temperature. The resulting Ti samples decorated with Ca, P and Zn-doped TiO_2 nanotubes were named as NT-Ca/P/Zn. After preparation, the samples were stored in a desiccator before performing tribocorrosion tests.

6.2.3. Surface and cross-section characterization of the TiO_2 nanotubular films

The surface morphology of TiO_2 nanotubular samples was investigated by scanning electron microscopy (SEM) using a JEOL JSM-6490LV. The surface chemistry of bio-functionalized nanotubes was accessed by energy-dispersive X-ray spectroscopy (EDS) (Pegasus X4M), using an acceleration voltage of 15 kV.

A dual beam instrument equipped with focused ion beam (FIB) with a gallium (Ga) ion source (TESCAN, LYRA 3) was used to obtain thin cross-sections (around 100 nm thick) of the TiO_2 nanotubular films. The samples surface was gold sputtered to improve the electrical conductivity during FIB preparation. To protect the thin cross-sections a platinum (Pt) layer of 1 µm was deposited in situ using a gas injection system and 1 nA Ga^+ ion current accelerated at 30 kV. Initial etching was conducted with 5 and 2 nA at 30 keV. Thinning was performed in 4 steps to obtain a lamella of ~ 100 nm: 1) 1 nA/30 keV; 2) 0.1 nA/10 keV; 3) 10 pA/5 keV; and 4) 3 keV. The cross-sections were observed at the Ti/TiO_2 nanotubes interface regions by dark-field scanning transmission electron microscopy (STEM-DF) using a JEOL 2100 F operating at an accelerating voltage of 200 kV. The length of the nanotubular films was measured from the samples observed by STEM.

6.2.4. Tribo-electrochemical experiments

The experimental approach used for tribo-electrochemical tests is similar to the one shown in a previous work by Souza *et al.* [13] The different groups of samples were fixed in an electrochemical cell with the desired surface facing upwards and in contact with the electrolyte. A modified Fusayama's artificial saliva (AS) [47] was used at 37 °C (pH = 5.5), with chemical

composition as follows: NaCl (0.4 g/L), KCl (0.4 g/L) , $CaCl_2.2H_2O$ (0.795 g/L), $Na_2S.9H_2O$ (0.005 g/L), $NaH_2PO_4.2H_2O$ (0.69 g/L) and Urea (1 g/L). This electrolyte has been widely used in previous investigations [13, 48-50] to simulate the highly corrosive oral cavity environment with Cl^-, F^-, and H^+ ions, playing a significant role on corrosion of dental implant materials [51]. Another reason for its use is related with the similar electrochemical behavior that metallic materials display in Fusayama´s saliva compared to the one in natural saliva [52]. The exposed surface area to AS was fixed at 0.63 cm^2.

The electrochemical cell was mounted on a CETR tribometer (Model UMT 2, Campbell, California, USA) in a pin-on-disk configuration, and an alumina (Al_2O_3) ball (Ø 10 mm) was selected as the counterbody material since it has high wear resistance, chemical inertness and electrical insulating properties [9]. A three-electrode setup was used with testing samples as the working electrode, a Pt counter electrode, and a saturated calomel electrode (SCE) (Hg/Hg_2Cl_2/saturated KCl solution; SCE = +244 mV *vs.* NHE) was used as the reference electrode.

For tribo-electrochemical experiments, the open circuit potential (OCP) was monitored prior to rubbing action until stabilization, during the whole duration of sliding and after the mechanical action, during 1800 s. The electrochemical measurements were carried out using a potentiostat Gamry Reference 600 coupled to Gamry framework software (Gamry Instruments, Warminster, PA, USA). The reciprocating sliding tests against alumina ball were performed at a normal load of 1 N, a sliding frequency of 1 Hz, and a linear displacement amplitude of 650 µm during 300 s and 1800 s. The tribometer was coupled to UMT-2 software (Campbell, California, USA) to monitor the tangential force during sliding, from which the friction coefficient (COF) was calculated. After testing, all the samples were ultrasonically cleaned with isopropanol during 10 minutes followed by distilled water for 5 minutes. Finally all the samples were dried at room temperature. It is noteworthy that all the experiments were performed for a minimum number of three samples for each condition, to assure the repeatability of the results.

6.2.5. Characterization of the wear tracks

After tribo-electrochemical experiments all the wear tracks were deeply analyzed. The morphological and chemical features of the wear scars were investigated by SEM (FEI Nova 200 (FEG/SEM)) and EDS (Pegasus X4M).

To calculate the volume of the degraded material from the samples exposed to tribo-electrochemical action (wear volume), the model previously described by Doni *et al.* [53] was followed. The wear track length was taken constant for all the tests as 650 µm, and the borders of the wear tracks were assumed as part of a calotte. The width and the deepness of the wear tracks were extracted from their profiles obtained by 2D profilometry (Veeco, Dektak 150) and

the data analysis was performed with the aid of the affiliated software (Dektak version 9.4). For each wear track, three 2D profiles were taken in its central region. The final wear volume was calculated through the following equation:

$$\mathbf{\Delta V} = [\frac{\mathbf{1}}{\mathbf{3}} * \boldsymbol{\pi} * \bar{\mathbf{D}}^{\mathbf{2}}(\mathbf{3R} - \bar{\mathbf{D}})] + \bar{\mathbf{A}}_{\mathbf{w}} * \mathbf{l} \qquad (1)$$

where ΔV is the total wear volume loss for each wear track in μm^3, $\bar{D}$ is the average deepness values, R is the radius of the alumina ball (counterbody), $\bar{A}_w$ is the average value of the wear loss area calculated from 2D profiles (obtained directly through the software), and l is the total length of the wear track (i.e. 650 μm). The final wear volume measurements were calculated from three wear tracks for each condition of test.

6.2.6. Statistical analysis

Data presented in this study are expressed as the arithmetic mean ± standard deviation (SD). The statistical tool SigmaStat 3.5 (Systat Software, San Jose, CA, USA) was used for statistical analysis. The evaluation of the data was carried out by one-way analysis of variance (ANOVA) in combination with Tukey HSD post hoc test for pair-wise comparisons between groups, with a significance level of $p < 0.05$.

6.3. Results

6.3.1. Characterization of TiO_2 nanotubular films

Titanium (Ti) smooth surfaces depicted in Fig. 6.1a were treated by two-step anodization in an ethylene glycol electrolyte containing fluoride (F^-) ions. Well-ordered Ti dioxide (TiO_2) nanotubes were grown from Ti surfaces, whose morphology is shown in Fig. 6.1b. The nanotubes are characterized by non-uniform diameters ranging from 50 – 90 nm as reported in a previous study [46]. The anodized Ti surfaces present a homogenous morphology, with TiO_2 nanotubular structures uniformly distributed along the surface area without film cracking. After bio-functionalization treatments by reverse polarization and anodization, zinc (Zn) was incorporated on nanotubular structures together with calcium (Ca) and phosphorous (P) without changing their surface morphology, as shown in Fig. 6.1c and Fig. 6.1d.

The cross-section of the nanotubular films, before and after bio-functionalization treatments, are shown in Fig. 6.2a and b respectively. Conventional anodic TiO_2 nanotubular films are characterized by a non-continuous interface as observed in Fig. 6.2a. The presence of a hollow space between the film and the Ti substrate is observed suggesting a poor adhesion of

the film. The interface of NT-Ca/P/Zn films present distinctive features as observed in Fig. 6.2b. This interface, beyond presenting some porosity at the nanoscale range, shows that the voided space existing before is not continuous anymore due to the formation of an oxide film during bio-functionalization treatments, with a thickness comprised between 230 – 250 nm.

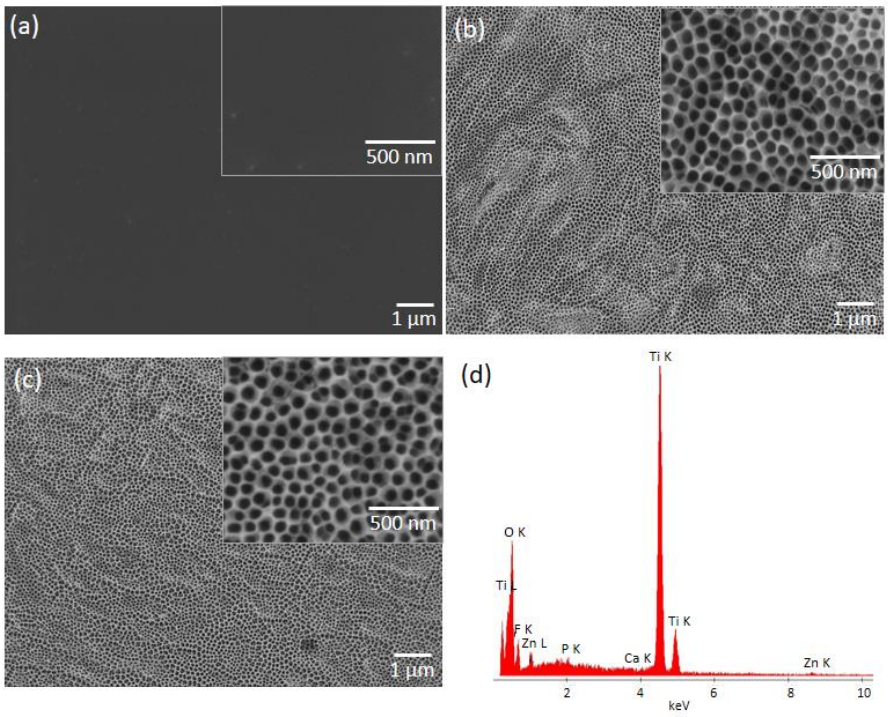

Fig. 6.1. SE SEM micrographs of (a) Ti, (b) NT and (c) NT-Ca/P/Zn surfaces. The inset images show the surface morphology in more detail. In (d) the EDS spectrum characteristic of NT-Ca/P/Zn samples is depicted.

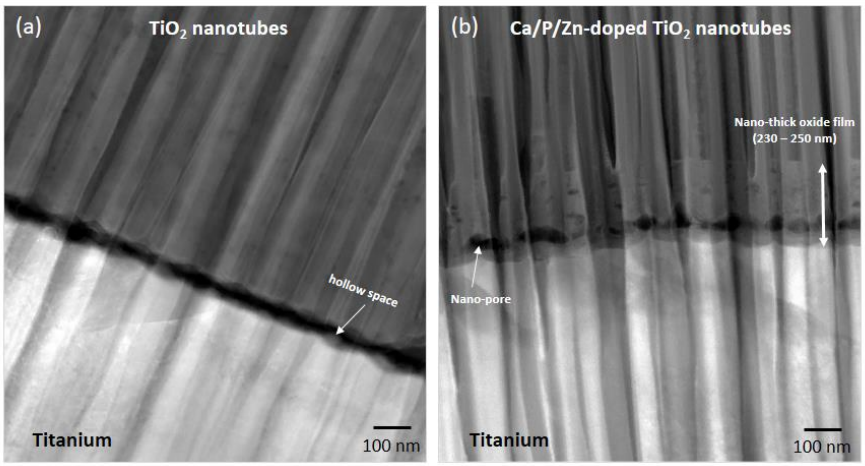

Fig. 6.2. STEM-DF micrographs of the FIB sections of (a) NT and (b) NT-Ca/P/Zn nanotubular films at the interface region. The inset white arrow in (a) highlights the hollow space existing between Ti substrate and NT film while in (b) shows the nano-pores existing at the interface instead of a continuous hollow space. In (b) is also depicted the nano-thick oxide film (230 – 250 nm) formed during bio-functionalization treatments.

6.3.2. Tribo-electrochemical behavior of TiO_2 nanotubular films

6.3.2.1. Electrochemical behavior before, during and after sliding

The evolution of the open circuit potential (OCP) before, during and after reciprocating sliding tests is shown in Fig. 6.3a. Before sliding Ti, NT and NT-Ca/P/Zn samples were immersed in artificial saliva (AS) and the OCP was recorded until stabilization. After the period of stabilization and before mechanical solicitations, the OCP of non-treated and Ti treated samples stabilized at different values, revealing their different tendencies to corrosion. As observed in Fig. 6.3a, NT-Ca/P/Zn samples display the highest OCP values (0.13 V *vs.* SCE) and so the lowest tendency to corrode, followed by NT (-0.15 V *vs.* SCE) and Ti smooth (-0.4 V *vs.* SCE) samples. The higher OCP values noticed for anodized Ti samples might be related with the presence of protective TiO_2 nanotubular films in their surfaces. The lower tendency to corrosion of TiO_2 nanotubes compared to Ti, has been already reported in previous studies [54, 55]. The improved electrochemical behavior observed for TiO_2 nanotubes after bio-functionalization processes maybe ascribed to the protective nano-thick oxide film formed at the interface region, as it will be further on discussed in more detail. This trend is kept during the whole duration of sliding and also afterwards.

As soon as the mechanical solicitations start on Ti smooth samples a fast and significant potential drop is observed from -0.4 V *vs.* SCE down to approximately -0.8 V *vs.* SCE, indicating the quick disruption and/or removal of the TiO_2 native layer (depassivation) due to the rubbing action of the alumina counterbody [9]. Once Ti oxide film is mechanically depassivated, the bare Ti surface becomes in contact with fresh electrolyte and thus exposed to its corrosive effects, which causes a lowering in the OCP, whose final value is dependent on the surface ratio of passive-to-active material [56]. Small variations in the OCP values are observed during the whole duration of rubbing action, due to the successive depassivation/repassivation phenomena taking place in between mechanical contact events in the wear track. This depassivation/repassivation behavior of Ti immersed in AS was already reported by Souza *et al.* [13]. At the time sliding is finished, the OCP immediately evolves to higher values due to the progressive re-growth of the passive film (repassivation) in the wear track.

As soon as NT samples are submitted to rubbing action (Fig. 6.3a – red curve) the OCP is maintained stable for approximately 100 s and then a monotonic decrease takes place during the whole duration of sliding, reaching the lowest value of -0.3 V *vs.* SCE. This behavior suggests that during the first moments of sliding the TiO_2 nanotubes were able to withstand the mechanical action and protect the Ti substrate against corrosion. As soon as the mechanical interaction is stopped the OCP progressively and slowly evolves to higher values, revealing a gradual repassivation of the wear track. It is evident that after the period of stabilization, the

OCP of NT samples reaches a lower value than the one initially recorded before sliding. This indicates that the electrochemical features in the worn area were changed after mechanical solicitations.

For NT-Ca/P/Zn samples a distinct behavior is observed compared to Ti and NT samples. As soon as the sliding starts the OCP drops and, immediately after, it goes back to noble values reaching a steady state for approximately 1000 s. After this plateau the OCP goes down until approximately -0.1 V and afterwards, it slightly evolves to higher values until the rubbing action is stopped. Once it is finished an uninterrupted repassivation occurs and at the end, the OCP reaches a stable and similar value to the one attained during the first plateau observed during the first 1000 s of sliding. For a better understanding of this behavior, additional reciprocating sliding tests were carried out for NT and NT-Ca/P/Zn samples for a shorter sliding period of 300 s. The OCP evolutions before, during and after the sliding tests carried out at this condition are depicted in Fig. 6.3b.

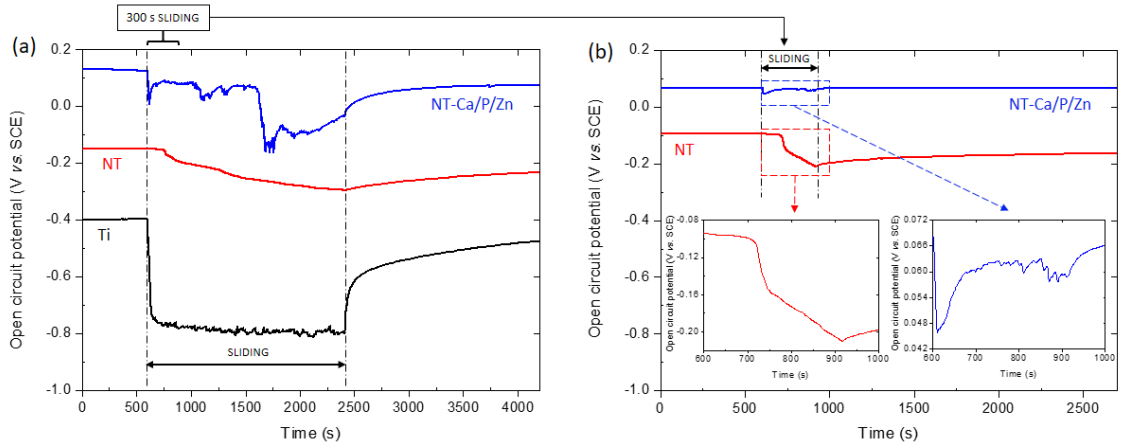

Fig. 6.3. Evolution of the open circuit potential (OCP) before, during and after reciprocating sliding tests in Ti, NT and NT-Ca/P/Zn samples during (a) 1800 s and (b) 300 s. The tribo-electrochemical experiments were performed in AS at a sliding frequency of 1 Hz, a load of 1N and a displacement of 650 µm.

Considering NT samples, as soon as the sliding starts no significant potential variation is detected during approximately 100 s, as previously observed. After this period, the OCP drops gradually down until the end of rubbing action, as can be seen in more detail in the inset graph in Fig. 6.3b (red curve). Once the sliding is stopped the OCP tends to slightly increase and stabilize in a lower value than the one reached before sliding. This behavior demonstrates that a short period of mechanical solicitations on NT surfaces is enough to modify the electrochemical features of the worn area. A distinctive behavior is observed for NT-Ca/P/Zn surfaces. As depicted in more detail in the inset graph in Fig. 6.3b (blue curve), the mechanical solicitations leads to a decrease in the OCP followed by a fast recovery to higher values, after which a steady is reached. As the mechanical solicitations are stopped, the OCP goes back to the level before

sliding, suggesting a complete recovery of the electrochemical properties of the film by repassivation in the wear track.

The evolution of the repassivation potential with time (repassivation kinetics) was calculated 300 s after the rubbing process was stopped, in accordance with the model reported by Hanawa *et al.* [57]. The repassivation kinetics was calculated using the following equation:

$$\Delta V = k_1 * log(t) + k_2 \quad (2)$$

where ΔV is the potential variation, t is the time after interrupting the sliding, k_1 represents the rate of repassivation and k_2 is a constant. These parameters were determined for sliding tests carried out for 1800 s, by fitting measured values to the equation 2. The repassivation kinetics is significantly higher ($p < 0.05$) for NT-Ca/P/Zn samples (0.046 ± 0.011 V/s) compared to NT samples (0.007 ± 0.002 V/s), which is in accordance with the significantly higher increase in the OCP after the end of sliding tests for bio-functionalized nanotubes (Fig. 6.3a – blue curve). As stated by Wood [15], the ability of a film to repassify quickly after its mechanical damage, is the key to being able to reduce the dissolution losses during wear-corrosion. As regards the repassivation rate of Ti samples (0.125 ± 0.01 V/s), it is significantly higher ($p < 0.001$) compared to both nanotubular samples.

6.3.2.2. Coefficient of friction evolution during sliding

The coefficient of friction (COF) evolution during sliding tests was recorded together with OCP and is shown in Fig. 6.4. For Ti smooth samples the COF was maintained relatively constant throughout the whole duration of sliding around a mean value of 0.5 (Fig. 6.4a). This is the expected value for the tribological pair Ti surface/alumina ball, as reported in previous studies [13, 58]. Some oscillations are observed in the COF measured during sliding, which may be ascribed to the release of wear particles in the contact region (third body particles), with part of them being either accumulated or ejected out of the contact region as sliding keeps on [9, 13].

Regarding NT samples, a short running-in-period is observed during the first 100 s, which is related with the period during which the OCP is maintained stable (Fig. 6.4b). Afterwards, as long as the OCP progressively decreases, the COF is kept stable around a mean value of 0.65. However, approximately 600 s before the sliding is finished, the COF tends to slightly decrease to values near 0.6. On the NT-Ca/P/Zn samples no differences in the COF are noticed during the OCP plateau achieved in the first 1000 s of sliding, along which the values are kept constant around 0.75 (Fig. 6.4c). However, the decrease in the OCP values after this period, is accompanied by a slight decrease in the COF from 0.75 down to 0.70. These COF values indicate the presence of Ti oxide film in the worn area, as they are characteristic of the tribological pair

Ti oxide/alumina. Similar steady state COF values comprised between 0.6 – 0.8 were reported for reciprocating sliding tests carried out against alumina ball on anodized Ti samples [48, 49, 58].

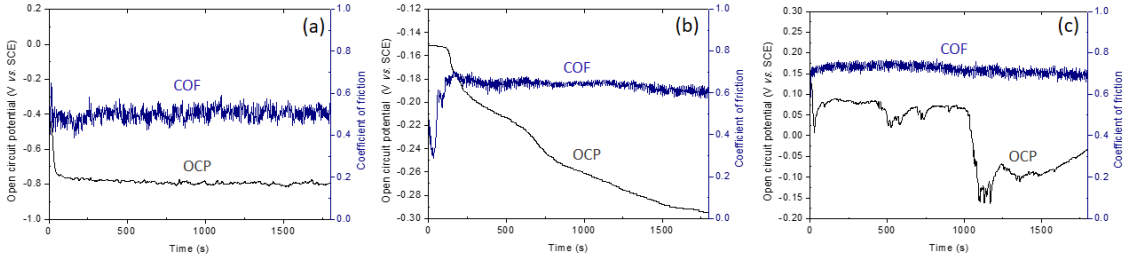

Fig. 6.4. Evolution of the open circuit potential (OCP) and the coefficient of friction (COF) during reciprocating sliding tests in (a) Ti, (b) NT and (c) NT-Ca/P/Zn samples during 1800 s. The tribo-electrochemical experiments were carried out in AS at a sliding frequency of 1 Hz, a load of 1N and a displacement of 650 µm.

6.3.2.3. Characterization of the wear tracks

The SEM micrographs representative of the wear tracks resulting from tribo-electrochemical tests are shown for Ti, NT and NT-Ca/P/Zn samples in Fig. 6.5a, b and c, respectively. The SEM images are shown both in secondary electrons (SE) and backscattered electrons (BSE) imaging modes, for a better understanding of the topographical and elemental features of the worn areas. The intensity of the BSE signal is related with the atomic number of the elements present in the sample since as higher the atomic number is, stronger the BSE signal. A region characterized by high atomic number elements is traduced in a brighter image and so, BSE images may provide important information on the elemental distribution along the wear tracks, with darker regions being related to the most oxidized areas (e.g. Ti oxides) once O has a lower atomic number than Ti.

The wear track morphology of Ti samples is shown in Fig. 6.5a, which presents curved borders, similar to the wear track morphology previously observed by Marques *et al.* [59] after reciprocating sliding tests on Ti immersed in AS with an alumina sphere. In Fig. 6.5b is clearly shown the irregular shape of the wear track of NT compared to Ti samples, as a result of nanotube film detachment from the Ti substrate. From BSE image, it is observed that a large part of the film was detached from the periphery of the contact area, since the brighter areas are correspondent to Ti substrate. This is an indicator of the poor adhesion of TiO_2 nanotubes to Ti. In the central area of this wear track, which corresponds to the sliding contact area, it is observed a darker region probably associated to wear debris resulting from film degradation, which have become entrapped and compacted generating a tribolayer. As observed in Fig. 6.5c the wear track on NT-Ca/P/Zn samples present huge differences compared to the one on NT samples. This wear track presents a completely different shape, with no signs of film detachment

on its periphery. From BSE image it is observed that the film has been removed from the central part of the wear track (brighter areas), however, a large area is still protected with film. This is an indicator that bio-functionalized nanotubes display an improved ability to withstand cyclic mechanical solicitations avoiding film detachment, probably due to the improved adhesion strength of bio-functionalized TiO_2 nanotubes to the Ti substrate. The higher mechanical destruction of NT samples is emphasized by their wear track length (1348 ± 37.5 µm), which is significantly higher ($p < 0.001$) compared to the maximum length measured on Ti (894.4 ± 62.8 µm) and NT-Ca/P/Zn (842 ± 37.4 µm) wear tracks.

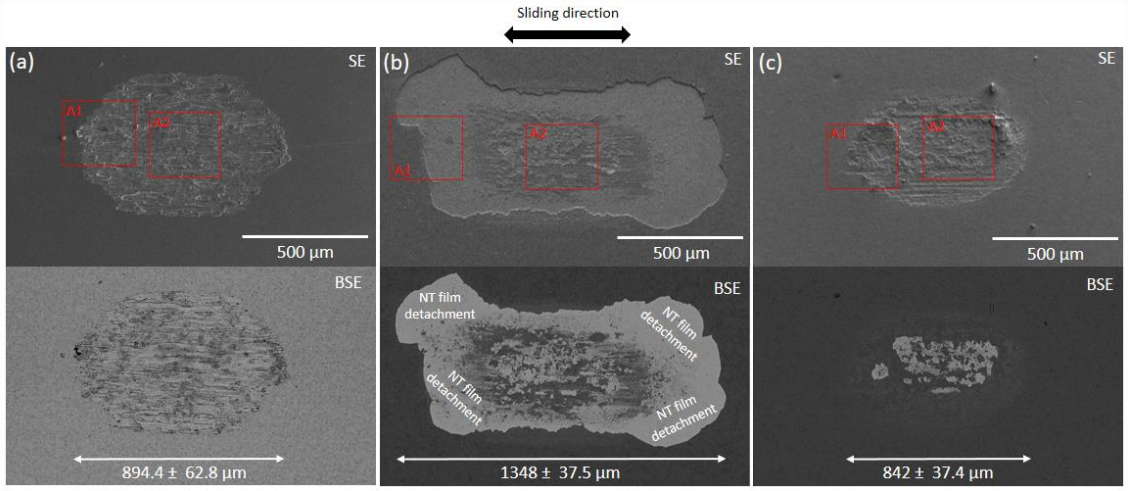

Fig. 6.5. SE/BSE SEM micrographs of the wear tracks resulting from tribo-electrochemical tests in (a) Ti, (b) NT and (c) NT-Ca/P/Zn samples for 1800 s of sliding duration. The maximum wear tracks length is included in BSE images for all the groups. The tribo-electrochemical experiments were carried out in AS at a sliding frequency of 1 Hz, a load of 1N and a displacement of 650 µm.

Higher magnification SEM images were took in the border (A1) and in the central region (A2) of the wear tracks, as indicated by the inset red squares in Fig. 6.5a, b and c. These images are shown in Fig. 6.6. Regarding Ti samples (Fig. 6.6a and b), ploughing lines aligned in the direction of the sliding movement are observed probably resulting from third body particles entrapped in the contact region leading to a predominant abrasive wear mechanism. Furthermore, extensive plastic surface deformation is observed along the wear track resulting from the high and continuous contact pressure applied on the surface during rubbing with the harder ceramic counterbody [59], with maximum Hertzian contact pressure being estimated as 400 MPa.

As observed in Fig. 6.6c, the irregular border of the wear track of NT samples shows clear signs of film detachment. The presence of cracks are identified in the film outside the worn area, which might suggest film degradation by fatigue wear and film delamination. In the middle part of the worn area (Fig. 6.6d) severe plastic deformation and ploughing lines are observed in

parallel to the direction of the counterbody movement showing evidences of abrasion. The wear debris coming out from film detachment may either act as abrasive bodies or get pressed between the two sliding bodies forming a compacted oxide layer between each other, as observed in Fig. 6.6d. As regards NT-Ca/P/Zn samples, abrasive wear marks are observed in SE image shown in Fig. 6.5c, along with plastic deformation of the nanotubular film (Fig. 6.6e and f). No signs of film detachment in the periphery of the wear track are observed, together with the absence of film cracking. For all the samples, mechanical wear also occurred by adhesion phenomena, through material transfer from the materials surface to the alumina ball, as observed under naked eyes after sliding tests. Wear of anodized Ti samples by abrasion and adhesion mechanisms have been previously identified in other studies [14, 59, 60].

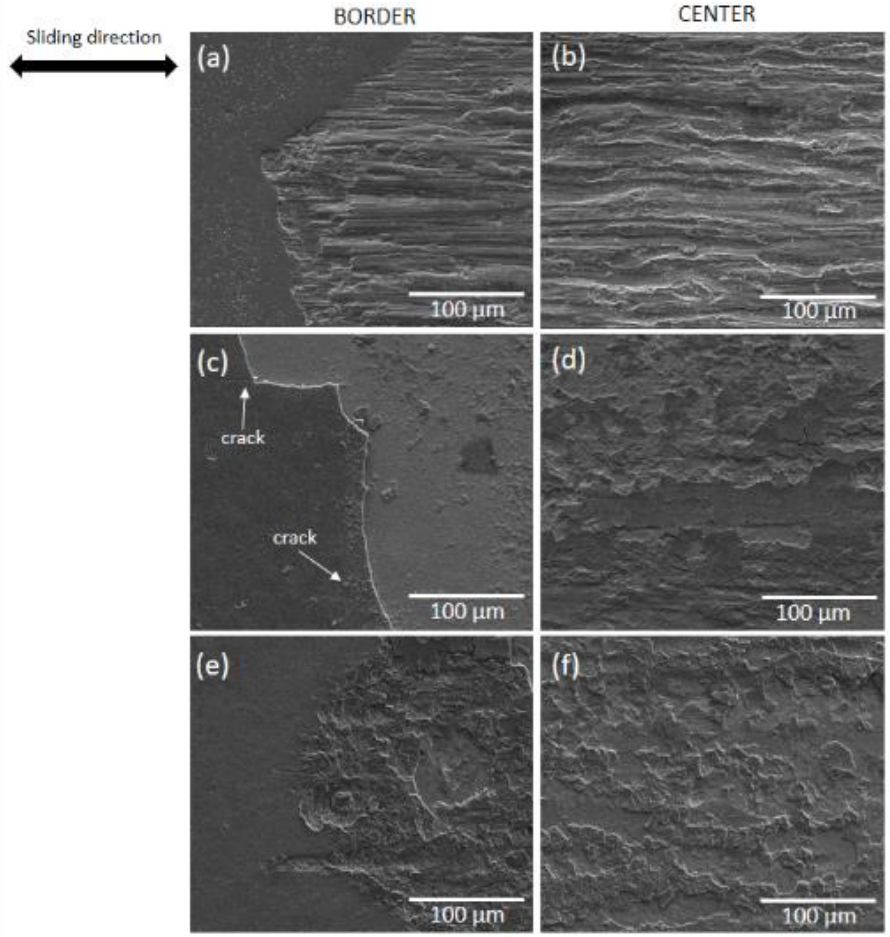

Fig. 6.6. SE SEM micrographs of the wear tracks of (a and b) Ti; (c and d) NT; (e and f) NT-Ca/P/Zn samples in the border and central regions. These are higher magnification images of the areas highlighted by the inset red squares in Fig. 6.5, named as A1 (border) and A2 (center). The tribo-electrochemical experiments were carried out in AS for 1800 s at a sliding frequency of 1 Hz, a load of 1N and a displacement of 650 µm.

Detailed SEM micrographs in the border and central regions of the wear tracks are shown in Fig. 6.7 for NT and NT-Ca/P/Zn samples. From BSE images shown in Fig. 6.7a is clear the entire detachment of TiO_2 nanotubes from the periphery of the sliding contact area. In the central

region of the wear track (Fig. 6.7b) it is observed part of the compacted oxide film (darker region) and the Ti substrate in the underlying plan (brighter region). From higher magnification images took in the border of the wear track of NT-Ca/P/Zn samples (Fig. 6.7c) is observed that the film is organized in different layers, which are structured in different plans. No signs of complete detachment of the film is found in this region, and interestingly, it is observed that the nanotubes still maintain their integrity in the subsurface plans (inset image in Fig. 6.7c). In the uppermost part of the film it seems that the wear debris became entrapped in the open pores of the nanotubes filling them up and, in some cases, covering the nanoporous structure. The wear track in the central region (Fig. 6.7d) presents similar characteristics with nanotube structures obstructed in the outermost part of the film, and remaining undamaged in the underlying plans (inset image in Fig. 6.7d). From BSE image it is evident that the nanotubular film detached from specific areas, as highlighted in the figure.

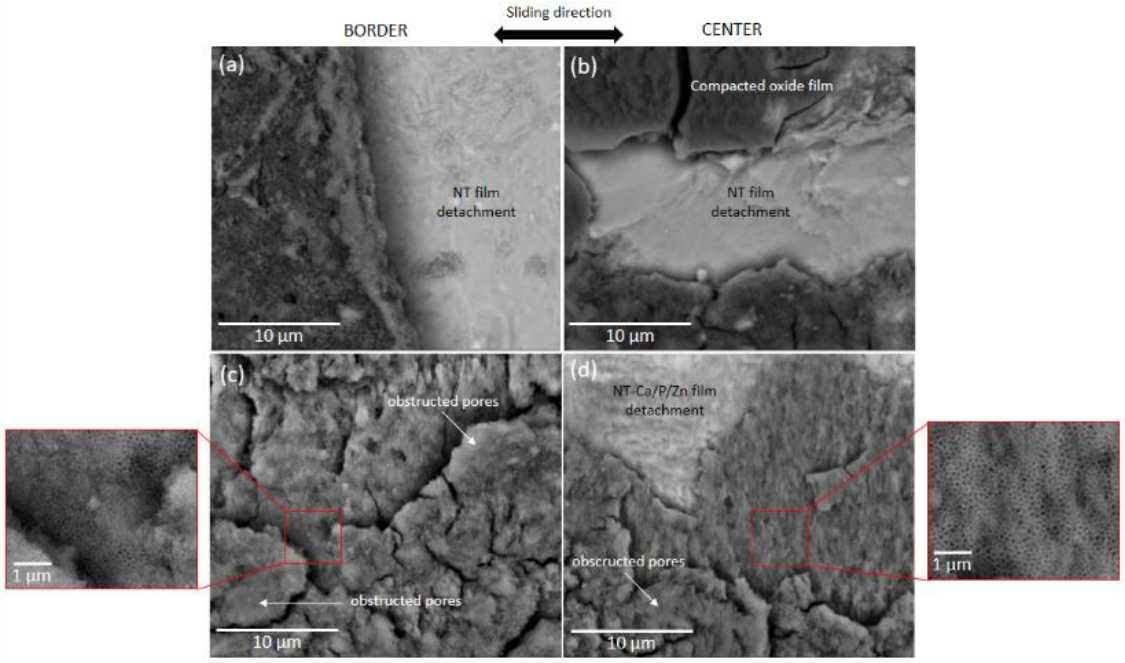

Fig. 6.7. BSE SEM micrographs of the wear tracks of (a and b) NT; (c and d) NT-Ca/P/Zn samples in the border and central regions. The inset images in (c) and (d) show that TiO_2 nanotubes survived both in the border and central regions of the worn NT-Ca/P/Zn samples. The tribo-electrochemical experiments were carried out in AS for 1800 s at a sliding frequency of 1 Hz, a load of 1N and a displacement of 650 µm.

The elemental composition of the wear tracks was investigated. EDS spectra were acquired from two different regions, the less oxidized (brighter areas – A1) and the most oxidized (darker areas – A2), as depicted in Fig. 6.8a and b for NT and NT-Ca/P/Zn wear tracks, respectively. From Fig. 6.8a it is confirmed both the presence of Ti in the brighter areas and the presence of Ti oxide in the darker ones. Elements present in the electrolyte such as P, potassium (K) and Ca were also detected in the oxidized regions. The same observations were found for

NT-Ca/P/Zn wear tracks. In this case, the detection of Ca and P elements may be also related with the composition of NT-Ca/P/Zn films.

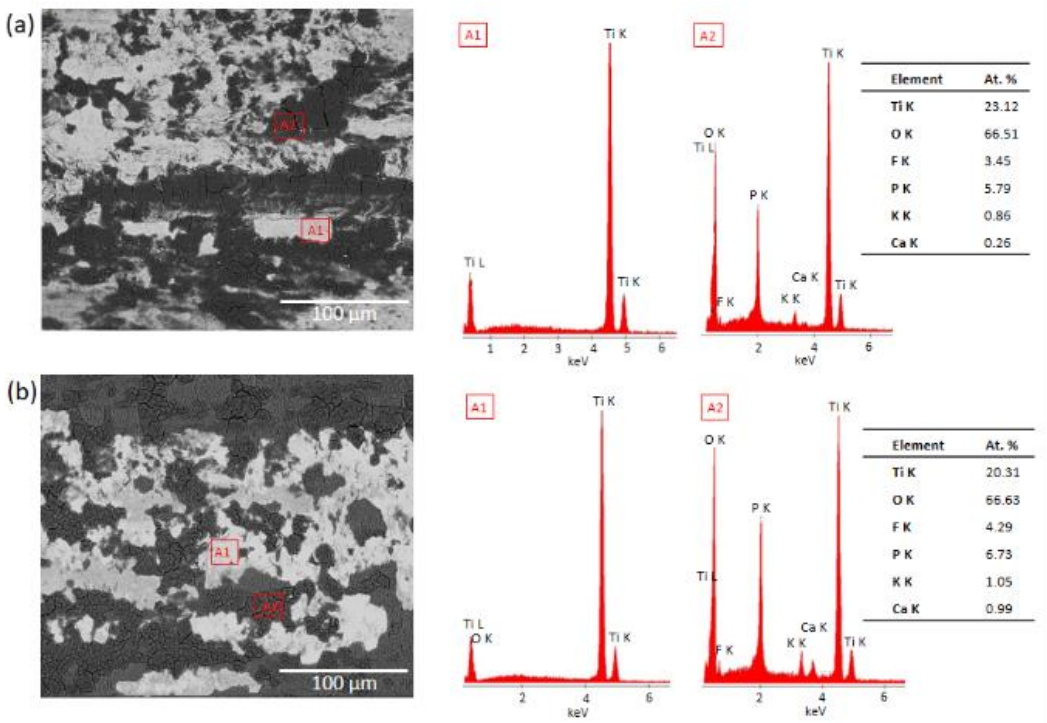

Fig. 6.8. BSE SEM micrographs in the central region of the wear tracks of (a) NT and (b) NT-Ca/P/Zn surfaces. The EDS spectra acquired from the inset squares (A1 and A2) are shown for both groups, together with the description of the chemical elements found and their atomic percentages (At. %). The tribo-electrochemical experiments were carried out in AS for 1800 s at a sliding frequency of 1 Hz, a load of 1N and a displacement of 650 µm.

In Fig. 6.9a and b the wear tracks of NT and NT-Ca/P/Zn samples resulting from 300 s sliding tests are shown, respectively. After 300 s of mechanical solicitations, the non-functionalized TiO_2 nanotubes detached from the contact region and neighboring areas, with part of the oxide film remaining in the central region of the wear track, as depicted in SE and BSE images in Fig. 6.9c, which are amplified from the inset red square in Fig. 6.9a. Scratches/grooves along with severe plastic deformation are visible inside the wear track aligned with the pin movement. From Fig. 6.9b it can be seen that bio-functionalized TiO_2 nanotubes present significantly lower mechanical damage with no signs of film detachment, as evident from higher magnification images shown in Fig. 6.9d.

6.3.2.4. Wear volume and wear track profiles

Wear volume measurements were carried out based on 2D profiles extracted from the central region of the wear tracks by 2D profilometry. The wear volumes calculated for all the groups of samples submitted to sliding tests during 1800 s and 300 s are shown in Fig. 6.10. The wear volume estimated from wear scar dimensions is the sum of wear loss due to corrosion and

the wear loss due to sliding wear [60]. After tribo-electrochemical tests carried out for 1800 s, the wear volume of NT samples was 2.9 ± 0.4 x 10^6 µm^3, significantly higher compared to Ti (1.9 ± 0.3 x 10^6 µm^3) and NT-Ca/P/Zn (1.2 ± 0.2 x 10^6 µm^3) samples. Similar results were acquired for sliding tests performed during 300 s, with NT samples presenting a significantly higher wear volume (3.2 ± 0.8 x 10^6 µm^3) compared to NT-Ca/P/Zn samples (0.5 ± 0.4 x 10^6 µm^3).

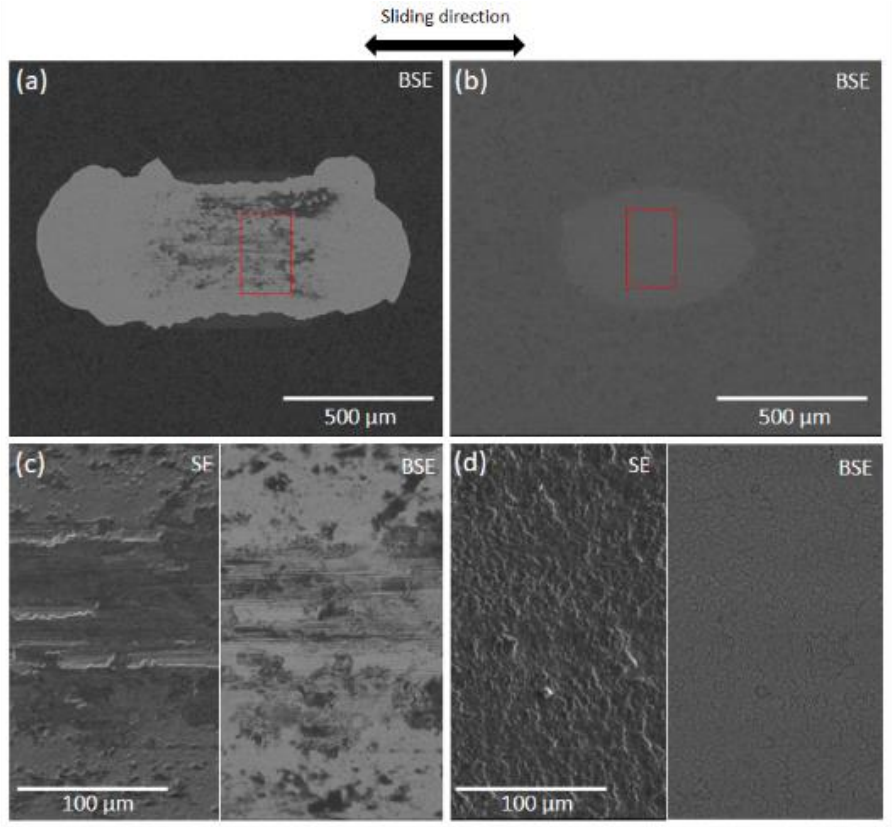

Fig. 6.9. BSE SEM micrographs of the wear tracks of (a) NT and (b) NT-Ca/P/Zn samples after 300 s of sliding. Higher magnification SE/BSE SEM images were obtained from the inset red squares and are shown in (c) for NT and in (d) for NT-Ca/P/Zn surfaces. The tribo-electrochemical experiments were carried out in AS at a sliding frequency of 1 Hz, a load of 1N and a displacement of 650 µm.

The 2D profiles representative of the wear tracks remaining on Ti, NT and NT-Ca/P/Zn samples after 1800 s sliding tests are depicted in Fig. 6.11a, while in Fig. 6.11b are shown the wear tracks profiles on NT and NT-Ca/P/Zn samples submitted to 300 s sliding tests. The maximum depth reached in the wear tracks is depicted in Table 6.1, jointly with the film thickness values for each different group of samples. The wear scar depth of Ti samples achieved a maximum value around 10.7 ± 0.4 µm, which is significantly higher than the ones measured on NT (7.9 ± 0.9 µm) and NT-Ca/P/Zn (7.1 ± 0.4 µm) samples. The maximum wear track depths measured on nanotubular samples are in the same order of magnitude of the films thickness (Table 6.1), indicating that in both cases the films were fully detached from the substrate. For sliding tests carried out for 300 s, the maximum depth of the wear track on NT samples (8.3 ±

1.2 µm) is significantly higher compared to NT-Ca/P/Zn samples (4.1 ± 0.1 µm) as clearly observed in Fig. 6.11b, which is in accordance with the significant lower wear volume measured for bio-functionalized samples.

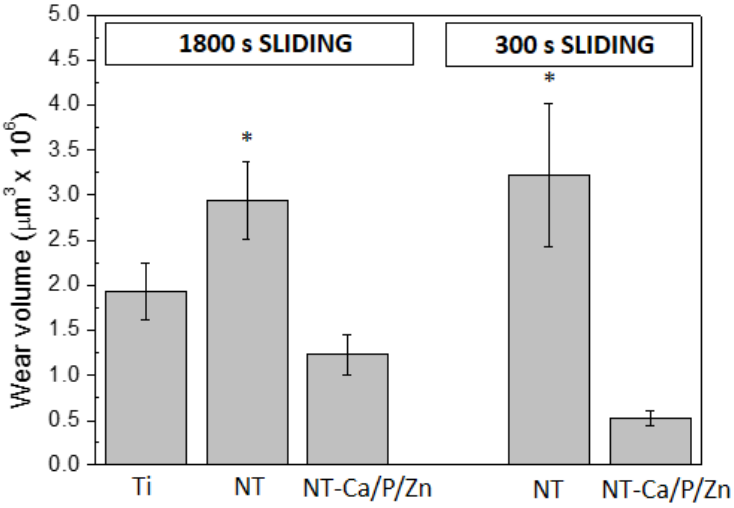

Fig. 6.10. Wear volume measurements after tribo-electrochemical tests carried out for 1800 s and 300 s sliding tests. For 1800 s SLIDING: (*) significantly different from Ti and NT-Ca/P/Zn, $p < 0.05$; for 300 s SLIDING: (*) significantly different from NT-Ca/P/Zn, $p < 0.001$. The tribo-electrochemical experiments were carried out in AS at a sliding frequency of 1 Hz, a load of 1N and a displacement of 650 µm.

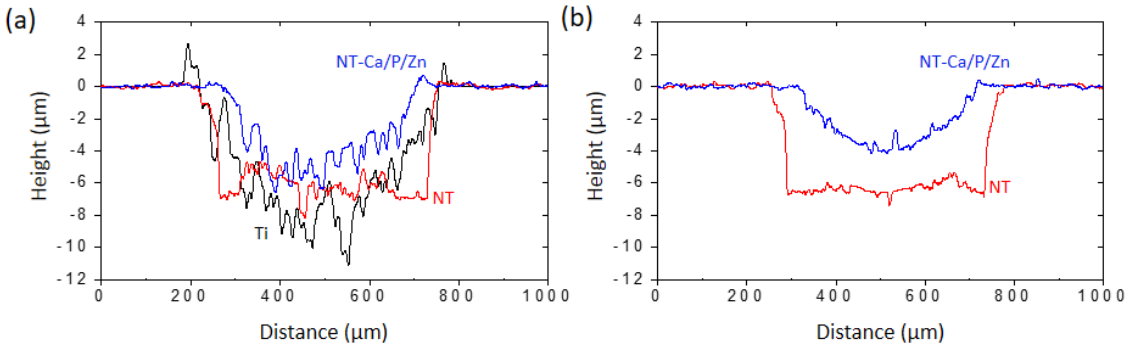

Fig. 6.11. 2D profiles obtained by profilometry in the central region of the wear tracks of Ti, NT and NT-Ca/P/Zn samples after sliding tests carried out for (a) 1800 and (b) 300 s. The tribo-electrochemical experiments were carried out in AS at a sliding frequency of 1 Hz, a load of 1N and a displacement of 650 µm.

Table 6.1. Maximum depth of the wear tracks on Ti, NT and NT-Ca/P/Zn samples after 1800 s and 300 s sliding tests. The thickness of NT and NT-Ca/P/Zn films is also presented.

Group	Maximum wear track depth (µm)		Film thickness (µm)
	1800 s SLIDING	300 s SLIDING	
Ti	10.7 ± 0.4	-	-
NT	7.9 ± 0.9 *	8.3 ± 1.2	6.1 ± 0.1
NT-Ca/P/Zn	7.1 ± 0.4 *	4.1 ± 0.1 #	4.6 ± 0.1

(*) significantly different from Ti, $p < 0.05$; (#) significantly different from NT, $p < 0.05$.

6.4. Discussion

6.4.1. Surface and interfacial features of TiO_2 nanotubular films

TiO_2 nanotubes were grown from Ti smooth surfaces presenting a bone-inspired morphology at a nanoscale (Fig. 6.1b). The well-ordered structure of the nanoarrays was achieved by two-step anodization of Ti in an organic electrolyte containing fluoride (F^-) ions. This methodology allows the synthesis of well-aligned nanotubular films with a specific morphology, which is preset by the first anodization step through the production of hemispherical footprints on Ti smooth surfaces. The mechanisms underlying the nanotube formation by two-step anodization in a fluoride containing electrolyte are well documented in literature [61-64]. The methodology to acquire the specific surface morphology depicted in Fig. 6.1b is reported in detail in a previous study [46], in which the mechanisms underlying nanotube formation are addressed and established a correlation with the final surface morphology achieved.

Beyond the morphology, the surface chemistry is also known to play a crucial role on cellular functions [65]. The doping of TiO_2 nanotubes with Ca and P elements natively present in bone, together with Zn, which is known to induce osteogenic differentiation and provide antibacterial activity [45], was successfully achieved by reverse polarization and anodization treatments of NT samples in a Ca/P/Zn-based electrolyte. The bio-functionalization treatments were applied without compromise the surface morphology previously achieved, as shown in Fig. 6.1c. Dissimilar features are found at the Ti/TiO_2 nanotubes interface before and after bio-functionalization treatments, as revealed in Fig. 6.2a and b, respectively. Anodization of TiO_2 nanotubes induces to the growth of a nano-thick oxide film (230 – 250 nm) at the interface region, which appears to improve the adhesion of the nanotubular film to Ti substrate. The features of Ti/TiO_2 nanotubes interface may influence the biomechanical stability of the film and thus the ability to withstand cyclic mechanical solicitations, which may compromise its long term success for osseointegrated implant applications. Beyond the wide range of studies reported in literature showing the promising features of TiO_2 nanotubes, most of them are concerned with their impact on biological performances. No information regarding the degradation behavior of the nanotubular systems by the simultaneous action of wear and corrosion is reported, which is a subject of paramount importance. The understanding of the tribo-electrochemical behavior of TiO_2 nanotubes before and after bio-functionalization treatments is the main aim of this work, and is addressed in the following section.

6.4.2. Tribo-electrochemical degradation mechanisms of TiO_2 nanotubes before and after bio-functionalization treatments

After immersion of Ti, NT and NT-Ca/P/Zn samples in AS, and before sliding tests, their OCP stabilized at different values, reflecting different surface activation stages (Fig. 6.3a). As reported by Ponthiaux *et al.* [16] the OCP provides information on the electrochemical state of a material, reflecting its active or passive state. An increase in the OCP (anodic shift) indicates a more passive state and on the contrary, a decrease (cathodic shift) indicates a more active state. After the period of OCP stabilization, a dense and passive oxide film of a few nanometers is expected to be present on Ti smooth surfaces [54, 66], while micron-length TiO_2 nanotubular films exist in both anodized Ti surfaces. The higher OCP achieved for NT and NT-Ca/P/Zn samples (Fig. 6.3a) is probably associated to the physical barrier created by TiO_2 nanotubular films with insulating properties, providing corrosion protection to the Ti substrate by hindering current flow. The less active state of TiO_2 nanotubes in different simulating body fluids has been reported in previous works [54, 55, 67, 68].

The fast and effective passivation behavior of NT samples was demonstrated before by potentiodynamic polarization studies in AS [46]. Demetrescu *et al.* [67] concluded that the low corrosion current density obtained for the TiO_2 nanotube samples tested in AS, was correlated to the formation of a strong passive barrier layer. Furthermore, Yu *et al.* [54, 55] demonstrated that TiO_2 nanotubes display better corrosion resistance compared to smooth Ti, which was also ascribed to the presence of a TiO_2 barrier layer. Thus, the less active state achieved for nanotubular samples immersed in AS, is also probably related to the formation of a passive oxide film which protects Ti substrate against corrosion. Interestingly, significantly higher OCP values were achieved after bio-functionalization treatments. Bio-functionalized TiO_2 nanotubes, beyond the fast and effective passivation ability, are also expected to display a significantly lower passive current in AS compared to conventional nanotubes [46], most likely due to the presence of a nano-thick oxide film at the interface region (Fig. 6.2b). The oxide film grown during bio-functionalization treatments might play a main role in corrosion, by restricting the movement of metal ions from the metallic surface to the surrounding medium [46].

Both groups of anodized Ti surfaces decorated with TiO_2 nanotubes present significantly higher OCP values before, during and after reciprocating sliding tests compared to Ti surfaces (Fig. 6.3a). It is known that the OCP recorded during sliding tests is a mixed potential reflecting the state of the unworn material and the state of the material in the wear track [16]. Garcia *et al.* [66] proposed the concept of active wear track area to investigate the wear-corrosion mechanisms of passive materials under sliding conditions. The active wear track area is defined

as the part of the surface area that loses its passive film under mechanical loading, becoming activated electrochemically and suffering corrosion.

At the time the alumina ball is loaded on NT samples and the sliding starts, the OCP keeps stable for approximately 100 s (Fig. 6.3a and b – red curves). This behavior indicates that the electrochemical passive state of the material in the wear track keeps unaltered. During this time the COF values are characteristic of alumina/Ti oxide tribological pair (Fig. 6.4b), thus indicating that the alumina ball is sliding against the TiO_2 nanotubular film. After this period of sliding, the OCP drops down (cathodic shift) suggesting that a more active state is achieved in the wear track, probably related to the detachment of the nanotubular film and the exposure of the metallic substrate to fresh electrolyte promoting corrosion. This may initiate a galvanic coupling between the passive surface and the bare Ti substrate, with consequent local dissolution of Ti [16]. For a better understanding of the OCP evolution during tribocorrosion, Vieira *et al.* [69] emphasized two different situations may happen: 1) the establishment of a galvanic coupling between the completely depassivated wear track and the surrounding passive area, or 2) a galvanic coupling within the wear track between depassivated and still passive areas [69]. Regarding NT samples the galvanic coupling is probably established according to the second case. As the sliding goes on the OCP slowly decreases indicating a gradual depassivation in the wear track area. In fact, after 1800 s of sliding the nanotubular film has been completely detached from the Ti substrate in the sliding contact area and from its periphery, as shown in Fig. 6.5b. As observed in Fig. 6.9a, the full detachment of the film occurred during the first 300 s of sliding.

The morphology of the wear debris resulting from tribo-electrochemical degradation of conventional TiO_2 nanotubes is shown in Fig. 6.12a. From these SEM micrographs it is clearly observed that the main mechanisms assisting TiO_2 nanotubular film degradation are tube smashing and densification in the top region, accompanied by delamination and full detachment of the nanotubes, through cracks formation and propagation from the surface to subsurface regions of the film. These mechanisms are schematically illustrated in Fig. 6.13a. It is clearly observed that most of the wear debris are either single or aggregated nanotubes, coming from nanotube film break in different parts along the film length, resulting in fragments of the tubes with variable dimensions. The densification of the nanotubes accompanied by wear and fracture was also previously observed by nanoindentation studies [36, 70]. Xu *et al.* [71] also studied the mechanical behavior of TiO_2 nanotube arrays by nanoindentation and observed that as the indentation depth increases the nanotubes break, interacting with neighboring nanotubes causing them to bend and fracture, with small fragments becoming compacted gradually, resulting in densification.

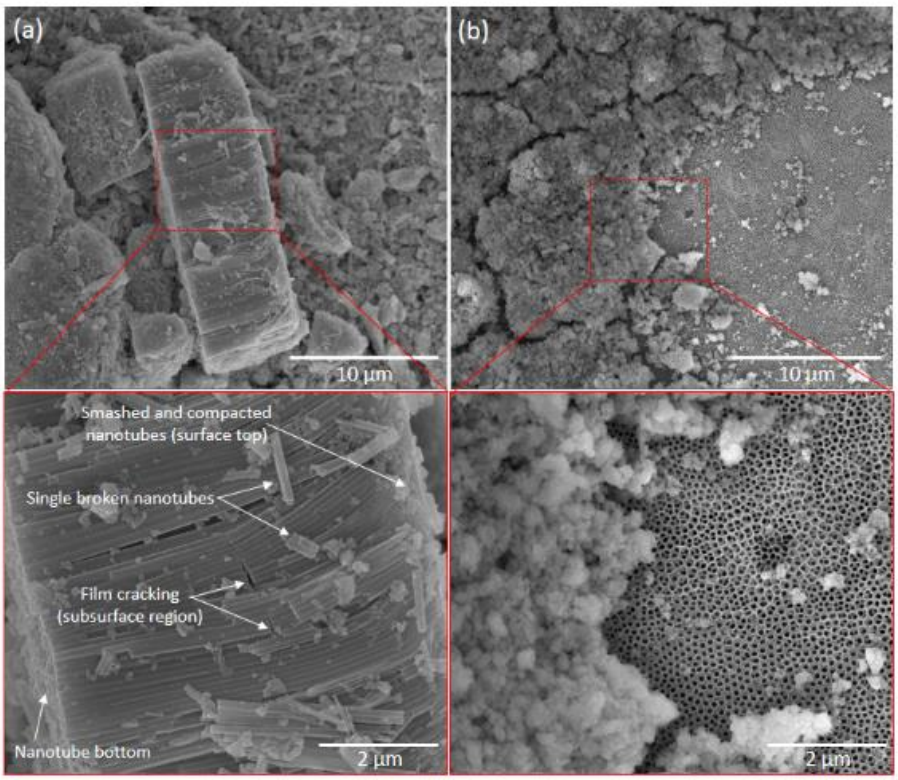

Fig. 6.12. SE SEM micrographs showing the wear debris morphology generated during tribo-electrochemical degradation of (a) NT and (b) NT-Ca/P/Zn samples.

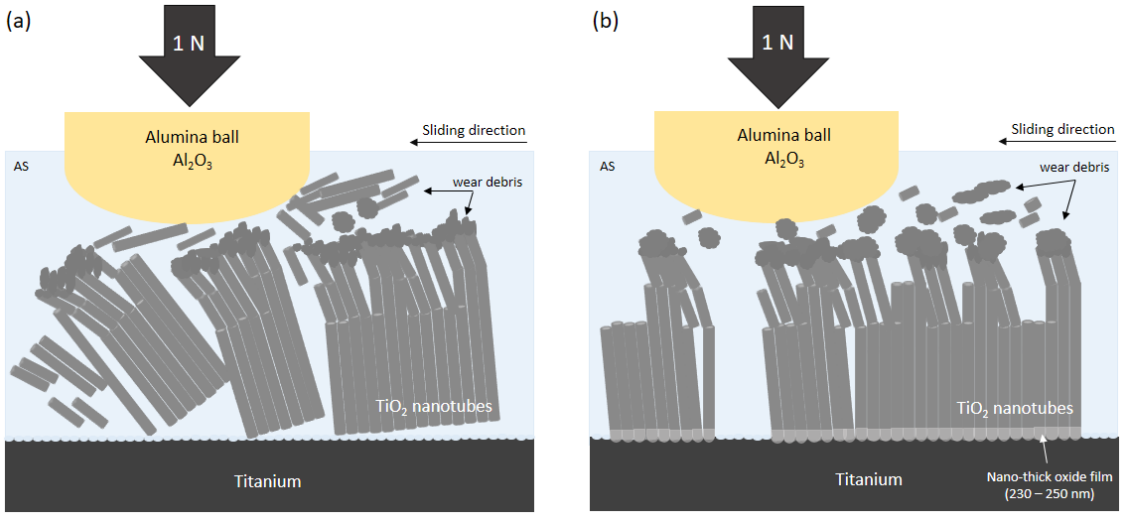

Fig. 6.13. Illustration of the tribo-electrochemical degradation mechanisms of TiO_2 nanotubes in (a) NT and (b) NT-Ca/P/Zn samples.

As a result of NT film detachment after 100 s of sliding, a large amount of film debris are released in the contact region, with part of them being either pushed out of the contact or becoming entrapped in it. As soon as the sliding goes on it is expected that the wear debris in the contact region are continuously exposed to mechanical and electrochemical solicitations,

and several actions are prone to take place simultaneously or sequentially interacting with each other in a complex way. One of them is the formation a compact oxide film in the central region of the wear track as a result of the continuous smashing/densification of the film debris, as observed after 1800 s (Fig. 6.5b, Fig. 6.6d and Fig. 6.7b) and 300 s (Fig. 6.9a and Fig 9c) sliding tests. The formation of this tribolayer may grant protection to the Ti substrate against corrosion and wear, and may explain both the COF and the gradual lowering of the OCP during sliding. A similar level of mechanical destruction of NT samples is observed after 300 s (Fig. 6.9a) and 1800 s (Fig. 6.5b) sliding tests. This suggests that after the catastrophic NT film degradation which takes place between 100 s – 300 s of sliding, the tribolayer formed in the contact region has the ability to protect the substrate against mechanical wear as long the sliding action takes place, as emphasized by the similar wear volumes measured after 300s and 1800 s sliding tests (Fig. 6.11). Simultaneously to tribolayer formation, it is expected that during sliding some of the debris are pushed against the nanotubular film which is surrounding the sliding contact region, along with the counterbody movement. This probably induces to cyclic compressive stresses, which may lead to the progressive structural damage of surface and subsurface regions of the film, with formation and propagation of cracks and consequent delamination. This reveals the poor adhesion strength of TiO_2 nanotubes to the Ti substrate and its brittleness. Because of the brittle nature of TiO_2 nanotubes, they probably elastically bend up to very small strain and consequently, they collapse [71]. Signs of fatigue wear are visible through cracks on the nanotubular film surface outside the wear track (Fig. 6.6c). It is noteworthy that within crack formation and propagation the electrolyte may penetrate into the substrate inducing corrosion, which may further contribute to film detachment.

As previously mentioned, the OCP measured during sliding is a mixed potential reflecting the intrinsic potentials of the materials in active and passive areas. This may explain the fact that beyond a large surface area of the Ti substrate is exposed to fresh electrolyte during sliding tests on NT samples, the minimum OCP achieved was around -0.3 V *vs.* SCE (Fig. 6.3a – red curve). Once the sliding is stopped the OCP evolves slightly to higher values and does not reach the initial OCP back, indicating that repassivation takes place at a rather limited oxidation rate. The electrochemical state of the material in the worn area was irreversibly modified as a consequence of sliding, with lower OCP values reflecting the more active electrochemical state of NT samples.

The tribo-electrochemical behavior of NT-Ca/P/Zn samples is significantly different compared to NT samples which may be both ascribed to the electrochemical and mechanical properties of the films as well to its adhesion strength to Ti substrate. After bio-functionalization treatments a nano-thick oxide film is formed at the interface of TiO_2 nanotubes (Fig. 6.2b)

providing corrosion protection to Ti [46]. In addition, this may contribute to the less active electrochemical state (noble OCP) that bio-functionalized TiO_2 nanotubes exhibit during the whole duration of sliding, this also suggests that the contribution of corrosion reactions on their tribo-electrochemical degradation behavior is lower compared to Ti and NT films. However, additional studies should be performed to confirm this assumption.

The chemical features of NT-Ca/P/Zn surfaces may also influence their OCP values. In this work X-ray photoelectron spectroscopy (XPS) studies were carried out, from which the presence of Zn was detected on these surfaces and mostly assigned to ZnO compounds (results not shown). From observation of potential-pH diagram of Zn it is known that zinc oxides and hydroxides are soluble in acid media, which is accompanied by the release of Zn^{2+} ions that in equilibrium conditions have a standard potential of -0.762 V/NHE (Zn^{2+}/Zn) [72]. As the pH of AS at 37 ^{o}C is 5.5, it is expected that once NT-Ca/P/Zn samples are immersed in solution, the ZnO compounds are dissolved with formation of Zn^{2+} ions. This may explain the OCP drop in the beginning of mechanical solicitations and the fluctuations (cathodic shifts) registered along the sliding tests (Fig. 6.3a and b – blue curves). Beyond Zn, NT-Ca/P/Zn samples are also composed of Ca and P. From literature it is known that the corrosion resistance of Ti in simulating body fluids (pH = 7.4, 37 ^{o}C) is enhanced after deposition of a calcium phosphate layer on its surface [73, 74]. Additionally, Alves *et al.* [58] studied the tribocorrosion behavior of anodic films produced in an electrolyte containing β-glycerophosphate and different concentrations of calcium acetate. The authors hypothesized that the reason for the improved tribocorrosion behavior of the anodic films, beyond the crystalline structure, could be the higher calcium content. Thus, it is believed that the Ca and P elements may have a beneficial effect on the tribo-electrochemical behavior of TiO_2 nanotubes, however, the underlying mechanisms are still unknown.

As soon as the mechanical solicitations starts, the OCP of NT-Ca/P/Zn samples drops and immediately after evolves to noble values reaching a steady state that is maintained during approximately 1000 s (Fig. 6.3a – blue curve). From sliding tests carried out for 300 s it is believed that the nanotubular film has not been fully detached out from the substrate during this first plateau, as suggested from SE and BSE images depicted in Fig. 6.9b and d. From wear track profiles shown in Fig. 6.11b it is confirmed the non-detachment of the film during the first 300 s of mechanical solicitations, since the maximum wear track depth is lower than the thickness of the film (Table 6.1) and significantly inferior to the maximum depth reached after 1800 s of sliding (Table 6.1). After 1000 s of sliding the OCP shifts down (cathodic shift) probably related to the detachment of the film with exposure of Ti substrate to the electrolyte, and thus achieving a more active state. As soon as the OCP decreases it is observed a slight decrease in the COF

values (Fig. 6.4c), which may be related with film detachment. Afterwards, the OCP slightly increases as long as the sliding keeps on, which might be related to the filling of the nanotubes with film debris, accompanied by their continuous smashing and compactness in the sliding track creating a kind of a compact oxide film blocking the passage of the electrolyte and protecting the Ti substrate from the corrosive attack. This behavior may also indicate the repassivation ability of these samples as long as the sliding occurs.

From Fig. 6.7c and d it is observed that after 1800 s of sliding, the nanotubular film is organized in different layers in the wear track, which are found in different plans. In the topmost part, the nanotubes are not visible probably as a consequence of the successive mechanical solicitations as the rubbing action goes on. In the central region are visible some parts from where the fully detachment of the film took place, together with others where the nanotubes still maintain their integrity with well-opened pores. This suggests that the degradation of the film occurs gradually and by layers probably by a cracking-assisted mechanism. As a consequence of cyclic and compressive stresses induced on the surface and subsurface regions of the film, the nanotubes may crush and be smashed from the top to the inner regions. Cracks are visible along the wear track which may induce to film delamination. On the contrary to NT samples, the film cracking is restricted to the contact region and no detachment occurs in the vicinity of the worn area.

The morphology of the wear debris observed after tribo- electrochemical degradation of bio-functionalized TiO_2 nanotubes is remarkable different compared to the one observed for non-functionalized nanotubes, as shown in Fig. 6.12b. Most of the wear debris present smaller dimensions and a non-defined morphology probably as a result of the mechanical/electrochemical solicitations at which were imposed for a longer period of time, as a consequence of the improved adhesion strength of the film and its resistance to detach as long as the sliding takes place. Contrarily to NT samples, the mechanical degradation of NT-Ca/P/Zn samples seems to occur gradually. The main mechanisms assisting the tribo-electrochemical degradation of bio-functionalized TiO_2 nanotubes may be summarized as smashing and densification in the top region, with gradual detachment of the film by layers, through cracks formation and propagation from the top to the inner regions of the film. These mechanisms are schematically illustrated in Fig. 6.13b. The results above discussed are in good agreement with the significantly lower wear volume measured for bio-functionalized nanotubes both after 300 s and 1800 s of sliding compared to conventional TiO_2 nanotubes (Fig. 6.10).

Finally it is noteworthy to highlight that on unloading, the OCP of NT-Ca/P/Zn samples immediately starts to increase and reaches, after some time, the OCP achieved during the first 1000 s of sliding (Fig. 6.3a – blue curve). On the other hand, if the sliding is finished after 300 s,

the OCP achieves the initial OCP back (Fig. 6.3b – blue curve). This suggests that if the nanotubular film is not completely detached during sliding, the material in the wear track has the ability of repassivation with the re-establishment of the initial surface passive state. However, once the nanotubular film peels off and comes out of the substrate, the passive state achieved in the first 1000 s of sliding is re-established instead of the initial one. This behavior shows the very strong repassivation ability of bio-functionalized nanotubes even when the nanotubular film is detached, suggesting that the higher OCP of these samples is related to the existence of the nano-thick oxide film at the interface.

As future work it would be of upmost important to investigate the mechanical properties of the TiO_2 nanotubes, before and after bio-functionalization. The information of the Young's modulus and hardness of the films must be addressed to understand their influence on the tribo-electrochemical degradation behavior of the films.

6.5. Conclusions

The tribo-electrochemical behavior of TiO_2 nanotubes before and after bio-functionalization treatments was investigated by reciprocating sliding tests carried out in artificial saliva. The tribo-electrochemical behavior of bio-functionalized TiO_2 nanotubes was significantly improved both from the electrochemical and the mechanical point of view. Hereafter follows the main outcomes of this study:

- The electrochemical stability of TiO_2 nanotubes is enhanced after bio-functionalization treatments, displaying a less active state during the whole duration of tribo-electrochemical tests.
- Bio-functionalized TiO_2 nanotubes display improved wear resistance, with the ability to withstand mechanical solicitations during 1000 s without fully film detachment.
- The improved tribo-electrochemical behavior of bio-functionalized nanotubes is granted by the nano-thick oxide film grown at Ti/TiO_2 nanotubes interface, which concedes electrochemical stability and improves the adhesion strength of the film to Ti substrate, resulting in a reduced wear volume loss.
- A first insight on the main degradation mechanisms of TiO_2 nanotubular films was proposed which relies on tube smashing and densification, accompanied by delamination and detachment of the tubes, through cracks formation and propagation from the surface to subsurface regions of the film.

This investigation provides, for the first time, new knowledge on the main degradation mechanisms of TiO_2 nanotubes before and after bio-functionalization treatments. The

methodology adopted for nanotubes functionalization, based on reverse polarization and anodization treatments, shows up as a very simple and effective way to create a multifunctional nano-thick oxide film at the interface region. This film has the ability to protect Ti substrate against corrosion and the simultaneous action of mechanical wear, by blocking the passage of current and enhancing the adhesion strength of the film to the substrate. This comes out as a very promising methodology to improve the long term biomechanical stability of TiO_2 nanotubes for osseointegrated implants applications.

Acknowledgements

This work was supported by FCT with the reference project UID/EEA/04436/2013 and by FEDER funds through the COMPETE 2020 – Programa Operacional Competitividade e Internacionalização (POCI) with the reference project POCI-01-0145-FEDER-006941.

The authors also acknowledge the financial support from FCT by the doctoral grant (Ref. SFRH/BD/88517/2012), CAPES (Proc. 99999.008666/2014-08), CNPq (Proc. 490761/2013-5) and UNESP. Also, the authors would like to thank LABNANO/CBPF (Brazilian Center for Research in Physics) for all the support in electron microscopy analyses. Tolou Shokuhfar is especially thankful to US National Science Foundation NSF-DMR CAREER award # 1564950.

References

[1] Niinomi M. Mechanical properties of biomedical titanium alloys, Materials Science and Engineering: A 243 (1998), 231-236.
[2] Oshida Y, Tuna EB, Aktören O, Gençay K. Dental implant systems, International journal of molecular sciences 11 (2010), 1580-1678.
[3] Demetrescu I, Pirvu C, Mitran V. Effect of nano-topographical features of Ti/TiO2 electrode surface on cell response and electrochemical stability in artificial saliva, Bioelectrochemistry 79 (2010), 122-129.
[4] Yao C, Slamovich EB, Webster TJ. Enhanced osteoblast functions on anodized titanium with nanotube-like structures, Journal of Biomedical Materials Research Part A 85 (2008), 157-166.
[5] Yang W-E, Hsu M-L, Lin M-C, Chen Z-H, Chen L-K, Huang H-H. Nano/submicron-scale TiO2 network on titanium surface for dental implant application, Journal of Alloys and Compounds 479 (2009), 642-647.
[6] Garcia-Alonso MC, Saldana L, Valles G, Gonzalez-Carrasco JL, Gonzalez-Cabrero J, Martinez ME, Gil-Garay E, Munuera L. In vitro corrosion behaviour and osteoblast response of thermally oxidised Ti6Al4V alloy, Biomaterials 24 (2003), 19-26.
[7] Johansson BI, Bergman B. Corrosion of titanium and amalgam couples: Effect of fluoride, area size, surface preparation and fabrication procedures, Dental Materials 11 (1995), 41-46.
[8] Manivasagam G, Dhinasekaran D, Rajamanickam A. Biomedical Implants: Corrosion and its Prevention - A Review, Recent Patents on Corrosion Science 2 (2010), 40-54.
[9] Vieira AC, Ribeiro AR, Rocha LA, Celis JP. Influence of pH and corrosion inhibitors on the tribocorrosion of titanium in artificial saliva, Wear 261 (2006), 994-1001.
[10] Ceschini L, Lanzoni E, Martini C, Prandstraller D, Sambogna G. Comparison of dry sliding friction and wear of Ti6Al4V alloy treated by plasma electrolytic oxidation and PVD coating, Wear 264 (2008), 86-95.
[11] Yerokhin AL, Leyland A, Matthews A. Kinetic aspects of aluminium titanate layer formation on titanium alloys by plasma electrolytic oxidation, Applied Surface Science 200 (2002), 172-184.
[12] Yetim AF. Investigation of wear behavior of titanium oxide films, produced by anodic oxidation, on commercially pure titanium in vacuum conditions, Surface and Coatings Technology 205 (2010), 1757-1763.
[13] Souza J, Barbosa S, Ariza E, Celis J-P, Rocha L. Simultaneous degradation by corrosion and wear of titanium in artificial saliva containing fluorides, Wear 292 (2012), 82-88.

[14] Oliveira FG, Ribeiro AR, Perez G, Archanjo BS, Gouvea CP, Araújo JR, Campos AP, Kuznetsov A, Almeida CM, et al. Understanding growth mechanisms and tribocorrosion behaviour of porous TiO 2 anodic films containing calcium, phosphorous and magnesium, Applied Surface Science 341 (2015), 1-12.
[15] Wood RJ. Tribo-corrosion of coatings: a review, Journal of Physics D: Applied Physics 40 (2007), 5502.
[16] Ponthiaux P, Wenger F, Drees D, Celis J-P. Electrochemical techniques for studying tribocorrosion processes, Wear 256 (2004), 459-468.
[17] Goodman SB. Wear particles, periprosthetic osteolysis and the immune system, Biomaterials 28 (2007), 5044-5048.
[18] Cobelli N, Scharf B, Crisi GM, Hardin J, Santambrogio L. Mediators of the inflammatory response to joint replacement devices, Nature Reviews Rheumatology 7 (2011), 600-608.
[19] Ribeiro AR, Gemini-Piperni S, Travassos R, Lemgruber L, C. Silva R, Rossi AL, Farina M, Anselme K, Shokuhfar T, et al. Trojan-Like Internalization of Anatase Titanium Dioxide Nanoparticles by Human Osteoblast Cells, Scientific reports 6 (2016), 23615.
[20] Tomsia AP, Launey ME, Lee JS, Mankani MH, Wegst UG, Saiz E. Nanotechnology approaches for better dental implants, The International journal of oral & maxillofacial implants 26 (2011), 25.
[21] Oh S, Daraio C, Chen L-H, Pisanic TR, Fiñones RR, Jin S. Significantly accelerated osteoblast cell growth on aligned TiO2 nanotubes, Journal of Biomedical Materials Research Part A 78A (2006), 97-103.
[22] Brammer KS, Frandsen CJ, Jin S. TiO2 nanotubes for bone regeneration, Trends in Biotechnology 30 (2012), 315-322.
[23] Zhao L, Wang H, Huo K, Cui L, Zhang W, Ni H, Zhang Y, Wu Z, Chu PK. Antibacterial nano-structured titania coating incorporated with silver nanoparticles, Biomaterials 32 (2011), 5706-5716.
[24] Brammer KS, Oh S, Cobb CJ, Bjursten LM, van der Heyde H, Jin S. Improved bone-forming functionality on diameter-controlled TiO2 nanotube surface, Acta Biomaterialia 5 (2009), 3215-3223.
[25] Das K, Bose S, Bandyopadhyay A. TiO2 nanotubes on Ti: influence of nanoscale morphology on bone cell–materials interaction, Journal of Biomedical Materials Research Part A 90 (2009), 225-237.
[26] Shokuhfar T, Hamlekhan A, Chang J-Y, Choi CK, Sukotjo C, Friedrich C. Biophysical evaluation of cells on nanotubular surfaces: the effects of atomic ordering and chemistry, International journal of nanomedicine 9 (2014), 3737.
[27] Lellouche J, Kahana E, Elias S, Gedanken A, Banin E. Antibiofilm activity of nanosized magnesium fluoride, Biomaterials 30 (2009), 5969-5978.
[28] Liao J, Anchun M, Zhu Z, Quan Y. Antibacterial titanium plate deposited by silver nanoparticles exhibits cell compatibility, International journal of nanomedicine 5 (2010), 337-342.
[29] Cao HL, Liu XY, Meng FH, Chu PK. Biological actions of silver nanoparticles embedded in titanium controlled by micro-galvanic effects, Biomaterials 32 (2011), 693-705.
[30] Vargas-Reus MA, Memarzadeh K, Huang J, Ren GG, Allaker RP. Antimicrobial activity of nanoparticulate metal oxides against peri-implantitis pathogens, International Journal of Antimicrobial Agents 40 (2012), 135-139.
[31] Al-Hazmi F, Alnowaiser F, Al-Ghamdi AA, Al-Ghamdi AA, Aly MM, Al-Tuwirqi RM, El-Tantawy F. A new large – Scale synthesis of magnesium oxide nanowires: Structural and antibacterial properties, Superlattices and Microstructures 52 (2012), 200-209.
[32] Lellouche J, Friedman A, Lellouche J-P, Gedanken A, Banin E. Improved antibacterial and antibiofilm activity of magnesium fluoride nanoparticles obtained by water-based ultrasound chemistry, Nanomedicine: Nanotechnology, Biology and Medicine 8 (2012), 702-711.
[33] Moseke C, Hage F, Vorndran E, Gbureck U. TiO2 nanotube arrays deposited on Ti substrate by anodic oxidation and their potential as a long-term drug delivery system for antimicrobial agents, Applied Surface Science 258 (2012), 5399-5404.
[34] Ercan B, Taylor E, Alpaslan E, Webster TJ. Diameter of titanium nanotubes influences anti-bacterial efficacy, Nanotechnology 22 (2011), 295102.
[35] Zhao Y, Xing Q, Janjanam J, He K, Long F, Low K-B, Tiwari A, Zhao F, Shahbazian-Yassar R, et al. Facile electrochemical synthesis of antimicrobial TiO2 nanotube arrays, International journal of nanomedicine 9 (2014), 5177.
[36] Crawford G, Chawla N, Das K, Bose S, Bandyopadhyay A. Microstructure and deformation behavior of biocompatible TiO2 nanotubes on titanium substrate, Acta Biomaterialia 3 (2007), 359-367.
[37] Rho J-Y, Tsui TY, Pharr GM. Elastic properties of human cortical and trabecular lamellar bone measured by nanoindentation, Biomaterials 18 (1997), 1325-1330.
[38] Soares P, Mikowski A, Lepienski CM, Santos E, Soares GA, Kuromoto NK. Hardness and elastic modulus of TiO2 anodic films measured by instrumented indentation, Journal of Biomedical Materials Research Part B: Applied Biomaterials 84 (2008), 524-530.
[39] Shokuhfar T, Arumugam GK, Heiden PA, Yassar RS, Friedrich C. Direct compressive measurements of individual titanium dioxide nanotubes, ACS nano 3 (2009), 3098-3102.
[40] Hu Y, Cai KY, Luo Z, Xu DW, Xie DC, Huang YR, Yang WH, Liu P. TiO2 nanotubes as drug nanoreservoirs for the regulation of mobility and differentiation of mesenchymal stem cells, Acta Biomaterialia 8 (2012), 439-448.
[41] Macdonald ML, Samuel RE, Shah NJ, Padera RF, Beben YM, Hammond PT. Tissue integration of growth factor-eluting layer-by-layer polyelectrolyte multilayer coated implants, Biomaterials 32 (2011), 1446-1453.

[42] Lee D-W, Yun Y-P, Park K, Kim SE. Gentamicin and bone morphogenic protein-2 (BMP-2)-delivering heparinized-titanium implant with enhanced antibacterial activity and osteointegration, Bone 50 (2012), 974-982.
[43] Gulati K, Ramakrishnan S, Aw MS, Atkins GJ, Findlay DM, Losic D. Biocompatible polymer coating of titania nanotube arrays for improved drug elution and osteoblast adhesion, Acta Biomaterialia 8 (2012), 449-456.
[44] Popat KC, Eltgroth M, LaTempa TJ, Grimes CA, Desai TA. Decreased Staphylococcus epidermis adhesion and increased osteoblast functionality on antibiotic-loaded titania nanotubes, Biomaterials 28 (2007), 4880-4888.
[45] Hu H, Zhang W, Qiao Y, Jiang X, Liu X, Ding C. Antibacterial activity and increased bone marrow stem cell functions of Zn-incorporated TiO2 coatings on titanium, Acta Biomaterialia 8 (2012), 904-915.
[46] Alves SA, Patel SB, Sukotjo C, Mathew MT, Filho PN, Celis J-P, Rocha LA, Shokuhfar T. Synthesis of calcium-phosphorous doped TiO2 nanotubes by anodization and reverse polarization: A promising strategy for an efficient biofunctional implant surface, Applied Surface Science 399 (2017), 682-701.
[47] Fusayama T, Katayori T, Nomoto S. Corrosion of Gold and Amalgam Placed in Contact with Each Other, Journal of Dental Research 42 (1963), 1183-1197.
[48] Alves S, Bayón R, Igartua A, Saénz de Viteri V, Rocha L. Tribocorrosion behaviour of anodic titanium oxide films produced by plasma electrolytic oxidation for dental implants, Lubrication science 26 (2014), 500-513.
[49] Alves S, Bayón R, de Viteri VS, Garcia M, Igartua A, Fernandes M, Rocha L. Tribocorrosion Behavior of Calcium-and Phosphorous-Enriched Titanium Oxide Films and Study of Osteoblast Interactions for Dental Implants, Journal of Bio-and Tribo-Corrosion 1 (2015), 1-21.
[50] Robin A, Meirelis J. Influence of fluoride concentration and pH on corrosion behavior of Ti-6Al-4V and Ti-23Ta alloys in artificial saliva, Materials and corrosion 58 (2007), 173-180.
[51] Souza JC, Barbosa SL, Ariza EA, Henriques M, Teughels W, Ponthiaux P, Celis J-P, Rocha LA. How do titanium and Ti6Al4V corrode in fluoridated medium as found in the oral cavity? An in vitro study, Materials Science and Engineering: C 47 (2015), 384-393.
[52] Holland R. Corrosion testing by potentiodynamic polarization in various electrolytes, Dental Materials 8 (1992), 241-245.
[53] Doni Z, Alves A, Toptan F, Gomes J, Ramalho A, Buciumeanu M, Palaghian L, Silva F. Dry sliding and tribocorrosion behaviour of hot pressed CoCrMo biomedical alloy as compared with the cast CoCrMo and Ti6Al4V alloys, Materials & Design 52 (2013), 47-57.
[54] Yu W-q, Qiu J, Xu L, Zhang F-q. Corrosion behaviors of TiO2 nanotube layers on titanium in Hank's solution, Biomedical Materials 4 (2009), 065012.
[55] Yu W-q, Qiu J, Zhang F-q. In vitro corrosion study of different TiO2 nanotube layers on titanium in solution with serum proteins, Colloids and surfaces B: Biointerfaces 84 (2011), 400-405.
[56] Diomidis N, Celis JP, Ponthiaux P, Wenger F. A methodology for the assessment of the tribocorrosion of passivating metallic materials, Lubrication science 21 (2009), 53-67.
[57] Hanawa T, Asami K, Asaoka K. Repassivation of titanium and surface oxide film regenerated in simulated bioliquid, Journal of biomedical materials research 40 (1998), 530-538.
[58] Alves A, Oliveira F, Wenger F, Ponthiaux P, Celis J-P, Rocha L. Tribocorrosion behaviour of anodic treated titanium surfaces intended for dental implants, Journal of Physics D: Applied Physics 46 (2013), 404001.
[59] Marques IdSV, Alfaro MF, da Cruz NC, Mesquita MF, Sukotjo C, Mathew MT, Barão VAR. Tribocorrosion behavior of biofunctional titanium oxide films produced by micro-arc oxidation: Synergism and mechanisms, Journal of the mechanical behavior of biomedical materials 60 (2016), 8-21.
[60] Runa M, Mathew M, Rocha L. Tribocorrosion response of the Ti6Al4V alloys commonly used in femoral stems, Tribology International 68 (2013), 85-93.
[61] Roy P, Berger S, Schmuki P. TiO2 nanotubes: synthesis and applications, Angewandte Chemie International Edition 50 (2011), 2904-2939.
[62] Ali G, Chen C, Yoo SH, Kum JM, Cho SO. Fabrication of complete titania nanoporous structures via electrochemical anodization of Ti, Nanoscale research letters 6 (2011), 1-10.
[63] Yuan X, Zheng M, Ma L, Shen W. High-speed growth of TiO2 nanotube arrays with gradient pore diameter and ultrathin tube wall under high-field anodization, Nanotechnology 21 (2010), 405302.
[64] Wang D, Yu B, Wang C, Zhou F, Liu W. A novel protocol toward perfect alignment of anodized TiO2 nanotubes, Advanced Materials 21 (2009), 1964-1967.
[65] Beutner R, Michael J, Schwenzer B, Scharnweber D. Biological nano-functionalization of titanium-based biomaterial surfaces: a flexible toolbox, Journal of the Royal Society Interface 7 (2010), S93-S105.
[66] Garcıa I, Drees D, Celis J-P. Corrosion-wear of passivating materials in sliding contacts based on a concept of active wear track area, Wear 249 (2001), 452-460.
[67] Demetrescu I, Pirvu C, Mitran V. Effect of nano-topographical features of Ti/TiO 2 electrode surface on cell response and electrochemical stability in artificial saliva, Bioelectrochemistry 79 (2010), 122-129.
[68] Grotberg J, Hamlekhan A, Butt A, Patel S, Royhman D, Shokuhfar T, Sukotjo C, Takoudis C, Mathew MT. Thermally oxidized titania nanotubes enhance the corrosion resistance of Ti6Al4V, Materials Science and Engineering: C 59 (2016), 677-689.
[69] Vieira AC, Rocha LA, Papageorgiou N, Mischler S. Mechanical and electrochemical deterioration mechanisms in the tribocorrosion of Al alloys in NaCl and in NaNO3 solutions, Corrosion Science 54 (2012), 26-35.

[70] Crawford G, Chawla N, Houston J. Nanomechanics of biocompatible TiO2 nanotubes by interfacial force microscopy (IFM), Journal of the mechanical behavior of biomedical materials 2 (2009), 580-587.
[71] Xu Y, Liu M, Wang M, Oloyede A, Bell J, Yan C. Nanoindentation study of the mechanical behavior of TiO2 nanotube arrays, Journal of Applied Physics 118 (2015), 145301.
[72] Delahay P, Pourbaix M, Van Rysselberghe P. Potential-pH Diagram of Zinc and its Applications to the Study of Zinc Corrosion, Journal of The Electrochemical Society 98 (1951), 101-105.
[73] Indira K, Kamachi Mudali U, Rajendran N. Corrosion behavior of electrochemically assembled nanoporous titania for biomedical applications, Ceramics International 39 (2013), 959-967.
[74] Cheng X, Roscoe SG. Corrosion behavior of titanium in the presence of calcium phosphate and serum proteins, Biomaterials 26 (2005), 7350-7356.

CHAPTER 7

Improved tribo-electrochemical performance of bio-functionalized TiO_2 nanotubes under multiple sliding actions in artificial saliva

Submitted for publication in Tribology International

Improved tribo-electrochemical performance of bio-functionalized TiO_2 nanotubes under multiple sliding actions in artificial saliva

Sofia A. Alves[1,2*], André L. Rossi[3], Ana R. Ribeiro[2,4,5], Fatih Toptan[1,6], Ana M. Pinto[1,6], Tolou Shokuhfar[7,8], Jean-Pierre Celis[9,10], Luís A. Rocha[1,2,11]

[1]*CMEMS – Center of MicroElectroMechanical Systems, Department of Mechanical Engineering, University of Minho, Azurém, 4800-058 Guimarães, Portugal*
[2]*IBTN/BR – Brazilian Branch of the Institute of Biomaterials, Tribocorrosion and Nanomedicine, Faculty of Sciences, UNESP – Universidade Estadual Paulista, 17033-360 Bauru, São Paulo, Brazil*
[3]*Brazilian Center for Research in Physics, 22290-180 Rio de Janeiro, Brazil*
[4]*Directory of Life Sciences Applied Metrology, National Institute of Metrology, Quality and Technology, 25250-020 Duque de Caxias – RJ, Brazil*
[5]*Postgraduate Program in Translational Biomedicine, University of Grande Rio, 25070-000 Duque de Caxias – RJ, Brazil*
[6]*Department of Mechanical Engineering, University of Minho, Azurém, 4800-058 Guimarães, Portugal*
[7]*Department of Bioengineering, University of Illinois at Chicago, 60607 Chicago, Illinois, USA*
[8]*IBTN/US – American Branch of the Institute of Biomaterials, Tribocorrosion and Nanomedicine, University of Illinois at Chicago, 60612 Chicago, Illinois, USA*
[9]*Department of Materials Engineering, KU Leuven, 3001 Leuven, Belgium*
[10]*Falex Tribology N.V., Wingepark 23B, 3110 Rotselaar, Belgium*
[11]*Faculdade de Ciências, Departamento de Física, UNESP – Universidade Estadual Paulista, 17033-360 Bauru, São Paulo, Brasil*
**e-mail: sofiafonso@msn.com*

Abstract

After insertion into bone, dental implants may be submitted to tribocorrosive conditions resulting in the release of metallic ions/wear debris, which can induce to peri-implant bone loss and loosening of the implant. Despite the promising ability of TiO_2 nanotubes (NTs) to improve osseointegration and avoid infection-related failures, the understanding of their degradation under the simultaneous action of wear and corrosion has not been explored. The main focus of this work is to study, for the first time, the tribo-electrochemical behavior of bio-functionalized TiO_2 NTs submitted to multiple wear actions, and compare it with conventional TiO_2 NTs.

TiO_2 NTs grown by anodization were doped with bioactive elements, namely calcium (Ca), phosphorous (P), and zinc (Zn), through reverse polarization anodization treatments. Characterization techniques such as scanning electron microscopy (SEM), energy dispersive X-ray spectroscopy (EDS), and scanning transmission electron microscopy (STEM), were used to characterize the films. Tribo-electrochemical tests were carried out in artificial saliva (AS) by two-cycle reciprocating sliding tests. The open circuit potential (OCP) was monitored before, during, and after both cycles of sliding, during which the coefficient of friction (COF) was calculated. The resulting wear scars were analyzed by SEM and EDS, and wear volume measurements were performed by 2D profilometry. Finally, the mechanical features of TiO_2 NTs were accessed by nanoindentation.

The results show that although all TiO_2 nanotubular films display a highly stable tribo-electrochemical response when submitted to multiple sliding actions, this was significantly improved after bio-functionalization. The enhanced electrochemical stability and wear resistance were granted by a nano-thick oxide film formed at Ti/TiO_2 NTs the interface, which increased significantly their adhesion strength and consequently their hardness. Additionally, the elastic modulus of TiO_2 NTs was significantly lower compared to Ti, and closer to that of natural bone. This study provides fundamental and new insights for the development of multifunctional TiO_2 NTs with long-term biomechanical stability and improved clinical outcomes.

Keywords: TiO_2 nanotubes; Bio-functionalization; Tribocorrosion; Film adhesion; Mechanical properties; Multiple sliding actions.

7.1. Introduction

Metallic implants made out of titanium (Ti) and Ti-based materials are the most commonly used for dental implants therapies owing their mechanical properties, excellent biocompatibility and high corrosion resistance [1, 2]. However, these materials present serious shortcomings as regards the absence of osteogenesis inducing ability and the lack of antimicrobial properties [1-3]. To overcome these issues, various studies on the modification of Ti surfaces features such as morphology/topography and chemistry, have been undertaken [2, 4-8]. A special focus has been devoted in the production of novel nanopatterned Ti implant surfaces and there is a strong believe that nano-functionalized surfaces will produce the new generation of dental implant materials [4, 9-12].

The exceptional features of TiO_2 NTs have been widely recognized to promote osseointegration and reduce infection, the most commonly reported complications of currently used Ti-based dental implants [1, 13-16]. These are very flexible structures for building of new functionalities and further achieve enhanced biocompatibility [17]. TiO_2 NTs may be easily coated with bioactive polymers [18] or nanoparticles [19], and have demonstrated excellent ability to act as efficient and controlled drug delivery systems, by encapsulation of drugs, bioactive molecules or inorganic elements into their hollow cavities [20-24]. The lack of biomechanical compatibility of metallic dental implants and bone is known to induce stress shielding effect and consequently bone resorption. This is an additional shortcoming that TiO_2 NTs have demonstrated ability to overcome, since they display lower elastic modulus than Ti and closer to that of natural bone [1, 3, 25-27].

Ti-based materials have a serious disadvantage since they are known to display low wear resistance [28] and this may induce various harmful consequences. During insertion, dental

implants are subjected to both wear and corrosion actions (tribocorrosion) that may lead to material degradation *in vivo.* Furthermore, dental implants may be also exposed to tribocorrosion in a long term, since cyclic micro-movements are known to take place at implant/bone interface as a consequence of chewing action [29, 30]. Consequently, dental implant material degradation by wear/corrosion processes, may result in the release of metallic ions/wear debris to adjacent tissues, which may induce to several biological complications [31-33]. Various studies have shown that TiO_2 nanoparticles are internalized by bone cells impairing their functions [34] and activating inflammatory reactions which may induce to osteolysis, and ultimately to implant failure [35-37]. In this light, the study of the degradation behavior of TiO_2 nanotubular surfaces is of crucial importance and this is still missing in literature. To further emphasize this need, it has been reported that TiO_2 NTs display poor adhesion strength to the substrate [38-40]. This is an issue of high priority since the poor adhesion of TiO_2 NTs may compromise their widespread applications.

In this contribution the tribo-electrochemical degradation behavior of TiO_2 NTs is studied before and after bio-functionalization treatments. To simulate *in vivo* harsh environmental conditions, for the first time, reciprocating sliding tests were carried out in artificial saliva at 37 °C under multiple cycles of sliding, intended to mimic the multiple mechanical solicitations that dental implants might be daily exposed. Here we describe the effects of bio-functionalization treatments on the tribo-electrochemical performance of TiO_2 NTs and correlate them with the adhesion strength and mechanical properties of the films.

7.2. Materials and Methods

7.2.1. Synthesis of TiO_2 NTs and bio-functionalization

To prepare TiO_2 NTs, two anodization steps were carried out in an optimized organic electrolyte composed of ethylene glycol (EG, Fluka Analytical, St. Louis, MO, USA), 0.3 wt. % ammonium fluoride (NH_4F, Ammonium Fluoride, Sigma-Aldrich, St. Louis, MO, USA) and 3 vol. % distilled water. In the first anodization step Ti smooth samples (anode) were immersed in the EG-based electrolyte together with a graphite rod (cathode), separated at a distance of about 2 cm, and a constant voltage of 60 V was applied for 1 h. Afterwards, the resultant nanotubular film was intentionally removed by sonication in isopropanol (15 min) and distilled water (5 min), leaving a nanotextured Ti surface for the second anodizing step. The second anodization step was conducted at the previous conditions for an anodization time of 30 min, to synthesize vertically aligned and ordered TiO_2 nanotubular films with a specific morphology. The resulting Ti samples with TiO_2 NTs were named as NT.

Bio-functionalization of TiO_2 NTs was conducted based on a novel methodology described

in a previous work [41], based on reverse polarization anodization treatments. The NT samples were subjected firstly to reverse polarization in an aqueous electrolyte composed of 0.35 M calcium acetate (Calcium acetate monohydrate, Sigma-Aldrich, St. Louis, MO, USA), 0.04 M β-glycerolphosphate (β-GP) (β-glycerolphosphate disodium salt pentahydrate, Sigma-Aldrich, St. Louis, MO, USA) and 0.35 M zinc acetate (Zinc acetate dihydrate, Sigma-Aldrich, St. Louis, MO, USA) as the source of calcium (Ca), phosphorous (P) and zinc (Zn), respectively. The reverse polarization step was carried out for 30 s in the Ca/P/Zn-based electrolyte, followed by anodization step in the same electrolyte for 30 min at 100 V. A graphite rod was used as the counter electrode and was placed about 2 cm away from the sample. After bio-functionalization, the nanotubular samples were named as NT-Ca/P/Zn. The outcomes of the tribo-electrochemical tests showed two dissimilar behaviors for these samples. Therefore, these were devided in two different groups named as NT-Ca/P/Zn#1 and NT-Ca/P/Zn#2.

NT, NT-Ca/P/Zn#1 and NT-Ca/P/Zn#2 samples, were cleaned in isopropanol (10 min), distilled water (5 min) and dried at room temperature. Finally, all the samples were stored in a desiccator until performing tribocorrosion tests.

A DC power supply (Keysight (Agilent) Technologies N5772A) was used for cathodic and anodic treatments with a limiting current of 2.5 A, and all of them were conducted at room temperature (22 – 24 °C) under stirring conditions.

7.2.2. Characterization of TiO_2 nanotubular films

The surface morphology of TiO_2 nanotubular samples was investigated before and after bio-functionalization treatments by scanning electron microscopy (SEM) using a FEI Helios NanoLab 650 equipped with a detector for energy dispersive X-ray spectroscopy (EDS). Elemental analyses of the samples were performed by EDS, using an acceleration voltage of 10 kV.

Thin cross-sections (around 100 nm thick) of TiO_2 nanotubular films were obtained by a dual beam instrument equipped with focused ion beam (FIB) with a gallium (Ga) ion source (TESCAN, LYRA 3). A platinum (Pt) layer of 1 µm was deposited in situ using a gas injection system and 1 nA Ga^+ ion current accelerated at 30 kV aiming to protect the thin cross-sections. The initial etching was conducted with 5 and 2 nA at 30 keV, and thinning was performed in 4 steps to obtain a lamella of ~ 100 nm: 1) 1 nA/30 keV; 2) 0.1 nA/10 keV; 3) 10 pA/5 keV; and 4) 3 keV. The Ti/TiO_2 NTs interface was observed by imaging the FIB-sections by dark-field scanning transmission electron microscopy (STEM-DF) using a JEOL 2100 F operating at an accelerating voltage of 200 kV.

7.2.3. Tribo-electrochemical experiments

A tribo-electrochemical approach was used to investigate the degradation behavior of nanotubular samples under the simultaneous action of wear and corrosion. The samples were fixed in an electrochemical cell, with an exposed surface area of 0.63 cm^2 to the test solution. A modified Fusayama's artificial saliva (AS) [42] was used at 37 °C (pH = 5.5), with chemical composition as follows: NaCl (0.4 g/L), KCl (0.4 g/L), $CaCl_2.2H_2O$ (0.795 g/L), $Na_2S.9H_2O$ (0.005 g/L), $NaH_2PO_4.2H_2O$ (0.69 g/L) and Urea (1 g/L). This solution has been previously used in various studies [43-46] to mimic the extremely corrosive oral environment composed of Cl^-, F^-, and H^+ ions, which play a significant role on corrosion of dental implant materials [47]. Furthermore, it is known that metallic materials display a similar electrochemical behavior in Fusayama´s saliva and natural saliva [48]. The tests were conducted in a pin-on-disk CETR tribometer (Model UMT 2, Campbell, California, USA) with a reciprocating sliding configuration, and an alumina (Al_2O_3) ball (Ø 10 mm) was used as the counterbody. In a three-electrode setup the testing samples were used as the working electrode, a platinum counter electrode, and a saturated calomel electrode (SCE) (Hg/Hg_2Cl_2/saturated KCl solution; SCE = +244 mV *vs.* NHE) was used as the reference electrode.

The reciprocating sliding tests were performed at a normal load of 1 N, a sliding frequency of 1 Hz and a linear displacement amplitude of 650 µm. Two independent cycles of sliding were carried out for 1800 s, with an interval of 2000 s between both. The open circuit potential (OCP) was monitored using a potentiostat Gamry Reference 600 coupled to Gamry framework software (Gamry Instruments, Warminster, PA, USA) before the first period of sliding until stabilization, during both cycles of sliding and afterwards, during their correspondent periods of stabilization of 2000 s. During both periods of sliding the tribometer was coupled to UMT-2 software (Campbell, California, USA) to monitor the tangential force during sliding, through which the coefficient of friction (COF) was calculated. At the end, all the samples were ultrasonically cleaned with isopropanol (10 min) followed by distilled water (5 min). To assure the repeatability of the results, all the tests were accomplished for a minimum number of three samples for each group.

7.2.4. Characterization of the wear tracks

After tribo-electrochemical testing, the morphological and chemical features of the wear scars were investigated by SEM (FEI Nova 200 (FEG/SEM)) and EDS (Pegasus X4M).

To calculate the wear volume of the samples, the model previously described by Doni *et al.* [49] was strictly followed. The wear track length was taken constant for all the tests as 650 µm. The width and the deepness of the wear tracks were extracted from the profiles obtained

by 2D profilometry (Veeco, Dektak 150) and the data analysis was performed with the software (Dektak version 9.4). The final wear volume measurements were calculated from three wear tracks for each condition of test.

7.2.5. Nanoindentation tests

The mechanical properties of Ti polished samples (mirror-finishing) and TiO_2 nanotubular samples were measured using a nanoindentation system (Micro Materials NanoTest), with a load resolution of 50 nN.

To avoid the influence of substrate, preliminary experiments were carried out to select the most appropriate load to be applied, in such a way that the maximum indentation depth was always less than 10 % of the thickness of the films [27]. Afterwards, the maximum applied load during nanoindentation was set as 5 mN and the holding time was 5 s.

The reduced modulus (E_r) and hardness were determined from indentation load-displacement data following the Oliver and Pharr methodology [50]. The hardness is determined from the maximum load and the projected area of contact. The E_r combines the mechanical properties of the indenter and the sample, and is given by the following equation:

$$\frac{1}{E_r} = \frac{(1-\nu_1{}^2)}{E_1} + \frac{(1-\nu_2{}^2)}{E_2} \quad (1)$$

where ν_1 and E_1 are the Poisson´s ratio and Young's modulus of the specimen and, ν_2 and E_2 are the Poisson's ratio and Young's modulus of the indenter, respectively. For the diamond Berkovich indenter probe used, E_2 = 1140 GPa and ν_2 = 0.07. The ν_1 of TiO_2 NTs was chosen to be the same as that bulk TiO_2 (i.e. 0.28) [51], while the ν_1 of Ti was assumed as 0.32. The elastic modulus (E) of TiO_2 NTs and Ti samples was calculated by fitting the measured E_r values in equation (1). The minimum of six indentations per each sample were used for elastic modulus and hardness calculations.

7.2.6. Statistical analysis

In this study the data is presented as the arithmetic mean ± standard deviation (SD). The statistical analysis was conducted by means of statistical tool SigmaStat 3.5 (Systat Software, San Jose, CA, USA). Data analysis was performed by one-way analysis of variance (ANOVA) in combination with Tukey HSD post hoc test, with a significance level of $p < 0.05$.

7.3. Results

7.3.1. Characterization of TiO_2 nanotubular films

The surface morphology of TiO_2 NTs synthesized by two-step anodization of titanium (Ti) surfaces is shown in Fig. 7.1a. After bio-functionalization of NT samples in the Ca/P/Zn-based electrolyte by reverse polarization and anodization processes, the morphology of the NTs was preserved as shown in Fig. 7.1b. Both nanotubular surfaces are characterized by NTs with non-uniform diameters ranging from 50 – 90 nm as reported in a previous study [41]. The chemical features of NT and NT-Ca/P/Zn samples were determined by semi-quantitative EDS analysis, and the atomic % of the elements detected is depicted in Table 7.1. Both groups of samples are composed of Ti, oxygen (O) and fluorine (F), and NT-Ca/P/Zn samples are additionally constituted of Ca, P and Zn elements. In a previous work, XPS studies conducted in NT samples showed that Ti and O were mainly found as TiO_2 [41].

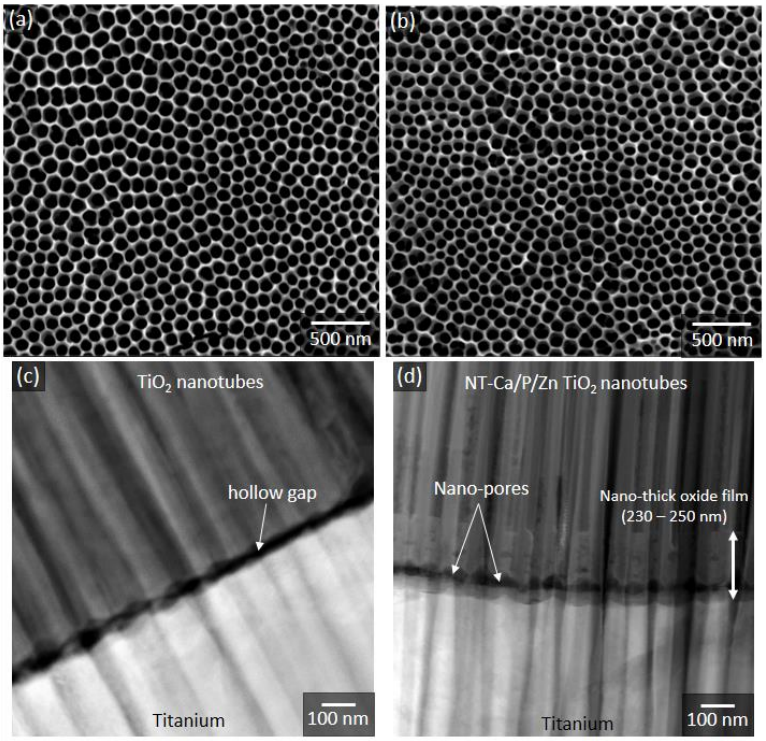

Fig. 7.1. SE SEM micrographs of (a) NT and (b) NT-Ca/P/Zn surfaces. Dark-field STEM micrographs at the interface of (c) NT and (d) NT-Ca/P/Zn nanotubular films. In (c) the inset white arrow shows the lacuna between Ti substrate and NT film while in (d) shows the nano porosity at the interface instead of a continuous hollow gap. In (d) is also highlighted the nano-thick oxide film grown during bio-functionalization (230 – 250 nm).

Table 7.1. Atomic percentage (At. %) of the elements detected in NT and NT-Ca/P/Zn samples by EDS.

Element	NT (At. % ± SD)	NT-Ca/P/Zn (At. % ± SD)
Ti K	21.82 ± 1.64	23.66 ± 1.05
O K	53.18 ± 1.26	51.70 ± 3.98
F K	8.90 ± 0.53	9.46 ± 0.73
Ca K	-	0.26 ± 0.04
P K	-	0.33 ± 0.03
Zn L	-	1.35 ± 0.12

The interfacial features of TiO_2 nanotubular films were studied before and after bio-functionalization treatments. Although no differences were found on NTs morphology, bio-functionalization induced significant changes in the interface between Ti substrate and TiO_2 NTs. The Ti/TiO_2 NTs interface is shown in Fig. 7.1c and d for NT and NT-Ca/P/Zn samples respectively. For conventional TiO_2 NTs a non-continuous interface characterized by a hollow space between Ti substrate and TiO_2 film is observed (Fig. 7.1c), suggesting a poor adhesion strength of the NTs. On the other hand, after bio-functionalization treatments, the hollow gap existing before is no longer continuous along the interfacial region due to the formation of a nano-thick oxide film (230 – 250 nm thickness). This newly formed film at the interface, beyond present some porosity at the nanoscale range, induced the formation of a more continuous interface which appears to improve the adhesion of the film to the Ti substrate.

7.3.2. Tribo-electrochemical behavior of TiO_2 nanotubular films submitted to two-cycle sliding tests

7.3.2.1. Open circuit potential and coefficient of friction evolutions

The open circuit potential (OCP) evolution before two-cycle sliding tests in NT and NT-Ca/P/Zn samples is shown in Fig. 7.2a. It is noteworthy that two different trends were observed during sliding tests carried out in NT-Ca/P/Zn samples and both trends are reported as NT-Ca/P/Zn#1 and NT-Ca/P/Zn#2. Before mechanical solicitations, all the samples were immersed in artificial saliva (AS) until OCP stabilization. The OCP reflects the electrochemical surface activation stage (active *vs.* passive), revealing its tendency to corrosion so that a higher OCP indicates a lower corrosion trend. After the period of stabilization both group of samples stabilized at significantly different OCP values. NT samples achieved a stable OCP around -0.14 V *vs.* SCE that differs strikingly from NT-Ca/P/Zn samples potential, which stabilized around 0.11 – 0.12 V *vs.* SCE. Higher OCP values were found for NT-Ca/P/Zn samples as compared to NT samples during the whole duration of two-cycle sliding tests. These differences might be related with the different interfacial features of TiO_2 nanotubular films before and after bio-functionalization treatments, as will be further on discussed in more detail (discussion section).

As soon as the first cycle of sliding starts on NT samples (SLIDING 1), it is observed that the OCP is kept stable for approximately 100 s and afterwards, a gradual decrease takes place during its whole duration reaching the lowest value of -0.3 V *vs.* SCE. As soon as the sliding is finished the OCP gradually evolves to noble values during the whole 2000 s stabilization period. Once the second cycle of sliding starts (SLIDING 2), the OCP starts to decrease immediately and a gradual lowering is observed during its complete duration reaching a minimum value of -0.3 V *vs.* SCE. Interestingly, it is noticed that after the end of SLIDING 2, the OCP tends to stabilize at a value similar to that achieved previously in the final stage of SLIDING 1. The coefficient of

friction (COF) evolution during SLIDING 1 is shown in Fig. 7.2b. It is observed that in the first period of 300 s of sliding the COF is around 0.7 – 0.75, and after this period it decreases and tends to stabilize in values around 0.66 – 0.67. As observed in Fig. 7.2c, once the SLIDING 2 starts, the COF values are similar to the ones measured at the end of SLIDING 1 (i.e. 0.66 – 0.67) and these slightly drop down during SLIDING 2, reaching a minimum value of around 0.61 at the final stage.

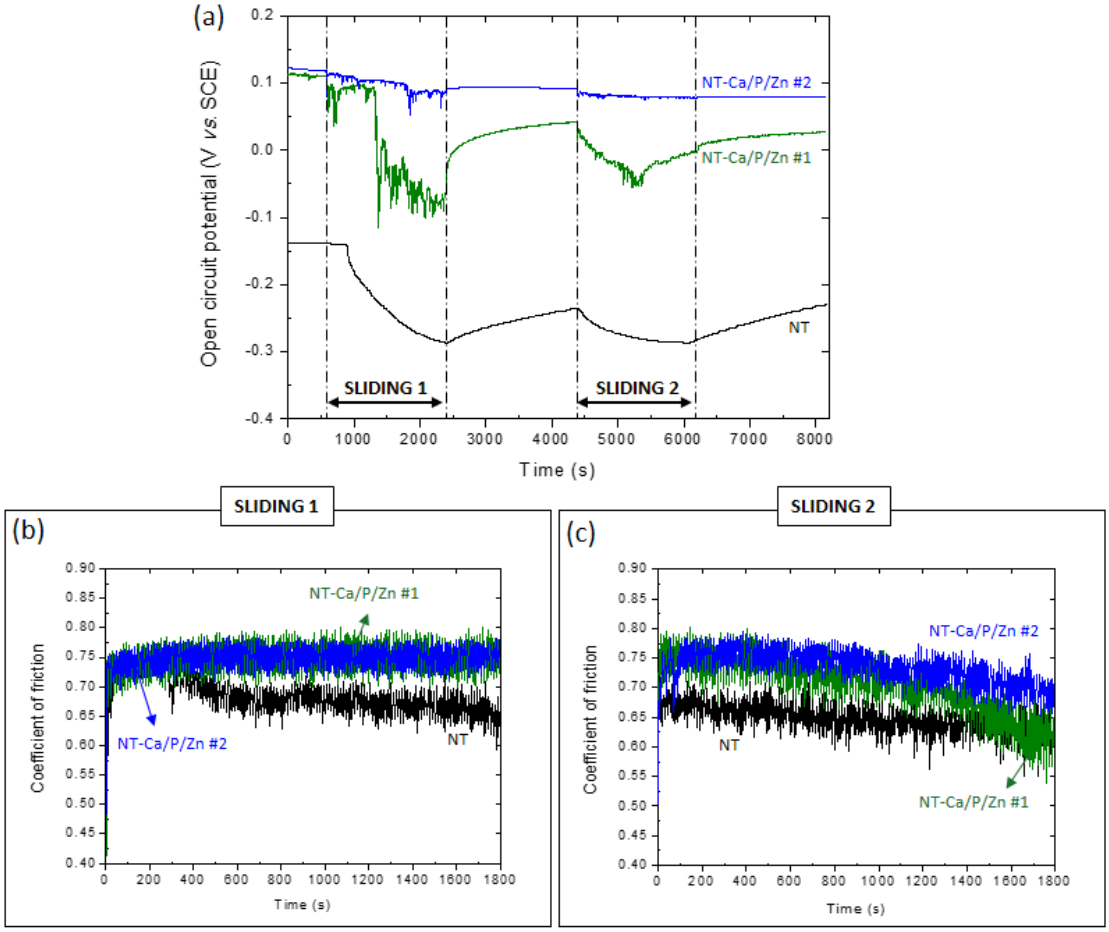

Fig. 7.2. (a) Evolution of the open circuit potential (OCP) before, during and after two-cycle reciprocating sliding tests in NT, NT-Ca/P/Zn#1 and NT-Ca/P/Zn#2 samples. The coefficient of friction values (COF) measured during the first sliding cycle (SLIDING 1) are shown in (b), while in (c) are depicted the COF values registered during the second sliding cycle (SLIDING 2). Both sliding periods lasted for 1800 s.

As referred above, two distinct electrochemical behaviors were observed for NT-Ca/P/Zn samples submitted to two-cycle sliding tests and both are presented in Fig. 7.2a as NT-Ca/P/Zn#1 and NT-Ca/P/Zn#2. As soon as the first cycle of mechanical solicitations starts on NT-Ca/P/Zn#1 samples, the OCP immediately drops a few mV and is maintained stable during approximately 800 s. After this time, the OCP drops until -0.1 V *vs.* SCE and immediately after goes up again, and then tends to slightly progress to lower values until SLIDING 1 is stopped, reaching a minimum value of 0.08 V *vs.* SCE. At the end of SLIDING 1 the OCP immediately and rapidly evolves to higher values, and after 2000 s stabilize at around 0.04 V *vs.* SCE. After the period of

stabilization when the second cycle of sliding starts, the OPC falls down and gradually reaches lower values during approximately 1000 s, after which the OCP starts to evolve to values increasingly high. As soon as SLIDING 2 is stopped, the OCP increases and reaches a similar value to the one initially recorded before the second sliding action. Concerning the COF evolution during SLIDING 1, this is maintained in a stable value of 0.75 during its total duration. When SLIDING 2 starts the COF is similar to the one attained at the end of SLIDING 1, and it slowly falls to lower values during the whole duration of mechanical solicitations. However, a remarkable higher drop is observed after 1000 s of sliding, which is coincident with the moment at which the OCP starts to increase (Fig. 7.2a).

In respect to NT-Ca/P/Zn#2 samples, as soon as SLIDING 1 starts the OCP drops only a few millivolts (around 0.01 V *vs.* SCE) and reaches a steady state for approximately 1200 s, after which the OCP falls down again a few millivolts and remain stable until the end of sliding. Once it is finished, the OCP evolves to more noble values reaching a stable value similar to the one achieved during the first plateau. After 2000 s stabilization period, the SLIDING 2 starts and the OCP slightly drops a few millivolts, and is maintained stable during the whole duration of sliding. Once mechanical action is finished, the OCP recovers and stabilizes in a value about 0.01 V *vs.* SCE, slightly inferior to the one recorded immediately before SLIDING 2. The COF evolution during the first cycle of sliding is similar to the one observed for NT-Ca/P/Zn#1 samples, which was kept in a stable value of 0.75. During SLIDING 2 duration, the COF measured is similar to the one registered at the end of SLIDING 1 and starts slowly decreasing after about 1000 s, which is coincident with the moment that COF values start decreasing for NT-Ca/P/Zn#1 during SLIDING 2 (Fig. 7.2c). It is noteworthy that the COF values measured during all the cycles are characteristic of the tribological pair Ti oxide/alumina of sliding and so they indicate the presence of Ti oxide film in the worn area.

7.3.2.2. Wear tracks characterization

Representative SEM images of the wear tracks on NT, NT-Ca/P/Zn#1 and NT-Ca/P/Zn#2 samples are shown in Fig. 7.3. The SEM images are shown both in secondary electron (SE) and backscattered (BSE) imaging modes aiming a better characterization of the topographical and chemical features of the worn areas resulting from two-cycle reciprocating sliding tests.

From SE/BSE SEM images of the wear track on NT samples (Fig. 7.3a) it is observed that TiO_2 nanotubular film detached from the Ti substrate, including from the periphery of the sliding contact area. Film detachment is transduced in a wear track with irregular borders and a significantly higher length when compared to the wear tracks on NT-Ca/P/Zn#1 (Fig. 7.3b) and NT-Ca/P/Zn#2 (Fig. 7.3c) samples. The brighter areas in BSE SEM images are related to those

regions characterized by a high atomic number, namely Ti, and contrast with those darker areas where elements with a low atomic number are present, such as O. In this light is it observed that the central region of the wear track of NT samples is characterized by the presence of oxidized areas, which are probably related to the formation of a tribofilm as a consequence of oxide film debris entrapment and compactness in the contact region. In contrast, both wear tracks on NT-Ca/P/Zn samples are characterized by curved borders with similar dimensions, and the detachment of the nanotubular film seems that have occurred mainly in the central region of the wear tracks, as suggested by the brighter contrast in BSE images (Fig. 7.3b and c).

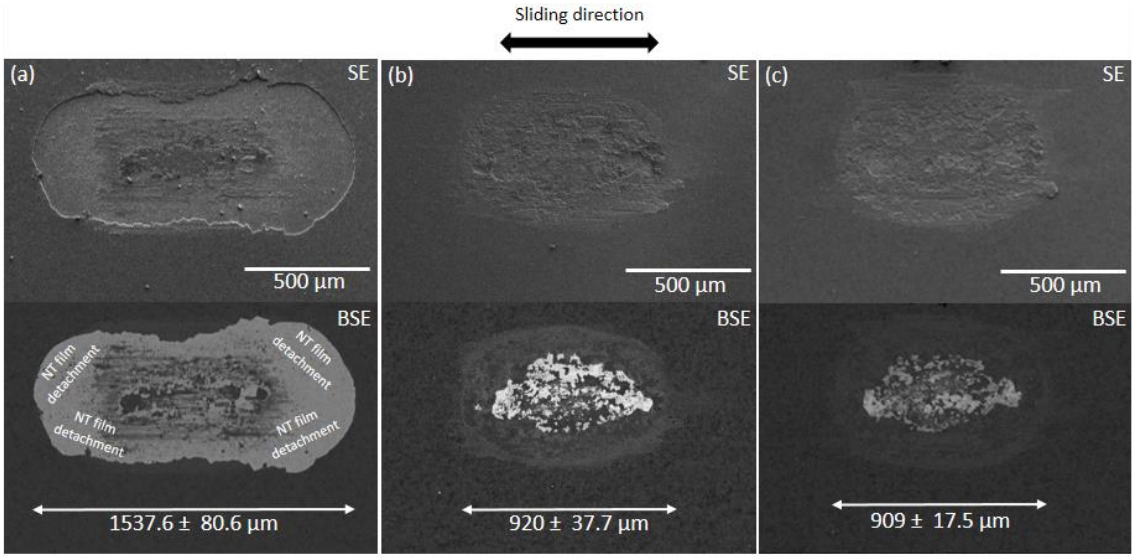

Fig. 7.3. SE/BSE SEM micrographs of the wear tracks in (a) NT, (b) NT-Ca/P/Zn#1 and (c) NT-Ca/P/Zn#2 samples after two-cycle reciprocating sliding tests in artificial saliva. The maximum wear tracks length is included in BSE images for all the groups.

A more detailed view of the wear tracks in the border and central regions is provided by BSE SEM images shown in Fig. 7.4a-b for NT samples. From these images it is confirmed that the film has been completely detached from the periphery of the contact region and Ti substrate became exposed to the aggressive environment provided by AS, and cracks are observed in the film remaining outside the wear track. In the central region, it is observed the presence of areas from where the nanotubular film was detached and others where the formation of a compact oxide film took place (tribofilm).

No significant differences were observed in the border and central regions of the wear tracks on NT-Ca/P/Zn#1 and NT-Ca/P/Zn#2 samples, and the representative images of their wear tracks are shown in Fig. 7.4c (border) and Fig. 7.4d (center). In the border region it is observed that the film is characterized by areas with dissimilar levels of damage: smooth areas that contrast with rougher regions with pores obstructed, and others where open tubes are still visible. In the central region, it is confirmed that NTs have been completely detached in some

areas, while in others still maintain their integrity. The obstruction of the pores in the topmost regions is also observed and indicated in Fig. 7.4d.

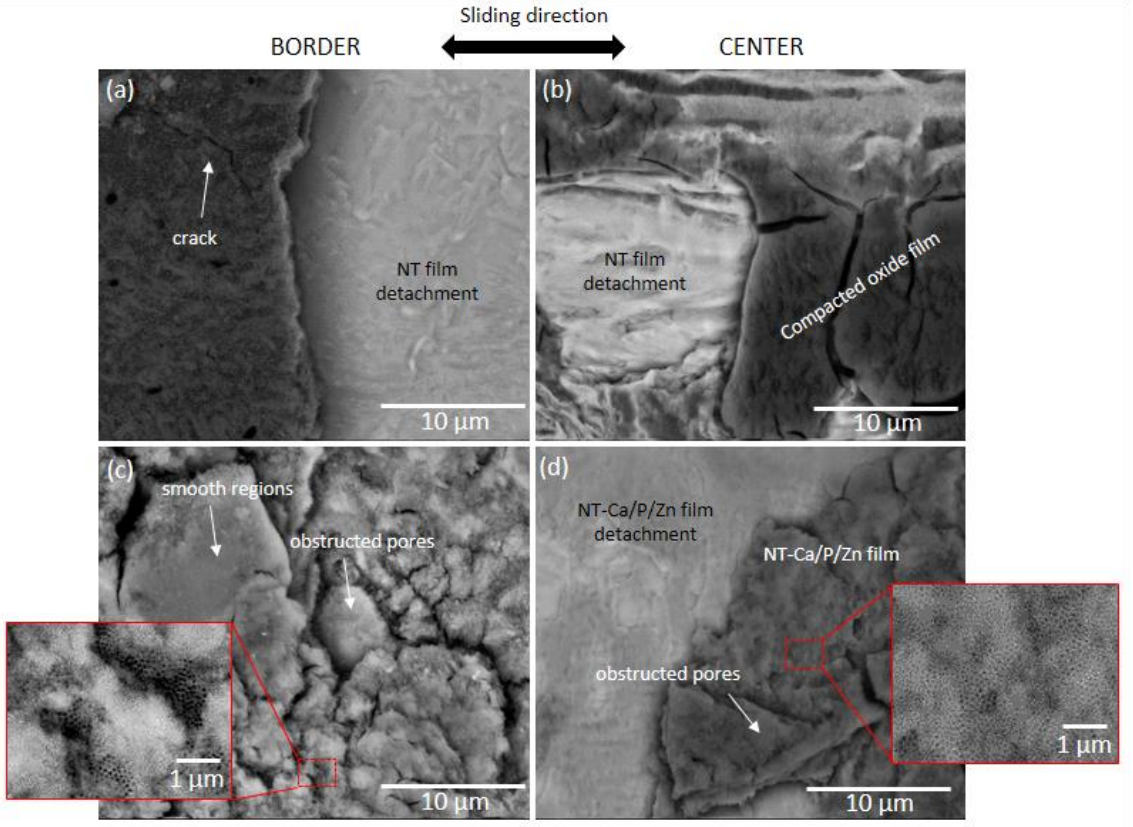

Fig. 7.4. BSE SEM micrographs of the wear tracks of (a and b) NT; (c and d) NT-Ca/P/Zn samples in the border and central regions. The inset images in (c) and (d) show the presence of TiO_2 NTs in the border and central regions.

7.3.2.3. Wear volume

After two-cycle tribo-electrochemical tests wear volume measurements were performed by 2D profilometry. The final wear volumes include both the contribution of wear due to corrosion and sliding wear, and are graphically presented in Fig. 7.5. The wear volume loss in conventional TiO_2 nanotubular samples was 4.05 ± 1.24 x 10^6 µm^3, significantly higher as compared to NT-Ca/P/Zn#1 and NT-Ca/P/Zn#2 samples whose wear volumes were measured as 1.22 ± 0.01 x 10^6 µm^3 and 1.58 ± 0.22 x 10^6 µm^3 respectively.

7.3.3. Mechanical properties of TiO_2 nanotubular films

The mechanical properties of TiO_2 nanotubular films were accessed before and after bio-functionalization treatments. An additional group of samples of pure Ti was included due to its relevance on clinical procedures in respect to dental implants. The elastic modulus and the hardness of Ti, NT and NT-Ca/P/Zn samples are depicted in Table 7.2.

TiO_2 NTs revealed a significantly lower elastic modulus when compared to pure Ti samples, both before and after bio-functionalization. As regards hardness measurements, Ti samples displayed significantly higher values in relation to both NT and NT-Ca/P/Zn samples. Interestingly, after bio-functionalization treatments an improvement in the hardness of the nanotubular films is observed, as shown by the significantly higher hardness (around 300 MPa) measured for NT-Ca/P/Zn as compared to NT samples (Table 7.2).

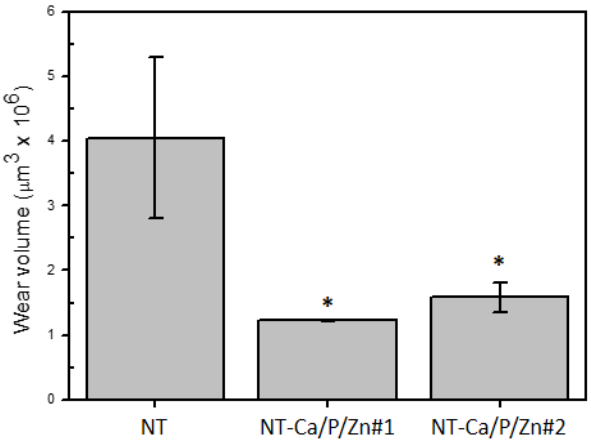

Fig. 7.5. Wear volume measurements after two-cycle reciprocating sliding tests in NT, NT-Ca/P/Zn#1 and NT-Ca/P/Zn#2 samples. (*) significantly different from NT, *p < 0.05*.

Table 7.2. Elastic modulus and hardness values measured for Ti, NT and NT-Ca/P/Zn samples.

Group	Elastic modulus (GPa ± SD)	Hardness (GPa ± SD)
Ti	127.25 ± 5.80	2.58 ± 0.12
NT	46.18 ± 4.03*	0.58 ± 0.08*
NT-Ca/P/Zn	46.99 ± 4.05*	0.89 ± 0.15*#

(*) significantly different from Ti, $p < 0.05$; (#) significantly different from NT, $p < 0.05$.

7.4. Discussion

7.4.1. Tribo-electrochemical degradation of TiO_2 nanotubular films under two-cycle sliding tests

The understanding of how new implant surfaces behave when submitted to the simultaneous action of sliding wear and corrosion is of paramount importance since dental implants might be exposed to these actions at early, mid and long term after insertion. Relative micro-movements take place between the implant surface and the surrounding bone tissue and may lead to several and harmful complications. In our present contribution we report on the synthesis of novel bio-functionalized TiO_2 nanotubular surfaces and their tribo-electrochemical performance. To simulate *in vivo* conditions, bio-functionalized TiO_2 NTs were submitted to multiple sliding actions in the presence of artificial saliva (AS) and their tribo-electrochemical response was compared with conventional TiO_2 NTs.

After immersion of NT samples in AS a stable OCP is achieved (Fig. 7.2a – black curve) and once SLIDING 1 takes place it is kept stable for 100 s, followed by a gradual decrease during the whole duration of sliding. Variations in OCP reflect the passive or active electrochemical state of the material. An increase (anodic shift) indicates a more passive state while a decrease (cathodic shift) suggests a more active state [52]. Furthermore, it is known that the OCP measured during sliding action is a mixed potential which reflects the electrochemical state of the material outside (unworn) and inside (worn) the wear track [52]. In this light, during the first 100 s of SLIDING 1 it seems that the electrochemical state of NT samples in the sliding contact area is kept unaltered, probably because TiO_2 NTs are able to withstand the mechanical actions and protect the underlying Ti substrate from AS. The gradual lowering of the OCP after this time suggests that the film is progressively degraded as sliding occurs. The COF monitored during this period indicates that the alumina ball is rubbing against an oxide film since 0.66 – 0.67 are typical COF values for alumina/Ti oxide tribological pair. Similar COF values comprised between 0.6 – 0.8 have been reported for sliding tests carried out on oxidized Ti surfaces against alumina ball [43, 44, 53]. When SLIDING 2 starts the OCP begins decreasing gradually and once it is finished it increasingly evolves to noble values, and interestingly it follows similar depassivation and repassivation rates of the ones registered during and after SLIDING 1, respectively. Although the COF during SLIDING 2 tends to decrease, it still indicates that an oxide film is present in the contact region, whose presence is confirmed by observation of the SEM BSE images of the wear scar remaining on NT samples (Fig. 7.3a and Fig. 7.4b). From these images it is observed that after two-cycle sliding a huge amount of NT film has been completely detached from the periphery of the contact area and the formation of a compact oxide film is observed in the central region, where the sliding contact took place. Possibly, one of the main mechanisms behind NT samples degradation relies in film detachment due to poor adhesion to the Ti substrate. Some cracks are visible in the film remaining outside the wear track (Fig. 7.4a) possibly resulting from cyclic compressive stresses generated during sliding, induced by film debris that are pushed against the film surrounding the contact area. The presence of cracks shows the brittleness of the film and suggests that it might have failed due to delamination.

The formation of the compact oxide film during tribo-electrochemical interactions (tribofilm) may grant both corrosion and wear protection to the substrate material as deduced from electrochemical behavior and COF measurements. Based on this knowledge it is presumed that the gradual decrease of the OCP during SLIDING 1 and SLIDING 2 is being influenced by the formation of this tribofilm. It is believed that the formation of this film occurs during sliding as a consequence of film debris release into the contact region, which are consequently entrapped and compacted as the rubbing action goes on. As Vieira et al. [54] highlighted, this may initiate

a galvanic coupling in the wear track between depassivated and still passive areas and strongly influence the evolution of the potential during tribocorrosion. This tribofilm is probably granting the stable electrochemical features of NT samples when submitted to multiple sliding actions, as observed from the similar depassivation and repassivation rates for both cycles of sliding.

Both NT-Ca/P/Zn samples show similar OCP values before mechanical solicitations (Fig. 7.2a – green and blue curves), and these are significantly higher compared to NT samples. The higher OCP reveals that TiO_2 NTs display a less active electrochemical state after bio-functionalization. This may be related with the fast and effective passivation ability of these samples immersed in AS, as previously deduced from potentiodynamic polarization studies of NT samples after bio-functionalization through the same methodology used in this study [41]. The improved electrochemical performance of bio-functionalized NTs is believed to be related with the formation of a nano-thick oxide film at the interface between Ti and TiO_2 NTs as observed in Fig. 7.1d, as a consequence of anodization process. Probably, the Ti^{4+} ions released from the Ti substrate at the moment of anodic polarization, reacted with O^{2-} ions moving in opposite direction (provided by H_2O or OH^- in the electrolyte), and formed a Ti oxide film at the interface [55]. As soon as mechanical solicitations start on NT-Ca/P/Zn#1 samples the OCP shifts down probably due to the wear of the topmost layers of the nanotubular film and after around 800 s, a more abrupt OCP fall takes place that may be related with the degradation of the film and exposure of the substrate to the harsh environment provided by AS. Immediately after the end of SLIDING 1, the OCP quickly recovers to higher values at a faster repassivation rate compared to NT samples, which highlights their ability of repassivation and the re-establishment of a noble potential close to the one attained during the first 800 s of sliding. During SLIDING 2, a different behavior is observed: the OCP slowly shifts down for around 1000 s, and afterwards it starts to evolve to values increasingly high towards the one achieved before sliding. Simultaneously to this noble evolution of the OCP, it is observed a decrease in the COF (Fig. 7.2c – green curve). This behavior suggests that repassivation of the wear track may be related with the formation of a tribofilm in the contact area with lubricant properties. To further investigate this phenomenon additional BSE SEM images were taken in the wear tracks of both NT and NT-Ca/P/Zn samples, however, before cleaning procedure. In this way, additional information on the morphological and chemical features of the scar region in direct contact with alumina counterbody could be obtained. These images are shown in Fig. 7.6a and b for NT and NT-Ca/P/Zn samples, respectively. In the central region of the wear tracks remaining on NT and NT-Ca/P/Zn samples the presence of compacted mixed oxide films were found with a smooth topography, contrasting with less oxidized regions from where most of the film has been probably detached. The presence of smooth regions was observed in a higher extension for NT-

Ca/P/Zn samples, including in the border region of the wear track after samples cleaning as observed in Fig. 7.4c. From observation of Fig. 7.6a and EDS spectra extracted from regions A1 and A2 indicated in the figure, it is observed that the smooth oxide films are characterized by a significantly higher at. % of P. The presence of P-rich oxide films are also found on NT-Ca/P/Zn samples as observed from Fig. 7.6b and the correspondent EDS spectra in areas A1 and A2. The smooth areas found in NT-Ca/P/Zn samples are composed additionally by Zn and a higher at. % of Ca as a result of their bio-functionalization with these elements.

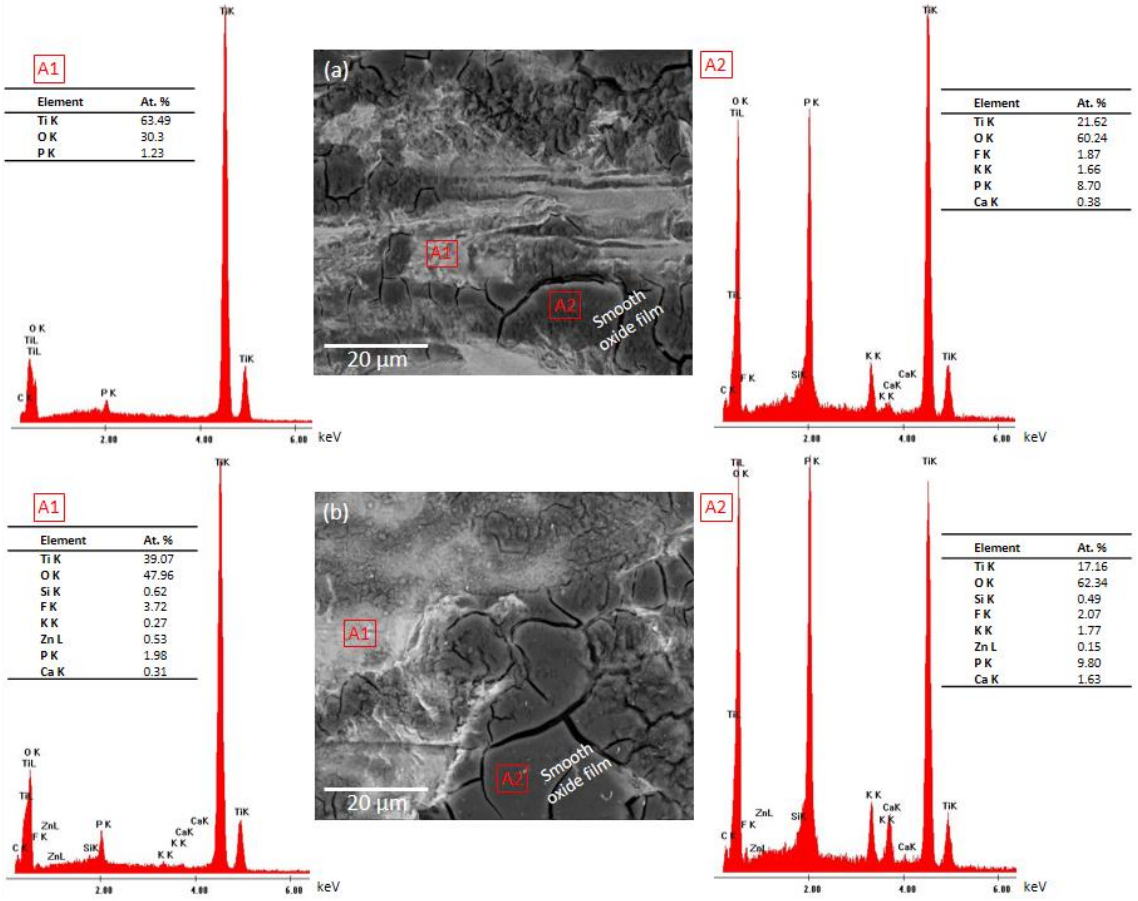

Fig. 7.6. BSE SEM micrographs in the central region of the wear tracks of (a) NT and (b) NT-Ca/P/Zn samples. The EDS spectra acquired from the inset red squares (A1 and A2) are depicted for both groups along with the insertion of the elemental composition and the atomic percentage (At. %) of the detected elements.

Hanawa et al. [56] reported that calcium phosphate is naturally formed on Ti surface immersed in a electrolyte solution containing inorganic ions found in biofluid, and approximately 60 % of the phosphate was PO_4^{3-}. The authors explained that the formation of a calcium phosphate layer on Ti surface was firstly dictated by the adsorption of hydrated phosphate ions to Ti. Furthermore, previous studies have also demonstrated the ability of anodic Ti oxide films to induce the formation of apatite when immersed in simulated body fluid [57, 58]. As soon as NT-Ca/P/Zn samples are immersed in AS and reciprocating sliding takes place, it is expected TiO_2

film debris are released and PO_4^{3-} ions in solution adsorb on their surface. Simultaneously, these are submitted to complex mechanical and electrochemical solicitations, during which film debris become entrapped in the contact region and are continuously smashed and compacted. This possibly induced the formation of a P-rich compact oxide film (tribofilm) in some areas of the wear track, most likely in those where the nanotubular film is thicker, as schematically illustrated in Fig. 7.7. Under wear action, PO_4^{3-} ions are known to undergo favorable reactions resulting in protective tribofilms [59, 60]. The presence of this tribofilm is most likely related with the increase of the OCP for NT-Ca/P/Zn#1 samples after 1000 s of SLIDING 2, and the simultaneous COF decrease (Fig. 7.2a and c – green curves). It is known that phosphate groups may act as lubricants [61], reducing the frictional force resisting to the relative sliding movement between neighboring surfaces, which is transduced in a lower COF. This might explain the smoothening effect observed on the surface of the film. Although not so evident for NT surfaces, a small trend is also observed for a gradual decrease in the COF during SLIDING 2 (Fig. 7.2c – black curve) and the formation of this P-rich film may also be a reasonable explanation for that. On the other hand, another possibility is that once TiO_2 nanotubular film has undergone severe detachment, the alumina ball could be also in contact with the Ti substrate, which has a COF characteristic of around 0.45 [53].

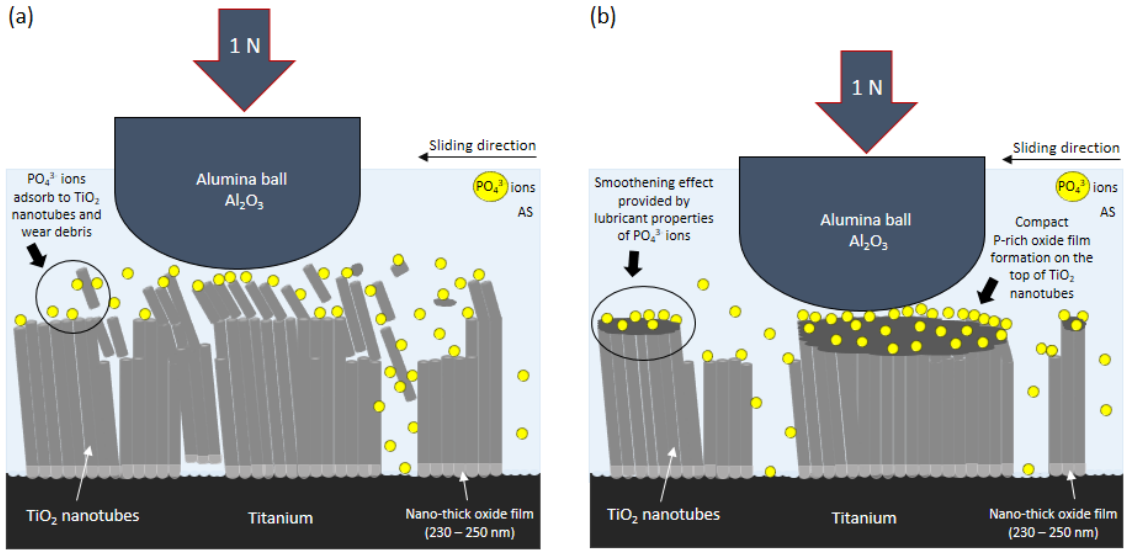

Fig. 7.7. Illustration of the formation mechanisms of the P-rich oxide film during tribo-electrochemical interactions on bio-functionalized TiO_2 NTs in AS. Firstly, PO_4^{3-} ions adsorb to TiO_2 NTs and wear debris generated during sliding as shown in (a) and then, as the tribo-electrochemical interactions take place there is the formation of a compact P-rich oxide film on the top of bio-functionalized TiO_2 NTs as depicted in (b). The smoothening effect observed on the surface of the film is related with the lubricant properties of PO_4^{3-} ions.

Even though the OCP values measured during two-cycle sliding tests have been significantly different for NT-Ca/P/Zn#1 and NT-Ca/P/Zn#2 samples, the trend of OCP evolution was found quite similar between both during mechanical solicitations (Fig. 7.2a – green and blue curves). In both cases two steady-states were achieved during SLIDING 1 at different OCP values, and at different time periods. Although during SLIDING 2 the OCP decreased only a few millivolts for NT-Ca/P/Zn#2 samples, the trend for COF decrease after 1000 s is similar to NT-Ca/P/Zn#1 samples (Fig. 7.2c – green and blue curves). No significant differences were found in the wear volume loss measured between NT-Ca/P/Zn#1 and NT-Ca/P/Zn#2 samples (Fig. 7.5), and therefore the differences in the OCP between both seem not be related with the level of mechanical damage of the nanotubular films. Most probably, the experimental conditions used for reciprocating sliding tests are close to the threshold conditions for NTs withstand mechanical solicitations without failure, which is dependent on their mechanical properties. Furthermore, the OCP might be also influenced by the total extension and thickness of the tribofilm formed, which may be thinner or thicker as the OCP is lower or higher, respectively. It is noteworthy to highlight that the OCP fluctuations observed during two-cycle sliding tests for both NT-Ca/P/Zn samples, might be related with Zn^{2+} ions liberation that have standard potential of -0.762 V vs. NHE (Zn^{2+}/Zn) [62].

The wear volume loss was found significantly higher for NT than for both NT-Ca/P/Zn samples showed (Fig. 7.5). These differences may be related with the different adhesion strength of NT and NT-Ca/P/Zn films to the substrate, which seems be significantly higher for the latter. This is demonstrated by the lower mechanical damage observed for NT-Ca/P/Zn samples (Fig. 7.3), in parallel with their significantly reduced wear volume loss (Fig. 7.5). No detachment is observed in the area outside the contact region for these samples and the survival of NTs is found even in the border and central regions of their wear tracks (Fig. 7.4c and d). As a consequence of bio-functionalization of TiO_2 NTs and the formation of a nano-thick oxide film at the interface, the interfacial bonding to the substrate increased significantly, and consequently their ability to withstand to both electrochemical and mechanical solicitations possibly by minimizing initiation and propagation of cracks.

For all the samples the main wear mechanisms identified include abrasion evidenced by abrasion grooves induced by third body particles, along with plastic deformation of the nanotubular film (Fig. 7.3 and Fig. 7.6). Furthermore, adhesion phenomenon also occurred as observed from material transfer to the counterbody after sliding tests.

7.4.2. Mechanical properties of TiO_2 NTs: significance and impact on wear resistance

The design of new implant systems with excellent mechanical properties is a requirement

for long term implant success. After bio-functionalization treatments the hardness of TiO_2 nanotubular films became significantly higher as compared to conventional TiO_2 NTs (Table 7.2). The hardness values for NT and NT-Ca/P/Zn samples were measured as 0.58 ± 0.08 GPa and 0.89 ± 0.15 GPa, respectively. Xu et al. [51] also studied the mechanical behavior of TiO_2 nanotube arrays and found out their hardness as 0.94 GPa, which is in the same order of magnitude of our results. This improvement may be related with the nano-thick oxide film formed at the interface Ti/TiO_2 NTs after anodization treatments in the Ca/P/Zn-based electrolyte. The growth of this film at the interface improved significantly the adhesion strength of TiO_2 NTs to the substrate, as previously deduced from the different tribo-electrochemical responses observed between NT and NT-Ca/P/Zn samples. It has been previously reported that the hardness is dependent on the film adhesion properties to the substrate, in such a way that as higher the adhesion strength higher the hardness [63, 64]. A film with good adhesion to the substrate will constrain its plastic flow making the indentation more difficult that is transduced in a higher hardness than the one with poor adhesion [63, 65]. This is also in good agreement with the significantly reduced wear loss in NT-Ca/P/Zn samples when compared to NT samples (Fig. 7.5), since a higher hardness is generally correlated with an improved wear resistance [53, 66-68]. Once NT-Ca/P/Zn films display improved adhesion properties to the substrate, consequently they display an improved ability to resist to mechanical wear.

Our results show that the hardness and elastic modulus of Ti surfaces are 2.58 ± 0.12 GPa and 127.25 ± 5.80 respectively. These are in agreement with Soares et al. [27] who measured the hardness and elastic modulus of Ti polished surfaces by nanoindentation as 2.6 ± 0.7 GPa and 143 ± 23 GPa, respectively. In our work, the elastic modulus of TiO_2 NTs was significantly lower (around 63%) than that of Ti and was comprised between 42 – 52 GPa, both for NT and NT-Ca/P/Zn samples (Table 7.2). Existing literature describes elastic modulus of TiO_2 nanotube arrays ranging 4 – 43 GPa [1, 69]. Our results are in accordance with the study performed by Crawford et al. [69] who reported an elastic modulus for TiO_2 NTs of approximately 36 – 43 GPa, also found significantly lower than that of the Ti substrate. This reduction may be related with the porous structure of TiO_2 nanotubular films [27]. TiO_2 nanotubular surfaces display an elastic modulus approaching that of natural bone, which is around 11 – 30 GPa [26]. Therefore these surfaces are expected to have improved biomechanical compatibility than pure Ti, by reducing stress shielding effect [70] which is very well known to induce bone resorption at implant bone interface.

7.5. Conclusions

The tribo-electrochemical performance of conventional and bio-functionalized TiO_2 NTs was investigated when submitted to multiple sliding actions in artificial saliva. Furthermore, the mechanical properties of those films were investigated and correlations were found with their tribo-electrochemical responses. The main conclusions are as follows:

- TiO_2 NTs display a highly stable tribo-electrochemical response when submitted to multiple sliding actions.
- The tribo-electrochemical behavior of TiO_2 NTs was significantly improved after bio-functionalization treatments both from the electrochemical and mechanical point of view.
- Bio-functionalization of TiO_2 NTs by reverse polarization anodization induced the formation of a nano-thick oxide film at the interface region which improved significantly the adhesion strength of the NTs to Ti substrate.
- The improved adhesion of bio-functionalized TiO_2 NTs was correlated with their increased hardness, and consequently linked to the significantly enhanced wear resistance of these films.
- TiO_2 NTs display the ability to induce the formation of a protective P-rich tribofilm when submitted to tribo-electrochemical actions in AS, which appears to grant both electrochemical protection and mechanical wear resistance.
- The elastic modulus of TiO_2 NTs is significantly lower compared to that of smooth Ti, and close that of natural bone.

In brief, bio-functionalized TiO_2 NTs through reverse polarization anodization display an improved ability to withstand multiple tribo-electrochemical solicitations. These show up as multifunctional surfaces able to simultaneously provide corrosion protection, resistance to mechanical degradation and avoid bone resorption by reducing stress shielding effect. This study provides fundamental and new insights for the development of TiO_2 NTs in Ti surfaces with long term biomechanical compatibility and stability towards the new generation of dental implants.

Acknowledgements

This work was supported by FCT with the reference project UID/EEA/04436/2013 and by FEDER funds through the COMPETE 2020 – Programa Operacional Competitividade e Internacionalização (POCI) with the reference project POCI-01-0145-FEDER-006941.

The authors also acknowledge the financial support from FCT by the doctoral grant (Ref. SFRH/BD/88517/2012), CAPES (Proc. 99999.008666/2014-08), CNPq (Proc. 490761/2013-5) and UNESP. Moreover, the authors are grateful to LABNANO/CBPF (Brazilian Center for Research in

Physics) for all the support provided in electron microscopy analyses. Finally, Tolou Shokuhfar is also thankful to US National Science Foundation NSF-DMR CAREER award # 1564950.

References

[1] Crawford G, Chawla N, Houston J. Nanomechanics of biocompatible TiO 2 nanotubes by interfacial force microscopy (IFM), Journal of the mechanical behavior of biomedical materials 2 (2009), 580-587.
[2] Zhang W, Wang G, Liu Y, Zhao X, Zou D, Zhu C, Jin Y, Huang Q, Sun J, et al. The synergistic effect of hierarchical micro/nano-topography and bioactive ions for enhanced osseointegration, Biomaterials 34 (2013), 3184-3195.
[3] Zhao L, Wang H, Huo K, Cui L, Zhang W, Ni H, Zhang Y, Wu Z, Chu PK. Antibacterial nano-structured titania coating incorporated with silver nanoparticles, Biomaterials 32 (2011), 5706-5716.
[4] Mendonça G, Mendonça DBS, Simões LGP, Araújo AL, Leite ER, Golin AL, Aragão FJL, Cooper LF. Nanostructured implant surface effect on osteoblast gene expression and bone-to-implant contact in vivo, Materials Science and Engineering: C 31 (2011), 1809-1818.
[5] Chen J, Rungsiyakull C, Li W, Chen Y, Swain M, Li Q. Multiscale design of surface morphological gradient for osseointegration, Journal of the mechanical behavior of biomedical materials 20 (2013), 387-397.
[6] Yazici H, Fong H, Wilson B, Oren EE, Amos FA, Zhang H, Evans JS, Snead ML, Sarikaya M, et al. Biological response on a titanium implant-grade surface functionalized with modular peptides, Acta Biomaterialia 9 (2013), 5341-5352.
[7] Holmberg KV, Abdolhosseini M, Li Y, Chen X, Gorr S-U, Aparicio C. Bio-inspired stable antimicrobial peptide coatings for dental applications, Acta Biomaterialia 9 (2013), 8224-8231.
[8] Arenas MA, Pérez-Jorge C, Conde A, Matykina E, Hernández-López JM, Pérez-Tanoira R, de Damborenea JJ, Gómez-Barrena E, Esteba J. Doped TiO 2 anodic layers of enhanced antibacterial properties, Colloids and Surfaces B: Biointerfaces 105 (2013), 106-112.
[9] Tomsia AP, Launey ME, Lee JS, Mankani MH, Wegst UG, Saiz E. Nanotechnology approaches for better dental implants, The International journal of oral & maxillofacial implants 26 (2011), 25.
[10] Puckett SD, Taylor E, Raimondo T, Webster TJ. The relationship between the nanostructure of titanium surfaces and bacterial attachment, Biomaterials 31 (2010), 706-713.
[11] Liu X, Chu PK, Ding C. Surface nano-functionalization of biomaterials, Materials Science and Engineering: R: Reports 70 (2010), 275-302.
[12] Zhao L, Mei S, Chu PK, Zhang Y, Wu Z. The influence of hierarchical hybrid micro/nano-textured titanium surface with titania nanotubes on osteoblast functions, Biomaterials 31 (2010), 5072-5082.
[13] Ercan B, Taylor E, Alpaslan E, Webster TJ. Diameter of titanium nanotubes influences anti-bacterial efficacy, Nanotechnology 22 (2011), 295102.
[14] Popat KC, Leoni L, Grimes CA, Desai TA. Influence of engineered titania nanotubular surfaces on bone cells, Biomaterials 28 (2007), 3188-3197.
[15] Brammer KS, Oh S, Cobb CJ, Bjursten LM, van der Heyde H, Jin S. Improved bone-forming functionality on diameter-controlled TiO 2 nanotube surface, Acta Biomaterialia 5 (2009), 3215-3223.
[16] Shokuhfar T, Hamlekhan A, Chang J-Y, Choi CK, Sukotjo C, Friedrich C. Biophysical evaluation of cells on nanotubular surfaces: the effects of atomic ordering and chemistry, International journal of nanomedicine 9 (2014), 3737.
[17] Vasilev K, Poh Z, Kant K, Chan J, Michelmore A, Losic D. Tailoring the surface functionalities of titania nanotube arrays, Biomaterials 31 (2010), 532-540.
[18] Gulati K, Ramakrishnan S, Aw MS, Atkins GJ, Findlay DM, Losic D. Biocompatible polymer coating of titania nanotube arrays for improved drug elution and osteoblast adhesion, Acta Biomaterialia 8 (2012), 449-456.
[19] Gao A, Hang R, Huang X, Zhao L, Zhang X, Wang L, Tang B, Ma S, Chu PK. The effects of titania nanotubes with embedded silver oxide nanoparticles on bacteria and osteoblasts, Biomaterials 35 (2014), 4223-4235.
[20] Hu Y, Cai K, Luo Z, Xu D, Xie D, Huang Y, Yang W, Liu P. TiO 2 nanotubes as drug nanoreservoirs for the regulation of mobility and differentiation of mesenchymal stem cells, Acta Biomaterialia 8 (2012), 439-448.
[21] Gulati K, Aw MS, Losic D. Drug-eluting Ti wires with titania nanotube arrays for bone fixation and reduced bone infection, Nanoscale research letters 6 (2011), 571.
[22] Popat KC, Eltgroth M, LaTempa TJ, Grimes CA, Desai TA. Decreased Staphylococcus epidermis adhesion and increased osteoblast functionality on antibiotic-loaded titania nanotubes, Biomaterials 28 (2007), 4880-4888.
[23] Shokuhfar T, Sinha-Ray S, Sukotjo C, Yarin AL. Intercalation of anti-inflammatory drug molecules within TiO 2 nanotubes, RSC Advances 3 (2013), 17380-17386.
[24] Kodama A, Bauer S, Komatsu A, Asoh H, Ono S, Schmuki P. Bioactivation of titanium surfaces using coatings of TiO2 nanotubes rapidly pre-loaded with synthetic hydroxyapatite, Acta Biomaterialia 5 (2009), 2322-2330.
[25] Crawford G, Chawla N, Das K, Bose S, Bandyopadhyay A. Microstructure and deformation behavior of biocompatible TiO 2 nanotubes on titanium substrate, Acta Biomaterialia 3 (2007), 359-367.
[26] Rho J-Y, Tsui TY, Pharr GM. Elastic properties of human cortical and trabecular lamellar bone measured by nanoindentation, Biomaterials 18 (1997), 1325-1330.

[27] Soares P, Mikowski A, Lepienski CM, Santos E, Soares GA, Kuromoto NK. Hardness and elastic modulus of TiO2 anodic films measured by instrumented indentation, Journal of Biomedical Materials Research Part B: Applied Biomaterials 84 (2008), 524-530.
[28] Budinski KG. Tribological properties of titanium alloys, Wear 151 (1991), 203-217.
[29] Rodrigues T, Moreira F, Guerra F, Nicolau P, Neto MA. Clinical trial—in vivo endosseous implants micromovements measuring with 3D Digital Image Correlation method, Biodental Engineering III (2014), 77.
[30] Szmukler-Moncler S, Salama H, Reingewirtz Y, Dubruille JH. Timing of loading and effect of micromotion on bone-dental implant interface: review of experimental literature, Journal of biomedical materials research 43 (1998), 192-203.
[31] Rocha L, Oliveira F, Cruz H, Sukotjo C, Mathew M. Bio-Tribocorrosion in Biomaterials and Medical Implants, In Bio-tribocorrosion in dental applications, Elsevier Inc. (2013), 223-249.
[32] Cruz HV, Souza JCM, Henriques M, Rocha LA. Tribocorrosion and bio-tribocorrosion in the oral environment: the case of dental implants, Biomedical tribology Nova Science Publishers Inc, New York (2011), 1-30.
[33] Olmedo DG, Paparella ML, Brandizzi D, Cabrini RL. Reactive lesions of peri-implant mucosa associated with titanium dental implants: a report of 2 cases, International Journal of Oral and Maxillofacial Surgery 39 (2010), 503-507.
[34] Ribeiro AR, Gemini-Piperni S, Travassos R, Lemgruber L, Silva RC, Rossi AL, Farina M, Anselme K, Shokuhfar T, et al. Trojan-like internalization of anatase titanium dioxide nanoparticles by human osteoblast cells, Scientific reports 6 (2016).
[35] Cobelli N, Scharf B, Crisi GM, Hardin J, Santambrogio L. Mediators of the inflammatory response to joint replacement devices, Nature Reviews Rheumatology 7 (2011), 600-608.
[36] Ingham E, Fisher J. The role of macrophages in osteolysis of total joint replacement, Biomaterials 26 (2005), 1271-1286.
[37] Ingham E, Fisher J. Biological reactions to wear debris in total joint replacement, Proceedings of the Institution of Mechanical Engineers, Part H: Journal of Engineering in Medicine 214 (2000), 21-37.
[38] Miraghaei S, Ashrafizadeh F, Raeissi K, Santamaria M, Di Quarto F. An Electrochemical Investigation on the Adhesion of As-Formed Anodic TiO2 Nanotubes Grown in Organic Solvents, Electrochemical and Solid-State Letters 14 (2011), K8-K11.
[39] Zhao M, Li J, Li Y, Wang J, Zuo Y, Jiang J, Wang H. Gradient Control of the Adhesive Force between Ti/TiO2 Nanotubular Arrays Fabricated by Anodization, Scientific reports 4 (2014).
[40] Yu D, Zhu X, Xu Z, Zhong X, Gui Q, Song Y, Zhang S, Chen X, Li D. Facile method to enhance the adhesion of TiO2 nanotube arrays to Ti substrate, ACS applied materials & interfaces 6 (2014), 8001-8005.
[41] Alves SA, Patel SB, Sukotjo C, Mathew MT, Filho PN, Celis J-P, Rocha LA, Shokuhfar T. Synthesis of calcium-phosphorous doped TiO2 nanotubes by anodization and reverse polarization: A promising strategy for an efficient biofunctional implant surface, Applied Surface Science 399 (2017), 682-701.
[42] Fusayama T, Katayori T, Nomoto S. Corrosion of Gold and Amalgam Placed in Contact with Each Other, Journal of Dental Research 42 (1963), 1183-1197.
[43] Alves S, Bayón R, Igartua A, Saénz de Viteri V, Rocha L. Tribocorrosion behaviour of anodic titanium oxide films produced by plasma electrolytic oxidation for dental implants, Lubrication science 26 (2014), 500-513.
[44] Alves S, Bayón R, de Viteri VS, Garcia M, Igartua A, Fernandes M, Rocha L. Tribocorrosion Behavior of Calcium- and Phosphorous-Enriched Titanium Oxide Films and Study of Osteoblast Interactions for Dental Implants, Journal of Bio-and Tribo-Corrosion 1 (2015), 1-21.
[45] Souza J, Barbosa S, Ariza E, Celis J-P, Rocha L. Simultaneous degradation by corrosion and wear of titanium in artificial saliva containing fluorides, Wear 292 (2012), 82-88.
[46] Robin A, Meirelis J. Influence of fluoride concentration and pH on corrosion behavior of Ti-6Al-4V and Ti-23Ta alloys in artificial saliva, Materials and corrosion 58 (2007), 173-180.
[47] Souza JC, Barbosa SL, Ariza EA, Henriques M, Teughels W, Ponthiaux P, Celis J-P, Rocha LA. How do titanium and Ti6Al4V corrode in fluoridated medium as found in the oral cavity? An in vitro study, Materials Science and Engineering: C 47 (2015), 384-393.
[48] Holland R. Corrosion testing by potentiodynamic polarization in various electrolytes, Dental Materials 8 (1992), 241-245.
[49] Doni Z, Alves A, Toptan F, Gomes J, Ramalho A, Buciumeanu M, Palaghian L, Silva F. Dry sliding and tribocorrosion behaviour of hot pressed CoCrMo biomedical alloy as compared with the cast CoCrMo and Ti6Al4V alloys, Materials & Design 52 (2013), 47-57.
[50] Oliver WC, Pharr GM. An improved technique for determining hardness and elastic modulus using load and displacement sensing indentation experiments, Journal of Materials Research 7 (1992), 1564-1583.
[51] Xu Y, Liu M, Wang M, Oloyede A, Bell J, Yan C. Nanoindentation study of the mechanical behavior of TiO2 nanotube arrays, Journal of Applied Physics 118 (2015), 145301.
[52] Ponthiaux P, Wenger F, Drees D, Celis J-P. Electrochemical techniques for studying tribocorrosion processes, Wear 256 (2004), 459-468.
[53] Alves A, Oliveira F, Wenger F, Ponthiaux P, Celis J-P, Rocha L. Tribocorrosion behaviour of anodic treated titanium surfaces intended for dental implants, Journal of Physics D: Applied Physics 46 (2013), 404001.

[54] Vieira A, Rocha L, Papageorgiou N, Mischler S. Mechanical and electrochemical deterioration mechanisms in the tribocorrosion of Al alloys in NaCl and in NaNO 3 solutions, Corrosion Science 54 (2012), 26-35.
[55] Roy P, Berger S, Schmuki P. TiO2 nanotubes: synthesis and applications, Angewandte Chemie International Edition 50 (2011), 2904-2939.
[56] Hanawa T, Ota M. Calcium phosphate naturally formed on titanium in electrolyte solution, Biomaterials 12 (1991), 767-774.
[57] Yang B, Uchida M, Kim H-M, Zhang X, Kokubo T. Preparation of bioactive titanium metal via anodic oxidation treatment, Biomaterials 25 (2004), 1003-1010.
[58] Cui X, Kim HM, Kawashita M, Wang L, Xiong T, Kokubo T, Nakamura T. Preparation of bioactive titania films on titanium metal via anodic oxidation, Dental Materials 25 (2009), 80-86.
[59] Somers AE, Howlett PC, MacFarlane DR, Forsyth M. A review of ionic liquid lubricants, Lubricants 1 (2013), 3-21.
[60] Dai W, Kheireddin B, Gao H, Kan Y, Clearfield A, Liang H. Formation of Anti-Wear Tribofilms via α-ZrP Nanoplatelet as Lubricant Additives, Lubricants 4 (2016), 28.
[61] Yang Y, Zhang C, Wang Y, Dai Y, Luo J. Friction and wear performance of titanium alloy against tungsten carbide lubricated with phosphate ester, Tribology International 95 (2016), 27-34.
[62] Delahay P, Pourbaix M, Van Rysselberghe P. Potential-pH Diagram of Zinc and its Applications to the Study of Zinc Corrosion, Journal of The Electrochemical Society 98 (1951), 101-105.
[63] Stone D, LaFontaine WR, Alexopoulos P, Wu TW, Li C-Y. An investigation of hardness and adhesion of sputter-deposited aluminum on silicon by utilizing a continuous indentation test, Journal of Materials Research 3 (1988), 141-147.
[64] Azadmanjiri J, Wang JY, Berndt CC, Kapoor A, Zhu DM, Ang ASM, Srivastava VK. Tantalum-and silver-doped titanium dioxide nanosheets film: Influence on interfacial bonding structure and hardness of the surface system, Industrial & Engineering Chemistry Research (2016).
[65] LaFontaine WR, Yost B, Li C-Y. Effect of residual stress and adhesion on the hardness of copper films deposited on silicon, Journal of Materials Research 5 (1990), 776-783.
[66] Karthikeyan S, Vijayaraghavan L. Influence of Nano Al2O3 Particles on the Adhesion, Hardness and Wear Resistance of Electroless NiP Coatings, International Journal of Materials, Mechanics and Manufacturing 4 (2016), 106-110.
[67] Marques IdSV, Alfaro MF, Da Cruz NC, Mesquita MF, Takoudis C, Sukotjo C, Mathew MT, Barão VAR. Tribocorrosion behavior of biofunctional titanium oxide films produced by micro-arc oxidation: Synergism and mechanisms, Journal of the mechanical behavior of biomedical materials 60 (2016), 8-21.
[68] Oliveira FG, Ribeiro AR, Perez G, Archanjo BS, Gouvea CP, Araújo JR, Campos AP, Kuznetsov A, Almeida CM, et al. Understanding growth mechanisms and tribocorrosion behaviour of porous TiO 2 anodic films containing calcium, phosphorous and magnesium, Applied Surface Science 341 (2015), 1-12.
[69] Crawford G, Chawla N, Das K, Bose S, Bandyopadhyay A. Microstructure and deformation behavior of biocompatible TiO2 nanotubes on titanium substrate, Acta Biomaterialia 3 (2007), 359-367.
[70] Mohseni E, Zalnezhad E, Bushroa A. Comparative investigation on the adhesion of hydroxyapatite coating on Ti–6Al–4V implant: A review paper, International Journal of Adhesion and Adhesives 48 (2014), 238-257.

CHAPTER 8

General results and discussion
Final conclusions

8.1. General results and discussion

The main aim of this project was to synthesize bone-inspired TiO_2 nanotubes (NTs) with multiple functionalities, aiming to address, simultaneously, three of the main causes of failures in implant dentistry: tribocorrosion, infection and poor osseointegration. To achieve the main aim, a systematic and multidisciplinary approach was followed, through which new scientific knowledge was produced in research fields not yet explored in literature. The development of this project comprised several independent studies, which were reported in different scientific papers all interrelated with each other.

The possibilities for surface functionalization are countless. In this work, a simple and novel methodology was followed based in a well-known and widely used technique for surface functionalization, including by dental implant companies, i.e. anodization. Biocompatible TiO_2 nanotubular surfaces were synthesized and enriched with bioactive elements, namely calcium (Ca), phosphorous (P), and zinc (Zn). Beyond surface chemistry, the novel methodology adopted induced to modification of TiO_2 NTs/Ti substrate interface features, which are known to dictate the adhesion strength of the film to the substrate and subsequently its tribo-electrochemical performance. Henceforward are described the main results of this project, which were reported in five scientific papers from chapter 3 to chapter 7. The interrelation existing between the main outcomes of each chapter were established, and some important topics were additionally discussed.

8.1.1. Reverse polarization anodization of TiO_2 NTs: a simple and novel methodology to achieve bio-multifunctionalization

In this study conventional TiO_2 NTs were functionalized by reverse polarization anodization that emerged as a simple, versatile, cost-effective, and novel methodology to provide them multiple and key functionalities for osseointegrated implants applications.

One of the main routes seeking the synthesis of bio-functionalized TiO_2 NTs was, firstly, the optimization of the production protocol of conventional TiO_2 NTs. As primarily described in chapter 3, and further confirmed in the following chapters, TiO_2 NTs were synthesized by two-step anodization processes that relied in the growth of highly ordered nano-arrays with non-uniform diameters ranging from 50 – 90 nm. A bone-inspired surface morphology was achieved and the mechanisms behind the growth formation of such micron-length NTs were addressed in chapter 3 and chapter 4. The strategies for bio-functionalization of TiO_2 NTs were, for the first time, described in chapter 3, in which reverse polarization anodization was found as the most promising to achieve an efficient biofunctional implant surface.

From all the studies described from chapter 3 to chapter 7 it is observed that reverse polarization anodization of TiO_2 NTs influenced their surface chemistry without compromising their morphological/topographical features. After bio-functionalization treatments, TiO_2 NTs displayed similar diameters as compared to the conventional ones, and their thickness was around 4.5 – 5.6 μm (chapter 3 and chapter 4). The versatility of this new methodology is shown by the enrichment of TiO_2 NTs with distinct bioactive elements, namely Ca, P, and Zn, by simply changing the anodization electrolyte composition. As pointed out in chapter 4, not only the surface chemistry of the NTs was changed, but also their chemical features along their length, even in the region near the interface with the Ti substrate. Two main groups of bio-functionalized NTs were synthesized and named in accordance with their chemical composition as NT-Ca/P and NT-Ca/P/Zn samples. Through XPS studies Ca, P and Zn were found mainly assigned to $Ca_3(PO_4)_2$, CaO, PO_4^{2-} groups, and ZnO compounds adsorbed to TiO_2 (chapter 3 and chapter 5). As discovered in chapter 3, reverse polarization appeared as an essential step to be applied before anodization, to induce the formation of additional compounds on NTs, such as CaO. This finding was reported to be possibly related with the improved biocompatibility of reverse polarized NTs, as compared to the ones functionalized only by single anodization.

The nanotubular surfaces, before and after bio-functionalization, were found more hydrophilic as compared to conventional Ti smooth surfaces (chapter 3), which is known to influence cell functionalities, together with surface morphology/topography and chemistry. The biocompatibility of NT-Ca/P samples for osteoblast-like cells was firstly proved in chapter 3, and then confirmed in chapter 5. In this latter chapter in-depth biological studies were conducted for NT-Ca/P and NT-Ca/P/Zn samples from which their biocompatibility was evidenced both for osteoblast-like and human mesenchymal stem cells (hMSCs).

Bringing together reverse polarization and anodization steps, TiO_2 NTs were granted with multiple and crucial functionalities for the production of enhanced implant surfaces. While reverse polarization arose as a fundamental step for the synthesis of biocompatible Ca/P and Ca/P/Zn-doped TiO_2 NTs, the anodization step was found to play a key role on the improvement of their electrochemical and tribo-electrochemical responses in artificial saliva (AS). This improved ability to withstand both to corrosive and tribocorrosive environments, was linked with the formation of a nano-thick oxide film at the interface region as a consequence of anodization. These findings resulted from the studies reported in chapter 3, 4, 6 and 7 and will be discussed in more detail in the following sections.

8.1.2. Understanding the influence of TiO_2 NTs bio-functionalization on human cells and bacterial responses: impact on osseointegration and infection

The incorporation of bioactive elements natively present in bone such as Ca and P, is a well-known approach to improve the bio-functionality of Ti-based surfaces [1, 2]. Based on this knowledge, these elements were chosen to enrich TiO_2 NTs intended for dental and orthopedic applications, along with Zn that plays an important role in osteoblast differentiation and bone formation, and also display antimicrobial properties [3, 4].

As clearly shown in chapter 5, nanotubular surfaces modulated the morphology of osteoblast-like and hMSCs, by inducing to a highly stretched shape compared to cells on smooth and micro/nano-roughened Ti surfaces. Furthermore, early adhesion studies showed that cells interacted faster with nanotubular surfaces, and after 2 h of adhesion the formation of stress fibers along with well-developed lamellipodia and filopodia suggested an improved adhesion ability. It is believed that the cell adhesion process has been controlled by nanotubular surface features, namely morphology, topography, chemistry, and energy. These characteristics may play, separately or together, key roles on the initial protein adsorption to NTs, and consequently interfere in cell functionalities such as adhesion, cytoskeleton organization, proliferation and differentiation [5]. The topographical/morphological and physicochemical characteristics of TiO_2 NTs are known to control the adhesion of extracellular matrix (ECM) proteins and subsequently modulate cell adhesion through integrin receptors [6, 7].

As reported in chapter 7, NTs display a lower elastic modulus as compared to smooth Ti, whose values are around 42 – 52 GPa and 121 – 134 GPa, respectively. The reorganization of actin cytoskeleton may be modulated by focal adhesion complexes via integrin receptors, which are sensitive to substrate stiffness and may induce to mechanotransduction activating intracellular signaling pathways [8-10]. Stiff matrix is known to induce cell spreading size, well-aligned stress fibers and enhanced focal adhesion assembly, features generally assigned to osteogenic phenotype. Therefore, it is believed that beyond the effect of morphological/topographical and physicochemical surface features on cell adhesion, the mechanical properties of TiO_2 NTs may also induce to mechanotransduction stimuli, and synergistically modulate cell shape. This is in accordance with previous studies in which TiO_2 NTs triggered intracellular cascades, which are known to regulate mechanotransduction and MSCs commitment to osteoblastic differentiation [11-13]. Shih et al. [8] provided evidences that the matrix stiffness affects osteogenic phenotype of MSCs by mechanotransduction events mediated by α_2-integrin. The authors showed that substrate stiffness regulates the activity of several kinase activities involved in osteogenic differentiation (e.g. ROCK, FAK and ERK 1/2). The lower elastic modulus of TiO_2 NTs is also expected to reduce stress shielding effect, since it is

closer to that of natural bone (11 – 30 GPa) [14, 15]. Stress shielding is usually a consequence of the mismatch of mechanical properties between bone and implant materials, and is widely known to induce bone resorption [16]. Therefore, Ti surfaces decorated with TiO_2 NTs are expected to improve the biomechanical compatibility of implant materials and so, their long-term success.

An additional interesting outcome from the study reported in chapter 5, is related with the key role of Zn to induce osteogenic differentiation of hMSCs by regulating the expression levels of bone morphogenetic protein 2 (BMP-2), which is known to control osteogenic differentiation [17]. It is believe that the higher expression of BMP-2 might have stimulated osteopontin (OPN) expression, a major structural protein of bone matrix [18]. Furthermore, nanotubular surfaces, with or without zinc, induced hMSCs to release significantly higher amount of vascular endothelial growth factor (VEGF), when compared to smooth and micro/nano-roughened Ti surfaces. VEGF synthesis is being probably modulated by the unique surface morphological/topographical and/or physicochemical characteristics of TiO_2 NTs. VEGF is known to play a significant role in angiogenesis and vascularization, which play main roles in bone healing and formation [19]. Beyond promoting cellular functions, NT-Ca/P/Zn surfaces showed the ability to impair *S. aureus* viability, and thus behave as bio-selective surfaces.

In brief, NT-Ca/P/Zn surfaces are biocompatible both for osteoblast-like and hMSCs, able to modulate cell adhesion and osteogenic differentiation, and stimulate the release of VEGF, when compared to adequate controls. In addition to their antimicrobial properties and the ability to reduce stress-shielding effect, these results suggest that TiO_2 nanotubular-textured surfaces and their enrichment with Zn is a very promising approach to design new bio-selective functional surfaces for osseointegrated Ti implants, by improving osseointegration and simultaneously avoiding infection. Based on these outcomes, these surfaces were selected for tribo-electrochemical tests, which are fully reported in chapter 6 and 7 of this thesis.

8.1.3. Improved tribo-electrochemical behavior of bio-functionalized TiO_2 NTs under single and multiple sliding actions

It is very well-known that TiO_2 NTs may effectively enhance cell functionalities and display antimicrobial properties. However, their widespread biological applications may be compromised by the poor adhesion strength of NTs to the Ti substrate [20], and no studies have been undertaken neither to investigate this main issue nor to find a way to overcome it.

One of the main objectives of this work was the in-depth characterization of the morphological features of the interface between TiO_2 NTs and Ti substrate, before and after bio-functionalization treatments. This study is reported in chapter 4, and one of the main outcomes

relied on the poor adhesion of conventional NTs, through observation of a non-continuous interface characterized by a hollow space between the nanotubular film and the substrate. After bio-functionalization treatments remarkable changes were observed at the Ti/TiO_2 NTs interface region, due to the formation of a nano-thick oxide film (230 – 250 nm) during anodization process, which appeared to improve NTs adhesion to Ti. The formation of this nano-thick oxide film at the interface confirmed the hypothesis postulated in chapter 3, to explain the significantly lower passive current measured for bio-functionalized NTs as compared to the conventional ones and smooth Ti in AS. This nano-thick oxide film is acting as a protective barrier against the passage of current, therefore effectively protecting the substrate against corrosion.

The adhesion properties and degradation mechanisms of TiO_2 NTs were investigated by tribo-electrochemical tests carried out in AS under single and multiple sliding actions, to better mimic real *in vivo* conditions that dental implants might be exposed to in real life. These studies were reported in chapter 6 and 7 and, for the first time, several fundamental findings were achieved. The poor adhesion of conventional TiO_2 NTs was undoubtedly confirmed and bio-functionalization came out as a very promising approach to overcome it. Besides the more active electrochemical state, conventional TiO_2 NTs suffered catastrophic destruction right after 100 – 300 s sliding actions accompanied by significantly higher wear volume loss as compared to bio-functionalized NTs, either when submitted to single or multiple sliding actions in AS. The improved tribo-electrochemical behavior after bio-functionalization was correlated with the significantly higher adhesion strength of the NTs to the substrate, granted by the nano-thick interfacial film formed by anodization. The high adhesion strength was correlated with the higher hardness measured for these films, which consequently enhanced their mechanical wear resistance. From these studies a first insight on the main degradation mechanisms of TiO_2 NTs was proposed that relies on tube smashing and densification, along with delamination and detachment of the tubes, through cracks formation and propagation from the surface to subsurface regions of the film.

An additional important outcome from the study reported in chapter 7 is the ability of TiO_2 NTs to induce the formation of a protective P-rich tribofilm with lubricant properties during tribo-electrochemical solicitations. This film may help to explain the open circuit potential (OCP) evolution during sliding, both for conventional and bio-functionalized NTs, as well as the high electrochemical stability observed in both cases when submitted to multiple sliding actions. Beyond the improved electrochemical properties, the formation of this tribofilm is believed to synergistically improve the wear resistance ability of TiO_2 NTs. Conventional NTs showed similar degradation by mechanical wear after sliding tests carried out for 300 s and 1800 s, and furthermore, this trend was kept after 2-cycle sliding periods undertaken for 1800 s each. As

concerns bio-functionalized NTs, a trend of a gradual degradation was observed for sliding tests carried out for 300 s and 1800 s, and no significant differences were registered when 2-cycle sliding tests were carried out. These results highlight the ability of NTs to withstand multiple cycles of mechanical solicitations, and suggest that the degradation induced by mechanical wear in the beginning of sliding actions, dictate their long term degradation. This ability of nanotubular films to avoid further mechanical degradation as long mechanical solicitations take place, is believed to be strongly related with the formation of the compact P-rich tribofilm, which grants both protection against corrosion and wear.

The outcomes reported in this section are of tremendous clinical significance since aseptic loosening of dental implants is generally ascribed to peri-implant inflammatory reactions induced by the liberation of metallic ions and solid wear debris, as a consequence of material surface degradation [21, 22]. Ribeiro et al. [23] showed that TiO_2 nanoparticles are internalized by human osteoblasts inducing modifications on their behavior. Furthermore, Wang et al. [24] suggested that chronic exposure of hMSCs to Ti wear debris *in vivo*, may contribute to decreased bone formation at the implant/bone interface by reducing population of viable hMSCs and compromising their differentiation into functional osteoblasts. Peri-implant inflammation is currently associated to periprosthetic bone resorption (osteolysis) with subsequent implant failure, along with the need of an additional surgery to the patient, always painful and expensive. Bio-functionalized TiO_2 NTs display superior resistance to withstand corrosive and tribocorrosive actions, as compared to pure Ti and conventional TiO_2 NTs. Therefore, these are very promising candidates to minimize implant degradation *in vivo*, and subsequently contribute for the establishment of a stable bone-implant anchorage, enhancing the implant life span.

8.2. Final conclusions

This thesis focused on the development of multifunctional TiO_2 NTs through reverse polarization anodization, an easy and innovative strategy which provide them the ability to overcome the main risk factors known to induce dental implant failures. The main outcomes of this work are summarized as follows:

- Reverse polarization anodization is a simple and effective methodology to modify the chemistry of TiO_2 NTs without compromising their morphology. These two steps complement each other: while reverse polarization is fundamental to provide biocompatibility, anodization is key step to improve the interfacial features of conventional TiO_2 NTs.

- Ti surfaces decorated with hydrophilic TiO_2 NTs were fabricated with a bone-inspired morphology. These surfaces displayed an elastic modulus closer to that of bone, modulated osteoblast-like and hMSCs morphologies and reduced *S. aureus* viability, compared to pure Ti.

- TiO_2 NTs displayed angiogenic properties by stimulating the synthesis of VEGF, and their enrichment with Zn supplied them with osteogenic properties by modulating the expression of osteogenesis-related genes.

- Bio-functionalized TiO_2 NTs displayed improved corrosion and tribo-electrochemical properties as compared to pure Ti and conventional NTs. These improvements were suited by the formation of nano-thick oxide film at the interface by anodization, with insulating and adhesion strengthening properties. While the insulator properties of the film granted TiO_2 NTs enhanced corrosion protection, the adhesion strengthening increased their hardness and consequently their wear resistance.

- All the nanotubular films displayed a highly stable tribo-electrochemical behavior when submitted to multiple cycles of mechanical solicitations. The formation of a P-rich oxide tribofilm during tribo-electrochemical solicitations protects effectively the substrate against long-term degradation by wear and corrosion.

In this project, efforts to achieve TiO_2 NTs with improved functionalities have been made. By comparing with the available literature, this thesis remarkably shows that significant improvements have been achieved. By means of a simple approach, key functionalities of conventional TiO_2 NTs were improved which are expected to have huge clinical impact as regards the biological, microbiological and tribo-electrochemical performances of Ti-based implant materials. The new methodology discovered may bring new insights to improve already existing implant systems, or even to create new surfaces with enhanced functionalities. This study takes along a fundamental and insightful contribution by providing new knowledge on the mechanisms behind tribocorrosive degradation of nanotubular films, and simultaneously, by contributing with an effective and low cost method to overcome it.

One aspect of paramount importance is that the findings reported in this thesis find possibility of practical implementation. They may be translated and applied in dental and orthopedic industries, launched into the market and effectively help people by providing them a better quality of life, while at the same time saving companies' resources.

To finalize, the main aim of this thesis was successfully achieved and the central hypothesis validated: **Titanium surfaces decorated with TiO_2 NTs display multiple bio-functionalities: tribo-electrochemical resistance, antibacterial activity and osseointegration ability**.

References

[1] Dorozhkin SV and Epple M. Biological and medical significance of calcium phosphates, Angewandte Chemie International Edition 41 (2002), 3130-3146.

[2] Ducheyne P, Radin S, Heughebaert M and Heughebaert JC. Calcium phosphate ceramic coatings on porous titanium: effect of structure and composition on electrophoretic deposition, vacuum sintering and in vitro dissolution, Biomaterials 11 (1990), 244-254.

[3] Jin G, Cao H, Qiao Y, Meng F, Zhu H and Liu X. Osteogenic activity and antibacterial effect of zinc ion implanted titanium, Colloids and Surfaces B: Biointerfaces 117 (2014), 158-165.

[4] Huo K, Zhang X, Wang H, Zhao L, Liu X and Chu PK. Osteogenic activity and antibacterial effects on titanium surfaces modified with Zn-incorporated nanotube arrays, Biomaterials 34 (2013), 3467-3478.

[5] Brammer KS, Frandsen CJ and Jin S. TiO2 nanotubes for bone regeneration, Trends in biotechnology 30 (2012), 315-322.

[6] Kulkarni M, Mazare A, Gongadze E, Perutkova Š, Kralj-Iglič V, Milošev I, Schmuki P, Iglič A and Mozetič M. Titanium nanostructures for biomedical applications, Nanotechnology 26 (2015), 062002.

[7] Park J, Bauer S, von der Mark K and Schmuki P. Nanosize and vitality: TiO2 nanotube diameter directs cell fate, Nano letters 7 (2007), 1686-1691.

[8] Shih YRV, Tseng KF, Lai HY, Lin CH and Lee OK. Matrix stiffness regulation of integrin-mediated mechanotransduction during osteogenic differentiation of human mesenchymal stem cells, Journal of Bone and Mineral Research 26 (2011), 730-738.

[9] Li G, Song Y, Shi M, Du Y, Wang W and Zhang Y. Mechanisms of Cdc42-mediated rat MSC differentiation on micro/nano-textured topography, Acta Biomaterialia 49 (2016), 235-246.

[10] Engler AJ, Sen S, Sweeney HL and Discher DE. Matrix elasticity directs stem cell lineage specification, Cell 126 (2006), 677-689.

[11] Zhang H, Cooper LF, Zhang X, Zhang Y, Deng F, Song J and Yang S. Titanium nanotubes induce osteogenic differentiation through the FAK/RhoA/YAP cascade, RSC Advances 6 (2016), 44062-44069.

[12] Gulati K, Maher S, Findlay DM and Losic D. Titania nanotubes for orchestrating osteogenesis at the bone–implant interface, Nanomedicine 11 (2016), 1847-1864.

[13] McBeath R, Pirone DM, Nelson CM, Bhadriraju K and Chen CS. Cell shape, cytoskeletal tension, and RhoA regulate stem cell lineage commitment, Developmental cell 6 (2004), 483-495.

[14] Rho J-Y, Tsui TY and Pharr GM. Elastic properties of human cortical and trabecular lamellar bone measured by nanoindentation, Biomaterials 18 (1997), 1325-1330.

[15] Mohseni E, Zalnezhad E and Bushroa A. Comparative investigation on the adhesion of hydroxyapatite coating on Ti–6Al–4V implant: A review paper, International Journal of Adhesion and Adhesives 48 (2014), 238-257.

[16] Noyama Y, Miura T, Ishimoto T, Itaya T, Niinomi M and Nakano T. Bone loss and reduced bone quality of the human femur after total hip arthroplasty under stress-shielding effects by titanium-based implant, Materials Transactions 53 (2012), 565-570.

[17] Beederman M, Lamplot JD, Nan G, Wang J, Liu X, Yin L, Li R, Shui W, Zhang H, et al. BMP signaling in mesenchymal stem cell differentiation and bone formation, Journal of biomedical science and engineering 6 (2013), 32.

[18] Terai K, Takano-Yamamoto T, Ohba Y, Hiura K, Sugimoto M, Sato M, Kawahata H, Inaguma N, Kitamura Y, et al. Role of osteopontin in bone remodeling caused by mechanical stress, Journal of Bone and Mineral Research 14 (1999), 839-849.

[19] Wernike E, Montjovent M-O, Liu Y, Wismeijer D, Hunziker EB, Siebenrock K-A, Hofstetter W and Klenke FM. VEGF incorporated into calcium phosphate ceramics promotes vascularisation and bone formation in vivo, European Cell Materials 19 (2010), 30-40.

[20] Zhao M, Li J, Li Y, Wang J, Zuo Y, Jiang J and Wang H. Gradient Control of the Adhesive Force between Ti/TiO2 Nanotubular Arrays Fabricated by Anodization, Scientific Reports 4 (2014).

[21] Goodman SB. Wear particles, periprosthetic osteolysis and the immune system, Biomaterials 28 (2007), 5044-5048.

[22] Huber M, Reinisch G, Trettenhahn G, Zweymüller K and Lintner F. Presence of corrosion products and hypersensitivity-associated reactions in periprosthetic tissue after aseptic loosening of total hip replacements with metal bearing surfaces, Acta Biomaterialia 5 (2009), 172-180.

[23] Ribeiro AR, Gemini-Piperni S, Travassos R, Lemgruber L, Silva RC, Rossi AL, Farina M, Anselme K, Shokuhfar T, et al. Trojan-like internalization of anatase titanium dioxide nanoparticles by human osteoblast cells, Scientific Reports 6 (2016), 23615.

[24] Wang ML, Nesti LJ, Tuli R, Lazatin J, Danielson KG, Sharkey PF and Tuan RS. Titanium particles suppress expression of osteoblastic phenotype in human mesenchymal stem cells, Journal of Orthopaedic Research 20 (2002), 1175-1184.

CHAPTER 9

Unanswered questions and future work

9.1. Unanswered questions

Throughout the different stages of development of this thesis a few research questions have arisen, for which neither always a plausible answer has been found based on the existing literature. Henceforward are described some of those unanswered questions:

- One of the main outcomes resulting from the study reported in chapter 3, highlights reverse polarization as a critical step to enhance surface biocompatibility, which was ascribed to the formation of CaO compounds on TiO_2 nanotubes (NTs). However, little knowledge still exists on the effect of CaO on cell functionalities and further studies must be carried out to clarify this hypothesis. Furthermore, it should be elucidated why cell functions (i.e. metabolic activity and adhesion) are compromised, as compared to conventional NTs, if reverse polarization is not applied before anodization step.
- Fluoride ions (F^-) adsorbed on TiO_2 NTs were thought to impair hMSCs differentiation towards osteoblast phenotype, and also to display bactericidal activity against *S. aureus*. Even though this topic has been discussed in chapter 5 based on literature review, the mechanisms behind such biological effects still remained unclear. Additional studies should be undertaken to better understand the possible role of F^- ions on human cells and bacterial functions.
- Although all the nanotubular surfaces displayed the ability to impair bacterial viability, as shown in chapter 5, the mechanisms behind such effect need to be in-depth investigated.
- The metabolic activity of hMSCs cultured in osteogenic medium for six days, was lower for those cells adhered on bio-functionalized NTs as compared to the ones on micro/nano-roughened Ti surfaces. This trend was reported in chapter 5, and it was assumed to be simultaneously influenced by surface features and osteoblastic differentiation of hMSCs. However, the influence of these factors on metabolic activity and proliferation of hMSCs remained uncertain, and additional studies should be performed for clarification.
- Biological studies have demonstrated improved cell adhesion properties on TiO_2 NTs, with cells presenting a very well stretched morphology as compared to smooth and micro/nano-roughened Ti surfaces (chapter 5). However, it remained unclear the effect of surface morphology on cell adhesion, and consequently on its shape. Once surface morphology is dictated by NTs diameter and wall-thickness, additional studies should be performed by changing the nanotube features and assessing their influence on cell responses.
- The poor adhesion strength of conventional TiO_2 NTs was firstly demonstrated in chapter 4, and further confirmed in chapter 6 and 7 by tribo-electrochemical testing. Nevertheless, little knowledge still exists on the real mechanisms governing film detachment.

9.2. Future work

Academic knowledge builds upon the work of others… there is no an end for research! Hereafter are proposed a few topics considered important to be undertaken for further improvements on the current findings, or to provide new insights for exploring other subjects:

- The execution of in-depth studies for understanding the mechanisms underlying cell adhesion process would be of upmost important. To achieve this knowledge an interesting approach would be the quantification of extracellular matrix (ECM) proteins (e.g. albumin and fibronectin) adsorbed to TiO_2 NTs, and the labeling of cell membrane proteins associated to focal adhesion complexes involved in cell adhesion process (e.g. vinculin and paxillin).
- The understanding of the relation existing between cell morphology and osteoblastic differentiation could be achieved by western blot analysis, to study focal adhesion kinase activities involved in intracellular signaling pathways that regulate osteoblast phenotype.
- An in-depth study on the osteoblastic differentiation ability of hMSCs in contact with bio-functionalized NTs should be undertaken. This could be achieve, for example, through quantification of alkaline phosphatase activity (ALP) and bone morphogenetic protein-2 (BMP-2) synthesized by cells in contact with nanotubular surfaces. Furthermore, it would be of upmost relevance to understand the mineralization ability of cells after 21 days of culture.
- The study of the release profile of chemical elements constituting bio-functionalized TiO_2 NTs (i.e. F, Ca, P and Zn) would also of highest significance. This could be achieved by immersion tests in simulating body fluid, and quantification of ionic species release by inductively coupled plasma atomic emission spectroscopy (ICP-AES). This information is of crucial importance to understand the influence of these elements on cell functionalities.
- An additional topic of profound importance would be the study of osteoblasts ability to internalize wear particles released from degradation of bio-functionalized NTs by tribocorrosion, as well as their toxicity potential.
- The use of additional electrochemical techniques to quantify the ionic current released during mechanical solicitations, would be also an interesting approach to study the tribocorrosion behavior of bio-functionalized TiO_2 NTs.
- To explore thermal treatments of bio-functionalized NTs, as a way to improve their multiple functionalities. This seems be a promising strategy to further improve biological performance, antibacterial activity and also achieve enhanced tribocorrosion resistance.
- Bio-functionalized NTs are versatile systems that may be conjugated with other techniques to achieve enhanced bio-functionalities. In particular, TiO_2 NTs have been widely recognized as efficient controlled delivery systems of a wide range of bioactive compounds.